5-2011

SYNTHESIS, CHARACTERIZATION, AND REACTIVITY OF BIOLOGICALLY RELEVANT COPPER(I) SELONE AND THIONE COMPLEXES

Martin Kimani
Clemson University, mkimani@clemson.edu

SYNTHESIS, CHARACTERIZATION, AND REACTIVITY OF BIOLOGICALLY RELEVANT COPPER(I) SELONE AND THIONE COMPLEXES

A Dissertation
Presented to
The Graduate School of
Clemson University

In Partial Fulfillment
of the Requirements for the Degree
Doctor of Philosophy
Chemistry

---

by
Martin Mucheru Kimani
May 2011

Accepted by:
Dr. Julia Brumaghim, Committee Chair
Dr. Gautam Bhattacharyya
Dr. Meredith Newby
Dr. Shiou-Jyh Hwu

ABSTRACT

In Fenton-like reactions, Cu^{+} localized on DNA reduces hydrogen peroxide to form hydroxyl radical ($^{\bullet}OH$), resulting in oxidative DNA damage. This DNA damage causes mutation and cell death, which can lead to diseases such as cancer, Alzheimer's, and arteriosclerosis. Sulfur and selenium antioxidants have been investigated for the prevention and treatment of these diseases, and studies have shown that sulfur- and selenium-containing antioxidants prevent DNA damage from copper-generated hydroxyl radical and that metal coordination is required for the observed antioxidant activity.

To determine how copper coordination results in DNA damage inhibition, Cu^{+} complexes with selone and thione ligands were synthesized with the aim of studying their electrochemistry and reactivity with H_2O_2. Tris(pyrazolyl)methane and -borate ligands are used to synthesize the target metal complexes, since they mimic metal coordination environments in biological systems. *N,N'*-1,3-dimethyl-imidazole thione (dmit), and selone (dmise) ligands are used since they resemble ergothioneine and selenoneine, sulfur and selenium-containing antioxidants naturally found in plants and animals. Selone coordination to Cu^{+} significantly stabilizes Cu^{2+} more effectively than thione coordination by an average of 224 mV. The copper-selone complexes of the formula $[Tpm^{R}Cu(dmise)]^{+}$ and Tp*Cu(dmise) (Tpm^{R} = tris(pyrazolyl)methane, R = H; Tpm, R = Me; Tpm*, R = *i*Pr; Tpm^{iPr}; Tp* = tris(1,3-dimethylpyrazolyl)borate) have potentials from -283 mV to -390 mV, while the analogous thione complexes ($[Tpm^{R}Cu(dmit)]^{+}$ and Tp*Cu(dmit)) have potentials ranging from 70 mV to -232 mV. If similar Cu-Se

complexes are formed *in vivo*, these potentials may be low enough to inhibit Cu^{2+} reduction by NADH and prevent copper redox cycling.

The reactivity of dmise, dmit, and their tris(3,5-dimethylpyrazolyl)methane copper complexes [Tpm*Cu(L) (L = dmise or dmit) with H_2O_2 was explored. Dmise and dmit are both reactive towards H_2O_2 and may be effective scavengers of H_2O_2. Treatment of $[Tpm*Cu(dmise/dmit)]^+$ with H_2O_2 showed sacrificial oxidation of the chalcogenone without oxidation of the Cu^+ metal center, and if similar copper-selenium or –sulfur complexes form *in vivo*, these complexes may scavenge H_2O_2 and inhibit copper-mediated oxidative damage.

A comparative coordination chemistry and density functional theory study of selone and thione with cuprous halides was also performed, and the resulting complexes have varied geometries and stochiometries depending on the type of halide and chalcogenone ligand used, intramolecular π-π interactions, and degree of short contact interactions between X-H (X = I, Br, Cl, Se or S) atoms in the solid state structures. Cu^+ complexes of the bidentate thio- and seleno-imidazolyl ligands bis(thioimidazolyl)methane, bis(selenoimidazolyl)methane, bis(thioimidazolyl)ethane, and bis(selenoimidazolyl)ethane were synthesized, and these complexes preferentially formed dinuclear, three- and four-coordinate Cu^+ complexes. The $Cu^{2+/+}$ reduction potentials of these copper complexes with bidentate chalcogenone ligands vary within a range of 471 mV, a difference that would have significant effects in redox-mediated reactions. The results presented give more insight on the antioxidant activity of selone and thione compounds in the prevention of copper-mediated oxidative damage. These

results also reveal the diverse coordination chemistry of Cu^{+} with selone and thione and elucidates the effects of this coordination on $Cu^{2+/+}$ reduction potentials.

DEDICATION

I dedicate this dissertation to my wife and daughter, Jennifer and Jennise Kimani; parents, Francis and Alice Kimani, and brothers, Charles and Sospeter Kimani and sister Eunice Hahn for their love and encouragement. The constant encouragement from my dad and unceasing prayers from my mom made me believe that all things are possible.

ACKNOWLEDGEMENTS

Firstly, am mostly grateful to my advisor, Dr. Julia L. Brumaghim, for allowing me to conduct air-sensitive bio-inorganic chemistry research in her lab. Her training, encouragement, supervision and support from the preliminary to the concluding level enabled me to develop an understanding of bioinorganic chemistry especially metal coordination chemistry and electrochemistry. I would like to thank Dr. Brumaghim for always being open to new ideas and helping me develop them to concrete projects.

I would also like to thank Dr. Don VanDerveer for X-ray crystal and powder data collection training and for always having his door open for discussion. He truly made me a good crystallographer. I would like to thank Prof. Bill Pennington for a lot of help on X-ray powder data interpretation. Special thanks to Carolyn Quarles for conducting ESI mass spectroscopy experiments. Special acknowledgement to the entire staff in the chemistry department for their helpful services. I would like to acknowledge my collaborator, Dr. Craig Bayse for conducting DFT studies.

I would especially like to thank my family and friends in Kenya and USA for their continuous love, support, and guidance throughout my academic career. Special thanks to my wife Jennifer for her non-ending support and to my wonderful daughter Jennise for giving me a new perspective in life. I would also like to acknowledge my lab-mate Hsiao Wang (Sabina) for her friendship, witty comments, encouragement, and very informative scientific discussions. Special thanks to Brumaghim group members, both past and present for their sense of humor, support and friendship, which made research an enjoyable experience.

TABLE OF CONTENTS

LIST OF TABLES

List of Tables (Continued)

Table Page

List of Tables (Continued)

Table Page

LIST OF FIGURES

List of Figures (Continued)

Figure Page

List of Figures (Continued)

Figure Page

List of Figures (Continued)

Figure Page

List of Figures (Continued)

Figure Page

List of Figures (Continued)

Figure Page

List of Figures (Continued)

Figure Page

List of Figures (Continued)

Figure Page

List of Figures (Continued)

Figure Page

List of Schemes

Scheme Page

CHAPTER ONE

ANTIOXIDANT AND METAL COORDINATION PROPERTIES OF BIOLOGICAL CHALCOGENONES

Antioxidant and biological effects of selenium and sulfur.

Selenium is an essential micronutrient for both humans and animals with a RDA (recommended dietary allowance) ranging from 55-350 μg/day for humans.[1] It is incorporated as selenocysteine in the active site of many antioxidant proteins, including glutathione peroxidases, thioredoxin reductases, and thyroid hormone deiodinases.[2-3] In humans, selenium deficiency can lead to Keshan, Kashin-Beck, and neurodegenerative diseases, whereas selenium overload may lead to garlic breath, poisoning, and selenosis.[4] Selenocysteine coordinates nickel in Ni-Fe-Se hydrogenase, a microbial enzyme that catalyze the reversible and selective interconversion of H_2 and $2H^+/2e^-$.[5] Selenocysteine also coordinates molybdenum and tungsten in the formate dehydrogenases of *E. coli*[6,7] and *Clostridium thermoaceticum*,[8] respectively. Metal coordination of selenium antioxidant compounds prevents Fe^{2+}- and Cu^+-mediated oxidative DNA damage,[9-11] and selenium antioxidants play protective roles against heart disease, as well as prostate, lung, and colon cancer.[12,13] Recently, the selenium containing compound selenoneine (Figure 1.1) was isolated from the blood of blue tuna and was shown to be a very potent antioxidant.[14]

Sulfur is found in numerous proteins and low molecular weight compounds in plants and animals and plays a major role in redox processes, metal binding, and catalytic

reactions.[15] Major sulfur-containing compounds in the body include methioneine, cysteine, taurine, glutathione, *N*-acetylcysteine, and ergothioneine, and these compounds are involved in protein synthesis and antioxidant defense mechanisms. In biological systems, sulfur coordination to metals is found in

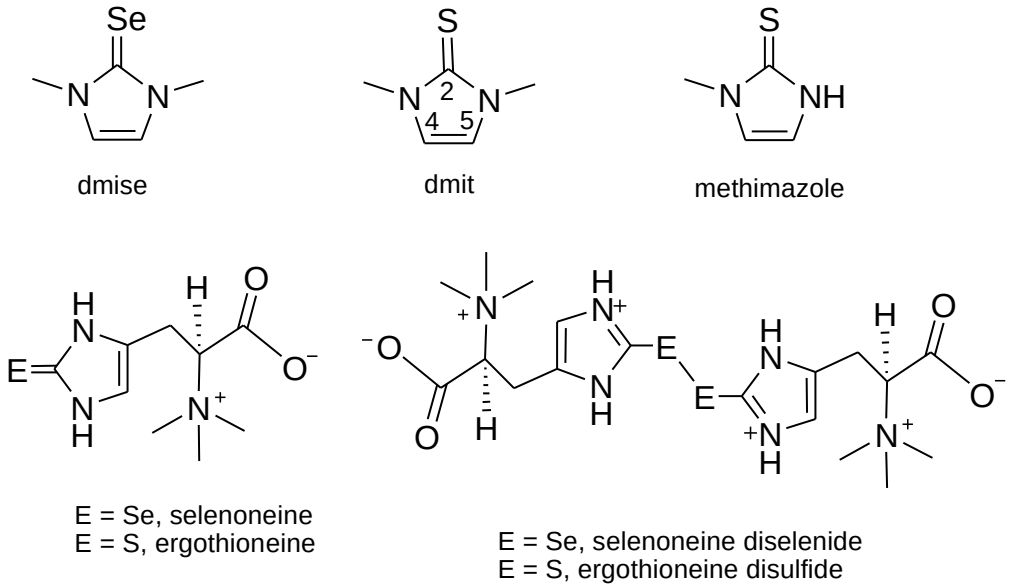

Figure 1.1. Thione and selone ligands described in this

blue copper proteins,[16-18] copper transport proteins,[19] iron-sulfur clusters,[20] ferrodoxins,[21,22] Rieske proteins,[23] and zinc fingers.[24] Sulfur antioxidants also prevent Fe^{2+}- and Cu^{+}-mediated DNA oxidative damage through metal coordination.[25,26] Sulfur-containing compounds such as *N*-acetyl-L-cysteine and D-penicillamine are used to treat heavy metal poisoning, whereas allicin and other sulfur containing compounds from garlic exhibit antimicrobial, antibacterial and antifungal properties.[27-30] The thione compound ergothioneine (Figure 1.1) is a biological antioxidant capable of binding divalent metal ions.[31-33]

Antioxidant and metal binding properties of biological chalcogenones.

Selenoneine (2-selenohistidine trimethylbetaine or 2-selenyl-N_α,N_α,N_α-trimethyl-L-histidine) is a seleno-histidine first identified by Yamashita and Yamashita in 2010 after isolation from the blood of blue tuna, *Thunnus orientalis*.[14] Selenoneine is also the primary source of selenium in chicken gizzard, liver, and heart as well as in squid hepatopancreas. The highest concentration of selenoneine (430-437 nmol of selenium/g) are found in tuna and mackerel blood.[14] Selenoneine was first isolated in its oxidized diselenide form that was then reduced to the monomeric selone form by treatment with dithiothreitol or glutathione. In solution, selenoneine exhibits selenol-selone tautomerism and exists primarily in the selone form under physiological conditions.[14]

As an antioxidant, selenoneine is a potent radical scavenger and has shown greater antioxidant activity than the analogous sulfur antioxidant ergothioneine in scavenging the 1-diphenyl-2-picrylhydrazyl (DPPH) radical *in vitro*.[14] The high concentrations of selenoneine found in animal tissues suggest that this molecule may play an important role in physiological redox and antioxidant processes.[14] Because selenium antioxidants can inhibit oxidative damage by binding to Cu^+ and Fe^{2+},[9-11] and because selenoneine likely coordinates metal ions through the selenium and nitrogen atoms of the five-membered ring, the coordination chemistry of selenoneine may contribute to its antioxidant behavior. Thus, understanding the binding properties of similar selone compounds will provide insight into metal binding as a novel antioxidant mechanism for selenoneine.

Ergothioneine (2-mecarptohistidine trimethylbetaine) is a thiohistidine first isolated in 1909 from ergot, and it is also found in plants, animals, and humans.[34] Similar to selenoneine, ergothioneine exhibits thione-thiol tautomerism, but exists primarily in the thione form under physiological conditions.[27] Ergothioneine binds divalent metals ions such as Cu^{2+} without undergoing autooxidation to the disulfide dimer due to its more negative reduction potential relative to other thiols.[27]

The antioxidant abilities of ergothioneine inhibition of peroxynitrite-dependent nitration of nitrotyrosine,[35] and prevention of xanthine and hypoxanthine formation, compounds implicated in inflammatory conditions such as gout.[36] Similar to selenoneine, ergothioneine also scavenges DPPH radical but it is less potent compared to selenoneine.[14] Several studies have shown that ergothioneine can neutralize reactive oxygen species such as hydroxyl radical and peroxynitrite,[37,38] and that ergothioneine protects rat kidneys and livers from oxidative damage by Fe/H_2O_2,[34] despite studies showing that the reaction of ergothioneine with H_2O_2 is very sluggish.[39,40]

In addition, ergothioneine coordinates redox-active metals such as Cu^{2+}, Cu^{+}, Hg^{2+}, and Fe^{2+}, by binding through sulfur or nitrogen atoms. To determine how this metal coordination ability may be related to its observed antioxidant activity, it is necessary to investigate the coordination chemistry of ergothioneine analogs.

The thione methimazole is the most common drug used in the treatment of hyperthyroidism.[41] The mechanism of inhibition of hyperthyroidism using thiourea drugs such as methimazole is not fully understood, but these compounds are proposed to block

thyroid hormone biosynthesis by inhibiting thyroid peroxidases catalyzed iodination of tyrosine residues in thyroglobulin.[41,42] Numerous studies have also shown that methimazole is a potent scavenger of hydroxyl radical and peroxynitrite and that it prevents thyroperoxidase and DNA damage.[43-45] Medicinal studies of methimazole have shown its ability to prevent oxidative stress and chemical-induced gastropathy in rats,[46] to inhibit melanin synthesis in cultured B16 melanocytes,[47] and to upregulate T-cell-derived cytokines.[48]

The rich coordination chemistry of transition metals with methimazole has previously been investigated in detail.[49-52] The coordination of methimazole to Cu^{+} results in diverse architectures ranging from mononuclear complexes to polynuclear networks with several methimazole binding modes, including monodentate and bridging via coordination of the sulfur and non-alkylated nitrogen atom.[53-55]

The research presented in this dissertation involves understanding the antioxidant mechanisms of chalcogenone compounds similar to selenoneine, ergothioneine, and methimazole. The selone and thione ligands used throughout these chapters resemble selenoneine,[14] ergothioneine,[56] and methimazole (Figure 1.1).[41] The work presented in Chapter 2 investigates the effects of *N,N'*-1,3-dimethylimidazole selone (dmise) and thione (dmit; Figure 1.1) ligand coordination on the redox properties of Cu^{+}.[57] Tris(pyrazolyl)methane and -borate ligands are used to synthesize the target Cu^{+} complexes, since they mimic metal coordination environments in biological systems.[58] Research described in Chapter 3 focuses on the reactivity of dmise, dmit, and their tris(pyrazolyl)methane Cu^{+} complexes with H_2O_2. Work outlined in Chapter 4

investigates the ability of dmise and dmit to reduce Cu^{2+} to Cu^{+} as well as the coordination and electrochemistry of bis(1-methylimidazolyl) diselenide with Cu^{2+}. The work presented in Chapters 2, 3, and 4 enhances further understanding of selenium and sulfur antioxidant activity through their ability to alter $Cu^{2+/+}$ reduction potential upon coordination to Cu^{+} or through the ability of selenium and sulfur antioxidant compounds to scavenge reactive oxygen species such as H_2O_2.

Work described in Chapter 5 investigates the comparative coordination chemistry of dmise and dmit with Cu^{+} halides, resulting in complexes with varied geometries and stochiometries. Tetrameric and monomeric copper complexes were synthesized and compared using density functional theory calculations to determine ligand effects as well as the effects of inter- and intramolecular forces on solid state geometries of the complexes.[59] The research described in Chapter 6 focuses on the coordination and electrochemistry studies of the bidentate thio- and seleno-imidazolyl ligands bis(thioimidazolyl)methane, bis(selenoimidazolyl)methane, bis(thioimidazolyl)ethane, and bis(selenoimidazolyl)ethane ligands with Cu^{+}. Overall the work presented in this dissertation reveals the diverse coordination chemistry of Cu^{+} with selone and thione ligands and elucidates the effect of this coordination on $Cu^{2+/+}$ reduction potentials and reactivity with H_2O_2. It also sheds light on the mechanisms of antioxidant activity of selone and thione compounds in the prevention of copper-mediated oxidative damage.

References

(1) Schrauzer, G. N. *J. Am. Coll. Nutr.* **2001**, *20*, 1-4.

(2) Combs, G. F.; Gray, W. P. *Pharmacol. Ther.* **1998**, *79*, 179-192.

(3) Takahashi, M.; Sato, T.; Shinohara, F.; Echigo, S.; Rikiishi, H. *Int. J. Oncol.* **2005**, *27*, 489-495.

(4) Papp, L. V.; Holmgren, A.; Khanna, K. K. *Antioxid. Redox Signal.* **2010**, *12*, 793-795.

(5) Parkin, A.; Goldet, G.; Cavazza, C.; Fontecilla-Camps, J. C.; Armstrong, F. A. *J. Am. Chem. Soc.* **2008**, *130*, 13410-13416.

(6) Gladyshev, V. N.; Boyington, J. C.; Khangulov, S. V.; Grahame, D. A.; Stadtman, T. C.; Sun, P. D. *J. Biol. Chem.* **1996**, *271*, 8095-8100.

(7) Boyington, J. C.; Gladyshev, V. N.; Khangulov, S. V.; Stadtman, T. C.; Sun, P. D. *Science* **1997**, *275*, 1305-1308.

(8) Laukel, M.; Chistoserdova, L.; Lidstrom, M. E.; Vorholt, J. A. *Eur. J. Biochem.* **2003**, *270*, 325-333.

(9) Battin, E. E.; Perron, N. R.; Brumaghim, J. L. *Inorg. Chem.* **2006**, *45*, 499-501.

(10) Battin, E. E.; Brumaghim, J. L. *Cell Biochem. Biophys.* **2009**, *55*, 1-23.

(11) Ramoutar, R. R.; Brumaghim, J. L. *J. Inorg. Biochem.* **2007**, *101*, 1028-1035.

(12) Reid, M. E.; Duffield-Lillico, A. J.; Slate, E.; Natarajan, N.; Turnbull, B.; Jacobs, E.; Combs, G. F.; Alberts, D. S.; Clark, L. C.; Marshall, J. R. *Nutr. Cancer* **2008**, *60*, 155-163.

(13) Lippman, S. M.; Klein, E. A.; Goodman, P. J.; Lucia, M. S.; Thompson, I. M.; Ford, L. G.; Parnes, H. L.; Minasian, L. M.; Gaziano, J. M.; Hartline, J. A.; Parsons, J. K.; Bearden, J. D.; Crawford, E. D.; Goodman, G. E.; Claudio, J.; Winquist, E.; Cook, E. D.; Karp, D. D.; Walther, P.; Lieber, M. M.; Kristal, A. R.; Darke, A. K.; Arnold, K. B.; Ganz, P. A.; Santella, R. M.; Albanes, D.; Taylor, P. R.; Probstfield, J. L.; Jagpal, T. J.; Crowley, J. J.; Meyskens, F. L.; Baker, L. H.; Coltman, C. A. *J. Am. Med. Assoc.* **2009**, *301*, 39-51.

(14) Yamashita Y.; Yamashita M. *J. Biol. Chem.* **2010**, *285*, 18134-18138.

(15) Jacob, C.; Giles, G. L.; Giles, N. M.; Sies, H. *Angew. Chem. Int. Ed.* **2003**, *42*, 4742-4758.

(16) Barrett, M. L.; Harvey, I.; Sundararajan, M.; Surendran, R.; Hall, J. F.; Ellis, M. J.; Hough, M. A.; Strange, R. W.; Hillier, I. H.; Hasnain, S. S. *Biochemistry* **2006**, *45*, 2927-2939.

(17) Bertrand, T.; Jolivalt, C.; Briozzo, P.; Caminade, E.; Joly, N.; Madzak, C.; Mougin, C. *Biochemistry* **2002**, *41*, 7325-7333.

(18) Ando, K. *J. Chem. Phys.* **2010**, *133*, 175101-175109.

(19) Rubino, J. T.; Riggs-Gelasco, P.; Franz, K. J. *J. Biol. Inorg. Chem.* **2010**, *15*, 1033-1049.

(20) Liochev, S. I. *Free Radic. Res.* **1996**, *25*, 369-384.

(21) Elsen, S.; Efthymiou, G.; Peteinatos, P.; Diallinas, G.; Kyritsis, P.; Moulis, J. M. *BMC Microbiol.* **2010**, *10*, 271-281.

(22) Meyer, J. *J. Biol. Inorg. Chem.* **2008**, *13*, 157-170.

(23) Schneider, D.; Schmidt, C. L. *Biochim. Biophys. Acta-Bioenerg.* **2005**, *1710*, 1-12.

(24) Klug, A. In *Annual Review of Biochemistry*; Annual Reviews: Palo Alto, 2010; Vol. 79, pp 213-231.

(25) Ramoutar, R. R.; Brumaghim, J. L. *Cell Biochem. Biophys.* **2010**, *58*, 1-23.

(26) Ramoutar, R. R.; Brumaghim, J. L. *Main Group Chem.* **2007**, *6*, 143-153.

(27) Jacob, C. *Nat. Prod. Rep.* **2006**, *23*, 851-863.

(28) Bat-Chen, W.; Golan, T.; Peri, I.; Ludmer, Z.; Schwartz, B. *Nutr. Cancer* **2010**, *62*, 947-957.

(29) Kang, S. S.; Lim, D. R.; Kyung, K. H. *J. Med. Food* **2010**, *13*, 1247-1253.

(30) Arzanlou, M.; Bohlooli, S. *J. Med. Microbiol.* **2010**, *59*, 1044-1049.

(31) Hartman, Z.; Hartman, P. E. *Chem. Biol. Interact.* **1992**, *84*, 153-168.

(32) Reid, R. S.; Rabenstein, D. L. *J. Am. Chem. Soc.* **1982**, *104*, 6733-6737.

(33) Motohashi, N.; Mori, I.; Sugiura, Y. *Chem. Pharm. Bull.* **1976**, *24*, 2364-2368.

(34) Hand, C. E.; Honek, J. F. *J. Nat. Prod.* **2005**, *68*, 293-308.

(35) Aruoma, O. I.; Whiteman, M.; England, T. G.; Halliwell, B. *Biochem. Biophys. Res. Commun.* **1997**, *231*, 389-391.

(36) Rahman, I.; Gilmour, P. S.; Jimenez, L. A.; Biswas, S. K.; Antonicelli, F.; Aruoma, O. I. *Biochem. Biophys. Res. Commun.* **2003**, *302*, 860-864.

(37) Franzoni, F.; Colognato, R.; Galetta, F.; Laurenza, I.; Barsotti, M.; Di Stefano, R.; Bocchetti, R.; Regoli, F.; Carpi, A.; Balbarini, A.; Migliore, L.; Santoro, G. *Biomed. Pharmacother.* **2006**, *60*, 453-457.

(38) Aruoma, O. I.; Spencer, J. P. E.; Mahmood, N. *Food Chem. Toxicol.* **1999**, *37*, 1043-1053.

(39) Arduini, A.; Eddy, L.; Hochstein, P. *Free Rad. Biol. Med.* **1990**, *9*, 511-513.

(40) Akanmu, D.; Cecchini, R.; Aruoma, O. I.; Halliwell, B. *Arch. Biochem. Biophys.* **1991**, *288*, 10-16.

(41) Cooper, D. S. *N. Engl. J. Med.* **2005**, *352*, 905-917.

(42) Das, D.; Roy, G.; Mugesh, G. *J. Med. Chem.* **2008**, *51*, 7313-7317.

(43) Kahmann, C.; Wunderlich, G.; Freudenberg, R.; Zophel, K.; Oehme, L.; Kotzerke, J. *Int. J. Radiat. Biol.* **2010**, *86*, 811-816.

(44) Roy, G.; Mugesh, G. *J. Am. Chem. Soc.* **2005**, *127*, 15207-15217.

(45) Ferreira, A. C. F.; Cardoso, L. D.; Rosenthal, D.; de Carvalho, D. P. *Eur. J. Biochem.* **2003**, *270*, 2363-2368.

(46) Al Moutaery, A. *Exp. Toxicol. Pathol.* **2003**, *55*, 277-285.

(47) Kasraee, B.; Hugin, A.; Tran, C.; Sorg, O.; Saurat, J. H. *J. Invest. Dermatol.* **2004**, *122*, 1338-1341.

(48) Kocjan, T.; Wraber, B.; Kocijancic, A.; Hojker, S. *J. Endocrinol. Invest.* **2004**, *27*, 302-307.

(49) Raper, E. S. *Coord. Chem. Rev.* **1996**, *153*, 199-255.

(50) Raper, E. S. *Coord. Chem. Rev.* **1997**, *165*, 475-567.

(51) Raper, E. S.; Creighton, J. R.; Bell, N. A.; Clegg, W.; Cucurull-Sanchez, L. *Inorg. Chim. Acta* **1998**, *277*, 14-20.

(52) Pettinari, C.; Pettinari, R.; Pellei, M.; Lobbia, G. G. *Polyhedron* **1999**, *18*, 1941-1951.

(53) Lobana, T. S.; Sultana, R.; Hundal, G.; Castineiras, A. *Polyhedron* **2009**, *28*, 1573-1577.

(54) Lobana, T. S.; Sharma, R.; Butcher, R. J. *Z. Anorg. Allg. Chem.* **2008**, *634*, 1785-1790.

(55) Raper, E. S. *Coord. Chem. Rev.* **1994**, *129*, 91-156.

(56) Ey, J.; Schomig, E.; Taubert, D. *J. Agric. Food Chem.* **2007**, *55*, 6466-6474.

(57) Kimani, M. M.; Brumaghim, J. L.; Vanderveer, D. *Inorg. Chem.* **2010**, *49*, 9200-9211.

(58) Field, D. L.; Messerle, B. A.; Soler, L. P.; Hambley, T. W.; Turner, P. *J. Organomet. Chem.* **2002**, *655*, 146-157.

(59) Kimani, M. M.; Brumaghim, J. L.; Bayse, C. A. *Dalton Trans.*, submitted.

CHAPTER TWO

PROBING THE ANTIOXIDANT ACTION OF SELENIUM AND SULFUR USING Cu(I)-CHALCOGENONE TRIS(PYRAZOLYL) METHANE AND -BORATE COMPLEXES

Introduction

Reactive oxygen species, (ROS) which include superoxide ($O_2^{\bullet-}$), hydrogen peroxide (H_2O_2), hydroxyl radical ($^{\bullet}OH$), singlet oxygen ($^1O_2$) and peroxyl radical ($RO_2^{\bullet}$), are involved in oxidative damage to lipids, proteins and DNA.[1] Copper(I) participates in the Fenton-like reaction (reaction 1) in which hydroxyl radical is generated from the reduction of less-damaging hydrogen peroxide.[2] This copper-mediated hydroxyl radical generation is catalytic *in vivo* if cellular reductants, such as NADH are available to reduce Cu^{2+} to Cu^{+}. Numerous studies have linked damage from copper-generated hydroxyl radical to Alzheimer's disease, cardiovascular diseases, and cancer.[3,4]

$$Cu^{+} + H_2O_2 \rightarrow Cu^{2+} + HO^{\bullet} + OH^{-} \quad (1)$$

Selenium- and sulfur-containing compounds have been widely studied as potential antioxidants for the prevention or reduction of oxidative DNA damage.[5] Selenium is an essential micronutrient for both humans and animals, with a recommended dietary allowance ranging from 55-350 μg/day.[6] Organoselenium compounds are of particular interest because they appear to be more bioavailable relative to inorganic selenium compounds.[7]

Using copper-mediated DNA damage studies and UV-vis spectroscopy, our group has identified copper coordination as an explanation for selenium and sulfur antioxidant activity.[5,8-10] This novel metal binding antioxidant hypothesis is separate from the traditional explanation that focuses on the ability of selenium compounds to decompose hydrogen peroxide in a manner similar to glutathione peroxidase (GPx).[11]

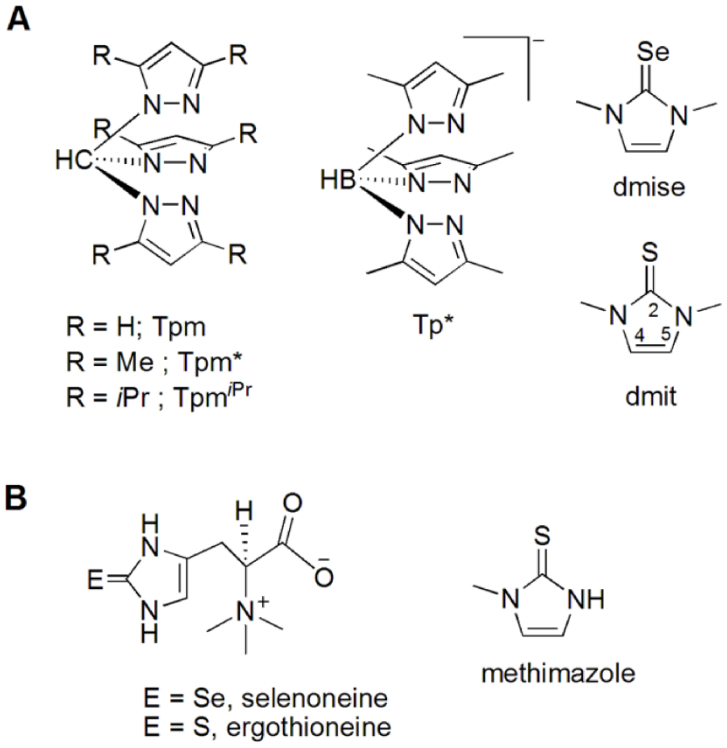

Figure 2.1. A) Tris(pyrazolyl) and heterocyclic thione and selone ligands used in this study. Numbering scheme is shown for dmit. B) Structures of naturally-occurring selone and thione antioxidants and the drug methimazole.

As part of our efforts to understand the role of Se/S-Cu coordination in the prevention of metal-mediated DNA damage, biologically relevant Cu^{+} selone and thione

complexes with tris(pyrazolyl)methane or tris(pyrazolyl)borate ligands have been synthesized, with the aim of studying their copper coordination and electrochemistry. Scorpionate nitrogen donor ligands first introduced by Trofimenko[12] (Figure 2.1A) were employed, since they mimic biological coordination.[13] The heterocyclic selones and thiones used in this study (Figure 2.1A) resemble methimazole, a drug currently used in the treatment of hyperthyroidism (Figure 2.1B).[14] Dmit and dmise are also structurally similar to ergothioneine,[15] and selenoneine,[16] respectively, antioxidant compounds widely found in plant and animal tissues (Figure 2.1B).

The heterocyclic chalcogenones used in this study are good σ- and π-donors, and similar compounds, such as imidazoline-2-thiones, display a diversity of bonding modes.[17] The coordination chemistry of selones and thiones with transition metals and halogens has been previously reviewed by Raper,[18] Akrivos,[19] Spicer, *et al.*,[20] and Pettinari,[21] as well as studied by Devillanova, *et al*.,[22] Williams, *et al*.,[23-27] Rabinovich, *et al*.,[28,29] and Parkin, *et al*.[30,31] Many reports describe the coordination chemistry of thiones with Cu^{+},[17,32-34] but reports of analogous selone complexes are few.[35-37] Herein, we report the synthesis and characterization of mononuclear, four coordinate-copper(I) complexes: Tp*Cu(L) and $[Tpm^{R}Cu(L)]^{+}$ where (L = *N,N'*-dimethylimidazole selone, dmise; *N,N'*-dimethylimidazole thione, dmit; Tp* = hydrotris(3,5-dimethylpyrazolyl)borate; Tpm^{R} = tris(pyrazolyl)methane, R = H; Tpm, R = Me; Tpm*, R = *i*Pr; Tpm^{iPr}). Brumaghim, *et al.*,[8,10,38] and others[39] have determined that the antioxidant activities of analogous selenium and sulfur compounds can be very distinct. Thus, we have investigated the geometries and spectroscopic properties of both copper-selone and -thione complexes.

Because selenium and sulfur coordination to copper is necessary for prevention of copper mediated DNA damage, comparative electrochemical studies of selone and thione complexes will help determine changes in the reduction potentials of $Cu^{2+/+}$ upon coordination. These comparative studies will provide insights into the effects of selenium and sulfur coordination and antioxidant activity *in vivo*. "This work is reproduced from Kimani, *et al*. *Inorg. Chem.* **2010**, *49,* 9200-9211. Copyright 2010 American Chemical Society." The copyright permission is in Appendix A, page 221.

Results and Discussion

Synthesis of Cu(I) selone and thione complexes. The target copper(I) complexes with the BF_4^- counterion were synthesized using two different routes. Method 1 involves a two-step, one-pot procedure via the treatment of equimolar amounts of $[Cu(NCCH_3)_4][BF_4]$ and *N,N'*-dimethylimidazole selone (dmise) or *N,N'*-dimethylimidazole thione (dmit) in acetonitrile followed by cannula addition of the desired tripodal ligand in acetonitrile. Method 2 involves treating $[Tpm^RCu(NCCH_3][BF_4]$ with one molar equivalent of dmise or dmit in dichloromethane (Scheme 2.1). Compared to method 1, method 2 generally results in slightly higher yields with shorter reaction times. Copper complexes with the chloride counterion were synthesized by reaction of equimolar amounts of CuCl and the chalcogenone in a mixed solvent system of methanol and acetonitrile, followed by cannula addition of the tripodal ligand in acetonitrile (Scheme 2.1).

The neutral copper complexes were synthesized by combining CuCl and dmise/dmit in methanol and acetonitrile, respectively, followed by cannula addition of tris(3,5-dimethylpyrazolyl)borate (Tp*) in acetonitrile (Scheme 2.1). These neutral complexes can also be synthesized by reaction of Tp*Cu($NCCH_3$) with molar equivalent of dmit or dmise in dichloromethane (Scheme 2.1). All of the target metal complexes are fairly stable to air for about 5-10 h as solids but are easily oxidized from Cu^+ to Cu^{2+} in solution.

Scheme 2.1

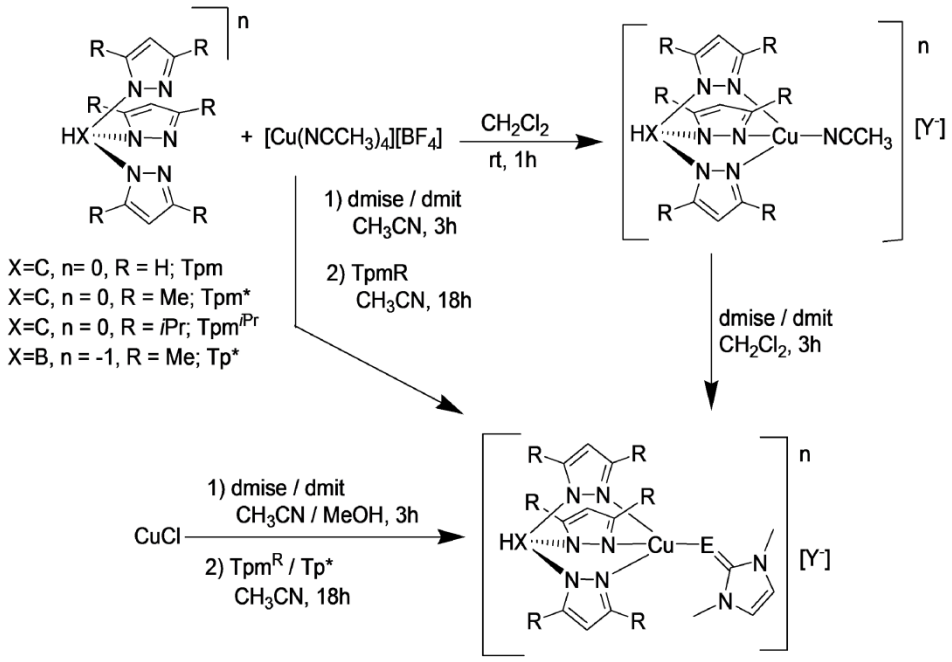

[$Tpm^RCu(dmise)$][BF_4]; E = Se, Y = BF_4, n = 1, X = C, R = H (**3**), R = Me (**1**), R = *i*Pr (**6**)
[$Tpm^RCu(dmit)$][BF_4]; E = S, Y = BF_4, n = 1, X = C, R = H (**4**), R = Me (**2**), R = *i*Pr (**5**)
[$Tpm^RCu(dmise)$][Cl]; E = Se, Y = Cl, n = 1, X = C, R = Me (**9**), R = *i*Pr (**12**)
[$Tpm^RCu(dmit)$][Cl]; E = S, Y = Cl, n = 1, X = C, R = Me (**10**), R = *i*Pr (**11**)
Tp*Cu(dmit) (**7**); E = S, n = 0, X = B
Tp*Cu(dmise) (**8**); E = Se, n = 0, X = B

NMR spectroscopy of copper thione and selone complexes. In the ^{1}H NMR spectra of [Tpm^{R}Cu(L)][X] (R = H; Tpm, R = Me; Tpm*, R = *i*Pr; Tpm^{iPr}; L = $NCCH_3$, dmise, or dmit; X = BF_4^- or Cl^-), the apical CH proton resonance of the tris(pyrazolyl)methane ligand bound to copper is shifted upfield by δ 0.1 to 0.5 from its position in the free ligand. This same upfield shift was observed by Fujisawa and co-workers for the [Tpm^{iPr}Cu($NCCH_3$)]$^+$ complex.[40] All other proton signals of both the tripodal ligand (Tpm^{R}) and the chalcogenone (dmise and dmit) are shifted downfield upon Cu^+ complexation. This downfield shift of the ligand resonance upon copper coordination is a result of increased deshielding effects on the protons upon metal binding. For copper complexes with tris(pyrazolyl)borate ligands, the resonance for the BH proton is not observed, as is common.[40]

^{1}H and ^{13}C{^{1}H} NMR spectroscopy data for the complexed and uncomplexed selone and thione ligands are given in Table 2.1 (ligand numbering scheme in Figure 2.1A). A substantial shift of the C-2 resonance of the dmise and dmit ligands, are observed upon complexation to copper. Shifts of δ 3 to 8 for both the C=Se and C=S carbons are also observed upon copper binding, attributed to the shift of the electron density from the selenocarbonyl or thiocarbonyl group to the neighboring N-C bond. This electron density shift reduces the double bond character of the C=Se or C=S bond while increasing that of the C-N single bond, resulting in an upfield shift for the C-2 resonance.[32,41-43] This upfield shift is characteristic of selone or thione bound to copper via the selenium and sulfur atoms. The increased electron density of the C-N bond upon copper complexation results in a minor increases in deshielding effects on C-4 and C-5,

as supported by observed downfield shifts of the C-4 and C-5 resonances. In the ^{1}H and $^{13}C\{^{1}H\}$ NMR spectra, H-4/5 and are shifted downfield and C-2 resonances are shifted upfield for the selone copper complexes (δ 6.93 - 7.18 and δ 120.3 - 122.2, respectively) and thione copper complexes (δ 6.82 - 7.04 and δ 118.6 - 119.9, respectively) relative to the free selone (δ 6.77 and δ 119.7) and thione (δ 6.64 and δ 117.6) compounds (Table 2.1). These NMR shifts upon selone and thione complexation are consistent with copper binding stabilizing the resonance form that places the positive charge into the heterocyclic ring (Figure 2.2).

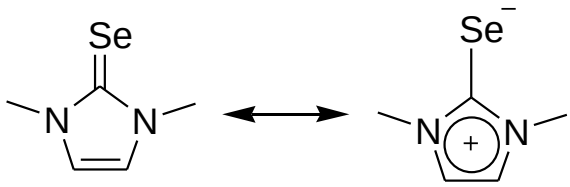

Figure 2.2. Resonance structures for the selone.

The $^{77}Se\{^{1}H\}$ NMR resonances for the tris(pyrazolyl) copper selone complexes **1**, **3**, **6**, and **8** are shifted upfield (δ -31.5 to -95.6) upon selone coordination to copper relative to the free dmise ligand (δ -6). The charge of the ligand of the tri(pyrazolyl) ligand has the most profound effect on the shift of the $^{77}Se\{^{1}H\}$ NMR resonance upon coordination of dmise to copper. The $^{77}Se\{^{1}H\}$ NMR resonance in the neutral Tp*Cu(dmise) (**8**) complex resulted in an upfield shift of δ 25.5 while the charged complexes $[Tpm^{R}Cu(dmise)]^{+}$ (R = H; Tpm; **3**, R = Me; Tpm*; **1**, R = *i*Pr; **6**) show an average upfield shift of δ 86.8.

Notably, the copper complexes with Cl^{-} counterions have smaller downfield shift

on the methyl and olefinic protons and smaller upfield C-2 resonance shifts of the heterocyclic chalcogenones relative to analogous complexes with BF_4^- counterions. Because Cl^- is significantly more coordinating than BF_4^-, the Cl^- counterion may compete slightly with the selone ligand for binding to labile Cu^+.[44,45] The presence of mononuclear copper complexes with dmise and dmit ligands can be clearly seen from their ESI-mass spectra. The fragmentation patterns found for all the complexes are consistent with their calculated isotopic distribution.

Table 2.1. $^{13}C\{^1H\}$, ^1H and $^{77}Se\{^1H\}$ NMR chemical shifts of selone and thione ligands before and after copper complexation.

	$^{13}C\{^1H\}$ shift (δ)		^1H shift (δ)		$^{77}Se\{^1H\}$ shift (δ)
Ligand or Cu(I) complex	**C-2**	**C-4/5**	**CH_3**	**H-4/5**	
Dmise	155.57	119.71	3.53	6.77	-6
[TpmCu(dmise)][BF_4] (**3**)	148.90	122.24	3.73	7.15	-95.6
[Tpm*Cu(dmise)][BF_4] (**1**)	147.61	121.60	3.88	7.17	-87.5
[Tpm$^{i\mathrm{Pr}}$Cu(dmise)][BF_4] (**6**)	148.12	121.47	3.85	7.18	-95.6
[Tpm*Cu(dmise)][Cl] (**9**)	153.22	119.98	3.75	6.97	
[Tpm$^{i\mathrm{Pr}}$Cu(dmise)][Cl]	152.03	120.54	3.79	6.98	
Tp*Cu(dmise)	151.63	120.27	3.75	6.93	-31.5
dmit	162.42	117.60	3.53	6.64	
[TpmCu(dmit)][BF_4] (**4**)	154.66	119.90	3.82	7.04	
[Tpm*Cu(dmit)][BF_4] (**2**)	155.96	119.70	3.80	7.00	
[Tpm$^{i\mathrm{Pr}}$Cu(dmit)][BF_4] (**5**)	155.49	119.80	3.77	7.03	
[Tpm*Cu(dmit)][Cl]	156.54	119.42	3.73	6.86	
[Tpm$^{i\mathrm{Pr}}$Cu(dmit)][Cl]	159.52	118.58	3.70	6.82	
Tp*Cu(dmit) (**7**)	157.45	119.33	3.68	6.83	

Molar conductivities of the neutral complexes Tpm$^{i\mathrm{Pr}}$CuCl and Tpm*CuCl are low (18.4 and 19.2 S cm^2 mol^{-1}, respectively), indicating chloride coordination. In

contrast, molar conductivities of the cationic complexes **1**, **2**, **5**, and **6** with non-coordinating BF_4^- anions are significantly higher (89.7 – 118.4 S cm^2 mol^{-1}), indicating 1:1 ionic complexes. Conductivities of compounds with Cl^- anions (**9**, **10**, **11**, and **12)** range from 23.3 to 30.7 S cm^2 mol^{-1}, indicating that the Cl^- anions compete with thione and selone for copper binding. The ^{1}H NMR resonances for the H-4/5 protons of the copper chloride complexes **9**, **10**, **11**, and **12** (δ 6.82 - 6.98) are closer to the unbound ligands compared to complexes **1**, **2**, **5**, and **6** with non-coordinating BF_4^- counterions (δ 7.00 – 7.18), corroborating the conductivity measurements.

IR Spectroscopy. The acetonitrile copper complexes used as starting materials, [Tpm*Cu(NCCH$_3$)][BF$_4$] and [Tpm$^{i\text{Pr}}$Cu(NCCH$_3$)][BF$_4$] have N≡C stretching frequencies of 2272 and 2275 cm^{-1} respectively, comparable to literature reports.[46] The N≡C stretches in these copper acetonitrile complexes are shifted to higher wavenumbers relative to free acetonitrile (2250 cm^{-1}), indicating an increased N≡C bond strength due to donor bond formation upon Cu^+ complexation.[47] The IR spectrum of dmit shows a C=S stretching vibration at ~ 1181 cm^{-1}, whereas dmise has a C=Se stretching vibration at ~1148 cm^{-1}, consistent with previous reports for dmit, 1-mesitylimidazole selone, mbit = 1,1'-methylenebis(1,3-dihydro-3-methyl-2H-imidazole-2-thione), and mbis = 1,1'-methylene-bis(1,3-dihydro-3-methyl-2H-imidazole-2-selone).[48-50] Upon copper-dmit binding in complexes **2**, **4**, **5**, and **7** this C=S stretch shifts to lower energy, 1172-1178 cm^{-1}, indicative of weak backbonding to the thione ligand. Coordination of dmise to copper in Tpm^R complexes **1**, **3**, and **6** results in a slight shift of C=Se stretch to higher energy, 1150-1151 cm^{-1}, indicating that backbonding interactions with this ligand are not

significant. In contrast, the IR spectrum of Tp*Cu(dmise) (**8**) shows a slight shift to lower energy region for C=Se stretch (1145 cm^{-1}) upon coordination of dmise to copper.

Structural analysis of copper selone and thione complexes. Single crystal X-ray diffraction data were collected for [Tpm*Cu(dmise)][BF_4] (**1**), [Tpm*Cu(dmit)][BF_4] (**2**), [TpmCu(dmit)][BF_4] (**4**), [Tpm^{iPr}Cu(dmise)][BF_4] (**6**), Tp*Cu(dmit) (**7**) and Tp*Cu(dmise) (**8**) which crystallized as colorless prisms, and for [TpmCu(dmise)][BF_4] (**3**), which crystallized as colorless rods. Their structural parameters are summarized in Tables 2.5 to 2.11, and their structures are shown in Figures 2.3 to 2.5 and 2.7 to 2.10 while their packing diagrams are depicted in Figures 2.6, and 2.14 to 2.19. All the Cu^+ centers adopt distorted tetrahedral coordination geometry, bound to three nitrogen atoms from the tridentate ligand in a κ^3-fashion, and terminally bound to the heterocyclic chalcogenones. The distorted tetrahedral geometries can be seen in the N-Cu-N angles, ranging from 84.6 to 92.1º and arise from pinning back of Tpm^R and KTp* nitrogen atoms due to the small bite angles of these ligands.[51]

The crystal structure of [TpmCu(dmise)][BF_4] (**3**) is composed of two crystallographically-independent molecules in the same unit cell (Figure 2.3; Table 2.5). Each copper atom adopts a distorted tetrahedral coordination environment with average Cu-N distances of 2.12 Å for Cu(1)-N and 2.13 Å for Cu(1A)-N(A). Mean N-Cu-N angles are 87.2º for N-Cu(1)-N and 86.9º for N(A)-Cu(1A)-N(A), respectively. The Cu-Se bond lengths and Cu-Se-C bond angles are the major differences between the molecular geometry of these independent molecules, with the Cu(1A) molecule

exhibiting a bond length of 2.314 Å and an angle of 110.3º and the Cu(1) molecule a slightly shorter bond length of 2.294 Å and a much smaller angle of 100.4º.

Structures of the Tpm, Tpm*, Tpm^{iPr}, and Tp* copper selone complexes (**1**, **3**, **6** and **8**; (Figures 2.3, 2.4, 2.5, and 2 7; Table 2.2, 2.3, 2.4 and 2.5) are very similar despite the differences in steric bulk of their tris(pyrazolyl)methane ligands and overall charge of the ligands. In **1**, **3**, **6**, and **8** the dmise ligand is bound to the copper center with an average angle of 105.2º due to the presence of the lone pairs on the selenium atom. The Cu-Se bond lengths for **1** (2.30 Å), **3** (2.29 Å and 2.31 Å), and **6** (2.31 Å) are comparable, whereas the Cu-Se bond in **8** (2.33 Å) is slightly longer. The Cu-Se bond distances in **1**, **3**, **6**, and **8** are comparable to the Cu-Se bond distance of 2.30 Å in the Cu^{III}-bis-diselenolene complex reported by Ribas *et al.*,[52] but shorter than most reported copper-selenium complexes such as the selone [Cu(1,10-phen)$_2$($C_5H_{10}N_2Se$)][2ClO_4] (2.49 Å);[36] the selenolate [CuSe(2,4,6-*i*Pr$_3$$C_6H_2$)]$_2$[bipy]$_2$ (2.45 Å);[53] the selenoether [Cu(*o*- C_6H_4(SeMe)$_2$)$_2$][PF_6] (2.42 Å);[54]and the selenium macrocycle [Cu($C_{11}H_{14}Se_2$)$_2$][BF_4] (avg. 2.41 Å).[55] Short Cu-Se bond distances for **1**, **3**, **6**, and **8** imply stronger donor interactions between the soft selenium ligand and the soft copper metal ion, but only a limited number of non-bridging copper selone complexes are available for structural comparison.

Short interactions of 3.59 Å between selenium atoms are found within the unit cell of [Tpm^{iPr}Cu(dmise)][BF_4] (**6**), and these interactions are shorter than the sum of Se-Se van der Waals radii (3.80 Å).

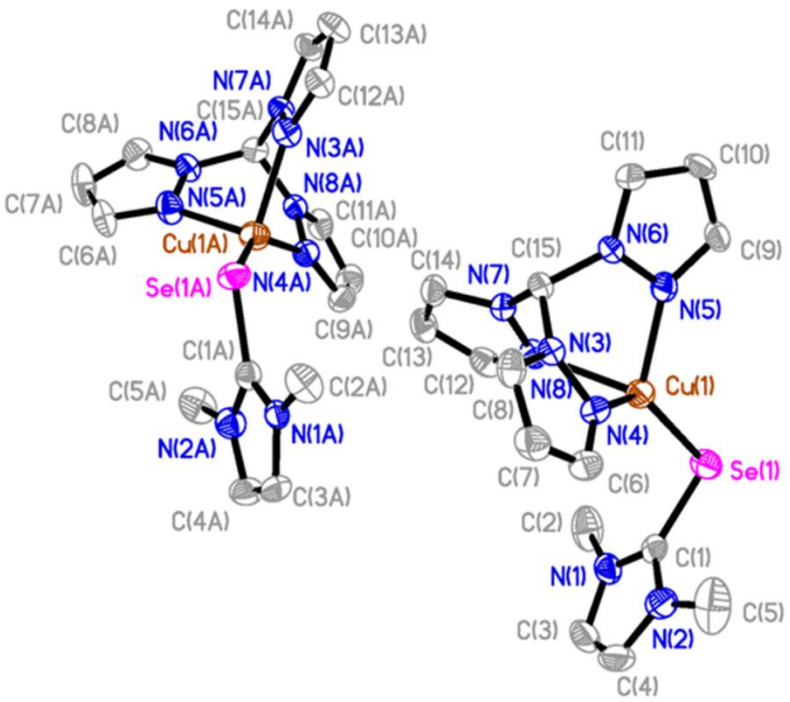

Figure 2.3. Crystal structure diagram (50% probability ellipsoids) of [TpmCu(dmise)][BF_4] (**3**) showing the two crystallographically independent molecules. Counterion and hydrogen atoms are omitted for clarity.

Table 2.2. Selected bond lengths (Å) and angles (°) for the two crystallographically independent molecules in complex **3**.

Cu(1)-N(3)	2.188(6)	N(4)-Cu(1)-N(5)	88.8(2)
Cu(1)-N(4)	2.111(6)	N(4)-Cu(1)-N(3)	86.6(2)
Cu(1)-N(5)	2.053(6)	N(5)-Cu(1)-N(3)	86.1(2)
Cu(1)-Se(1)	2.2941(13)	N(3)-Cu(1)-Se(1)	122.35(17)
C(1)-Se(1)		N(4)-Cu(1)-Se(1)	132.94(17)
		N(5)-Cu(1)-Se(1)	125.80(17)
Cu(1A)-N(3A)	2.111(6)	N(4A)-Cu(1A)-N(5A)	86.20(3)
Cu(1A)-N(4A)	2.094(7)	N(4A)-Cu(1A)-N(3A)	87.4(3)
Cu(1A)-N(5A)	2.184(7)	N(5A)-Cu(1A)-N(3A)	87.0(3)
Cu(1A)-Se(1A)	2.3120(13)	N(3A)-Cu(1A)-Se(1A)	114.74(17)
C(1A)-Se(1A)		N(4A)-Cu(1A)-Se(1A)	145.41(18)
		N(5A)-Cu(1A)-Se(1A)	119.49(18)

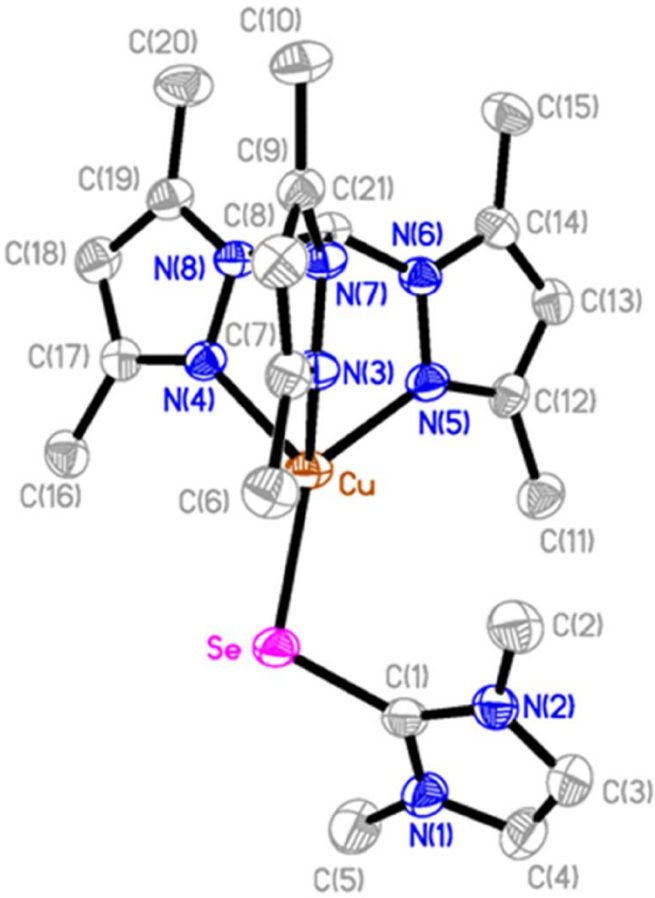

Figure 2.4. Crystal structure diagram of [Tpm*Cu(dmise)][BF_4] (**1**) displaying 50% probability density ellipsoids. Hydrogen atoms and counterion are omitted for clarity.

Table 2.3. Selected bond lengths (Å) and angles (°) for complex **1**.

Cu(1)-N(3)	2.126(2)	N(4)-Cu(1)-	88.66(10)
Cu(1)-N(4)	2.063(3)	N(4)-Cu(1)-	87.66(10)
Cu(1)-N(5)	2.089(2)	N(5)-Cu(1)-	85.67(9)
Cu(1)-Se(1)	2.2981(6)	N(3)-Cu(1)-	125.46(7)
Se(1)-C(1)	1.868(3)	N(4)-Cu(1)-	132.37(7)
		N(5)-Cu(1)-	123.04(7)
		C(1)-Se(1)-	108.24(10)

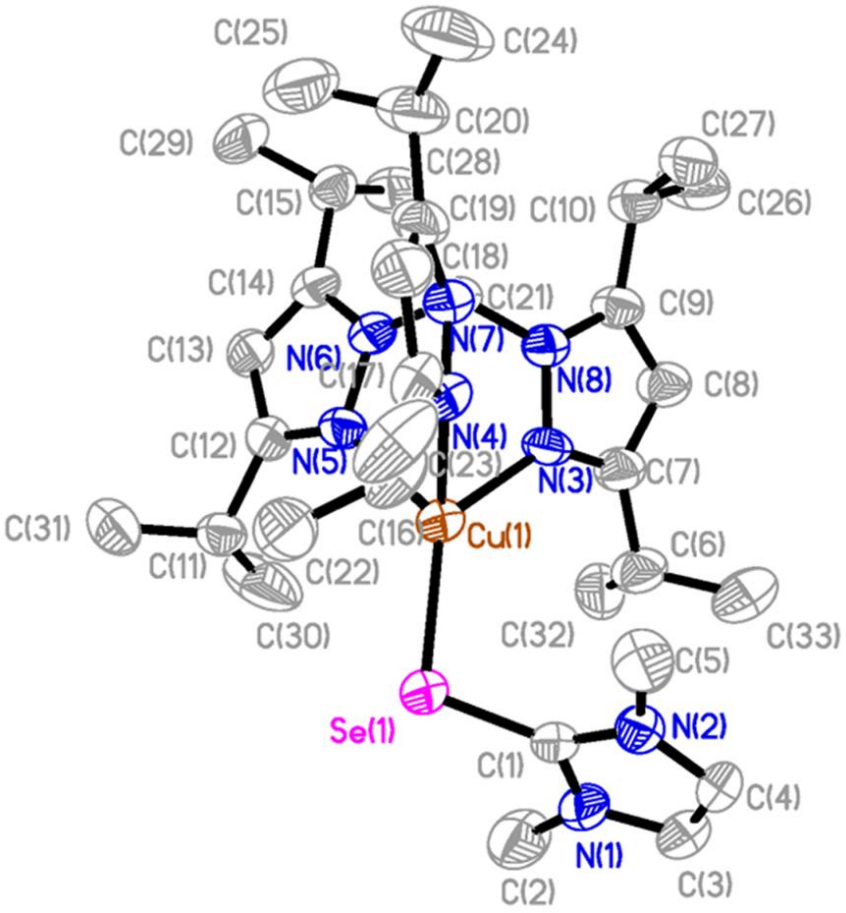

Figure 2.5. Crystal structure diagram of [Tpm^{iPr}Cu(dmise)][BF_4] (**6**) displaying 50% probability density ellipsoids. Hydrogen atoms and counterion are omitted for clarity.

Table 2.4. Selected bond lengths (Å) and angles (°) for complex **6**.

Cu(1)-N(3)	2.058(4)	N(4)-Cu(1)-N(5)	84.62(16)
Cu(1)-N(4)	2.095(4)	N(4)-Cu(1)-N(3)	88.44(16)
Cu(1)-N(5)	2.189(4)	N(5)-Cu(1)-N(3)	85.43(16)
Cu(1)-Se(1)	2.3126(8)	N(3)-Cu(1)-Se(1)	130.52(11)
Se(1)-C(1)	1.858(5)	N(4)-Cu(1)-Se(1)	124.40(11)
		N(5)-Cu(1)-Se(1)	128.71(10)
		C(1)-Se(1)-Cu(1)	104.62(13)

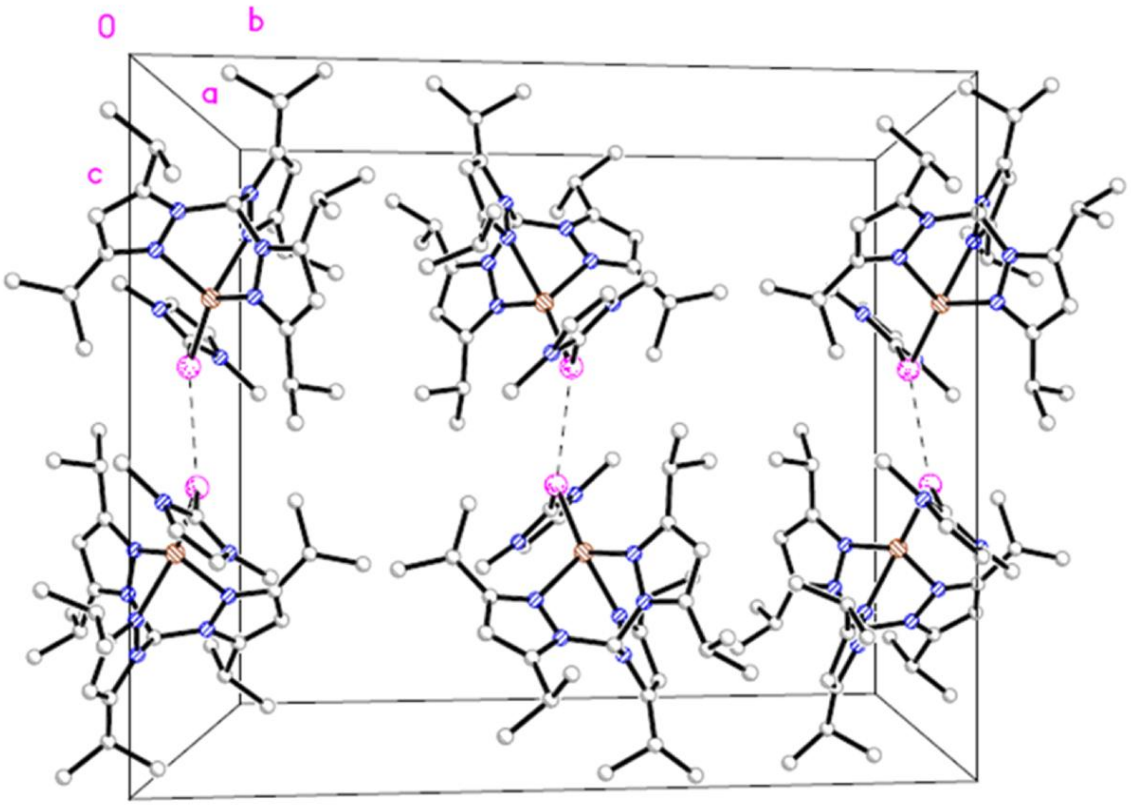

Figure 2.6. Crystal packing diagram of [Tpm^{iPr}Cu(dmise)][BF_4] (**6**) at 50% probability density ellipsoids displaying short Se-Se interactiona along the *a*-axis. Hydrogen atoms and counterion omitted for clarity.

The copper(I) thione complexes **2**, **4**, and **7** are tetrahedrally coordinated via the three nitrogen atoms of the Tpm* (**2**), Tpm (**4**), or Tp* (**7**), ligands and the sulfur atom of dmit (Figures 2.9, 2.10, and 2.11; Tables 2.8, 2.9, and 2.10). The average Cu-N distance of 2.10 Å in complex **7** is similar to complex **2**, but shorter compared to Cu-N distances of 2.12 Å in complex **4**.

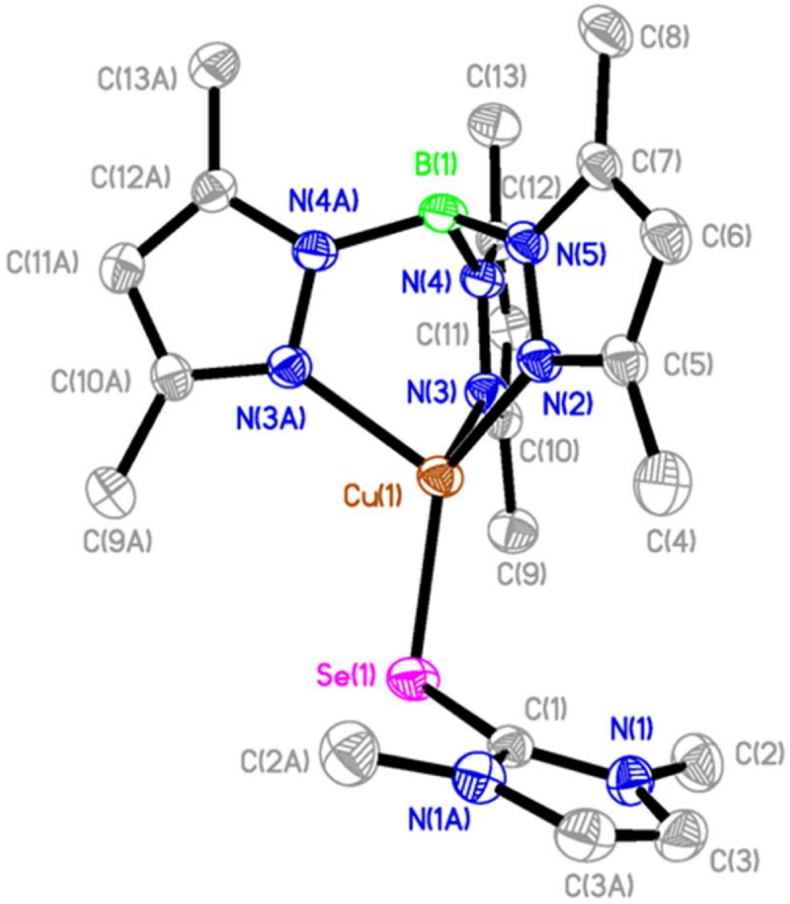

Figure 2.7. Crystal structure diagram of Tp*Cu(dmise) (**8**) displaying 50% probability density ellipsoids. Hydrogen atoms are omitted for clarity.

Table 2.5. Selected bond lengths (Å) and angles (°) for complex **8**.

Cu(1)-N(2)	2.033(4)	N(2)-Cu(1)-N(3)	92.05(10)
Cu(1)-N(3)	2.120(2)	N(2)-Cu(1)-N(3A)	92.05(10)
Cu(1)-N(3A)	2.120(2)	N(3)-Cu(1)-N(3A)	87.53(13)
Cu(1)-Se(1)	2.3299(9)	N(2)-Cu(1)-Se(1)	135.23(10)
Se(1)-C(1)	1.864(4)	N(3)-Cu(1)-Se(1)	118.86(7)
		N(3A)-Cu(1)-Se(1)	118.86(7)
		C(1)-Se(1)-Cu(1)	103.63(13)

The thione ligand is bound to the copper ion at almost identical C-S-Cu angles in complexes **4** (106.9º) and **7** (105.6º), but the angle increases to 111.3º in complex **2**. Complex **7** has a Cu-S bond distance of 2.22 Å, slightly longer than the observed bond length of 2.19 Å for complex **2** and 2.20 Å for complex **4**. The Cu-S bond lengths of complexes **2**, **4**, and **7** are shorter than previously-reported copper thione complexes such as $[Cu(PPh_3)_2(bzimH_2)Cl]$ (2.38 Å),[34] $[Cu(diditme)_2Cl]$ (2.23 Å),[56] $[CuCl(1\kappa S\text{-}imzSH)(PPh_3)_2]$ (2.36 Å),[57] and $[Cu(HB(3,5\text{-}^{i\text{Pr}}Pz)_3(SMeIm)]$ (2.45 Å);[58] however, the Cu-S bond lengths of complexes **2**, **4**, and **7** are longer than those copper thiolate complexes such as $[Cu(SC_6F_5)(HB(3,5\text{-}i\text{PrPz})_3)]$ (2.18 Å),[59] and $[Cu(SCPh_3)(HB(3,5\text{-}i\text{PrPz})_3)]$ (2.12 Å).[59]

Changing the alkyl substituents on the 3 and 5 positions of the pyrazole ring has minor effects on Cu-Se/S bond distances and Cu-Se/S-C(1) bond angles. In addition, the overall charge of the tris(pyrazolyl) ligand has very little effect on the structure of copper thione complexes. Complex **7** with the negatively charged Tp* ligand has slightly larger N-Cu-N angles (avg. 90.5º) compared to the neutral Tpm and Tpm* ligands (avg. 87.2º). The Cu-S bond distance of 2.19 Å in $[Tpm^*Cu(dmit)][BF_4]$ (**2**) is slightly shorter relative to 2.22 Å in the neutral complex Tp*Cu(dmit) (**7**).

The average Cu-N bond lengths and N-Cu-N angles in complexes **1**, **2**, **3**, **4**, and **6** are comparable to other tris(pyrazolyl)methane copper(I) complexes such as $[TpmCu(NCCH_3)][BF_4]$ (2.05-2.14 Å, 87.8º),[60] $[Tpm^*Cu(1,4\text{-}CNC_6H_4NC)][BF_4]$ (2.06-2.09 Å, 87.2º),[60] $[Tpm^{3\text{-}t\text{Bu}}Cu(NCCH_3)][PF_6]$ (2.06-2.14 Å, 89.2º),[51] and

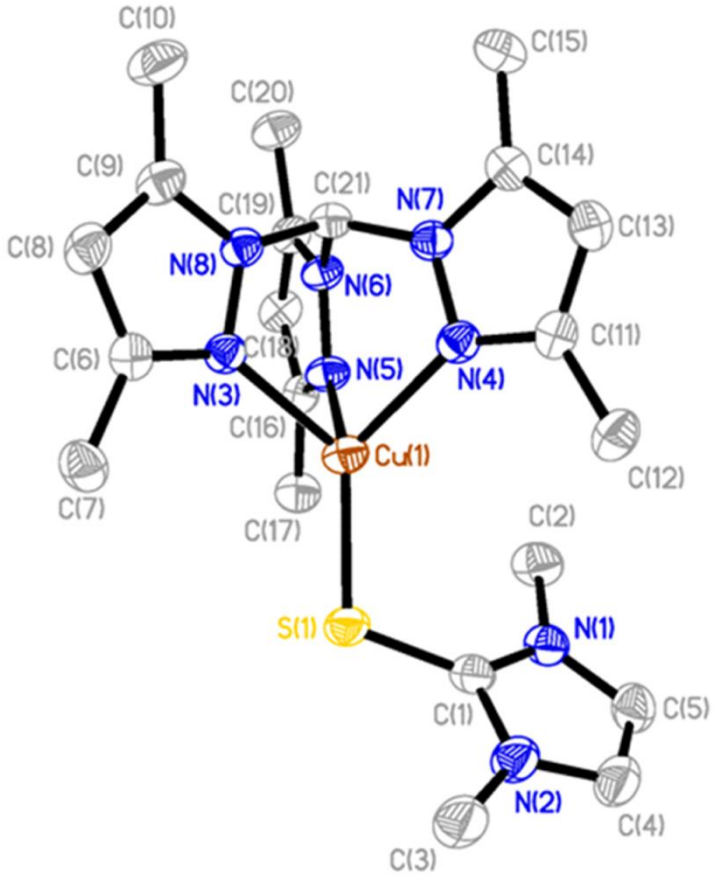

Figure 2.8. Crystal structure diagram of [Tpm*Cu(dmit)][BF_4] (**2**) showing 50% probability density ellipsoids. Hydrogen atoms and counterion are omitted for clarity.

Table 2.6. Selected bond lengths (Å) and angles (°) for complex **2**.

Cu-N(3)	2.095(2)	N(3)-Cu-N(4)	88.49(8)
Cu-N(4)	2.077(2)	N(3)-Cu-N(5)	85.23(8)
Cu-N(5)	2.1334(19)	N(4)-Cu-N(5)	87.40(8)
Cu-S	2.191(8)	N(3)-Cu-S	125.20(6)
S-C(1)	1.709(3)	N(4)-Cu-S	130.45(6)
		N(5)-Cu-S	126.07(6)
		C(1)-S-Cu	111.30(9)

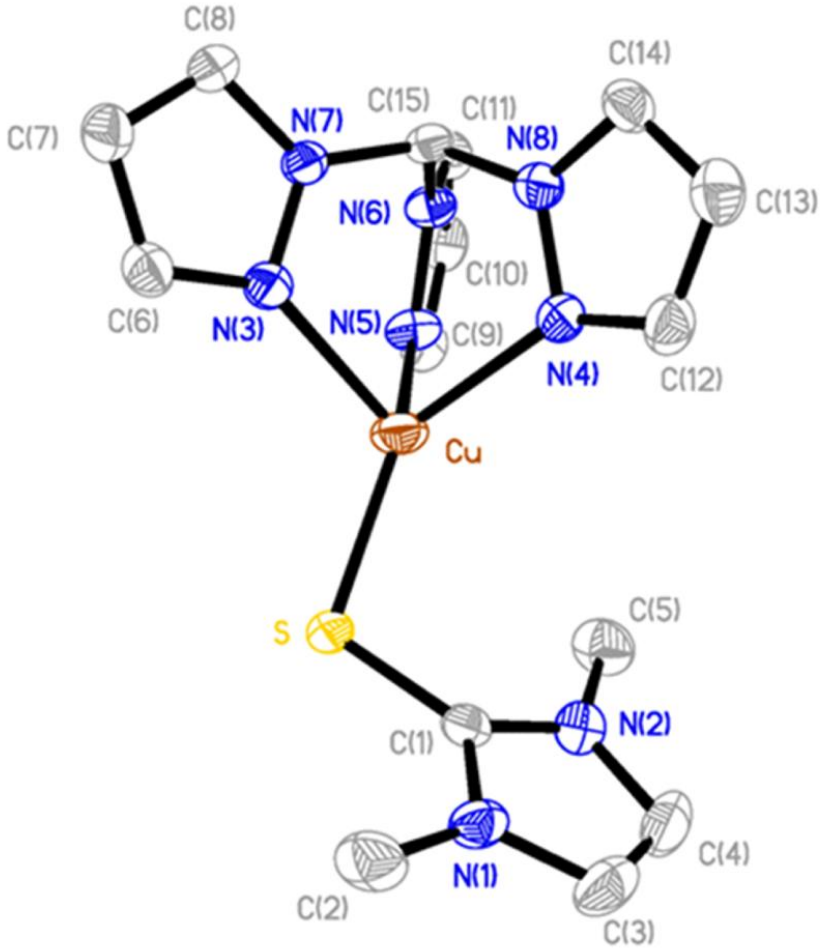

Figure 2.9. Crystal structure diagram of [TpmCu(dmit)][BF_4] (**4**) showing 50% probability density ellipsoids. Hydrogen atoms and counterion are omitted for clarity.

Table 2.7. Selected bond lengths (Å) and angles (°) for complex **4**.

Cu-N(3)	2.128(2)	N(3)-Cu-N(4)	88.73(9)
Cu-N(4)	2.121(2)	N(3)-Cu-N(5)	87.82(9)
Cu-N(5)	2.117(2)	N(4)-Cu-N(5)	85.5(10)
Cu-S	2.202(7)	N(3)-Cu-S	111.8(6)
S-C(1)	1.711(3)	N(4)-Cu-S	133.15
		N(5)-Cu-S	134.51
		C(1)-S-Cu	106.8(9)

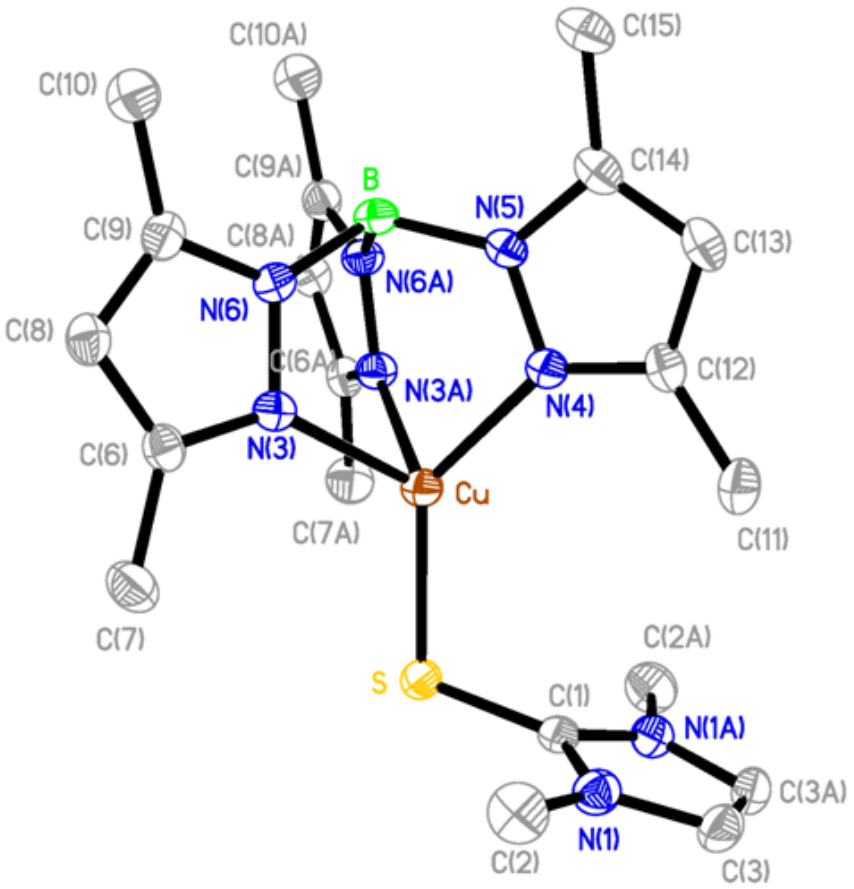

Figure 2.10. Crystal structure diagram of Tp*Cu(dmit) (**7**) showing 50% probability density ellipsoids. Hydrogen atoms are omitted for clarity.

Table 2.8. Selected bond lengths (Å) and angles (°) for complex **7**.

Cu-N(3)	2.1248(16)	N(3)-Cu-N(4)	92.09(7)
Cu-N(3A)	2.1248(16)	N(3A)-Cu-N(5)	92.09(7)
Cu-N(4)	2.039(2)	N(4)-Cu-N(5)	87.23(9)
Cu-S	2.219(9)	N(3)-Cu-S	119.14(5)
S-C(1)	1.708(3)	N(3A)-Cu-S	119.14(5)
		N(4)-Cu-S	134.84(7)
		C(1)-S-Cu	105.62(10)

[Tpm^{iPr}Cu(CO)][PF_6] (avg. 2.05 Å,88.1º).[40] The neutral Tp* complexes **7** and **8** have average N-Cu-N bond angles of 90.5º, larger than those of complexes **1** (87.3º), **2** (87.1º), **3** (87.3º and 86.9º), **4** (87.4º), **6** (86.2°) and K[Tp*Cu($SC_6H_4NO_2$)]·$2C_3H_6O$ (88.9º),[61] but similar to or slightly smaller than the previously reported Tp^{iPr}Cu(CO) (90.9º) and Tp^{iPr}Cu(SMeIm) (90.6º)[58] complexes.

Coordination of the dmise ligand to copper results in slightly shorter Se-C(1) bond lengths of 1.87 Å in complex **1** and 1.86 Å in complexes **6** and **8** relative to that of the uncoordinated ligand (1.89 Å),[27] whereas for complex **3**, this bond length is relatively unchanged compared to unbound dmise (1.89, Se(1)-C(1A) and 1.87 Å, Se(1A)-C(1A)). This slight shortening of the C=Se bond may be a result of donor bond formation between dmise and copper. Coordination of the thione ligand to copper in complexes **2**, **4**, and **7** results in almost identical S-C(1) bond distances (1.71 Å), longer than the S-C(1) bond distance (1.68 Å) in the free thione ligand.[62] Thus, the C=S bond is weakened due to back bonding from the copper. Based upon IR data and C=S/Se bond distances of the ligands before and after coordination, dmit is a better pi-acceptor than dmise but is a weak pi-acceptor relative to ligands such as CO that show slight elongation of the CO bond distance and a large shift of the C-O bond stretch to lower wavenumbers (~50 cm^{-1}) in the IR spectrum upon copper coordination.[40]

It has been reported that the strength of the metal-chalcogenone bond can be correlated to the degree of $^{13}C\{^1H\}$ NMR shift difference for the C-2 resonance upon complexation of selone or thione ligands.[42,63,64] Popovic, *et al.*,[42] showed a correlation

between C-2 $^{13}C\{^{1}H\}$ NMR resonance shifts vs. Hg-S bond lengths for three complexes, but this reported trend does not correlate with a shift of ν(C=S) to lower energies in the reported IR spectra. Isab and coworkers,[63,64] make this claim based solely on $^{13}C\{^{1}H\}$ NMR data with no corresponding structural data. To determine whether our data suggested such a trend, we compared the $^{13}C\{^{1}H\}$ NMR C-2 resonance shifts for our complexes (Table 4) with their Cu-S/Se bond lengths from the X-ray crystallographic data. For the copper selone complexes, the largest C-2 resonance shift of δ 8 compared to unbound dmise was found for [Tpm*Cu(dmise)][BF_4] (**1**), but its Cu-Se bond length of 2.298 Å is not statistically different from the average bond length of 2.303 Å for [TpmCu(dmise)][BF_4] (**3**) with a C-2 resonance shift of δ 6. [Tpm$^{i\mathrm{Pr}}$Cu(dmise)][BF_4] (**6**) and Tp*Cu(dmise) (**8**) have C-2 resonance shifts of δ 7 and δ 4, respectively, compared to unbound dmise and slightly longer Cu-Se bond lengths of 2.313 Å and 2.330 Å, respectively. For the copper thione complexes, the largest C-2 resonance shift of δ 8 relative to the unbound dmit was found for [TpmCu(dmit)][BF_4] (**4**) with the second-shortest Cu-S bond distance of 2.20 Å. [Tpm*Cu(dmit)][BF_4] (**2**) has the shortest Cu-S bond distance of 2.19 Å and a C-2 resonance shift of δ 7. The neutral complex Tp*Cu(dmit) (**7**) has a C-2 resonance shift of δ 5 compared to the unbound dmit and a slightly longer Cu-S bond distance of 2.22 Å. Thus, although we observed consistent upfield shifts of the C-2 resonance in the $^{13}C\{^{1}H\}$ NMR spectra of complexes **1** to **12** upon dmise and dmit coordination to copper, no specific correlation is observed between Cu-S/Se bond distances determined from the X-ray structures and C-2 NMR resonance shifts.

Electrochemical studies of selone and thione ligands and their copper complexes. The electrochemical behavior of the chalcogenone ligands and their copper(I) complexes were examined by cyclic voltammetry to determine the difference in redox potentials between dmise and dmit as well as the change in the $Cu^{2+/+}$ redox potential upon Cu-selone or Cu-thione coordination. The free selone has a more negative reduction potential ($E°$) compared to the thione: $E_{1/2}$ = -367 mV and -169 mV, respectively, versus normal hydrogen electrode (NHE), and both ligands exhibit quasi-reversible electrochemical behavior (Figure 2.11). The lower reduction potential of the selone relative to that of the thione implies that selone is a better reducing agent, thus it may possess greater antioxidant ability to neutralize reactive oxygen species.[65,66]

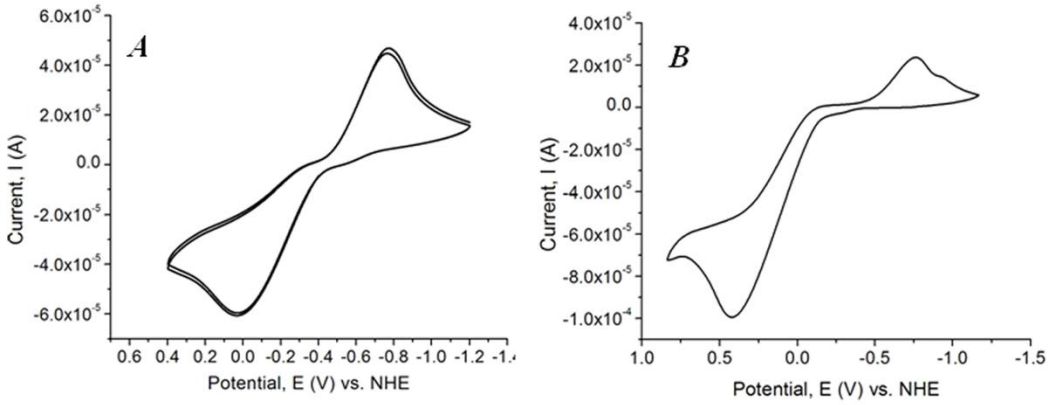

Figure 2.11. Cyclic voltammetry (CV) scans for dmise (***A***) and dmit (***B***). All data collected with 1 mM complex in acetonitrile. Potentials are reported versus NHE.

The $Cu^{2+/+}$ redox potentials of the copper selone and thione complexes versus NHE are given in Table 2.12. The cyclic voltammograms (CV) of these complexes

exhibit two one-electron, chemically reversible potential waves belonging to the $Cu^{2+/+}$ and $Cu^{+/0}$ reduction and oxidation processes, as shown in Figure 2.12 (CV spectra for all complexes are provided in Figures 2.13). At negative potentials, a peak corresponding to the $Cu^{+/0}$ reduction commences at potentials more negative than -1242 mV. After switching the scan direction, the Cu^0 is then stripped off the electrode at a potential close to -742 mV.[67,68]

The acetonitrile complexes [Tpm$^{i\text{Pr}}$Cu(NCCH$_3$)][BF$_4$], [Tpm*Cu(NCCH$_3$)][BF$_4$], and [TpmCu(NCCH$_3$)][BF$_4$] show large peak separations between the cathodic and anodic waves for the $Cu^{2+/+}$ oxidation and reduction potentials compared to the copper selone and thione complexes, suggesting quasi-reversible electrochemical behavior. This large separation may indicate that the oxidized or reduced products are not stable enough to remain intact, due to slow electron transfer kinetics during the voltammetry sweep,[69] or may indicate a large reorganization energy upon shifting from a distorted tetrahedral Cu^+ complex to a five-coordinate Cu^{2+} complex.[70]

The redox potentials of the copper selone complexes decrease significantly compared to those of the thione copper complexes. Complexation of selone and thione ligand to [Tpm*Cu(NCCH$_3$)][BF$_4$] lowers the $Cu^{2+/+}$ redox potential by 635 mV and 374 mV, respectively, whereas upon complexation to [Tpm$^{i\text{Pr}}$Cu(NCCH$_3$)][BF$_4$] the $Cu^{2+/+}$ redox potential is reduced by 847 mV and 617 mV, respectively. Thus, dmise coordination stabilizes the Cu^{2+} metal center more effectively than dmit coordination by an average of 224 mV.

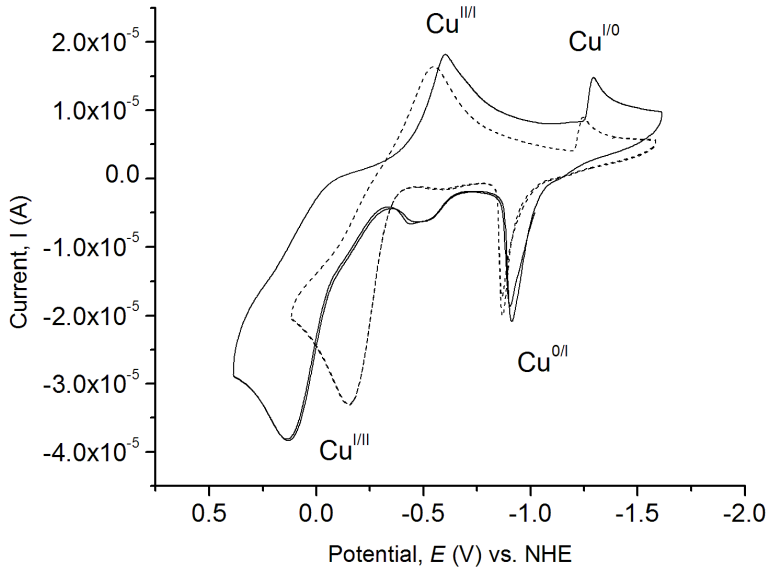

Figure 2.12. Cyclic voltammetry (CV) scan for Tp*Cu(dmise) (dashed line) and Tp*Cu(dmit) (solid line) in acetonitrile.

Effect of ligands and counterions on the $Cu^{+/2}$ *redox potential*. For the copper selone and thione complexes (**1**, **2**, **3**, **4**, **5**, and **6**) the bulkier the tris(pyrazolyl)methane ligand on the 3 and 5 positions of the pyrazole rings, the more negative the $Cu^{2+/+}$ redox potentials. The electron donating ability of the alkyl substituents is: *i*Pr > Me > H. For the copper selone complexes, the redox potentials are shifted to lower voltages in the following order: [TpmCu(dmise)][BF_4] (**3**) (-283 mV) > [Tpm*Cu(dmise)][BF_4] (**1**) (-366 mV) > [Tpm^{iPr}Cu(dmise)][BF_4] (**6**) (-0.390 mV). Despite the analogous copper thione complexes having higher positive potentials, the same trend is observed: [TpmCu(dmit)][BF_4] (**4**) (70 mV) > [Tpm*Cu(dmit)BF_4] (**2**) (-105 mV) > [Tpm^{iPr}Cu(dmit)][BF_4] (**5**) (-160 mV). The partially-negatively-charged chalcogenone species coupled with its σ and π donation abilities, stabilizes Cu^{2+} relative to Cu^{+} and

results in a more negative $Cu^{2+/+}$ redox potential. In contrast, for the acetonitrile complexes $[Tpm^{R}Cu(NCCH_3)][BF_4]$ (R = H, Me, *i*Pr), increased steric bulk of the alkyl substituents on the 3 and 5 position of the pyrazole rings results in a more positive $Cu^{2+/+}$ potential: $[TpmCu(NCCH_3)][BF_4]$ (-219 mV) < $[Tpm*Cu(NCCH_3)][BF_4]$ (269 mV) < $[Tpm^{iPr}Cu(NCCH_3)][BF_4]$ (457 mV). Thus, increasing the steric bulk on the 3 and 5 positions of the pyrazole rings results in increased thermodynamic stability of the copper(I) acetonitrile complexes, due to increased electron donating ability of the alkyl groups on the 3 and 5 positions of the pyrazole ring. The same increase to more positive $Cu^{2+/+}$ potentials with increased steric bulk and electron donating ability on the 3 position of the pyrazole ring in copper acetonitrile complexes with tris(pyrazolyl)methane type ligands was observed by Fujisawa *et al*.[40]

The selone compound **1** with the neutral Tpm* ligand has slightly more negative $Cu^{2+/+}$ potentials (-366 mV) relative to the complex **8** with anionic Tp* ligand (-346 mV). For the copper thione complexes, complex **7** with the anionic Tp* ligand has significantly more negative potential (-232 vs. -105 mV) compared to complex **2** with the neutral Tpm* ligand, an effect similarly observed for $Tp*Cu(NCCH_3)$ (-349 mV) vs. $[Tpm*Cu(NCCH_3)][BF_4]$ (269 mV). Fujisawa *et al*. also observed more negative potentials for $Tp^{iPr}Cu(NCCH_3)$ relative to $[Tpm^{iPr}Cu(NCCH_3)][PF_6]$ and determined that the borate ligands are more electron donating than the methane ligands.[40] It is expected that the negatively-charged borate ligands coupled with the partially-negatively-charged chalcogenone will stabilize Cu^{2+} relative to Cu^{+} vs. the neutral Tpm* ligand, resulting in a more negative reduction potential.

Table 2.9. Redox potentials of selone and thione ligands and $Cu^{2+/+}$ and $Cu^{+/0}$ potentials of synthesized copper complexes vs. NHE.

		$Cu^{2+/+}$				$Cu^{+/0}$			
Complex or ligand		E_{pa}	E_{pc}	ΔE	$E_{1/2}$	E_{pa}	E_{pc}	ΔE	$E_{1/2}$
[TpmCu(dmise)][BF_4]	(**3**)	-30	-536	506	-283	-915	-1303	324	-760
[Tpm*Cu(dmise)][BF_4]	(**1**)	-88	-644	556	-366	-905	-1494	589	-1199
[Tpm^{iPr}Cu(dmise)][BF_4]	(**6**)	-49	-729	680	-390	-888	1257	370	-1070
Tp*Cu(dmise)	(**8**)	-122	-570	448	-346	-1072	-1444	372	-1258
[Tpm*Cu(dmise)][Cl]	(**9**)	-30	-752	722	-376	-803	-1305	502	-1053
[Tpm^{iPr}Cu(dmise)][Cl]	(**12**)	11	-643	654	-316	-920	-1448	525	-1184
[TpmCu($NCCH_3$)][BF_4]		203	-641	844	-219	-598	-922	324	-760
[Tpm*Cu($NCCH_3$)][BF_4]		1158	-620	1778	269	-363	-1297	934	-830
Tp*Cu($NCCH_3$)		-51	-647	596	-349	-824	-1247	423	-1036
Tpm*CuCl		46	-450	496	-202	-723	-1645	922	-1184
dmise[a]		39	-773	812	-367				
[TpmCu(dmit)][BF_4]	(**4**)	392	-252	644	70	-932	-1295	363	-1113
[Tpm*Cu(dmit)][BF_4]	(**2**)	307	-518	825	-105	-789	-1371	582	-1080
[Tpm^{iPr}Cu(dmit)][BF_4]	(**5**)	187	-507	694	-160	-967	-1181	214	-1074
Tp*Cu(dmit)	(**7**)	147	-611	758	-232	-980	-1566	586	-1273
[Tpm*Cu(dmit)][Cl]	(**10**)	-15	-341	326	-163	-785	-1349	564	-1067
[Tpm^{iPr}Cu(dmit)][Cl]	(**11**)	9	-291	300	-141	-908	-1442	534	-1175
[Tpm^{iPr}Cu($NCCH_3$)][BF_4]		1254	-340	1594	457	-332	-1248	916	-790
Tpm^{iPr}CuCl		280	-18	298	131	-467	-1370	903	-918
dmit[a]		424	-761	1158	-167				

[a]Reported redox potentials are for the uncomplexed ligand.

Biological significance of selenium coordination. Although dmit and dmise are not found *in vivo*, they are structurally similar to ergothioneine[15] and selenoneine,[16] respectively, which are sulfur and selenium containing antioxidants found in plants and animals. Yamashita, *et al*.[16] found that selenoneine is the major selenium compound found in tuna and mackerel blood (~0.45 μM concentration) and is a very potent radical scavenger. Dmit is also structurally similar to methimazole,[14] a thione drug currently used for treatment of hyperthyrodism. Mugesh, *et al*. has demonstrated the abilities of dmit and dmise to protect against peroxynitrite-mediated protein tyrosine nitration[71] and similar compounds such as selenoneine have been shown to be very potent radical

scavengers.[16] Dmise and dmit also prevent copper-mediated DNA damage.[72] The electrochemical data obtained from the target metal complexes provides insight as to whether similar Se-Cu complexes formed *in vivo* could cycle between the $Cu^{2+/+}$ forms. Complexes with reduction potentials lower than -324 mV (versus NHE) cannot be reduced by cellular reductants such as NADH.[73] The copper selone complexes have a reduction potential range of -283 to -390 mV, whereas copper thione complex potentials range from 70 to -232 mV versus NHE. Thus, copper selenium complexes have significantly lower potentials than analogous copper-sulfur complexes, and most are more negative than that of NADH. Therefore, if similar complexes are formed *in vivo*, these potentials may be low enough to prevent Cu^{2+} reduction by NADH, making the Fenton-like reaction of copper non-catalytic, and inhibiting generation of hydroxyl radical (reaction 1).

Conclusions

Biologically relevant Cu^{+} selone and thione complexes with tris(pyrazolyl)methane and tris(pyrazolyl)borate ligands have been synthesized and characterized, and their electrochemistry has been investigated and compared. The copper-selone complexes [Tpm*Cu(dmise)][BF_4] (**1**), [TpmCu(dmise)][BF_4] (**3**), [Tpm$^{i\mathrm{Pr}}$Cu(dmise)][BF_4] (**6**), and Tp*Cu(dmise) (**8**) possess the shortest copper-selone bond distances reported. The copper-thione complexes [Tpm*Cu(dmit)][BF_4] (**2**), [TpmCu(dmit)][BF_4] (**4**), and Tp*Cu(dmit) (**7**) have Cu-S bond lengths ranging from

2.19 - 2.22 Å. Changing the alkyl groups on the 3 and 5 positions of the pyrazole ring has little effect on the Cu-Se or Cu-S bond lengths, but has dramatic effects on the $Cu^{2+/+}$ redox potentials of complexes. The $^{13}C\{^{1}H\}$ NMR data predicts stronger Cu-Se bonding in [Tpm*Cu(dmise)][BF_4] (**1**) relative to [TpmCu(dmise)][BF_4] (**3**) and [Tpm$^{i\text{Pr}}$Cu(dmise)][BF_4] (**6**), although little variation is observed in the Cu-Se bond distances. The dmise ligand coordination stabilizes the Cu^{2+} center more effectively than dmit coordination by an average of 224 mV. The results obtained in this study give us insight into possible alternative explanation about the antioxidant abilities of selenium and sulfur compounds. Since reduction potentials of the copper selone complexes are more negative than the copper thione complexes, if similar complexes are formed *in vivo*, these potentials may be low enough to inhibit Cu^{2+} reduction by NADH and prevent copper redox cycling.

Experimental section

Materials. The synthesis and manipulation of all copper complexes was performed under an inert atmosphere of argon or nitrogen using standard Schlenk techniques. Acetonitrile, methanol, and ether were purified using standard procedures and freshly distilled under argon atmosphere prior to use. The following compounds were synthesized according to published procedures: 3,5-diisopropyl pyrazole,[59] hydrotris(3,5-diisopropyl-1-pyrazoyl)methane (Tpm$^{i\text{Pr}}$),[40] potassium hydro-tris(3,5-dimethylpyrazolyl)borate (Tp*),[74] *N,N'*-dimethylimidazole selone (dmise), *N,N'*-

dimethylimidazole thione (dmit),[75] $[Cu(NCCH_3)_4][BF_4]$,[76] Tpm*CuCl, $[Tpm^*Cu(NCCH_3)]^+$,[51] hydrotris(3,5-dimethyl-1-pyrazoyl)methane (Tpm*),[77] $Tpm^{iPr}CuCl$ and $[Tpm^{iPr}Cu(NCCH_3)]^+$.[40] The following reagents were used as received: cuprous chloride (Aldrich), 3,5-dimethyl-1-pyrazole (Aldrich), tetra-*n*-butylammonium bromide (Aldrich), sodium carbonate (VWR), selenium powder, sulfur powder, cuprous oxide (stabilized; Aldrich), diisobutyrylmethane (VWR), hydrazine monohydrate (VWR), 1-methylimidazole (VWR), and methyliodide (VWR).

Instrumentation. ^1H, $^{13}C\{^1H\}$, $^{77}Se\{^1H\}$, and $^{19}F\{^1H\}$ NMR spectra were obtained on Bruker-AVANCE 300 and 500 MHz NMR spectrometers. $^{11}B\{^1H\}$ NMR spectra were obtained on a Joel 300 MHz NMR spectrometer. ^1H and $^{13}C\{^1H\}$ NMR chemical shifts are reported in δ relative to tetramethylsilane (TMS) and referenced to solvent. $^{19}F\{^1H\}$ NMR and $^{11}B\{^1H\}$ NMR spectra were externally referenced to CCl_3F (δ 0)[78] and neat $BF_3{\cdot}OEt_2$ (δ -19.4),[79] respectively. $^{77}Se\{^1H\}$ NMR chemical shifts were externally referenced to diphenyl diselenide (δ 461),[80] and reported relative to dimethyl selenide (δ 0).

Electrochemical experiments were performed with a BAS 100B potentiostat. A three compartment cell was used with an Ag/AgCl reference electrode, Pt counter electrode, and a glassy carbon working electrode. Freshly-distilled acetonitrile was used as the solvent with tetra-*n*-butylammonium phosphate as the supporting electrolyte (0.1 M). Solutions containing 1 mmol analyte were deaerated for 2 min by vigorous nitrogen purge. The measured potentials were corrected for junction potentials relative to

ferrocenium/ferrocene (0.543 mV vs. Ag/AgCl).[81] All $E_{1/2}$ values were calculated from $(E_{pa} + E_{pc})/2$ at a scan rate of 100 mV/s, and $\Delta E = E_{pa} - E_{pc}$. Cyclic voltammograms of selone and thione ligands (Figure 11) and their copper complexes showing the $Cu^{+/2+}$ potentials are given in Figures 13-15. Resistivity for each complex was measured in DMF solution (0.1 mM) at 25°C using a GDT-11 multimeter and converted to molar electrical conductivity.

Infrared spectra were obtained using Nujol mulls on KBr salt plates with a Magna 550 IR spectrometer. Abbreviations used in the description of vibrational data are as follows: vs, very strong; s, strong; m, medium; w, weak; b, broad. Electrospray ionization mass spectrometry (ESI-MS) was conducted using a QSTAR XL Hybrid MS/MS System from Applied Biosystems via direct injection of sample (0.05 mL/min flow rate) into a Turbo Ionspray ionization source. Samples were run under positive mode, with ionspray voltage of 5500 V, and TOF scan mode. Melting points were determined using a Barnstead Electrothermal 9100 apparatus in silicon-grease-sealed glass capillary tubes. Absorption spectra were collected using a Varian Cary-50 Bio spectrophotometer in quartz cuvettes with a path length of 1 cm. Elemental analysis was performed by Atlantic Microlabs, Inc.*Preparation of complexes. [Tpm*Cu(dmise)][BF$_4$] (**1**) Method 1*: The dmise ligand (176 mg, 1 mmol) was dissolved in acetonitrile (20 mL) and was cannula transferred into a solution of $[Cu(CNCH_3)_4][BF_4]$ (312 mg, 1 mmol) in acetonitrile (20 mL). The reaction mixture was stirred at room temperature for 3 h until it was clear and colorless. An equimolar amount of Tpm* (298 mg, 1 mmol) was then dissolved in acetonitrile (10 mL) and cannula transferred into the reaction mixture and stirred for an

additional 18 h. The solvent volume in the reaction mixture was reduced to about 4 mL and the product was precipitated with diethyl ether to afford an off-white solid that was dried *in vacuo* and analyzed. Yield 78% (486 mg, 0.78 mmol).

Method 2: [Tpm*Cu($NCCH_3$)][BF_4][51] (250 mg, 0.5 mmol) was dissolved in dichloromethane (10 mL) and into this was cannula transferred dmise (90 mg, 0.5 mmol) in dichloromethane (10 mL). The reaction mixture was stirred for 3 h, and the solvent volume reduced to about 3 mL. The product was precipitated with diethyl ether to afford an off-white solid that was dried *in vacuo* and analyzed. Single crystals for X-ray analysis were grown from slow vapor diffusion of ether into acetonitrile solution. Yield: 89% (277 mg, 0.445 mmol). ^{1}H NMR (CD_2Cl_2): 2.18 (s, 9H, $3CH_3$), 2.541 (s, 9H, $3CH_3$), 3.88 (s, 6H, $2CH_3$ [dmise]), 5.99 (s, 3H, 3CH [Pz]), 7.17 (s, 2H, 2CH [dmise]), 7.77 (s, 1H, CH). ^{13}C{^{1}H} NMR (CD_2Cl_2): 10.72 (CH_3), 13.16 (CH_3), 37.58 (CH_3 [dmise], 67.86 (CH), 106.76 (C-4 [Pz]), 121.60 (2CH [dmise]), 139.60 (C-3 [Pz]), 147.61 (C=Se), 150.79 (C-5 [Pz]). ^{19}F{^{1}H} NMR: -152.46, -152.52 (s, $^{10}BF_4$, $^{11}BF_4$). ^{11}B{^{1}H} NMR (CD_3CN): -1.397. ^{77}Se{^{1}H} NMR (CD_2Cl_2): -87.5. IR (cm^{-1}): 481 s, 520 vs, 582 s, 610 s, 630 vs, 661 vs, 703 s, 739 vs, 793 vs, 815 s, 853 w, 900 vs, 980 s, 1031 b, 1150 vs, 1239 b, 1306 w, 1454 w, 1569 s, 1688 s, 2362 s, 2722 s, 3141 s, 3171 s, 3423 b. UV-vis (CH_3CN): 273 nm. Mp: 169-172°C. Mass spectrum (ESI-MS): *m/z* 537.1 [Tpm*Cu(dmise)]$^{+}$, 361.1 [Tpm*Cu]$^{+}$. Molar conductivity: 90.42 S cm^2 mol^{-1}. Anal. Calc. for $C_{21}H_{30}BCuF_4N_8Se$: C, 40.43; N, 17.96; H, 4.86. Found: C, 40.19; N, 17.74; H, 4.84.

*[Tpm*Cu(dmit)][BF_4] (**2**).* Complex **2** was prepared following the procedure for **1** using both methods except that dmit (1 mmol, 129 mg) was used in place of dmise. Yield: method 1, 64% (368 mg, 0.640 mmol); method 2, 78% (451 mg, 0.780 mmol). Single crystals for X-ray analysis were grown from slow vapor diffusion of ether into acetonitrile solution. ^{1}H NMR (CD_2Cl_2): 2.18 (s, 9H, $3CH_3$), 2.53 (s, 9H, $3CH_3$), 3.80 (s, 6H, $2CH_3$ [dmit]), 6.00 (s, 3H, 3CH [Pz]), 7.00 (s, 2H, 2CH [dmit]), 7.76 (s, 1H, CH). ^{13}C{^{1}H} NMR: 10.72 (CH_3), 13.11 (CH_3), 35.82 (CH_3 [dmit]), 67.79 (CH), 106.74 (C-4 [Pz]), 119.70 (2CH [dmit]), 139.58 (C-3 [Pz]), 150.78 (C-5 [Pz]), 155.96 (C=S). ^{19}F{^{1}H} NMR: -152.56, 152.61 (s, $^{10}BF_4$, $^{11}BF_4$). ^{11}B{^{1}H} NMR (CD_3CN): -1.43. IR (cm^{-1}): 481 s, 520 s, 582 s, 611 m, 630 vs, 672 vs, 703 s, 734 vs, 751 vs, 795 m, 816 s, 854 m, 900 vs, 976 s, 1058 b, 1149 vs, 1171 vs, 1239 m, 1306 s, 1393 b, 1570 s, 1676 s, 2723 s, 3141 vs, 3171 vs, 3351 w. UV-vis (CH_3CN): 273 nm. Mp: 167-170°C. Mass spectrum (ESI-MS): *m/z* 489.1 [Tpm*Cu(dmit)]$^{+}$, 361.1 [Tpm*Cu]$^{+}$, 319.0 [Cu-$(dmit)_2$]$^{+}$, 191.0 [Cu-dmit]$^{+}$. Molar conductivity: 89.74 S cm^2 mol^{-1}. Anal. Calc. for $C_{21}H_{30}BCuF_4N_8S$: C, 43.72; N, 19.42; H, 5.24. Found: C, 43.78; N, 19.36; H, 5.27.

*[TpmCu(dmise)][BF_4] (**3**).* Complex **3** was prepared following the procedure for **1** using both methods except that Tpm (214 mg, 1 mmol) was used in place of Tpm*. Yield: method 1, 83% (447 mg, 0.83 mmol); method 2, 87% (471 mg, 0.87 mmol). Single crystals for X-ray analysis were grown from slow vapor diffusion of ether into a methanol solution. ^{1}H NMR (CD_3CN): 3.73 (s, 6H, CH_3 [dmise]), 6.45 (b, 3H, CH [Pz]), 7.15 (s, 2H, CH [dmise]), 7.70 (b, 3H, CH [Pz]), 7.82 (b, 3H, CH [Pz]), 8.66 (s, H, CH). ^{13}C{^{1}H} NMR (CD_3CN): 38.02 (CH_3 [dmise]), 81.9 (CH), 107.87 (4-CH [Pz]), 122.24

(2CH [dmise]), 131.71 (3-CH [Pz]), 142.68 (5-CH [Pz]), 148.9 (C=Se). $^{19}F\{^{1}H\}$ NMR (CD_3CN): -149.557, -149.610 (s, $^{10}BF_4$, $^{11}BF_4$). $^{77}Se\{^{1}H\}$ NMR ($CDCl_3$): -95.6. IR (cm^{-1}): 521 w, 603 w, 611 w, 656 w, 723 s, 761 vs, 799 vs, 815 vs, 917 w, 961 w, 978 w, 1093 b, 1208 w, 1233 s, 1275 s, 1307 vs, 1351 s, 1379 vs, 1396 s, 1458 vs, 1507 s, 1522 s, 1540 w, 1570 w, 1652 w, 1700 w, 2337 w, 2361 w, 2724 w, 2920 b, 3133 b. Mp: 204-206. UV-vis (CH_3CN): 275 nm. Mass spectrum (ESI-MS): *m/z* 452.9 $[TpmCu(dmise)]^+$, 277.0 $[TpmCu]^+$. Anal. Calc. for $C_{15}H_{18}BCuF_4N_8Se$: C, 33.38; N, 20.76; H, 3.36. Found: C, 33.17; N, 20.55; H, 3.34

*[TpmCu(dmit)][BF$_4$] (**4**).* Complex **4** was prepared following the procedure for **1** using both methods except that Tpm (214 mg, 1 mmol) and dmit (129 mg, 1 mmol) were used in place of Tpm* and dmise. Yield: method 1, 79% (389 mg, 0.791 mmol); method 2, 75% (368 mg, 0.749 mmol). Single crystals for X-ray analysis were grown from slow vapor diffusion of ether into a methanol solution. ^{1}H NMR (CD_2Cl_2): 3.82 (s, 6H, CH_3 [dmit]), 6.35 (t, J_{HH} = 2 Hz, 3H, CH [Pz]), 7.04 (s, 2H, CH [dmit]), 7.53 (d, J_{HH} = 2 Hz, 3H, CH [Pz]), 8.26 (d, J_{HH} = 2.5 Hz, 3H, CH [Pz]), 9.14 (s, H, CH). $^{13}C\{^{1}H\}$ NMR (CD_2Cl_2): 35.93 (CH_3 [dmit]), 76.08 (CH), 106.65 (4-CH [Pz]), 119.90 (2CH [dmit]), 132.07 (3-CH [Pz]), 141.64 (5-CH [Pz]), 154.66 (C=S). $^{19}F\{^{1}H\}$ NMR (CD_2Cl_2): -149.557, -149.610 (s, $^{10}BF_4$, $^{11}BF_4$). IR (cm^{-1}): 520 w, 613 vs, 661 w, 671 s, 719 vs, 750 vs, 772 vs, 794 vs, 851 vs, 921 w, 970 s, 1020 b, 1092 b, 1174 s, 1232 s, 1242 vs, 1258 w, 1288 vs, 1307 w, 1377 s, 1400 vs, 1464 vs, 1512 s, 1542 w, 1571 s, 2361 w, 2727 w, 2925 b, 3016 w, 3107 w, 3137 w, 3173 w. Mp: 205-207ºC. UV-vis (CH_3CN): 273 nm. Mass spectrum (ESI-MS): *m/z* 405.0 $[TpmCu(dmit)]^+$, 277.0 $[TpmCu]^+$, 191.0

[Cu-dmit]$^{+}$. Anal. Calc. for $C_{15}H_{18}BCuF_4N_8S$: C, 36.56; N, 22.74; H, 3.68. Found: C, 36.61; N, 22.77; H, 3.63.

*[Tpm^{iPr}Cu(dmit)][BF$_4$] (**5**)*. Complex **5** was prepared following the procedure for **1** using both methods except that Tpm^{iPr} (466 mg, 1 mmol) and dmit (129 mg, 1 mmol) were used in place of Tpm* and dmise, respectively. Yield: method 1, 83% (617 mg, 0.83 mmol).

Synthesis of complex **5** by method 2 was conducted following procedure for **1**, but with slight modifications. [Tpm^{iPr}Cu(NCCH$_3$)][BF$_4$][40] (660 mg, 1 mmol) was dissolved in dichloromethane (10 mL) and into this was cannula transferred dmit (128 mg, 1 mmol) in dichloromethane (10 mL). The reaction mixture was stirred for 3 h, and the solvent volume reduced to about 3 mL. The product was extracted with diethyl ether to afford a yellowish solution that was dried *in vacuo* and analyzed. Yield: 87% (648 mg, 0.872 mmol). Single crystals for X-ray analysis were grown via slow vapor diffusion of ether into dichloromethane solution. ^{1}H NMR (CD_2Cl_2) : 1.19 (d, J_{HH} = 7 Hz, 18H, 3(CH_3)$_2$) , 1.33 (d, J_{HH} = 7 Hz, 18H, 3(CH_3)$_2$) , 2.96 (sept, J_{HH} = 7 Hz, 3H, 3CH), 3.12 (sept, J_{HH} = 6.75 Hz, 3H, 3CH), 3.77 (s, 6H, 2CH_3 [dmit]), 6.05 (s, 3H, 3CH [Pz]), 7.03(s, 2H, 2CH [dmit]), 8.00 (s, 1H, CH). ^{13}C{^{1}H} NMR (CD_2Cl_2): 22.31 (CH(*CH_3*)$_2$), 22.88 (CH(*CH_3*)$_2$), 26.18 (CH(*CH_3*)$_2$), 27.84 (CH(*CH_3*)$_2$), 35.81 (CH_3 [dmit]), 67.28 (CH), 99.71 (4-CH [Pz]), 119.80 (2CH [dmit]), 150.85 (3-CH [Pz]), 155.49 (C=S), 160.99 (5-CH [Pz]). ^{19}F{^{1}H} NMR (CD_2Cl_2): -152.844, -152.896 (s, $^{10}BF_4$, $^{11}BF_4$). ^{11}B NMR (CD_2Cl_2): -4.69. IR (cm^{-1}): 520 s, 582 s, 633 s, 669 vs, 695 s, 723 s,743 s, 799 s, 821

vs,879 s, 902 s, 914 s, 1005 s, 1053 b, 1180 vs, 1235 vs, 1289 s, 1366 s, 1394 m, 1464 w, 1556 vs, 1569 s,1682 b, 1737 s, 2126 b, 2359 b, 2727 b, 3139 s, 3167 s, 3364 b. Mp: 232°C. UV-vis (CH_3CN): 261 nm. Mass spectrum (ESI-MS): *m/z* 657.2 $[Tpm^{iPr}Cu(dmit)]^+$, 529.2 $[Tpm^{iPr}Cu]^+$, 319.0 $[Cu\text{-}(dmit)_2]^+$, 191.0 $[dmit\text{-}Cu]^+$. Molar conductivity: 95.61 S cm^2 mol^{-1}. Anal. Calc. for $C_{33}H_{54}BCuF_4N_8S$: C, 53.23; N, 15.15; H, 7.26. Found: C, 53.44; N, 14.92; H, 7.42.

*$[Tpm^{iPr}Cu(dmise)][BF_4]$ (**6**)*. Complex **6** was prepared following the procedure for **1** using both methods except that Tpm^{iPr} (466 mg, 1 mmol) was used in place of Tpm*. Yield: method 1, 62% (491 mg, 0.619 mmol). Method 2 was modified as stated in procedure for **5**. Yield: 67% (530 mg, 0.67 mmol). Single crystals for X-ray analysis were grown via slow vapor diffusion of ether into dichloromethane solution. ^1H NMR (CD_2Cl_2): 1.17 (d, J_{HH} = 7 Hz, 18H, $3(CH_3)_2$), 1.32 (d, J_{HH} = 7 Hz, 18H, $3(CH_3)_2$), 2.98 (sept, J_{HH} = 6 Hz, 3H, 3CH), 3.11 (sept, J_{HH} = 6.75 Hz, 3H, 3CH), 3.85 (s, 6H, $2CH_3$ [dmise]), 6.04 (s, 3H, 3CH [Pz]), 7.18 (s, 2H, 2CH [dmise]), 8.01 (s, 1H, CH). $^{13}C\{^1H\}$ NMR (CD_2Cl_2): 22.40 ($CH(\mathit{CH_3})_2$), 22.87 ($CH(\mathit{CH_3})_2$), 26.19 ($CH(\mathit{CH_3})_2$), 27.82 ($CH(\mathit{CH_3})_2$), 37.57 (CH_3 [dmise]), 67.50 (CH), 99.64 (4-CH [Pz]), 121.47 (2CH [dmise]), 148.12 (C=Se), 150.81(3-CH [Pz]), 161.04(5-CH [Pz]). $^{19}F\{^1H\}$ NMR (CD_2Cl_2): -152.932, -152.984 (s, $^{10}BF_4$, $^{11}BF_4$). $^{11}B\{^1H\}$ NMR [(CD_3CN)]: -1.39. $^{77}Se\{^1H\}$ NMR ($CDCl_3$): -95.6. IR (cm^{-1}): 520 s, 583 s, 669 vs, 694 s, 723 s, 746 vs, 797 vs, 821 b, 878 s, 902 s, 914 vs, 928 s, 964 s, 1004 s, 1044 b, 1150 s, 1182 s, 1234 b, 1289 b, 1383 b, 1458 b, 1556 s, 1679 s, 2125 s, 2359 s, 2728 s, 3139 s, 3165 s, 3357 b. Mp: 234°C. UV-vis (CH_3CN): 273 nm. Mass spectrum (ESI-MS): *m/z* 705.2 $[Tpm^{iPr}Cu(dmise)]^+$, 529.2

[Tpm^{iPr}Cu]$^{+}$. Molar conductivity: 118.4 S cm^{2} mol^{-1}. Anal. Calc. for $C_{33}H_{54}CuN_8SeBF_4$: C, 50.04; N, 14.15; H, 6.87. Found: C, 49.92; N, 14.23; H, 6.99.

*Tp*Cu(dmit) (**7**). Method 1*: The dmit ligand (134 mg, 1 mmol) was dissolved in acetonitrile (20 mL) and was cannula transferred into a solution of CuCl (99 mg, 1 mmol) in methanol (20 mL). The reaction mixture was stirred at room temperature for 3 h, and an equimolar amount of KTp* (330 mg, 1 mmol) dissolved in acetonitrile was cannula transferred into the reaction mixture, stirred for 18 h and dried *in vacuo*. The target product was extracted using dichloromethane and the filtrate was dried *in vacuo* and analyzed. Single crystals suitable for X-ray structure determination were grown by slow diffusion of ether into methanol/dichloromethane solution. Yield 75% (365 mg, 0.75 mmol).

Method 2: [Tp*Cu(NCCH$_3$)] (200 mg, 0.5 mmol) was dissolved in dichloromethane (10 mL) and dmit (90 mg, 0.5 mmol) in dichloromethane (10 mL) was added. The reaction mixture was stirred for 3 h, dried *in vacuo* and the solid product washed with hexane to afford a white precipitate which was filtered, dried *in vacuo*, and analyzed. Yield 89% (217 mg, 0.445 mmol). ^{1}H NMR ($CDCl_3$): 1.70 (s, 9H, 3(CH_3)), 2.44 (s, 9H, 3(CH_3), 3.68 (s, 6H, 2CH_3 [dmit]), 5.73 (s, 3H, 3CH [Pz]), 6.83 (s, 2H, 2CH [dmit]). ^{13}C{^{1}H} NMR ($CDCl_3$): 13.25 (CH_3), 13.64 (CH_3), 36.08 (CH_3 [dmit]), 104.79 (C-4 [Pz]), 119.33 (2CH [dmit]), 144.60 (C-3 [Pz]), 148.31 (C-5 [Pz]), 157.45 (C=S). IR (cm^{-1}): 502 s, 516 s, 634 s, 656 s, 664 s, 679 s, 699 s, 743 s, 784 s, 813 s, 842 s, 979 s, 1036 s, 1059 s, 1082 s, 1175 b, 1235 s, 1262 s, 1386 b, 1542 s, 1571 s, 1653 s, 1673 s,

1695 s, 1734 s, 2341 s, 2362 s, 2509 s, 2735 s, 2853 b, 3034 s, 3118 s, 3155 s. Mp: 223-227°C. UV-vis (CH_3CN): 267 nm. Mass spectrum (ESI-MS): *m/z* 488.1 $[Tp^*Cu(dmit)]^+$, 360.1 $[Tp^*Cu]^+$, 318.9 $[Cu(dmit)_2]^+$, 190.9 $[Cu\text{-}dmit]^+$. Anal. Calc. for $CuC_{20}BH_{30}N_8S$: C, 49.13; N, 22.92; H, 6.20. Found: C, 48.83; N, 22.45; H, 6.18.

*Tp*Cu(dmise) (**8**)*. Complex **8** was prepared following the procedure for **7** using both methods except that dmise (175 mg, 1 mmol) was used in place of dmit. Single crystals suitable for X-ray analysis were grown by slow vapor diffusion of ether into dichloromethane and methanol solution. Yield: method 1, 59% (316 mg, 0.59 mmol); method 2, 74% (397 mg, 0.74 mmol). ^1H NMR ($CDCl_3$): 1.70 (s, 9H, 3(CH_3)), 2.44 (s, 9H, 3(CH_3), 3.75 (s, 6H, 2CH_3 [dmise]), 5.73 (s, 3H, 3CH [Pz]), 6.93 (s, 2H, 2CH [dmise]). $^{13}C\{^1H\}$ NMR ($CDCl_3$):): 13.25 (CH_3), 13.64 (CH_3), 37.45 (CH_3 [dmise]), 104.79 (C-4 [Pz]), 120.27 (2CH [dmise]), 144.60 (C-3 [Pz]), 148.30 (C-5 [Pz]), 151.63 (C=Se). $^{77}Se\{^1H\}$ NMR ($CDCl_3$): -31.5. IR (cm^{-1}): 599 s, 635 s, 655 s, 666 s, 699 s, 723 s, 748 s, 811 w, 839 s, 980 s, 1036 s, 1059 s, 1081 s, 1146 s, 1176 b, 1232 s, 1262 s, 1378 b, 1443 b, 1541 s, 1569 s, 1594 s, 1699 s, 2508 s, 2734 s, 2851 s, 3116 s, 3152 s. Mp: 223-227°C. UV-vis (CH_3CN): 270 nm. Mass spectrum (ESI-MS): *m/z* 536.1 $[Tp^*Cu(dmise)]^+$, 414.9 $[Cu(dmise)_2]^+$, 360.1 $[Tp^*Cu]^+$, 175.9 $[dmise]^+$. Anal. Calc. for $CuC_{20}BH_{30}N_8Se$: C, 46.04; N, 20.45; H, 5.52. Found: C, 45.05; N, 20.89; H, 5.69.

*[Tpm*Cu(dmise)][Cl] (**9**)*. The dmise ligand (176 mg, 1 mmol) was dissolved in acetonitrile (20 mL) and was cannula transferred to a solution of CuCl (99 mg, 1 mmol) in methanol (20 mL). The reaction mixture was stirred for 3 h at room temperature and an

equimolar amount of Tpm* (298 mg, 1 mmol) was dissolved in acetonitrile and cannula transferred into the reaction mixture and stirred for 18 h. The reaction mixture was pumped down to ~5 mL and the target product was precipitated using ether. The precipitate was dried *in vacuo* to yield a white powder. Yield 52% (297 mg, 0.52 mmol). ^{1}H NMR (CD_2Cl_2): 2.26 (s, 9H, $3CH_3$), 2.32 (s, 9H, $3CH_3$), 3.75 (s, 6H, $2CH_3$ [dmise]), 5.97 (s, 3H, 3CH [Pz]), 6.97 (s, 2H, 2CH [dmise]), 7.87 (s, 1H, CH). $^{13}C\{^{1}H\}$ NMR (CD_2Cl_2): 10.70 (CH_3), 13.37 (CH_3), 37.22 (CH_3 [dmise]), 106.99 (C-4 [Pz]), 119.98 (2CH [dmise]), 139.69 (C-3 [Pz]), 149.95 (C-5 [Pz]), 153.22 (C=Se). Mp: 256-258°C. IR (cm^{-1}): 628 s, 652 s, 700 vs, 705 vs, 738 s, 799 vs, 813 s, 850 vs, 900 vs, 975 vs, 1035 vs, 1098 w, 1150 s, 1240 vs, 1305 s, 1382 s, 1412 s, 1464 s, 1522 w, 1540 w, 1560 vs, 1653 s, 1733 s, 2338 w, 2361 w, 2936 b. UV-vis (CH_3CN): 273 nm. Mass spectrum (ESI-MS): *m/z* 537.1 $[Tpm*Cu(dmise)]^+$, 402.1 $[Tpm*Cu + MeOH]^+$, 361.1$[Tpm*Cu]^+$. Molar conductivity: 30.71 S cm^2 mol^{-1}. Anal. Calc. for $C_{21}H_{30}CuN_8SeCl$: C, 44.06; N, 19.57; H, 5.28. Found: C, 43.35; N, 19.43; H, 5.19.

*[Tpm*Cu(dmit)][Cl] (**10**)*. Complex **10** was prepared following the procedure for **9** except that dmit (129 mg, 1mmol) was used in place of dmise. Yield: 60% (315 mg, 0.60 mmol). ^{1}H NMR (CD_2Cl_2): 2.16 (s, 9H, $3CH_3$), 2.55 (s, 9H, $3CH_3$), 3.73 (s, 6H, $2CH_3$ [dmit]), 6.06 (s, 3H, 3CH [Pz]), 6.86 (s, 2H, 2CH [dmit]), 7.912 (s, 1H, CH). $^{13}C\{^{1}H\}$ NMR (CD_2Cl_2): 9.43 (CH_3), 12.04 (CH_3), 34.63 (CH_3 [dmit]), 68.59 (CH), 106.40 (C-4 [Pz]), 119.42 (CH [dmit]), 140.38 (C-3 [Pz]), 150.61 (C-5 [Pz]), 156.54 (C=S). IR (cm^{-1}): 630 s, 664 s, 670 s, 699 s, 706 s, 734 s, 749 s, 763 s, 817 s, 849 vs, 898 s, 977 s, 1035 s, 1087 s, 1181 b, 1240 s, 1306 s, 1387 b, 1465 b, 1521 s, 1567 s, 1623 b,

1653 b, 2915 b, 3074 b, 3105 b. Mp: 275-277ºC. UV-vis (CH_3CN): 273 nm. Mass spectrum (ESI-MS): *m/z* 489.1 $[Tpm^*Cu(dmit)]^+$, 402.1 $[Tpm^*Cu + MeOH]^+$, 361.1 $[Tpm^*Cu]^+$. Molar conductivity: 25.10 S cm^2 mol^{-1}. Anal. Calc. for $C_{21}H_{30}CuN_8SCl$: C, 47.91; N, 21.29; H, 5.71. Found: C, 47.65; N, 21.05; H, 5.69.

*[Tpm^{iPr}Cu(dmit)][Cl] (**11**).* Complex **11** was prepared following the procedure for **9** except that dmit (129 mg, 1 mmol) and Tpm^{iPr} (466 mg, 1 mmol) were used in place of dmise and Tpm*. Yield: 62% (430 mg, 0.62 mmol). ^{1}H NMR ($CDCl_3$): 1.22 (d, J_{HH} = 6 Hz, 36H, 6(CH_3)$_2$), 3.11 (sept, J_{HH} = 8.25 Hz, 3H, 3CH), 3.19 (br, 3H, 3CH), 3.70 (s, 6H, 2CH_3 [dmit]), 5.94 (s, 3H, 3CH [Pz]), 6.82 (s, 2H, 2CH [dmit]), 8.04(s, 1H, CH). ^{13}C{^{1}H} NMR ($CDCl_3$): 22.64 (CH(*CH_3*)$_2$), 23.13 (CH(*CH_3*)$_2$), 25.88 (CH(*CH_3*)$_2$), 27.73 (CH(*CH_3*)$_2$), 35.64 (CH_3 [dmit]), 63.43 (HC), 99.96 (4-C (Pz)), 118.58 (2CH_2 [dmit]), , 150.76 (3-C (Pz)), 159.5 (C=S), 160.09 (5-C (Pz)). IR (cm^{-1}): 670 vs, 691 s,722 vs, 747 vs, 763 vs, 797 vs, 806 s, 826 s, 861 s, 879 s, 903 s, 927 s, 961 s, 999 w, 1016 s, 1057 s, 1071 s, 1109 s, 1177 s, 1243 s, 1270 s, 1291 s, 1309 s, 1364 s,1380 s, 1465 w, 1552 s, 1571 s, 1621 s, 1656 b, 1729 s, 2722 b, 3038 b, 3079 s, 3104 s, 3148 s, 3196 b. Mp: 223-227°C. UV-vis (CH_3CN): 260 nm. Mass spectrum (ESI-MS): *m/z* 657.2 $[Tpm^{iPr}Cu(dmit)]^+$, 529.3 $[Tpm^{iPr}Cu]^+$, 319.0 $[Cu(dmit)_2]^+$, 232.0 [Cu-dmit + MeOH]$^+$, 191.0 [dmit-Cu]$^+$. Molar conductivity: 24.54 S cm^2 mol^{-1}. Anal. Calc. for $C_{33}H_{54}CuN_8SCl$: C, 57.14; N, 16.16; H, 7.79. Found: C, 56.40; N, 15.69; H, 7.88.

*[Tpm^{iPr}Cu(dmise)][Cl] (**12**).* Complex **12** was prepared following the above procedure for **9** except that Tpm^{iPr} (466 mg, 1 mmol) was used in place of Tpm*. Yield:

42% (311 mg, 0.42 mmol). ^{1}H NMR ($CDCl_3$): 1.22 (d, J_{HH} = 6 Hz, 36H, 6(CH_3)$_2$), 3.10 (sept, J_{HH} = 6 Hz, 3H, 3CH), 3.19 (sept, J_{HH} = 6 Hz, 3H, 3CH), 3.79 (s, 6H, 2CH_3 [dmise]), 5.94 (s, 3H, 3CH [Pz]), 6.98 (s, 2H, 2CH [dmise]), 8.04 (s, 1H, CH). ^{13}C{^{1}H} NMR ($CDCl_3$): 22.66 (CH(CH_3)$_2$), 23.13 (CH(CH_3)$_2$), 25.93 (CH(CH_3)$_2$), 27.72 (CH(CH_3)$_2$), 37.56 (CH_3 [dmise]), 71.1 (HC), 99.92 (4-CH [Pz]), 120.54 (2CH [dmise]), 150.81 (3-CH [Pz]), 152.03 (C=Se), 160.25 (5-CH [Pz]). IR (cm^{-1}): 668 vs, 722 vs, 740 vs, 752 vs, 797 vs, 806 s, 825 s, 860 s, 879 s, 903 s, 927 s, 1004 s, 1015 s, 1056 s, 1072 s, 1109 s, 1151 s, 1180 vs, 1234 s, 1270 vs, 1290 s, 1308 s, 1380 s, 1464 b, 1552 s, 1565 s, 1595 b, 1656 b, 2125 b, 3093 b, 3146 s. Mp: 234-236°C. UV-vis (CH_3CN): 205, 268 nm. Mass-spectrum (ESI-MS): *m/z* 705.2 [Tpm^{iPr}Cu(dmise)]$^{+}$, 570.3 [Tpm^{iPr}Cu + MeOH]$^{+}$, 529.2 [Tpm^{iPr}Cu]$^{+}$, 414.9 [Cu(dmise)$_2$]$^{+}$. Molar conductivities: 23.29 S cm^2 mol^{-1}. Anal. Calc. for $C_{33}H_{54}CuN_8SeCl$: C, 53.51; N, 15.14; H, 7.30. Found: C, 52.89; N, 15.21; H, 7.25.

X-ray Data Collection and Structural Determination. Single crystals grown from vapor diffusion were mounted on a glass filament with silicon grease and immediately cooled to 168 ± 2 K in a cold nitrogen gas stream. The crystals were grown by vapor diffusion of diethyl ether into an acetonitrile solution for [Tpm*Cu(dmise)][BF_4] (**1**) and [Tpm*Cu(dmit)][BF_4] (**2**); diethyl ether into a methanol solution for [TpmCu(dmise)][BF_4] (**3**) and [TpmCu(dmit)][BF_4] (**4**); diethyl ether into dichloromethane solution for [Tpm^{iPr}Cu(dmise)][BF_4] (**6**); and diethyl ether into a dichloromethane / methanol solution for Tp*Cu(dmit) (**7**) and Tp*Cu(dmise) (**8**). Intensity data were collected using a Rigaku Mercury CCD detector and an AFC8S

diffractometer. The space groups $P2_1/c$ for **1**, **2**, and **3**; $P2_12_12_1$ for **4**; $C2/c$ for **6** and $P2_1/m$ for **7** and **8** were determined from the observed systematic absences. Data reduction including the application of Lorentz and polarization (Lp) effects and absorption corrections used the CrystalClear program.[82] The structures were solved by direct methods and subsequent Fourier difference techniques, and refined anisotropically, by full-matrix least squares, on F^2 using SHELXTL 6.10.[83] The quantity minimized by the least square program was $\Sigma w = (F_o^2 - F_c^2)^2$ where $w = \{[\sigma^2(F_o^2)] + (0.0585P)^2 + 1.89P]\}$ for **1**, $w = \{[\sigma^2(F_o^2)] + (0.0843P)^2 + 1.58P]\}$ for **2**, $w = \{[\sigma^2(F_o^2)] + (0.0298P)^2 + 46.69P]\}$ for **3**, $w = \{[\sigma^2(F_o^2)] + (0.0469P)^2 + 0.34P]\}$ for **4**, $w = \{[\sigma^2(F_o^2)] + (0.0993P)^2 + 4.78P]\}$ for **6**, $w = \{[\sigma^2(F_o^2)] + (0.0619P)^2 + 0.93P]\}$ for **7**, $w = \{[\sigma^2(F_o^2)] + (0.0537P)^2 + 1.39P]\}$ for **8,** and $P = (Fo^2) + 2Fc^2)/3]$. In the final cycle of least and squares, independent anisotropic displacement factors were refined for the non-hydrogen atoms and the methyl hydrogen atoms were fixed in idealized positions with C-H = 0.96 Å. Their isotropic displacement parameters were set equal to 1.5 times U_{eq} of the attached carbon atom.

For complex **1,** the largest peak in the final Fourier difference map (0.81 $e \cdot A^{-3}$) was located 0.92 Å from F(2), and the lowest peak (-0.68 $e \cdot A^{-3}$) was located at a distance of 0.81 Å from Se. The largest peak for complex **2** in the final Fourier difference map (1.014 $e \cdot A^{-3}$) was located 0.02 Å from Cu, and the lowest peak (-0.676 $e \cdot A^{-3}$) was located at a distance of 0.76 Å from Cu. The largest peak for complex **3** in the final Fourier difference map (1.635 $e \cdot A^{-3}$) was located 0.29 Å from H(3AA), and the lowest peak (-0.740 $e \cdot A^{-3}$) was located at a distance of 0.80 Å from Se(1A). The largest peak for **4** in

the final Fourier difference map (0.77 $e \cdot A^{-3}$) was located 1.59Å from H(11A), and the lowest peak (-0.41 $e \cdot A^{-3}$) was located at a distance of 0.80 Å from Cu. The largest peak for **6** in the final Fourier difference map (0.94 $e \cdot A^{-3}$) was located 0.04 Å from Se(1), and the lowest peak (-0.60 $e \cdot A^{-3}$) was located at a distance of 0.89 Å from Se(1). The largest peak for **7** in the final Fourier difference map (0.583 $e \cdot A^{-3}$) was located 0.92 Å from H(20B), and the lowest peak (-0.628 $e \cdot A^{-3}$) was located at a distance of 0.11 Å from H(20A). The largest peak for **8** in the final Fourier difference map (0.71 $e \cdot A^{-3}$) was located 2.44 Å from H(13B), and the lowest peak (-0.51 $e \cdot A^{-3}$) was located at a distance of 0.81 Å from Se(1). Final refinement parameters for the structures of **1**, **2**, **3**, **4**, **6**, **7**, and **8** are given in Tables 2.10, 2.11, and 2.12. Crystal structure diagrams of the copper complexes are shown in Figures 2.3-2.5 and 2.7-2.10, and their crystal packing diagrams are shown in Figures 2.6 and 2.14-2.19.

Table 2.10. Summary of crystallographic data for complexes **1** and **2**.

	1	**2**
Chemical Formula	$C_{21}H_{30}BCuF_4N_8Se$	$C_{21}H_{30}BCuF_4N_8S$
F.W. (g/mol)	623.84	576.94
Space group	$P2_1/c$	$P2_1/c$
Crystal system	Monoclinic	Monoclinic
a, Å	12.199(2)	12.248(2)
b, Å	16.322(3)	16.233(3)
c, Å	13.043(3)	12.914(3)
α, °	90	90
β, °	93.54(3)	93.41(3)
γ, °	90	90
V, $Å^3$	2592.2(9)	2563.2(9)
Z	4	4
D_{cal}, Mg/m^3	1.598	1.495
Indices (min)	[-15, -20, -16]	[-15, -20, -16]
(max)	[12, 20, 15]	[13, 19, 16]
Parameters	333	333
F(000)	1264	1192
μ, mm^{-1}	2.302	0.990
2θ range,	2.50 - 26.71	3.01- 26.73
Collected reflections	21217	22159
Unique reflections	5472	5406
Final R (obs. Data)[a], R_1	0.0435	0.0508
wR_2	0.1101	0.1349
Final R (all data), R_1	0.0508	0.0557
wR_2	0.1163	0.1426
Goodness of fit (S)	1.110	1.098
Largest diff. Peak	0.808	1.014
Largest diff. Hole	-0.682	-0.676

[a] $R_1 = [\Sigma||F_0| - |F_c||]/ \Sigma|F_0|$; $wR_2 = \{[\Sigma w[(F_0)^2 - (F_c)^2]^2]\}^{1/2}$

Table 2.11. Summary of crystallographic data for complexes **3** and **4**.

	3	**4**
Chemical Formula	$C_{15}H_{18}BCuF_4N_8Se$	$C_{15}H_{18}BCuF_4N_8S$
F.W. (g/mol)	539.69	492.78
Space group	$P2_1/c$	*P2(1)2(1)2(1)*
Crystal system	Monoclinic	Orthorhombic
a, Å	10.176(2)	9.7241(19)
b, Å	17.734(3)	11.335(2)
c, Å	22.586(4)	18.262(4)
α, °	90	90
β, °	96.47(3)	90
γ, °	90	90
V, $Å^3$	4049.9(13)	2012.9(7)
Z	8	4
D_{cal}, Mg/m^3	1.770	1.626
Indices (min)	[-12, -21, -24]	[-8, -14, -23]
(max)	[11, 21, 26]	[12, 14, 23]
Parameters	546	274
F(000)	2144	1000
μ, mm^{-1}	2.932	1.245
2θ range,	2.96 – 25.05	2.76 – 26.72
Collected reflections	30276	16710
Unique reflections	7119	4255
Final R (obs. Data)[a], R_1	0.0692	0.0354
wR_2	0.1713	0.0845
Final R (all data), R_1	0.0741	0.0388
wR_2	0.1732	0.0871
Goodness of fit (S)	1.180	1.139
Largest diff. Peak	1.490	0.766
Largest diff. Hole	-0.619	-0.412

[a] $R_1 = [\Sigma||F_0| - |F_c||]/ \Sigma|F_0|$; $wR_2 = \{[\Sigma w[(F_0)^2 - (F_c)^2]^2]\}^{1/2}$

Table 2.12. Summary of crystallographic data for complexes **6**, **7**, and **8**.

	6	**7**	**8**
Chemical Formula	$C_{33}H_{54}BCuF_4N_8Se$	$C_{20}H_{30}BCuN_8S$	$C_{20}H_{30}BCuN_8Se$
F.W. (g/mol)	792.15	488.93	535.83
Space group	C2/*c*	$P2_1/m$	P21/*m*
Crystal system	Monoclinic	Monoclinic	Monoclinic
a, Å	23.822(5)	8.2925(17)	8.3319(17)
b, Å	16.733(3)	11.808(2)	11.771(2)
c, Å	19.931(4)	11.934(4)	12.082(2)
α, °	90	90	90
β, °	100.04(3)	91.32(3)	92.09(3)
γ, °	90	90	90
V, $Å^3$	7823(3)	1168.3(4)	1184.2(4)
Z	8	2	2
D_{cal}, Mg/m^3	1.345	1.390	1.503
Indices (min)	[-29, -20, -21]	[-10, -14, -14]	[-9, -14, -15]
(max)	[28, 20, 24]	[9, 14, 14]	[10, 14, 11]
Parameters	447	160	160
F(000)	3296	512	548
μ, mm^{-1}	1.541	1.048	2.483
2θ range,	2.43 – 26.32	3.02 – 26.74	3.02 – 26.29
Collected reflections	38614	11607	9538
Unique reflections	7938	2586	2494
Final R (obs. Data)[a], R_1	0.0628	0.0394	0.0383
wR_2	0.1619	0.1041	0.0953
Final R (all data)R_1	0.1023	0.0413	0.0465
wR_2	0.1969	0.1073	0.1021
Goodness of fit (S)	1.050	1.102	1.059
Largest diff. Peak	0.941	0.583	0.712
Largest diff. Hole	-0.598	-0.628	-0.513

[a] $R_1 = [\Sigma||F_0| - |F_c||]/ \Sigma|F_0|$; $wR_2 = \{[\Sigma w[(F_0)^2 - (F_c)^2]^2\}^{1/2}$

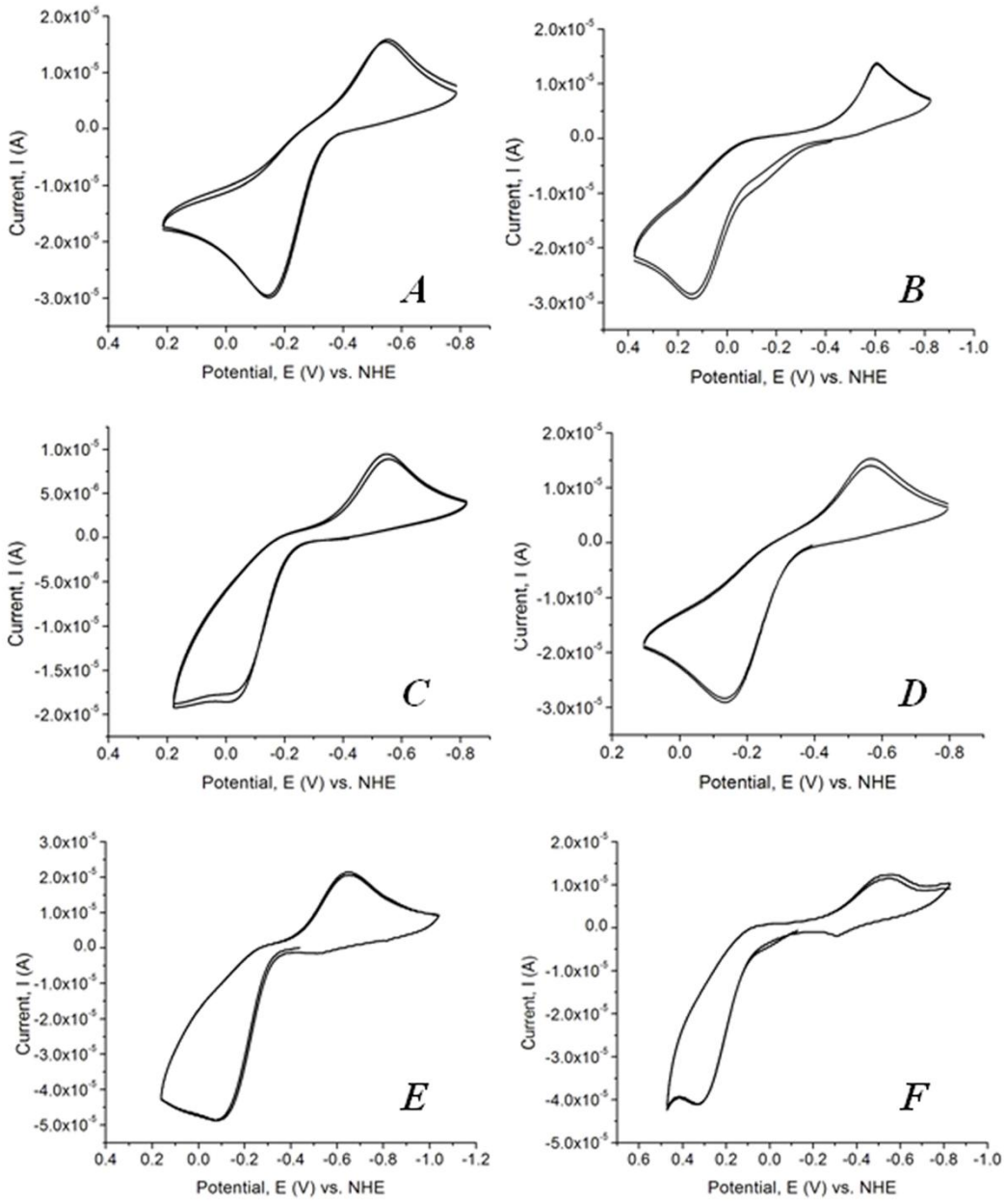

Figure 2.13. Cyclic voltammetry (CV) scans for A) Tp*Cu(dmise), B) Tp*Cu(dmit), C) [TpmCu(dmise)][BF_4], D) [TpmCu(dmit)][BF_4], E) [Tpm*Cu(dmise)][BF_4], F) [Tpm*Cu(dmit)][BF_4]. All data collected with 1 mM complex in acetonitrile. Potentials are reported versus NHE.

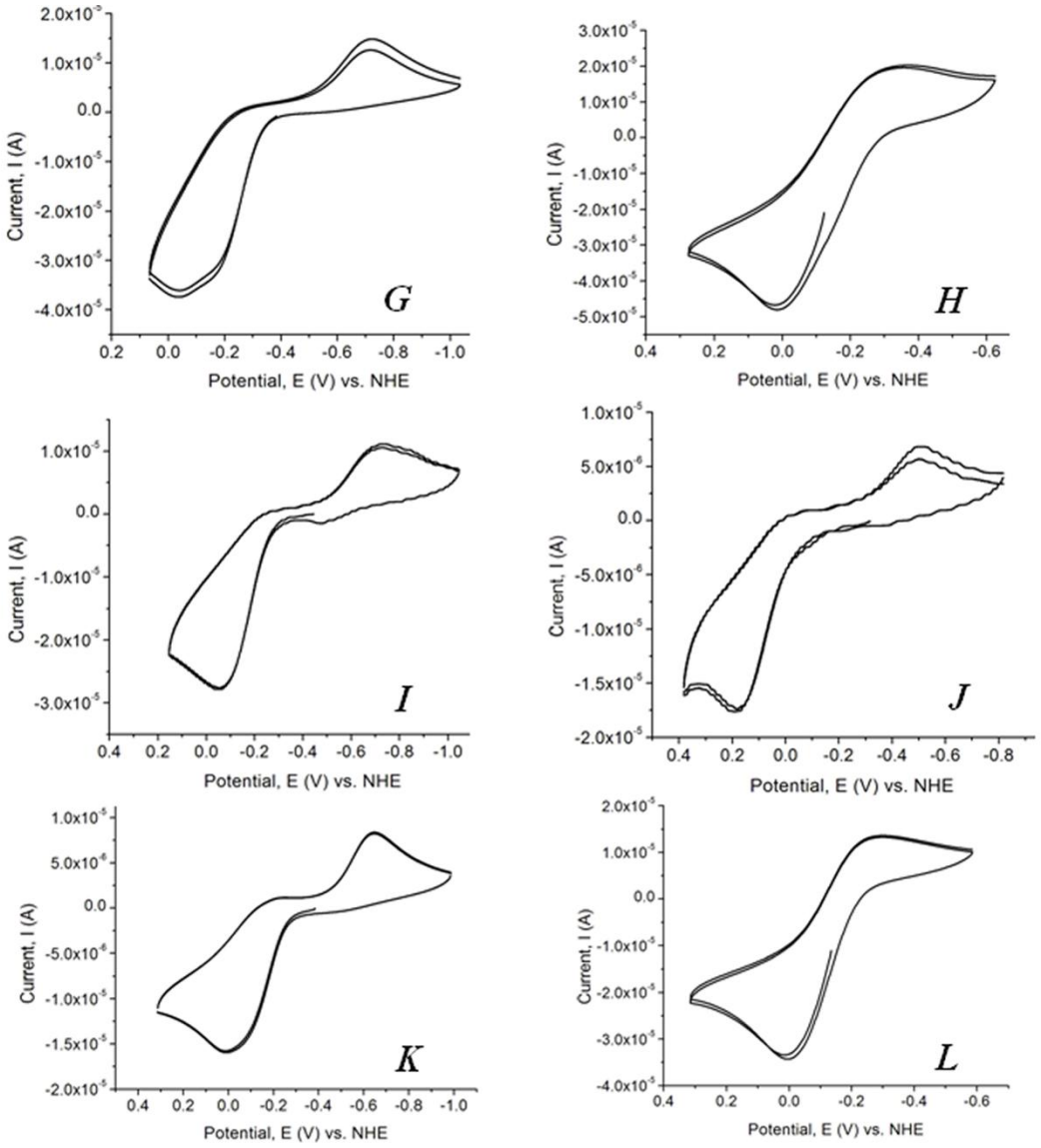

Figure 2.13 (cont.). Cyclic voltammetry (CV) scans for G) [Tpm*Cu(dmise)][Cl], H) [Tpm*Cu(dmit)][Cl], I) [Tpm^{iPr}Cu(dmise)][BF_4], J) [Tpm^{iPr}Cu(dmit)][BF_4], K) [Tpm^{iPr}Cu(dmise)][Cl], L) [Tpm^{iPr}Cu(dmit)][Cl]. All data collected with 10 mM complex in acetonitrile. Potentials are reported versus NHE.

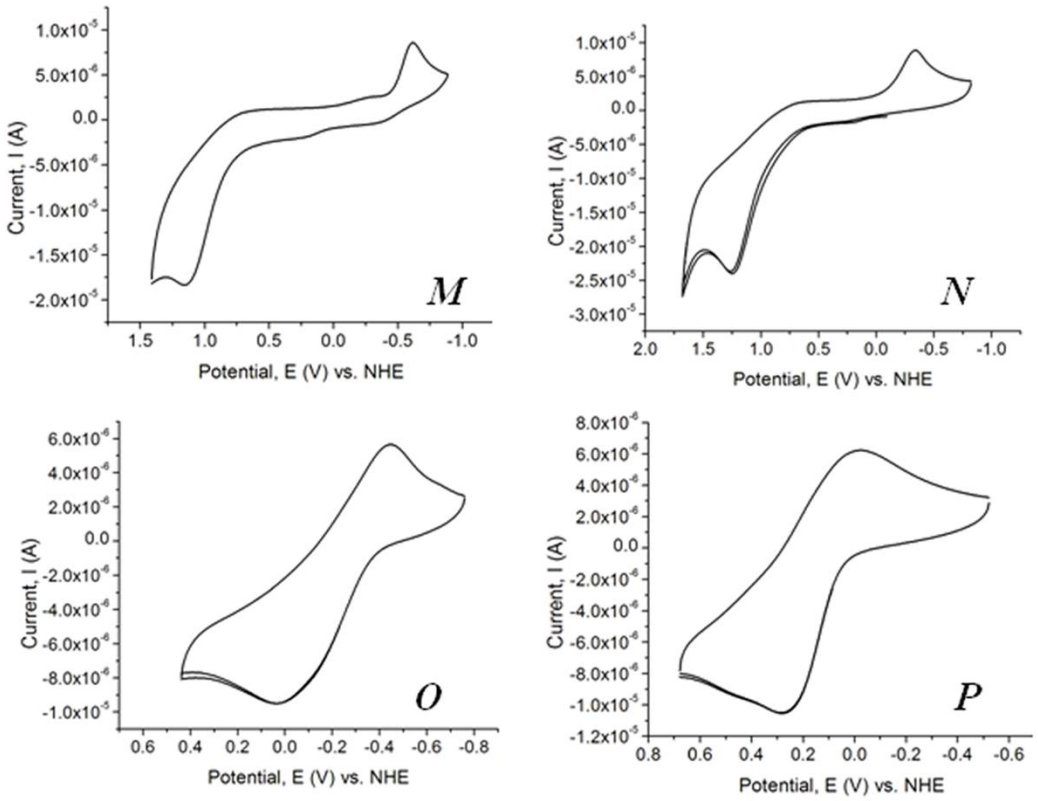

Figure 2.13 (cont.). Cyclic voltammetry (CV) scans for M) [Tpm*Cu(NCCH$_3$][BF$_4$], N) [Tpm^{iPr}Cu(NCCH$_3$][BF$_4$], O) Tpm*CuCl, P) Tpm^{iPr}CuCl. All data collected with 10mM complex in acetonitrile. Potentials are reported versus NHE.

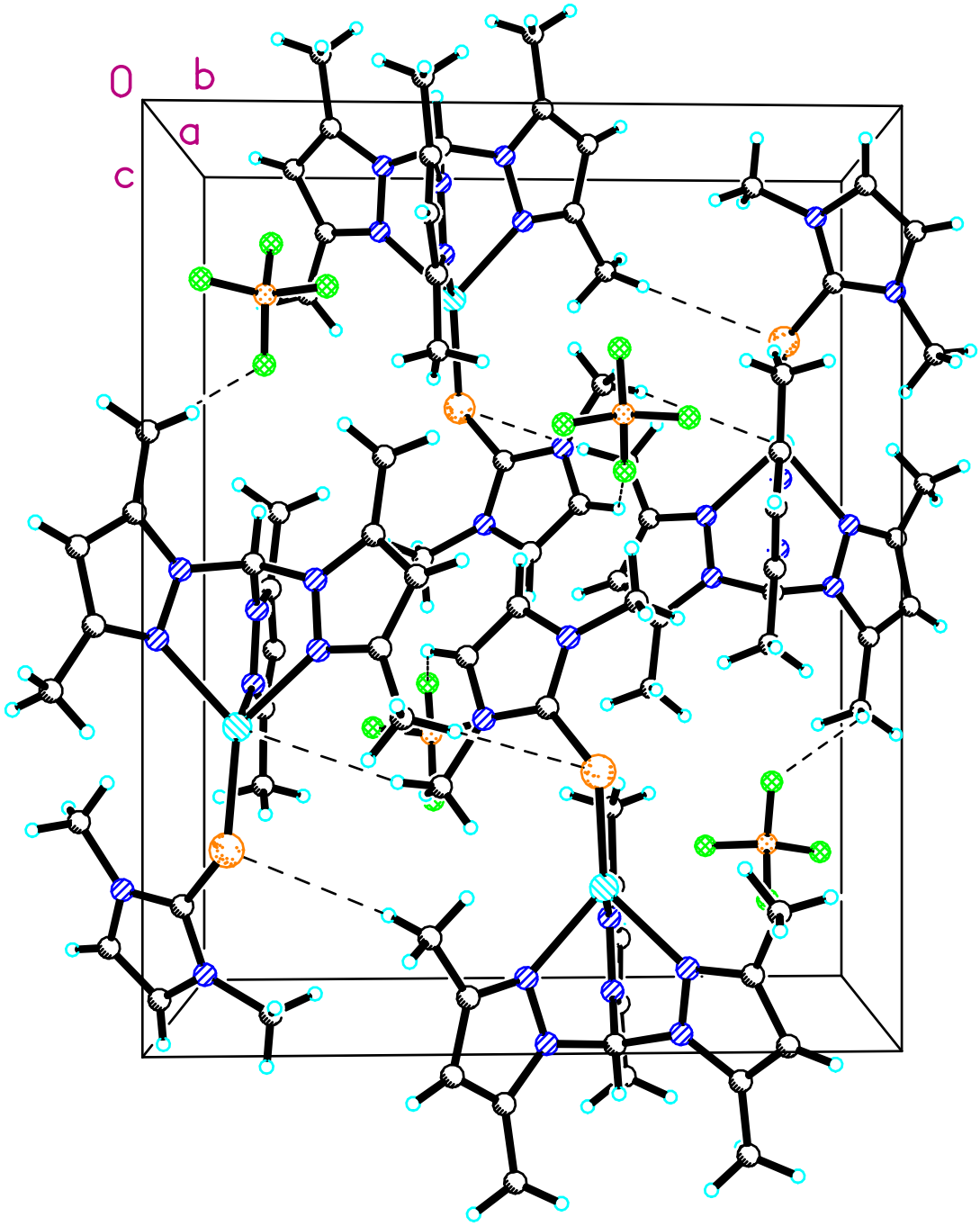

Figure 2.14. Crystal packing diagram of [Tpm*Cu(dmise)][BF_4] (**1**) at 50% probability density ellipsoids displaying H and F short contact interactions along the *a*-axis.

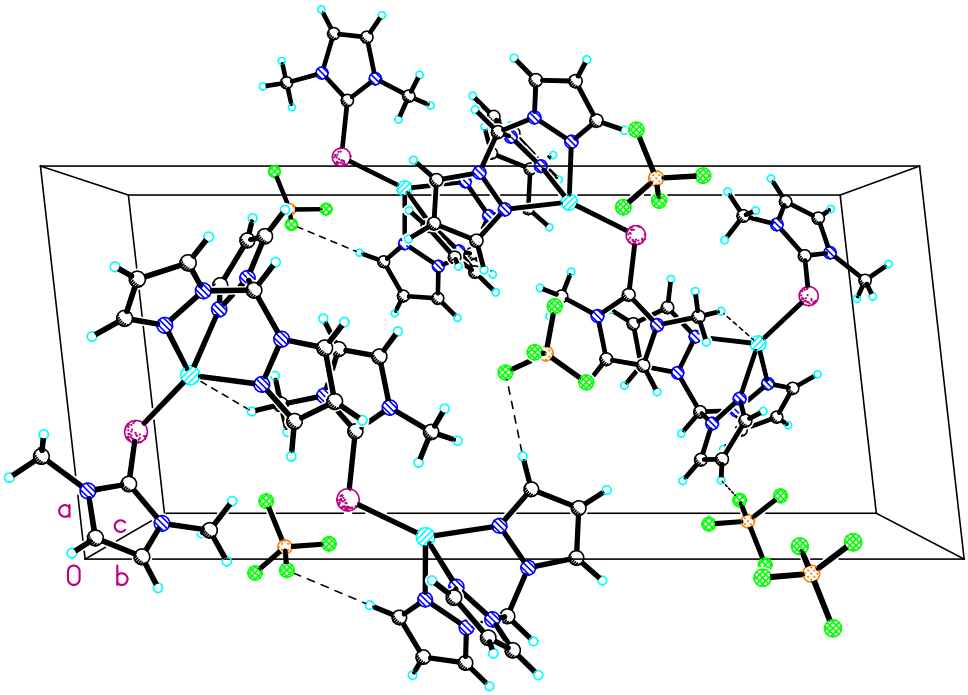

Figure 2.15. Crystal packing diagram of [TpmCu(dmise)][BF_4] (**3**) at 50% probability density ellipsoids displaying H and F short contact interactions along the *b*-axis.

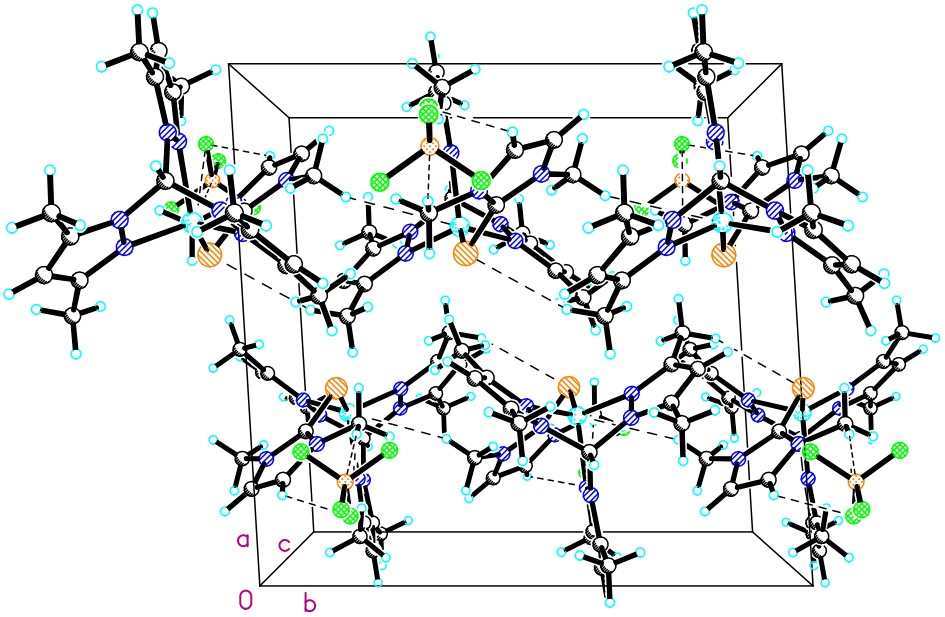

Figure 2.16. Crystal packing diagram of [Tpm*Cu(dmit)][BF_4] (**2**) at 50% probability density ellipsoids displaying H and F short contact interactions along the *b*-axis.

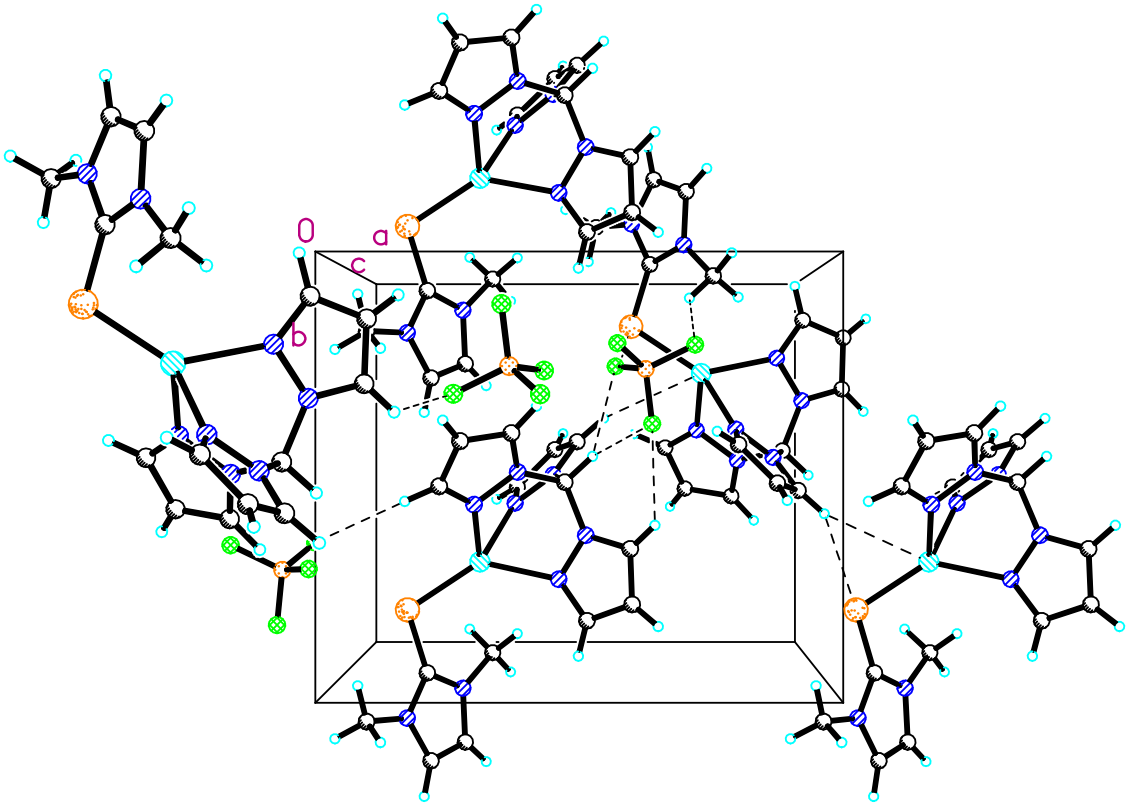

Figure 2.17. Crystal packing diagram of [TpmCu(dmit)][BF_4] (**4**) at 50% probability density ellipsoids displaying H and F short contact interactions along the *c*-axis.

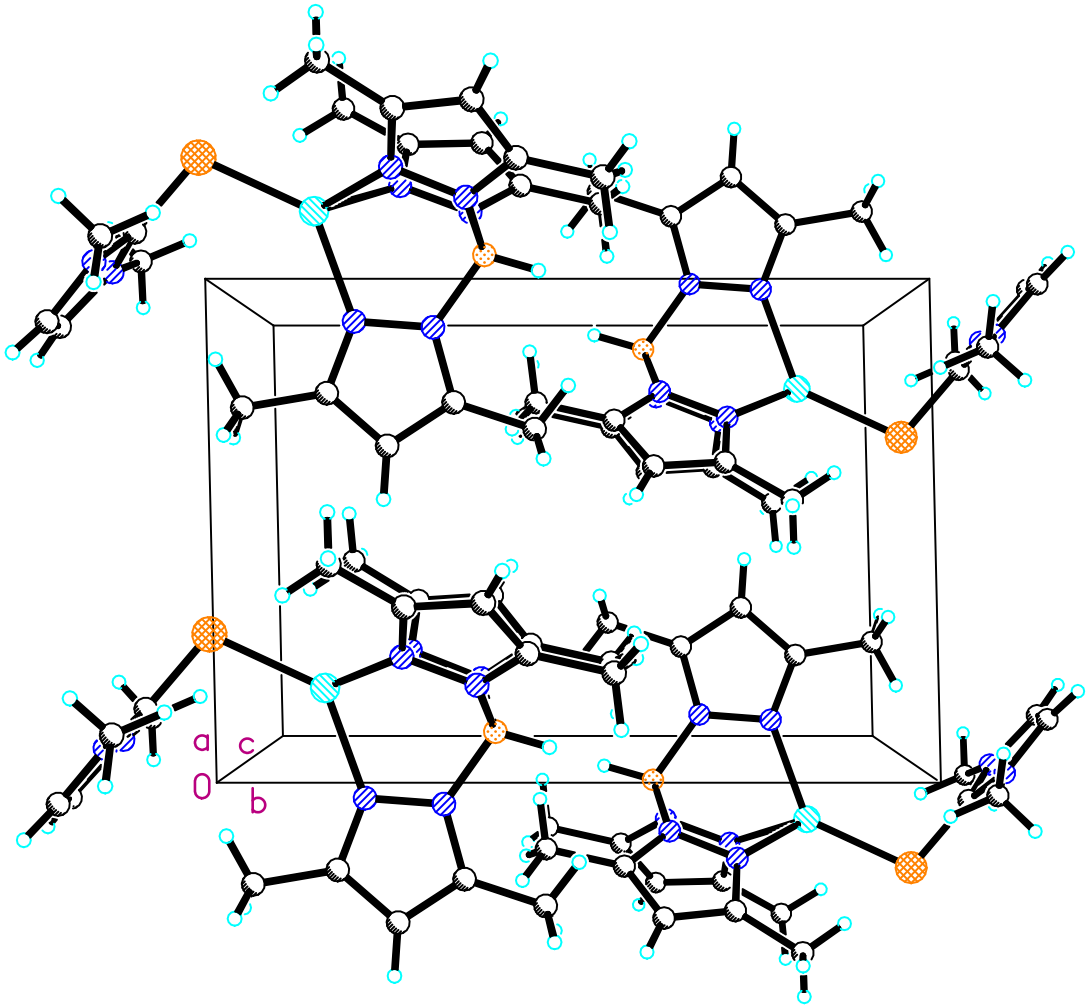

Figure 2.18. Crystal packing diagram of Tp*Cu(dmit) (**7**) at 50% probability density ellipsoids along the *b*-axis.

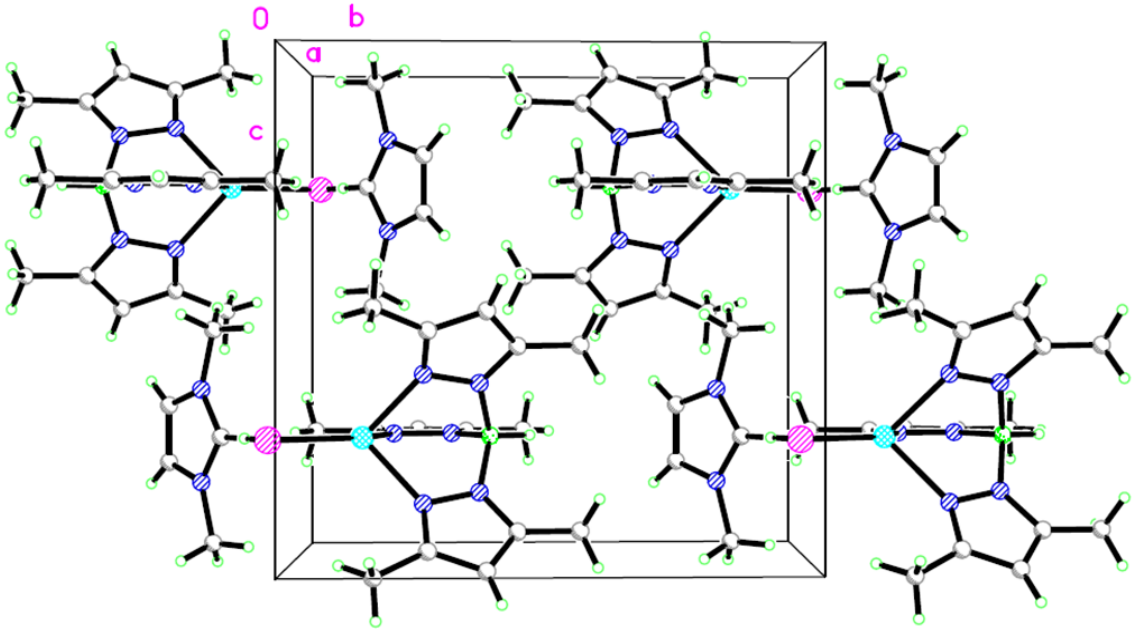

Figure 2.19. Crystal packing diagram of Tp*Cu(dmise) (**8**) at 50% probability density ellipsoids along the *a*-axis.

References

(1) Honglain, S.; Laurie, G. H.; Ke, J. L. *Free Rad. Biol. Med.* **2004**, *37*, 582-593.

(2) Stohs, S. J.; Bagchi, D. *Free Rad. Biol. Med.* **1995**, *18*, 321-336.

(3) De Flora, S.; Izzotti, A. *Mutat. Res.-Fundam. Mol. Mech. Mutagen.* **2007**, *621*, 5-17.

(4) Evans, M. D.; Dizdaroglu, M.; Cooke, M. S. *Mutat. Res.-Rev. Mutat. Res* **2004**, *567*, 1-61.

(5) Battin, E. E.; Brumaghim, J. L. *Cell Biochem. Biophys.* **2009**, *55*, 1-23.

(6) Schrauzer, G. N. *J. Am. Coll. Nutr.* **2001**, *20*, 1-4.

(7) Tapiero, H.; Townsend, D. M.; Tew, K. D. *Biomed. Pharmacother.* **2003**, *57*, 134-144.

(8) Battin, E. E.; Perron, N. R.; Brumaghim, J. L. *Inorg. Chem.* **2006**, *45*, 499-501.

(9) Ramoutar, R. R.; Brumaghim, J. L. *J. Inorg. Biochem.* **2007**, *101*, 1028-1035.

(10) Battin, E. E.; Brumaghim, J. L. *J. Inorg. Biochem.* **2008**, *102*, 2036-2042.

(11) Mugesh, G.; Singh, H. B. *Chem. Soc. Rev.* **2000**, *29*, 347-357.

(12) Trofimenko, S. *Chem. Rev.* **1993**, *93*, 943-980.

(13) Field, D. L.; Messerle, B. A.; Soler, L. P.; Hambley, T. W.; Turner, P. *J. Organomet. Chem.* **2002**, *655*, 146-157.

(14) Cooper, D. S. *N. Engl. J. Med.* **2005**, *352*, 905-917.

(15) Ey, J.; Schomig, E.; Taubert, D. *J. Agric. Food Chem.* **2007**, *55*, 6466-6474.

(16) Yamashita Y.; Yamashita M. *J. Biol. Chem.* **2010**, *285*, 18134-18138.

(17) Lobana, T. S.; Sharma, R.; Butcher, R. J. *Z. Anorg. Allg. Chem.* **2008**, *634*, 1785-1790.

(18) Raper, E. S. *Coord. Chem. Rev.* **1985**, *61*, 115-184.

(19) Akrivos, P. D. *Coord. Chem. Rev.* **2001**, *213*, 181-210.

(20) Spicer, M. D.; Reglinski, J. *Eur. J. Inorg. Chem.* **2009**, 1553-1574.

(21) Pattinari C. *Scorpionates II: Chelating Borate ligands dedicated to Swiatoslaw Trofimenko*; Imperial College Press: London, 2008, p. 381-415.

(22) Bigoli, F.; Demartin, F.; Deplano, P.; Devillanova, F. A.; Isaia, F.; Lippolis, V.; Mercuri, M. L.; Pellinghelli, M. A.; Trogu, E. F. *Inorg. Chem.* **1996**, *35*, 3194-3201.

(23) Williams, D. J.; McKinney, B. J.; Baker, B.; Gwaltney, K. P.; VanDerveer, D. *J. Chem. Crystallogr.* **2007**, *37*, 691-694.

(24) Williams, J. D.; Concepcion, J. J.; Koether, M. C.; Arrowood, A. K.; Carmack, A. L.; Hamilton, T. G.; Luck, S. M.; Ndomo, M.; Teel, R. C.; VanDerveer, D. *J. Chem. Crystallogr.* **2006**, *36*, 453-457.

(25) Williams, D. J.; White, K. M.; VanDerveer, D.; Wilkinson, A. P. *Inorg. Chem. Commun.* **2002**, *5*, 124-126.

(26) Williams, D. J.; Jones, T. A.; Rice, E. D.; Davis, K. J.; Ritchie, J. A.; Pennington, W. T.; Schimek, G. L. *Acta Crystallogr. Sect. C-Cryst. Struct. Commun.* **1997**, *53*, 837-838.

(27) Williams, D. J.; Fawcett, M. R. B.; Raye, R. R.; VanDerveer, D.; Pang, Y. T.; Jones, R. L.; Bergbauer, L. K. *Heteroatom Chem.* **1993**, *4*, 409-413.

(28) Patel, D. V.; Mihalcik, D. J.; Kreisel, K. A.; Yap, G. P.; Zakharov, L. N.; Kassel, W. S.; Rheingold, A. L.; Rabinovich, D. *Dalton Trans.* **2005**, 2410-2416.

(29) Maffett, L. S.; Gunter, K. L.; Kreisel, K. A.; Yap, G. P. A.; Rabinovich, D. *Polyhedron* **2007**, *26*, 4758-4764.

(30) Landry, V. K.; Buccella, D.; Pang, K. L.; Parkin, G. *Dalton Trans.* **2007**, 866-870.

(31) Parkin, G. *New J. Chem.* **2007**, *31*, 1996-2014.

(32) Lobana, T. S.; Castineiras, A. *Polyhedron* **2002**, *21*, 1603-1611.

(33) Kim, H. R.; Jung, I. G.; Yoo, K.; Jang, K.; Lee, E. S.; Yun, J.; Son, S. U. *Chem. Commun.* **2010**, *46*, 758-760.

(34) Aslanidis, P.; Hadjikakou, S. K.; Karagiannidis, P.; Cox, P. J. *Inorg. Chim. Acta* **1998**, *271*, 243-247.

(35) Devillanova, F. A.; Diaz, A.; Isaia, F.; Verani, G. *Transition Met. Chem.* **1989**, *14*, 153-154.

(36) Blake, A. J.; Lippolis, V.; Pivetta, T.; Verani, G. *Acta. Crystallogr. C* **2007**, *63*, m364-367.

(37) Minoura, M.; Landry, V. K.; Melnick, J. G.; Pang, K. L.; Marchio, L.; Parkin, G. *Chem. Commun.* **2006**, 3990-3992.

(38) Battin, E. E.; Ramoutar, R. R.; Quarles, C.; Zimmerman, M. T.; Brumaghim, J. L., in preparation.

(39) Collins, C. A.; Fry, F. H.; Holme, A. L.; Yiakouvaki, A.; Al-Qenaei, A.; Pourzand, C.; Jacob, C. *Org. Biomol. Chem.* **2005**, *3*, 1541-1546.

(40) Fujisawa, K.; Ono, T.; Ishikawa, Y.; Amir, N.; Miyashita, Y.; Okamoto, K.; Lehnert, N. *Inorg. Chem.* **2006**, *45*, 1698-1713.

(41) Beheshti, A.; Clegg, W.; Nobakht, V.; Mehr, M. P.; Russo, L. *Dalton Trans.* **2008**, 6641-6646.

(42) Popovic, Z.; Pavlovic, G.; Matkovic-Calogovic, D.; Soldin, Z.; Rajic, M.; Vikic-Topic, D.; Kovacek, D. *Inorg. Chim. Acta.* **2000**, *306*, 142-152.

(43) Bierbach, U.; Hambley, T. W.; Farrell, N. *Inorg. Chem.* **1998**, *37*, 708-716.

(44) Takeda, N.; Tanaka, Y.; Sakakibara, F.; Unno, M. *Bull. Chem. Soc. Jpn.* **2010**, *83*, 157-164.

(45) Parker, L. L.; Lacy, S. M.; Farrugia, L. J.; Evans, C.; Robins, D. J.; O'Hare, C. C.; Hartley, J. A.; Jaffar, M.; Stratford, I. J. *J. Med. Chem.* **2004**, *47*, 5683-5689.

(46) Balili, M. N. C.; Pintauer, T. *Acta Crystallogr. Sect. E.-Struct Rep. Online* **2007**, *63*, M988-M990.

(47) Swanson, B.; Shriver, D. F.; Ibers, J. A. *Inorg. Chem.* **1969**, *8*, 2182-2189.

(48) Williams, D. J.; Ly, T. A.; Mudge, J. W.; Vanderveer, D.; Jones, R. L. *Inorg. Chim. Acta* **1994**, *218*, 133-138.

(49) Landry, V. K.; Minoura, M.; Pang, K. L.; Buccella, D.; Kelly, B. V.; Parkin, G. *J. Am. Chem. Soc.* **2006**, *128*, 12490-12497.

(50) Jia, W. G.; Huang, Y. B.; Lin, Y. J.; Wang, G. L.; Jin, G. X. *Eur. J. Inorg. Chem.* **2008**, 4063-4073.

(51) Reger, D. L.; Collins, J. E. *Organometallics* **1996**, *15*, 2029-2032.

(52) Ribas, X.; Dias, J.; Morgado, J.; Wurst, K.; Almeida, M.; Veciana, J.; Rovira, C. *Cryst. Eng. Comm.* **2002**, *4*, 564-567.

(53) Ohlmann, C. M.; Marchland, C. M.; Schonberg, H. *Z. Anorg. Allg. Chem.* **1996**, *622*, 1349-1357.

(54) Black, J. R.; Champness, N. R.; Levason, W.; Reid, G. *Inorg. Chem.* **1996**, *35*, 1820-1824.

(55) Booth, D. G.; Levason, W.; Quirk, J. J.; Reid, G.; Smith, S. M. *J. Chem. Soc., Dalton Trans.* **1997**, 3493-3500.

(56) Devillanova, F. A.; Verani, G.; Battaglia, L. P.; Corradi, B. A. *Transition Met. Chem.* **1980**, *5*, 362-364.

(57) Lobana, T. S.; Sharma, R.; Butcher, R. J. *Z. Anorg. Allg. Chem.* **2008**, *634*, 1785-1790.

(58) Basumallick, L.; George, S. D.; Randall, D. W.; Hedman, B.; Hodgson, K. O.; Fujisawa, K.; Solomon, E. I. *Inorg. Chim. Acta* **2002**, *337*, 357-365.

(59) Kitajima, N.; Fujisawa, K.; Fujimoto, C.; Moro-oka, Y.; Hashimoto, S.; Kitagawa, T.; Toriumi, K.; Nakamura, A. *J. Am. Chem. Soc.* **1992**, *114*, 1277-1291.

(60) Hsu, S. C. N.; Chen, H. H. Z.; Lin, I.; Liu, J.; Chen, P. *J. Organomet. Chem.* **2007**, *692*, 3676-3684.

(61) Thompson, J. S.; Marks, T. J.; Ibers, J. A. *J. Am. Chem. Soc.* **1975**, *101*, 4180-4192.

(62) Tomlin, D. W.; Campbell, D. P.; Fleitz, P. A.; Adams, W. W. *Acta Cryst.* **1997**, *C53*, 1153-1154.

(63) Isab, A. A.; Wazeer, M. I. M.; Mohammed Fettouhi, M.; Ahmad, S.; Ashraf, W. *Polyhedron* **2006**, *25*, 2629-2636.

(64) Isab, A. A.; Wazeer, M. I.; Ashraf, W. *Spectrochim. Acta A, Mol. Biomol. Spectrosc.* **2009**, *72*, 218-221.

(65) Giles, G. I.; Tasker, K. M.; Johnson, R. J. K.; Jacob, C.; Peers, C.; Green, K. N. *Chem. Commun.* **2001**, 2490-2491.

(66) Giles, G. I.; Fry, F. H.; Tasker, K. M.; Holme, A. L.; Peers, C.; Green, K. N.; Klotz, L. O.; Sies, H.; Jacob, C. *Org. Biomol. Chem.* **2003**, *1*, 4317-4322.

(67) Falcomer, V. A. S.; Lemos, S. S.; Batista, A. A.; Ellena, J.; Castellano, E. E. *Inorg. Chim. Acta* **2006**, *359*, 1064-1070.

(68) Kogerler, P.; Williams, P. A. M.; Parajon-Costa, B. S.; Baran, E. J.; Lezama, L.; Rojo, T.; Muller, A. *Inorg. Chim. Acta.* **1998**, *268*, 239-248.

(69) Lee, D. H.; Hatcher, L. Y. Q.; Vance, M. A.; Sarangi, R.; Milligan, A. E.; Sarjeant, A. A. N.; Incarvito, C. D.; Rheingold, A. L.; Hodgson, K. O.; Hedman, B.; Solomon, E. I.; Karlin, K. D. *Inorg. Chem.* **2007**, *46*, 6056-6068.

(70) Balamurugan, R.; Palaniandavar, M.; Gopalan, R. S. *Inorg. Chem.* **2001**, *40*, 2246-2255.

(71) Bhabak, K. P.; Mugesh, G. *Chem. Eur. J.* **2010**, *16*, 1175-1185.

(72) Zimmerman, M. T.; Kimani, M. M.; Brumaghim, J. L., in preparation.

(73) Pierre, J. L.; Fontecave, M. *BioMetals* **1999**, *12*, 195-199.

(74) Trofimenko, S. *J. Am. Chem. Soc.* **1967**, *89*, 3170-3177.

(75) Roy, G.; Das, D.; Mugesh, G. *Inorg. Chim. Acta* **2007**, *360*, 303-316.

(76) Kubas, G. J. *Inorg. Synth.* **1990**, *28*, 68-70.

(77) Reger, G. L.; Grattan, T. C.; Brown, K. J.; Little, C. A.; Lamba, J. J. S.; Rheingold, A. L.; Sommer, R. D. *J.Organomet. Chem.* **2000**, *607*, 120-128.

(78) *NMR and the Periodic Table*; Harris, R. K.; Mann, B. E., Eds.; Academic Press: London, 1978, p. 99.

(79) Matsuo, H.; Miyazaki, Y.; Takemura, H.; Matsuoka, S.; Sakashita, H.; Yoshimura, K. *Polyhedron* **2004**, *23*, 955-961.

(80) Odom, J. D.; Dawson, W. H.; Ellis, P. D. *J. Am. Chem. Soc.* **1979**, *101*, 5815-5823.

(81) Connelly, N. G.; Geiger, W. E. *Chem. Rev.* **1996**, *96*, 877-910.

(82) Crystalclear; The Woodlands: Texas, USA, 1999.

(83) Sheldrick, G. M.; Bruker Analytical X-ray Systems Inc.: Madison, WI, 2000.

CHAPTER THREE

REACTIVITY OF BIOLOGICALLY RELEVANT CHALCOGENONES AND THEIR Cu(I) COMPLEXES WITH H_2O_2: INSIGHTS INTO SELENIUM AND SULFUR ANTIOXIDANT ACTIVITY

Introduction

Hydrogen peroxide (H_2O_2) is a byproduct of respiration and is reduced by copper (I) in the Fenton-like reaction, resulting in the formation of the damaging hydroxyl radical (reaction 1).[1] Cellular reductants can reduce Cu^{2+} to Cu^{+}, making $^{\bullet}OH$ formation catalytic.[2] The generated $^{\bullet}OH$ causes cellular DNA damage and can be enhanced by genetic diseases such as Wilson's and Menkes disease that result in mis-regulation of copper levels.[3] Copper-generated hydroxyl radical has been implicated as an underlying cause of diabetes, amyotrophic lateral sclerosis, cancer, inflammatory and neurodegenerative diseases, and Alzheimer's disease.[4-7]

$$Cu^{+} + H_2O_2 \rightarrow Cu^{2+} + HO^{\bullet} + OH^{-} \quad (1)$$

Selenium and sulfur antioxidants can prevent or reduce oxidative DNA damage[8-11] and may be important in preventing stomach, colorectal and prostate cancers, although their mechanism of action is not fully understood.[12-15] Two major clinical trials (NPC and SELECT) showed conflicting results on the ability of selenium supplementation to prevent prostate cancer, emphasizing the need for additional research into selenium antioxidant mechanisms.[16,17] Our previous research has determined that

metal coordination is required for inhibition of copper- mediated DNA damage by sulfur, oxo-sulfur, and selenium compounds,[8,9,18-21] and this copper binding mechanism is different from traditional mechanisms such as radical scavenging or glutathione peroxidase-like activity. [22]

To determine how coordination to sulfur and selenium inhibits copper mediated oxidative damage, biologically relevant Cu^{+}-*N,N'*-dimethylimidazole selone (dmise) and thione (dmit) complexes with tris(pyrazolyl)methane ligands have been synthesized,[23] and their reactivities examined with H_2O_2. The heterocyclic chalcogenone ligands used in this study resemble selenoneine,[24] and ergothioneine,[25] naturally occurring selenium and sulfur antioxidants found in animals and plants. Previous studies have shown that coordination of selone and thione ligands to copper in $[Tpm^*CuX]^{+}$ (Tpm* = tris(3,5-dimethylpyrazolyl)methane; X = dmise or dmit) results in more negative $Cu^{2+/+}$ reduction potentials.[23] If similar complexes form *in vivo*, this lowered copper potential may prevent reduction of Cu^{2+} by cellular reductants such as NADH, preventing Cu^{+} regeneration and inhibiting catalytic generation of $^{\bullet}OH$.

In addition to altering $Cu^{2+/+}$ reduction potentials, sulfur and selenium may also prevent DNA damage by acting as sacrificial antioxidants by reacting with H_2O_2 directly, preventing copper generation of $^{\bullet}OH$. If this sacrificial reactivity occurs, it is expected that the more oxophilic selone will be a more effective antioxidant than the thione.[26] The sacrificial antioxidant ability of selone and thione ligands was investigated by treating dmise and dmit with H_2O_2. Similarly, $[Tpm^*Cu(dmise)]^{+}$ and $[Tpm^*Cu(dmit)]^{+}$

complexes were treated with H_2O_2 to determine whether the chalcogenone ligand or Cu^+ reacts preferentially with H_2O_2. If the chalcogenone ligands are more reactive with H_2O_2 than Cu^+, the bound selenium or sulfur ligand will hinder oxidation of the Cu^+ center to Cu^{2+}. Sacrificial oxidation of copper-bound sulfur and selenium ligands would represent an alternative antioxidant mechanism compared to prevention of copper redox cycling.

Results and Discussion

Oxidation of dmise and dmit. The oxidation of the dmise and dmit ligands was conducted by treating the chalcogenones compounds with one or two equiv of H_2O_2, respectively, in methanol under an argon atmosphere. ^{1}H NMR spectra of the untreated dmise and dmit ligands have two resonances corresponding to the methyl protons (δ 3.60 and δ 3.56, respectively) and olefinic protons (δ 7.04 and δ 6.90, respectively; Figures 3.1 and 3.2).

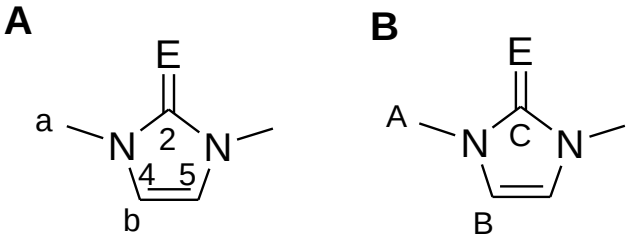

Figure 3.1. Structures of the heterocyclic chalcogenone ligands (E = S, dmit; E = Se, dmise) showing A) ^{1}H NMR resonance labels and B) ^{13}C{^{1}H} NMR resonance labels. Ring numbering is shown in A.

Upon treatment of dmise and dmit ligands with H_2O_2, the ^1H NMR spectra show shifted resonances that correspond to the methyl protons (δ 3.98 for both) and olefinic protons (δ 7.60 and δ 7.61 for dmise and dmit, respectively) along with the emergence of a new resonance at δ 8.91 (Figure 3.2). The methyl and olefinic protons of the H_2O_2-treated chalcogenone ligands are shifted downfield relative to untreated dmise and dmit. The new resonance at δ 8.91 suggests cleavage of the selenium or sulfur atom from the heterocyclic ring followed by hydrogen insertion. This new resonance at δ 8.90 is very similar to the H2 resonance of the 1,3-dimethylimidazolium cation.[27]

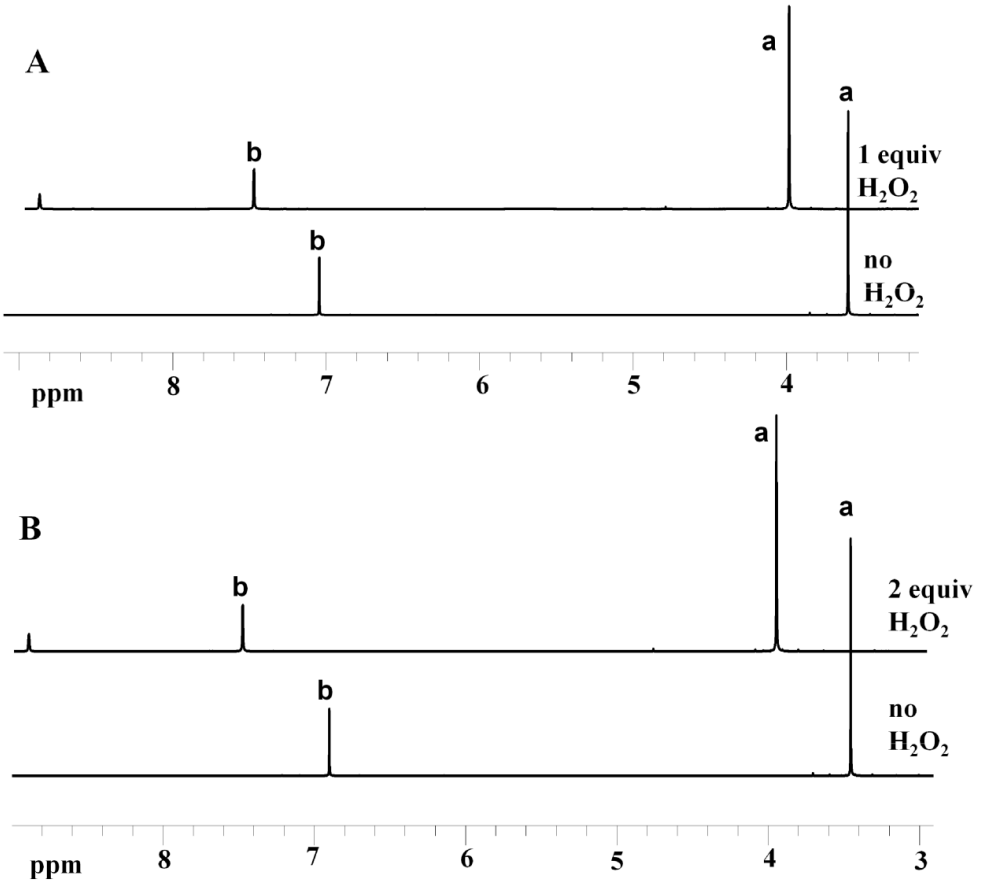

Figure 3.2. ^1H NMR spectra of A) dmise before and after treatment with 1 equiv H_2O_2, B) dmit before and after treatment with 2 equiv of H_2O_2.

The $^{13}C\{^{1}H\}$ NMR spectra of dmise and dmit show three resonances corresponding to the methyl carbons (δ 37.0 and δ 36.3, respectively), olefinic carbons (δ 120.5 and δ 119.2, respectively) and the quaternary carbon (δ 156.8 and 162.4, respectively; Figure 3.3). Upon treatment of dmise and dmit with H_2O_2, the $^{13}C\{^{1}H\}$ NMR resonances corresponding to the methyl carbons shift very little (δ 35.70 and δ 35.20, respectively). In contrast, the olefinic C-4 and C-5 carbons are slightly shifted downfield (δ 123.59 and δ 123.50, respectively), whereas the C-2 carbon is shifted upfield by about δ 20. This upfield shift of the C-2 carbon coupled with the ^{1}H NMR resonance at δ 8.90 indicates cleavage of the C=Se or C=S bonds from the heterocyclic rings and formation of the dimethylimidazolium cation.[26]

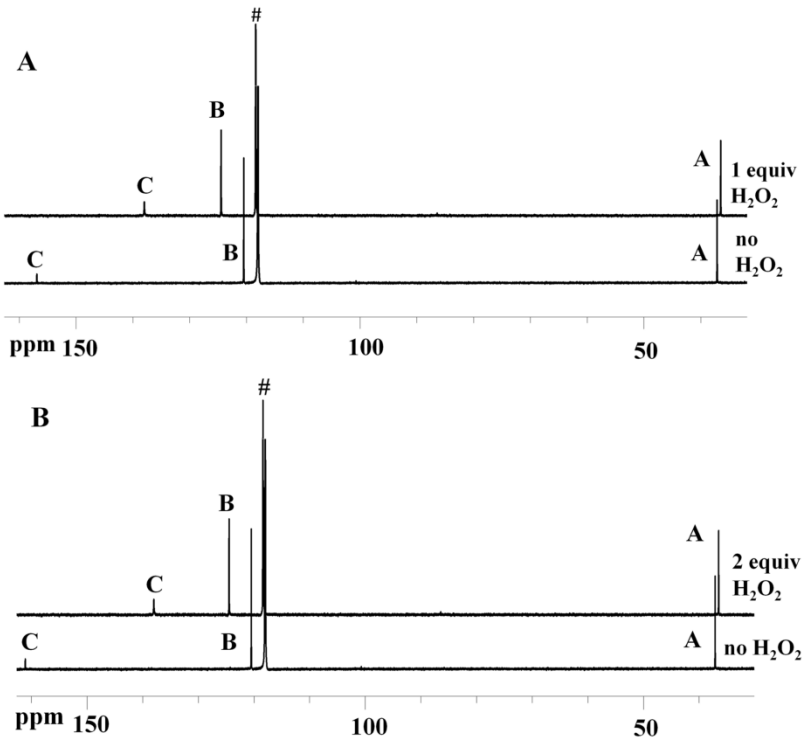

Figure 3.3. $^{13}C\{^{1}H\}$ NMR of A) dmise before and after treatment with 1 equiv H_2O_2 and B) dmit before and after treatment with 2 equiv H_2O_2. Solvent molecule labeled with the pound sign.

Electrospray ionization (ESI) mass spectra of the oxidized products obtained from the reaction of dmise or dmit with H_2O_2 confirm formation of the *N,N'*-dimethylimidazolium cation (*m/z* 97.071) as the major product in the positive ionization mode. Two oxidized sulfur products at *m/z* 96.99 $[SO_4H]^-$, 79.98 $[SO_3H]^-$ and one oxidized selenium product at *m/z* 112.96 $[SeO_2H]^-$ were identified in the negative ionization mode. The different oxidized species seen upon dmit and dmise oxidation may result from the higher concentration of H_2O_2 required for complete oxidation of dmit relative to dmise.

The identity of the oxidized selenium product was confirmed using $^{77}Se\{^1H\}$ NMR spectroscopy. The untreated dmise ligand has a selenium resonance at δ -29.5 in CD_3OD that shifts to δ 1345 upon treatment with 1 equiv H_2O_2 (Figure 3.4). A $^{77}Se\{^1H\}$ NMR resonance near δ 1345 is expected for the $[SeO_2H]^-$ ion.[20]

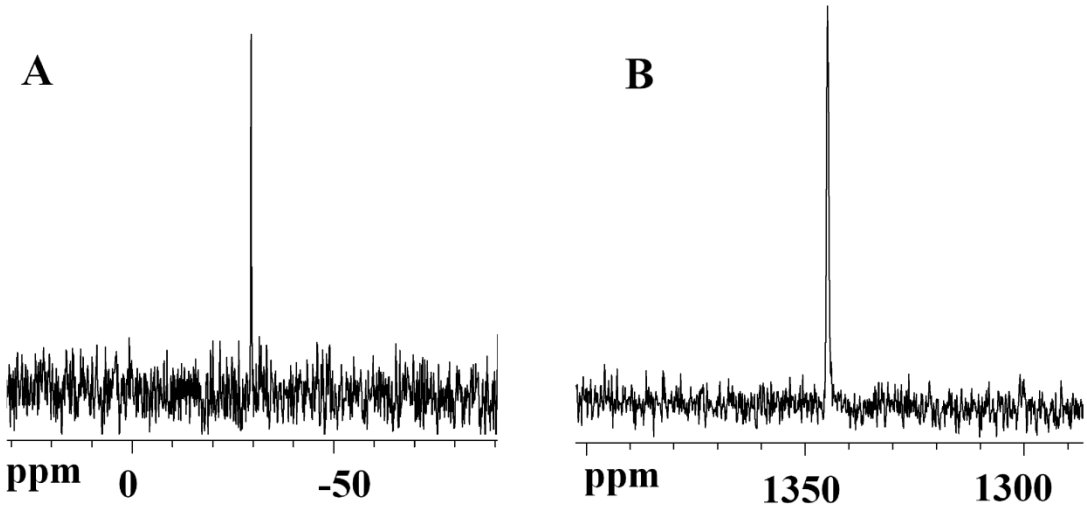

Figure 3.4. $^{77}Se\{^1H\}$ NMR spectra of A) dmise ligand and B) oxidized dmise ligand after reaction with H_2O_2.

Based on our experimental results, treatment of the chalcogenone ligands with H_2O_2 results in the oxidation and cleavage of selenium and sulfur atoms from the five-membered heterocyclic ring with the formation of the 1,3-dimethylimidazolium cation (Figure 3.5). Reactivity of dmise and dmit with the reactive oxygen species peroxynitrite has been investigated by Bhabak *et al.*[26] and the authors have determined that peroxynitrite oxidizes dmise and dmit to yield the 1,3-dimethylimidazolium cation and selenium and sulfur oxides, respectively. Elimination of the selenium and sulfur atoms from the five-membered rings occurs through formation of unstable selenic/sulfenic acids and seleninic/sulfinic acids. Theoretical DFT calculations conducted by our collaborator Dr. Craig Bayse (Old Dominion University) also suggest formation of unstable selenic/sulfenic and seleninic/sulfinic acid intermediates upon reaction of dmise or dmit with H_2O_2 leading to cleavage of C=Se or C=S bond.

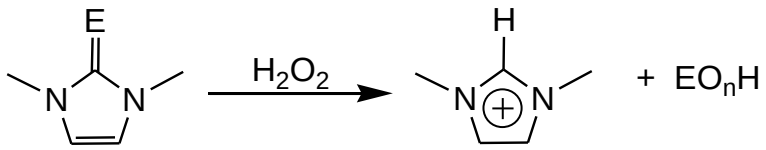

Figure 3.5. Reaction of dmise and dmit with H_2O_2 (E = Se, n = 2; E = S, n = 3, 4).

The higher oxophilicity of dmise relative to dmit is illustrated by the reactivity of this compound with H_2O_2. Upon reaction of dmise with 1 equiv of H_2O_2, the selenium atom is completely cleaved from the C-2 carbon, whereas the dmit ligand requires 2 equiv H_2O_2 to completely react. Thus, dmise is a more sensitive H_2O_2 scavenger compared to dmit and could prevent copper mediated oxidative damage by H_2O_2 more

effectively. These results are in agreement with results reported by Bhabak *et al*., indicating that selone containing compounds generally prevented more peroxynitrite mediated nitration of free tyrosine relative to analogous thione compounds.[26]

Reactivity of tris(3,5-dimethylpyrazolyl)methane Cu selone and thione complexes with H_2O_2. The tris(3,5-dimethylpyrazolyl)methane copper selone and thione complexes were treated with H_2O_2 to determine whether the Cu^+ or the chalcogenone atoms would preferentially react with H_2O_2. Acetonitrile solutions of the $[Tpm^*Cu(X)]^+$ (X = dmise or dmit) complexes were treated with 0.5, 1, and 2 molar equiv H_2O_2 for the selone complex or 1, 2, and 3 molar equiv H_2O_2 for the thione complex. ^1H NMR spectra of the oxidized $[Tpm^*Cu(X)]^+$ (X = dmise or dmit) copper complexes (Figure 3.6) show sharply-defined peaks, indicating that the diamagnetic Cu^+ center is not oxidized upon treatment with H_2O_2. The resonances corresponding to the tripodal Tpm* ligand do not shift upon H_2O_2 treatment, indicating that this reactive oxygen species only reacts with the dmise or dmit ligand.

The ^1H NMR spectra of the $[Tpm^*CuX]^+$ (X = dmise or dmit) copper complexes before treatment with H_2O_2 have dmise ligand resonances at δ 3.88 for the methyl protons and δ 7.17 for the olefinic protons, whereas the corresponding dmit resonances are observed at δ 3.87 and δ 7.00 respectively.[23] Upon treatment with H_2O_2, oxidized $[Tpm^*CuX]^+$ (X = dmise or dmit) copper complexes have dmise resonances at δ 3.86 for the methyl protons, δ 7.36 for the olefinic protons and a new resonance at δ 8.49 corresponding to an integration of one proton (Figure 3.6).

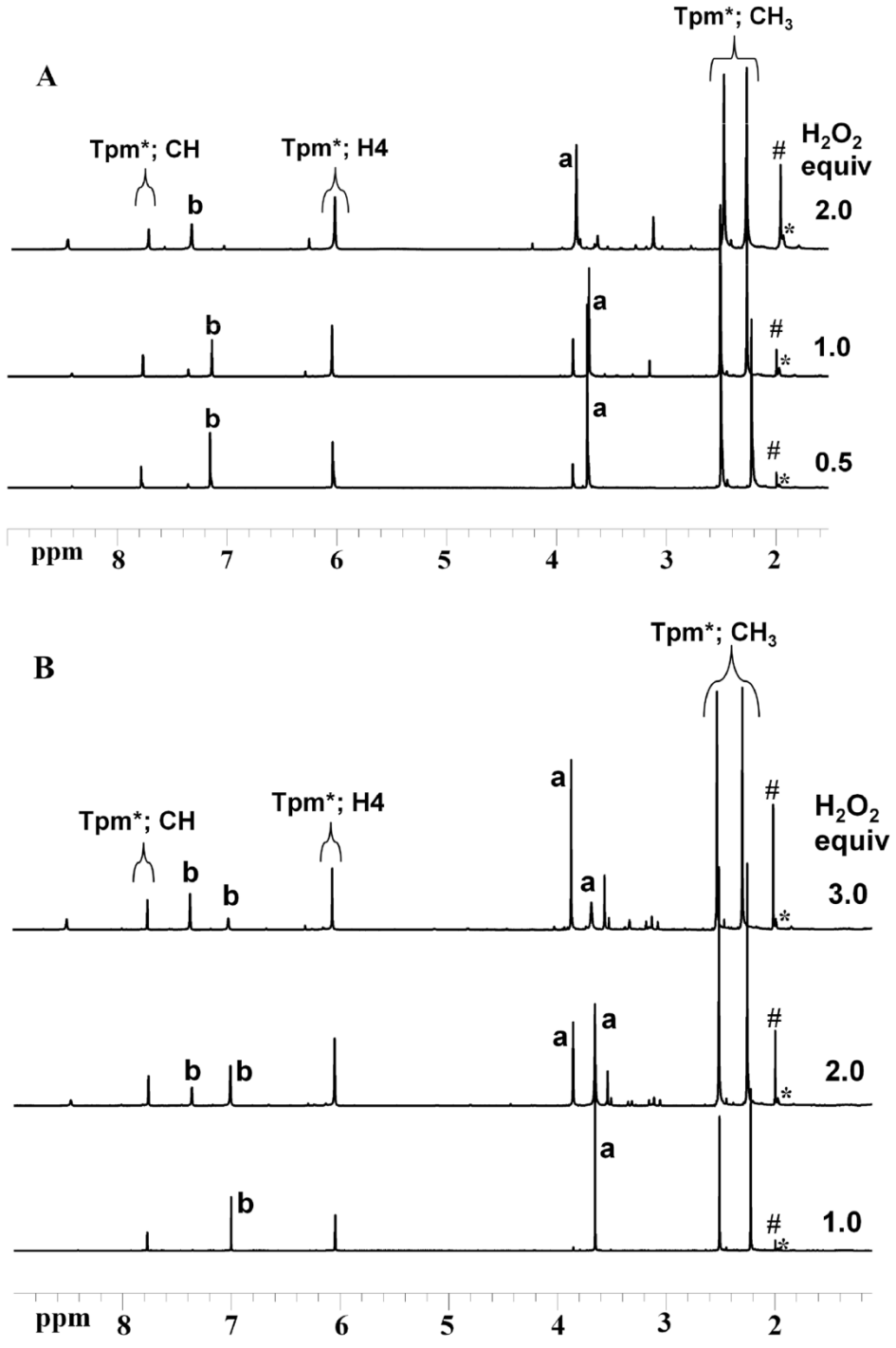

Figure 3.6. ^{1}H NMR spectra of A) [Tpm*Cu(dmise)][BF_4] upon treatment with 0.5, 1.0, and 2.0 equiv of H_2O_2 and B) [Tpm*Cu(dmit)][BF_4] upon treatment with 1.0, 2.0, and 3.0 equiv of H_2O_2. Solvent and H_2O resonances are labeled with an asterisk and pound sign respectively.

Upon similar oxidation, dmit resonances are observed at δ 3.85 for the methyl protons, δ 7.36 for the olefinic protons and a new resonance at 8.47 (Figure 3.6). The olefinic protons of the oxidized dmise and dmit ligands shift downfield relative to their resonances in the untreated copper selone or thione complexes.[23] This downfield shift upon oxidation coupled with the appearance of a new resonance ~ δ 8.48 indicates oxidation of the selenium and sulfur and formation of the 1,3-dimethylimidazolium cation, similar to the oxidation products of dmise and dmit. Complete oxidation of the selone ligand in $[Tpm^*Cu(dmise)]^+$ requires 2 equiv of H_2O_2, whereas the analogous copper-thione complex requires 3 equiv of H_2O_2 to completely react, indicating that the bound selone is more oxophilic relative to the bound thione. Both copper-bound selone and thione ligands sacrificially react with H_2O_2, and this reactivity prevents Cu^+ oxidation.

The ESI mass spectrometry data for the oxidized products obtained from the treatment of $[Tpm^*CuX]^+$ (X = dmise/dmit) complexes with H_2O_2 indicate formation of $[Tpm^*Cu(NCCH_3)]^+$ (*m/z* 402.12) and *N,N'*-dimethylimidazolium (*m/z* 97.071) in the positive ionization mode, corroborating ^1H NMR results. Negative ion ESI-MS results indicate several oxidized sulfur (*m/z* 79.98 $[SO_3H]^-$ and 96.99 $[SO_4H]^-$) and selenium products (112.96 $[SeO_2H]^-$). The different oxidized species arising from sulfur and selenium ligands may result from the higher concentration of H_2O_2 required for the complete oxidation of $[Tpm^*Cu(dmit)]^+$ complex (3 equiv H_2O_2) relative to $[Tpm^*Cu(dmise)]^+$ (2 equiv H_2O_2).

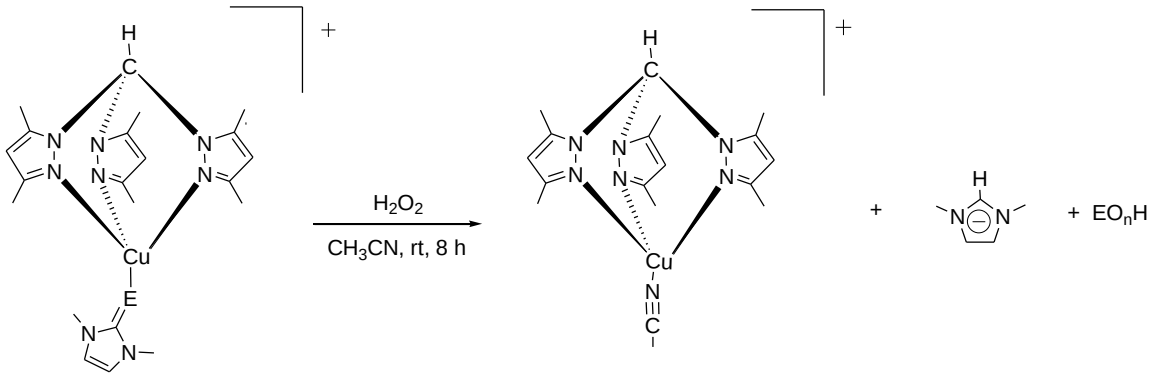

Figure 3.7. Reaction of $[Tpm^*CuX]^+$ (X = dmise or dmit) with H_2O_2 (E = Se, n = 2; E = S, n = 3, 4).

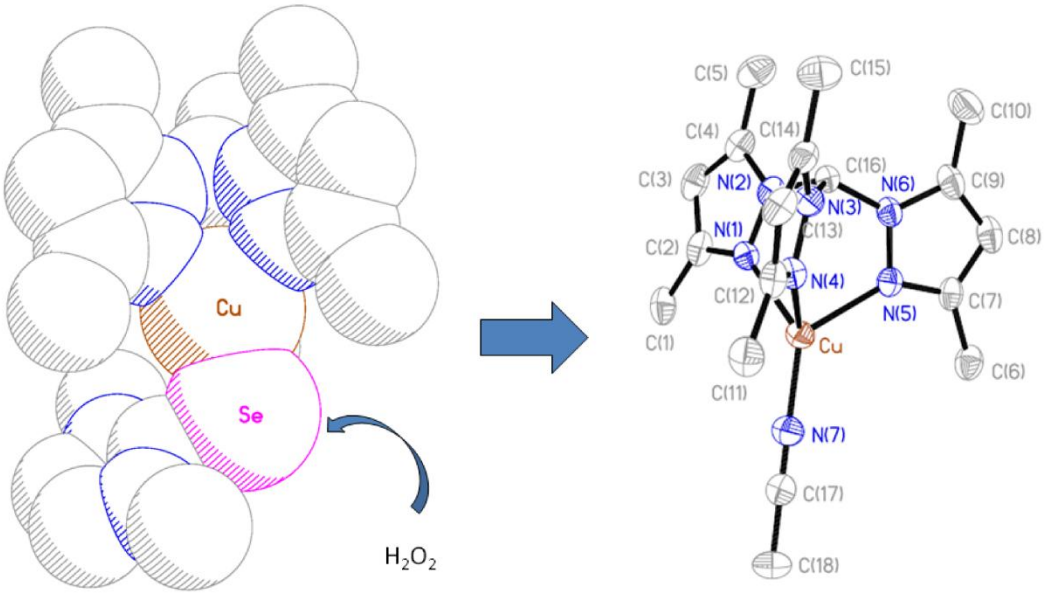

Figure 3.8. Space filling diagram of $[Tpm^*Cu(dmise)]^+$ and X-ray crystal structure of $[Tpm^*Cu(NCCH_3)]^+$ showing 50% probability density ellipsoids. Hydrogen atoms and counterions are omitted for clarity.

The overall reaction of $[Tpm^*CuX]^+$ (X = dmise or dmit) with H_2O_2 is given in Figure 3.7. Figure 3.8 reveals that both the Cu^+ center and selenium atoms are accessible for oxidation by H_2O_2, but H_2O_2 treatment preferentially oxidizes the chalcogenone

ligand without oxidation of the Cu^+ center. Similar to the results obtained in the oxidation of the unbound chalcogenones, dmise in $[Tpm^*Cu(dmise)]^+$ is a more sensitive H_2O_2 scavenger compared to dmit in $[Tpm^*Cu(dmit)]^+$. These results indicate that the copper selone complexes may prevent copper-mediated oxidative damage by H_2O_2 more effectively than their thione analogs.

Cu^+ complexes treated with O_2 and H_2O_2 form peroxo, side-on, end-on and oxo bridged dinuclear Cu^{2+} complexes.[28] Of particular interest is the reaction of $[Tpm^*Cu(NCCH_3)]^+$ with H_2O_2 that results in the formation of an oxo-bridged dicopper Tpm* complex, $[\{Tpm^*Cu(OH)\}_2]^{2+}$ with the oxidation of Cu^+ to Cu^{2+}.[29] The peroxo dicopper complexes previously obtained with tris(pyrazolyl)copper(I)-acetonitrile complexes and are usually characterized by formation of a deep purple solution at low temperatures,[30] a phenomenon that was absent in our system.

Treating $[Tpm^*CuX][BF_4]$ (X = dmise/dmit) with H_2O_2 in acetonitrile rresults in the formation of $[Tpm^*Cu(NCCH_3)][BF_4]$. The $[Tpm^*Cu(NCCH_3)][BF_4]$ complex can be independently synthesized from $[Cu(NCCH_3)_4][BF_4]$ and Tpm*,[31] but its structure has not been reported. The Cu^+ center in $[Tpm^*Cu(NCCH_3)][BF_4]$ (Figure 3.8) adopts distorted tetrahedral geometry, bound in a κ^3 fashion to three nitrogen atoms from the tridentate Tpm* ligand and terminally bound to an acetonitrile solvato ligand. The small bite angle of the Tpm* ligand results in pinning back of the nitrogen atoms upon coordination to copper, producing small N-Cu-N angles ranging from 85.9 to 89.9° (Table 3.1),[31] with Cu-N bond lengths of 2.08-2.09 Å. These C-N bond lengths and

N-Cu-N angles are comparable to other tris(pyrazolyl)methane copper(I) complexes such as [TpmCu(NCCH$_3$)][BF$_4$] (2.05-2.14 Å, 87.8º),[32] [Tpm*Cu(1,4-CNC$_6$H$_4$NC)][BF$_4$] (2.06-2.09 Å, 87.2º),[32] [Tpm$^{3\text{-}t\text{Bu}}$Cu(NCCH$_3$)][PF$_6$] (2.06-2.14 Å, 89.2º),[31] and [Tpm$^{i\text{Pr}}$Cu(CO)][PF$_6$] (avg. 2.05 Å, 88.1º).[33] The Cu-N bond distance of 1.87 Å for the terminal acetonitrile bond is comparable with previously reported Cu$^+$ acetonitrile complexes.[32,34,35]

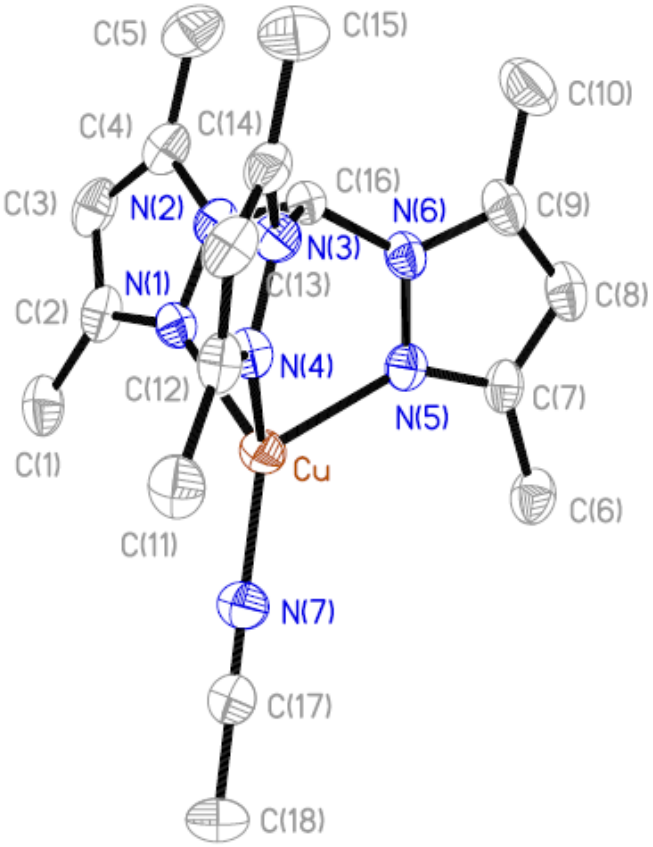

Figure 3.9. X-ray crystal structure diagram of [Tpm*Cu(NCCH$_3$)][BF$_4$] showing 50% probability density ellipsoids. Hydrogen atoms and counterions are omitted for clarity.

Table 3.1. Selected bond lengths (Å) and angles (deg) for [Tpm*Cu($NCCH_3$)][BF_4].

Cu-N(1)	2.088(4)	N(4)-Cu-N(1)	85.92(14)
Cu-N(4)	2.080(4)	N(4)-Cu-N(5)	89.93(14)
Cu-N(4)	2.089(3)	N(1)-Cu-N(5)	87.74(14)
Cu-N(7)	1.865(4)	N(7)-Cu-N(1)	130.26(16)
N(7)-C(17)	1.137(7)	N(7)-Cu-N(4)	124.68(16)
		N(7)-Cu-N(5)	125.35(16)

Treating [Tpm*CuX][BF_4] (X = dmise/dmit) with H_2O_2 in acetonitrile results in preferential oxidation of the dmise or dmit ligand and formation of oxidized selenium and sulfur species, the dimethylimidazolium cation and [Tpm*Cu($NCCH_3$)][BF_4]. Since these copper-selone and -thione complexes undergo sacrificial oxidation of chalcogenone atoms without oxidation of the Cu^+ center, if similar copper-selenium and -sulfur complexes are formed *in vivo*, such complexes may scavenge H_2O_2 and inhibit copper-mediated oxidative damage. These studies indicate that coordination of selenium and sulfur compounds to Cu^+ may prevent copper-mediated DNA damage in one of two ways: coordination of selone or thione to Cu^+ alters the $Cu^{2+/+}$ reduction potential hence preventing reduction of Cu^{2+} by NADH and inhibiting copper redox cycling or by efficiently scavenging H_2O_2 by bound selenium or sulfur compounds.

Conclusions

The reactivity of biologically relevant selone and thione ligands and their copper complexes with H_2O_2 has been determined and compared. Treatment of dmise and dmit with H_2O_2 results in cleavage of the C=Se or C=S bond and oxidation of the selenium

and sulfur atoms along with formation of the dimethylimidazolium cation. Treating [Tpm*CuX][BF_4] (X = dmise/dmit) with H_2O_2 in acetonitrile results in preferential oxidation of the dmise or dmit ligand and formation of oxidized selenium and sulfur species, the dimethylimidazolium cation and [Tpm*Cu($NCCH_3$)][BF_4]. In contrast, upon treating Cu^+ complexes without bound selenium or sulfur ligands with the same number of equivalents of H_2O_2, the Cu^+ is oxidized.[29] Since these copper-selone and -thione complexes undergo sacrificial oxidation of chalcogenone atoms without oxidation of the Cu^+ center, if similar copper-selenium and -sulfur complexes are formed *in vivo*, such complexes may scavenge H_2O_2 and inhibit copper-mediated oxidative damage.

Experimental Section

Materials. Methanol and acetonitrile were dried using standard procedures and freshly distilled prior to use. *N,N'*-dimethylimidazole selone (dmise),[36] *N,N'*-dimethylimidazole thione (dmit),[36] [Cu($NCCH_3$)$_4$][BF_4],[37] [Tpm*Cu(dmise)][BF_4], and [Tpm*Cu(dmit)][BF_4],[23] were synthesized according to published procedures. The following reagents were used as received: selenium powder (VWR), sulfur powder (VWR), cuprous oxide (stabilized, Aldrich), 1-methylimidazole (VWR), methyliodide (VWR), 3,5-dimethylpyrazole (VWR), and 30% H_2O_2 (VWR).

Instrumentation. ^1H, $^{13}C\{^1H\}$, and $^{77}Se\{^1H\}$ NMR spectra were obtained on Bruker AVANCE-500 or -300 NMR spectrometers. ^1H and $^{13}C\{^1H\}$ NMR chemical shifts are reported in δ vs. trimethylsilane (TMS; δ 0). $^{77}Se\{^1H\}$ NMR chemical shifts are

reported relative to dimethyl selenide (δ 0) and externally referenced to diphenyl diselenide (δ 461).[38] $^{19}F\{^{1}H\}$ NMR spectra were externally referenced to CCl_3F (δ 0).[39]

Infrared spectra were obtained using nujol mulls on KBr salt plates with a Magna 550 IR spectrometer. Abbreviations used in the description of vibrational data are as follows: vs, very strong; s, strong; m, medium; w, weak; b, broad. Electrospray ionization mass spectrometry (ESI-MS) was conducted using a QSTAR XL Hybrid MS/MS System from Applied Biosystems via direct injection of sample (0.05 mL/min flow rate) into a Turbo Ionspray ionization source. Samples were run under both positive and negative mode, with an ionspray voltage of 5500 V, and TOF scan mode. All the peak envelopes obtained match calculated isotopic abundances.

Reactivity of dmise with H_2O_2. Dmise (175 mg, 1 mmol) was dissolved in methanol (15 mL), and H_2O_2 (115 μL of 30%, 8.667 M; 1 mmol) was added. The reaction mixture was stirred for 5 h and dried *in vacuo* to afford a light brown oil. Yield of oxidized dmise: 100 % by ^{1}H NMR spectroscopy. ^{1}H NMR (CD_3OD): 3.978 (s, $2CH_3$), 7.579 (2H, 2CH), 8.91 (s, 1H, CH). $^{13}C\{^{1}H\}$ NMR (CD_3OD): 35.70 (CH_3), 123.59 (CH), 136.98 (CH (C-2)). $^{77}Se\{^{1}H\}$ NMR (CD_3OD): 1346.22. ESI-MS: *m/z*, positive ionization 97.07 $[C_5H_9N_2]^+$; negative ionization: 112.96 $[SeO_2H]^-$.

Reactivity of dmit with H_2O_2. Dmit (128 mg, 1 mmol) was dissolved in methanol (15 mL) and treated with 1equiv H_2O_2 (115 μL of 30%, 8.667 M; 1 mmol) or 2 equiv of H_2O_2 (230 μL of 30%, 8.667 M; 2 mmol). Yield of oxidized dmit: 100 % by ^{1}H NMR spectroscopy with 2 equiv H_2O_2. ^{1}H NMR (CD_3OD): 3.98 (s, $2CH_3$), 7.61 (2H, 2CH),

8.91 (s, 1H, CH). $^{13}C\{^{1}H\}$ NMR (CD_3OD): 35.20 (CH_3), 123.50 (CH), 137.31(CH (C-2)). ESI-MS: *m/z*, positive ionization 97.07 $[C_5H_9N_2]^+$; negative ionization: 96.99 $[SO_4H]^-$, 79.98 $[SO_3H]^-$.

*Reaction of [Tpm*Cu(dmise)][BF$_4$] with H$_2$O$_2$.* [Tpm*Cu(dmise)][BF_4] (320 mg, 0.5 mmol) was dissolved in acetonitrile (10 mL) and to this was added 0.5, 1.0, or 2.0 equiv of H_2O_2 (0.25, 0.5, or 1 mmol; 29, 58, or 115 μL). The reaction mixtures were stirred for 8 h and dried *in vacuo*. A control experiment using degassed water instead of H_2O_2 showed no reaction. Single crystals of [Tpm*Cu($NCCH_3$)][BF_4] were grown via slow diffusion of ether into acetonitrile solution. Yield of oxidized dmise: 85% by ^{1}H NMR spectroscopy with 2 equiv H_2O_2. ^{1}H NMR (CD_3CN): 2.31 (s, 9H, $3CH_3$), 2.51 (s, 9H, $3CH_3$), 3.86 (s, 6H, $2CH_3$), 6.05 (s, 3H, 3CH), 7.36 (s, 2H, 2CH (dmise)), 7.75 (s, 1H, CH), 8.49 (s, 1H, CH (dmise)). $^{13}C\{^{1}H\}$ NMR (CD_3CN): 11.05 (CH_3), 13.48 (CH_3), 36.64 (CH_3 (dmise)), 68.65 (CH), 107.22 (pz), 124.35 (CH (dmise)), 141.96 (CH (pz)), 151.52 (CH (pz)). IR (cm^{-1}): 520 w, 630 s, 662 s, 704 vs, 739 vs, 794 vs, 815 vs, 855 vs, 970 vs, 978 w, 1066 b, 1150 s, 1176 s, 1252 vs, 1307 vs, 1392 vs, 1417 vs, 1464 vs, 1568 vs, 1675 w, 2854 vs, 2924 b, 3142 s, 3171 s, 3501 w. ESI-MS: *m/z* positive ionization: 402.12 [Tpm*Cu($NCCH_3$)]$^+$, 380.10 [Tpm*Cu(OH) + 2H]$^+$, 361.09 [Tpm*Cu]$^+$, 97.07 $[C_5H_9N_2]^+$; negative ionization: 112.96 $[SeO_2H]^-$, 87.03 $[BF_4]^-$.

*[Tpm*Cu(dmit)][BF$_4$] with H$_2$O$_2$.* [Tpm*Cu(dmit)][BF_4] (273 mg, 0.5 mmol) were dissolved in acetonitrile (10 mL) and to this was added 1, 2, or 3 equiv of H_2O_2 (0.5, 1.0, or 1.5 mmol; 58, 115, or 173 μL). The reaction mixture was stirred overnight and

dried *in vacuo*. Yield of oxidized dmit: 68% by ^{1}H NMR spectroscopy with 3 equiv H_2O_2. ^{1}H NMR (CD_3CN): 2.28 (s, 9H, $3CH_3$), 2.51 (s, 9H, $3CH_3$), 3.85 (s, 6H, $2CH_3$), 6.05 (s, 3H, 3CH), 7.36 (s, 2H, 2CH (dmit)), 7.75 (s, 1H, CH), 8.47 (s, 1H, CH (dmit)). $^{13}C\{^{1}H\}$ NMR (CD_3CN): 11.04 (CH_3), 13.43 (CH_3), 36.61 (CH_3 (dmit)), 68.65 (CH), 107.24 (pz), 124.35 (CH (dmit)),141.98 (CH (pz)), 151.53 (CH (pz)). IR (cm^{-1}): 491 w, 521 s, 631 s, 672 vs, 704 vs, 740 s, 814 s, 857 vs, 907 vs, 1065 b, 1175 s, 1258 vs, 1286 w, 1308 vs, 1394 s, 1418 s, 1464 s, 1567 vs, 1676 w, 2917 b, 3144 s. ESI-MS: *m/z* positive ionization: 489.09 $[Tpm^*Cu(NCCH_3)][BF_4]^+$, 402.12 $[Tpm^*Cu(NCCH_3)]^+$, 380.10 $[Tpm^*Cu(OH) + 2H]^+$, 361.09 $[Tpm^*Cu]^+$, 97.07 $[C_5H_9N_2]^+$; negative ionization: 96.99 $[SO_4H]^-$, 79.98 $[SO_3H]^-$, 87.03 $[BF_4]^-$.

X-ray data collection and structural determination. Single crystals of $[Tpm^*Cu(NCCH_3)][BF_4]$ grown from vapor diffusion were mounted on a glass filament with silicon grease and immediately cooled to 168±2 K in a cold nitrogen gas stream. Intensity data were collected using a Rigaku Mercury CCD detector and an AFC8S diffractometer. The space groups C2/c for $[Tpm^*Cu(NCCH_3)][BF_4]$ was determined from the observed systematic absences. Data reduction including the application of Lorentz and polarization (Lp) effects and absorption corrections used the CrystalClear program.[40] The structures were solved by direct methods and subsequent Fourier difference techniques, and refined anisotropically, by full-matrix least squares, on F^2 using SHELXTL 6.10.[41]

Table 3.2. Summary of crystallographic data for [Tpm*Cu(NCCH$_3$)][BF$_4$].

Chemical Formula	$C_{18}H_{25}BCuF_4N_7$
F.W. (g/mol)	489.80
Space group	C2/*c*
Crystal system	Monoclinic
a, Å	25.997(5)
b, Å	7.598(15)
c, Å	25.019(5)
α, °	90
β, °	116.18(3)
γ, °	90
V, Å^3	4435.2(15)
Z	8
D_{cal}, Mg/m^3	1.467
Indices (min)	[-30, -7, -28]
(max)	[30, 9, 29]
Parameters	287
F(000)	2016
μ, mm^{-1}	1.038
2θ range,	1.81-25.05
Collected reflections	16722
Unique reflections	3917
Final R (obs. Data)[a], R_1	0.0636
wR_2	0.1724
Final R (all data), R_1	0.0823
wR_2	0.1948
Goodness of fit (S)	1.060
Largest diff. Peak	1.173
Largest diff. Hole	-0.761

[a] $R_1 = [\Sigma||F_0| - |F_c||]/ \Sigma|F_0|$; $wR_2 = \{[\Sigma w[(F_0)^2 - (F_c)^2]^2\}^{1/2}$

In the final cycle of least squares, independent anisotropic displacement factors were refined for the non-hydrogen atoms and the methyl hydrogen atoms were fixed in idealized positions with C-H = 0.96 Å. Their isotropic displacement parameters were set equal to 1.5 times U_{eq} of the attached carbon atom. The high wR_2 value results from disorder in the tetrafluoroborate counterion. Final refinement parameters for structure of [Tpm*Cu($NCCH_3$)][BF_4] are given in Table 3.1, and selected bond angles and distances are summarized in Table 3.2.

References

(1) Stohs, S. J.; Bagchi, D. *Free Radic. Biol. Med.* **1995**, *18*, 321-336.

(2) Pierre, J. L.; Fontecave, M. *BioMetals* **1999**, *12*, 195-199.

(3) Ala, A.; Walker, A. P.; Ashkan, K.; Dooley, J. S.; Schilsky, M. L. *Lancet* **2007**, *369*, 397-408.

(4) Brewer, G. J. *Exp. Biol. Med.* **2007**, *232*, 323-335.

(5) Cooper, G. J. S.; Chan, Y. K.; Dissanayake, A. M.; Leahy, F. E.; Keogh, G. F.; Frampton, C. M.; Gamble, G. D.; Brunton, D. H.; Baker, J. R.; Poppitt, S. D. *Diabetes* **2005**, *54*, 1468-1476.

(6) Leone, N.; Courbon, D.; Ducimetiere, P.; Zureik, M. *Epidemiology* **2006**, *17*, 308-314.

(7) Halliwell, B. *Biochem. J.* **2007**, *401*, 1-11.

(8) Battin, E. E.; Brumaghim, J. L. *Cell Biochem. Biophys.* **2009**, *55*, 1-23.

(9) Ramoutar, R. R.; Brumaghim, J. L. *Cell Biochem. Biophys.* **2010**, *58*, 1-23.

(10) Plano, D.; Baquedano, Y.; Ibanez, E.; Jimenez, I.; Palop, J. A.; Spallholz, J. E.; Sanmartin, C. *Molecules* **2010**, *15*, 7292-7312.

(11) Shen, Q. A.; Zhang, B. W.; Xu, R. H.; Wang, Y.; Ding, X. L.; Li, P. L. *Anaerobe* **2010**, *16*, 380-386.

(12) Tanaka, S.; Haruma, K.; Yoshihara, M.; Kajiyama, G.; Kira, K.; Amagase, H.; Chayama, K. *J. Nutr.* **2006**, *136*, 821S-826S.

(13) Alpers, D. H. *Curr. Opin. Gastroenterol.* **2009**, *25*, 116-121.

(14) Fleischauer, A. T.; Arab, L. *J. Nutr.* **2001**, *131*, 1032S-1040S.

(15) Facompre, N. D.; El-Bayoumy, K.; Sun, Y. W.; Pinto, J. T.; Sinha, R. *Cancer Prev. Res.* **2010**, *3*, 975-984.

(16) Reid, M. E.; Duffield-Lillico, A. J.; Slate, E.; Natarajan, N.; Turnbull, B.; Jacobs, E.; Combs, G. F.; Alberts, D. S.; Clark, L. C.; Marshall, J. R. *Nutr. Cancer* **2008**, *60*, 155-163.

(17) Lippman, S. M.; Klein, E. A.; Goodman, P. J.; Lucia, M. S.; Thompson, I. M.; Ford, L. G.; Parnes, H. L.; Minasian, L. M.; Gaziano, J. M.; Hartline, J. A.; Parsons, J. K.; Bearden, J. D.; Crawford, E. D.; Goodman, G. E.; Claudio, J.; Winquist, E.; Cook, E. D.; Karp, D. D.; Walther, P.; Lieber, M. M.; Kristal, A. R.; Darke, A. K.; Arnold, K. B.; Ganz, P. A.; Santella, R. M.; Albanes, D.; Taylor, P. R.; Probstfield, J. L.; Jagpal, T. J.; Crowley, J. J.; Meyskens, F. L.; Baker, L. H.; Coltman, C. A. *J. Am. Med. Assoc.* **2009**, *301*, 39-51.

(18) Battin, E. E.; Perron, N. R.; Brumaghim, J. L. *Inorg. Chem.* **2006**, *45*, 499-501.

(19) Ramoutar, R. R.; Brumaghim, J. L. *Main Group Chem.* **2007**, *6*, 143-153.

(20) Ramoutar, R. R.; Brumaghim, J. L. *J. Inorg. Biochem.* **2007**, *101*, 1028-1035.

(21) Battin, E. E.; Brumaghim, J. L. *J. Inorg. Biochem.* **2008**, *102*, 2036-2042.

(22) Mugesh, G.; Singh, H. B. *Chem. Soc. Rev.* **2000**, *29*, 347-357.

(23) Kimani, M. M.; Brumaghim, J. L.; Vanderveer, D. *Inorg. Chem.* **2010**, *49*, 9200-9211.

(24) Yamashita Y.; Yamashita M. *J. Biol. Chem.* **2010**, *285*, 18134-18138.

(25) Ey, J.; Schomig, E.; Taubert, D. *J. Agric. Food Chem.* **2007**, *55*, 6466-6474.

(26) Bhabak, K. P.; Mugesh, G. *Chem. Eur. J.* **2010**, *16*, 1175-1185.

(27) Herrmann, W. A.; Kocher, C.; Goossen, L. J.; Artus, G. R. J. *Chem.-Eur. J.* **1996**, *2*, 1627-1636.

(28) Hatcher, L. Q.; Karlin, K. D. *J. Biol. Inorg. Chem.* **2004**, *9*, 669-683.

(29) Cvetkovic, M.; Batten, S. R.; Moubaraki, B.; Keith S. Murray, K. S.; Spiccia, L. *Inorg. Chim. Acta.* **2001**, *324*, 131-140.

(30) Baldwin, M. J.; Root, D. E.; Pate, J. E.; Fujisawa, K.; Kitajima, N.; Solomon, E. I. *J. Am. Chem. Soc.* **1992**, *114*, 10421-10431.

(31) Reger, D. L.; Collins, J. E. *Organometallics* **1996**, *15*, 2029-2032.

(32) Hsu, S. C. N.; Chen, H. H. Z.; Lin, I.; Liu, J.; Chen, P. *J. Organomet. Chem.* **2007**, *692*, 3676-3684.

(33) Fujisawa, K.; Ono, T.; Ishikawa, Y.; Amir, N.; Miyashita, Y.; Okamoto, K.; Lehnert, N. *Inorg. Chem.* **2006**, *45*, 1698-1713.

(34) Schneider, J. L.; Carrier, S. M.; Ruggiero, C. E.; Young, V. G.; Tolman, W. B. *J. Am. Chem. Soc.* **1998**, *120*, 11408-11418.

(35) Lynch, W. E.; Kurtz, D. M.; Wang, S. K.; Scott, R. A. *J. Am. Chem. Soc.* **1994**, *116*, 11030-11038.

(36) Roy, G.; Das, D.; Mugesh, G. *Inorg. Chim. Acta* **2007**, *360*, 303-316.

(37) Kubas, G. J. *Inorg. Synth.* **1990**, *28*, 68-70.

(38) Odom, J. D.; Dawson, W. H.; Ellis, P. D. *J. Amer. Chem. Soc.* **1979**, *101*, 5815-5823.

(39) *NMR and the Periodic Table*; Harris, R. K.; Mann, B. E., Eds.; Academic Press: London, 1978, p. 99.

(40) Crystalclear; The Woodlands: Texas, USA, 1999.

(41) Sheldrick, G. M.; Bruker Analytical X-ray Systems Inc.: Madison, WI, 2000.

CHAPTER FOUR

REDUCTION OF Cu(II) BY *N,N'*-DIMETHYLIMIDAZOLE CHALCOGENONES AND THE COORDINATION CHEMISTRY OF BIS(1-METHYLIMIDAZOLYL) DISELENIDE TO Cu(II)

Introduction

The applications and coordination chemistry of heterocyclic selenoamides and thioamides with transition metals has been extensively studied for the past 20 years because of their applications in catalysis, their use as precursors for the synthesis of semiconductors via chemical vapor deposition (CVD), and their use as mimics for metalloproteins in bioinorganic chemistry.[1-6] Recently, we have investigated the ability of *N,N'*-dimethylimidazole selone (dmise) and thione (dmit) to reduce Cu^{2+} to Cu^{+} as well as the coordination chemistry of bis(1-methylimidazolyl) diselenide with Cu^{2+}. These selone and thione ligands are of interest because they resemble thiol-histidines such as ergothioneine[7,8] and ovothiols,[9] as well as the seleno-histidine selenoneine,[10] naturally occurring antioxidant sulfur and selenium compounds found in plants and animals (Figure 4.1).

Previous work has shown that Cu^{+} complexes of thio and selonoureas can be prepared via reduction of Cu^{2+} salts using an excess seleno- and thioamide containing ligands with concomitant oxidation of the seleno- and thioamide compounds.[11-14] Against this background, we carried out the reaction of $CuCl_2$ and $Cu(OTf)_2$ with molar equivalents of dmise or dmit to determine the products formed and the ability of these

heterocyclic chalcogenone ligands to reduce Cu^{2+} to Cu^{+}. In biological systems, most thiols are oxidized upon interacting with metal ions such as Cu^{2+} or by other redox processes. Thiol oxidation results in formation of disulfide bonds that play important role in cellular redox regulation.[15] Selenocysteine residues in SeI L selenoproteins or Grx3 mutants also can form diselenide bonds. The diselenide-containing protein SeI L is absent in mammals but present in aquatic organisms such as jawless fish, tunicates, and crustaceans. SeI L selenoproteins have very low reduction potential (-332 mV) which may have unique physiological and catalytic roles.[16]

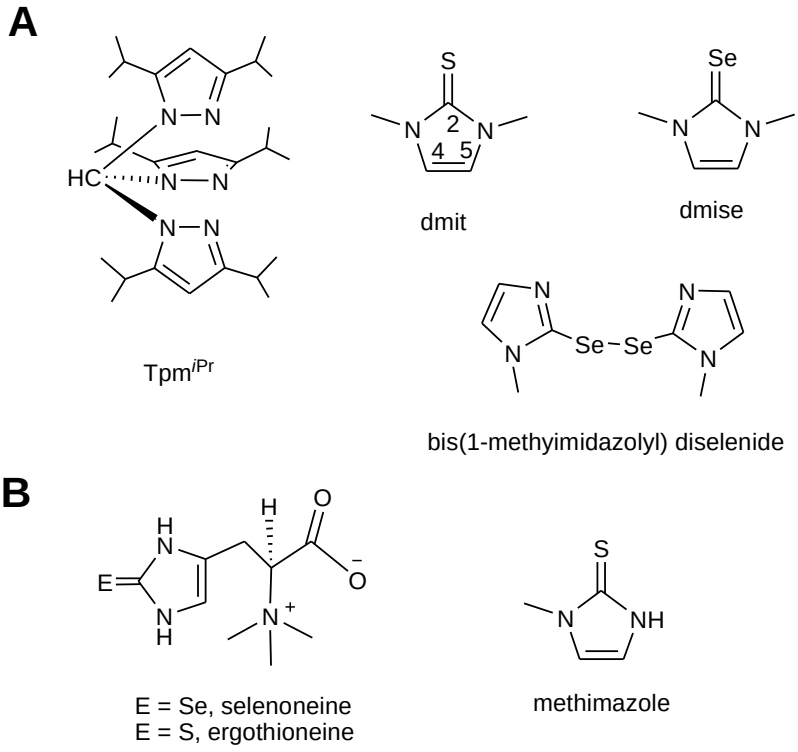

Figure 4.1. A) Ligands used in this study. B) Structures of naturally occurring selone and thione antioxidants and the drug methimazole.

Ergothioneine and selenoneine coordinate divalent metal ions such as $Cu^{2+}$and are easily oxidized to form ergothioneine disulfide and selenoneine diselenide.[9,17,18] The

metal binding properties of ergothioneine disulfide, and its selenium analog selenoneine diselenide, to transition metals (Fe^{2+}, Ni^{2+}, Co^{2+}, Zn^{2+}, and Cu^{+}) chlorides have been investigated by using bis(1-R-imidazolyl) disulfides and diselenides as coordination mimics (R = H, Me, Ph, ^{t}Bu; Figure 4.1).[18] These disulfide and diselenide mimics are excellent bidentate ligands, coordinating metals through the imidazolyl nitrogens and resulting in metal (Fe^{2+}, Ni^{2+}, Co^{2+}, and Zn^{2+}) complexes with distorted tetrahedral geometries.[18]

In this chapter, the coordination chemistry of Cu^{2+} with bis(1-methylimidazolyl) diselenide (MISeox) is explored to determine the potential binding modes of selenoneine diselenide. Cu^{2+} capping with the tripodal ligand tris(1,3-diisopropylpyrazolyl)methane (Tpm^{iPr}) ligand is used to ensure Cu^{2+} coordination to only one diselenide ligand. Electrochemical studies of the $[Tpm^{iPr}Cu(MISeox)]^{2+}$ cation will determine the effect of diselenide coordination on the $Cu^{2+/+}$ reduction potential.

Results and Discussion

Oxidation of dmise and dmit ligands. Oxidation of the chalcogenones dmise and dmit was performed by treating the anhydrous copper(II) salts $Cu(OTf)_2$ and $CuCl_2$ with 1 equiv of dmise or dmit in acetonitrile (Scheme 4.1) to yield the diselenide (**1** and **3**) and disulfide (**2**) dication salts. Both the diselenide and disulfide dications are indefinitely stable in air.

Scheme 4.1

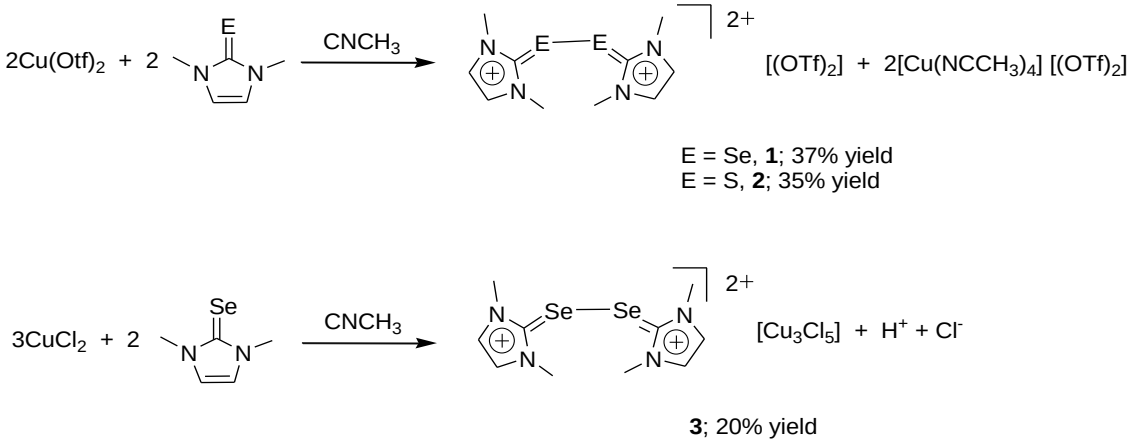

^{1}H NMR spectra of dmise and dmit show two sets of resonances corresponding to the methyl protons (δ 3.60 for dmise and δ 3.56 for dmit) and olefinic protons (δ 7.04 for dmise and δ 6.90 for dmit).[19] Upon oxidation of these chalcogenone compounds, these methyl and olefinic resonances shift downfield (δ 3.67 and 7.63 for **1**, and δ 3.73 and 7.64 for **2**). The presence of only two resonances for the oxidized dmise and dmit compounds, coupled with the significant downfield shift of the olefinic protons compared with the unoxidized compounds, suggest the formation of aromatic dichalcogenone dications.

The diselenide dication **1** has three ^{13}C{^{1}H} NMR resonances at δ 37.6 (CH_3 groups), δ 125.9 (olefinic carbon atoms) and δ 140.6 (C-Se). The methyl and olefinic carbons of **1** are slightly shifted downfield compared to dmise by δ 0.6 and 6.2, respectively.[19] In contrast, the C-2 carbon resonance of **1** is shifted upfield by δ 17 compared to dmise. This upfield shift is consistent with a shift of electron density from the selenocarbonyl group to the neighboring N-C bond and formation of an aromatic

imidazolium cation.[20-23] The $^{77}Se\{^{1}H\}$ NMR spectrum of the diselenide dication **1** shows a resonance at δ 329, significantly shifted downfield relative to that of dmise (δ -1).[19] The $^{13}C\{^{1}H\}$ NMR spectrum of the analogous disulfide **2** shows similar resonance shifts (δ +1, +9.3 and -20) for the methyl, olefinic, and S-C carbon atoms, respectively. The identities of the three diselenide and disulfide dications (**1**, **2**, and **3**) were confirmed by ESI mass spectrometry.

Structural analysis of the disulfide and diselenide dications. The X-ray crystal structure of $[(C_5N_2H_8S)_2]^{2+}$ (Figure 4.2) shows a $[(C_5N_2H_8S)_2]^{2+}$ dication with a S-S bond length of 2.10 Å (Table 4.1). Formation of the disulfide dication **2** results in significantly longer S-C (1.746(3) Å) bond distance relative to dmit (1.681(5) Å).[24] The bis(1,3-dimethylimidazolium) disulfide dication has a C(1)-S(1)-S(2)-C(6) torsion angle of 79.70°.

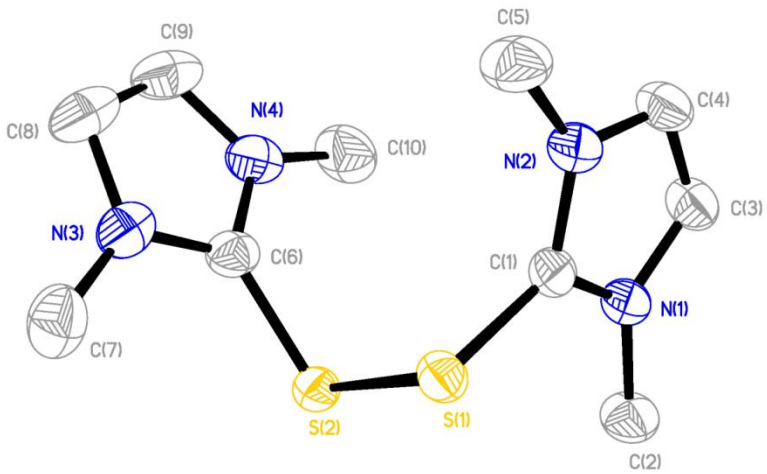

Figure 4.2. Crystal structure diagram of $[(C_5N_2H_8S)_2]^{2+}$ (**2**) showing 50% probability density ellipsoids. Hydrogen atoms and counterions omitted for clarity.

Table 4.1. Selected bond distances (Å) and angles (°) for **2**.

S(1)-S(2)	2.1015(10)	S(2)-S(1)-C(1)	100.17(9)
S(1)-C(1)	1.746(3)	S(1)-S(2)-C(6)	101.76(9)
S(2)-C(6)	1.744(3)		

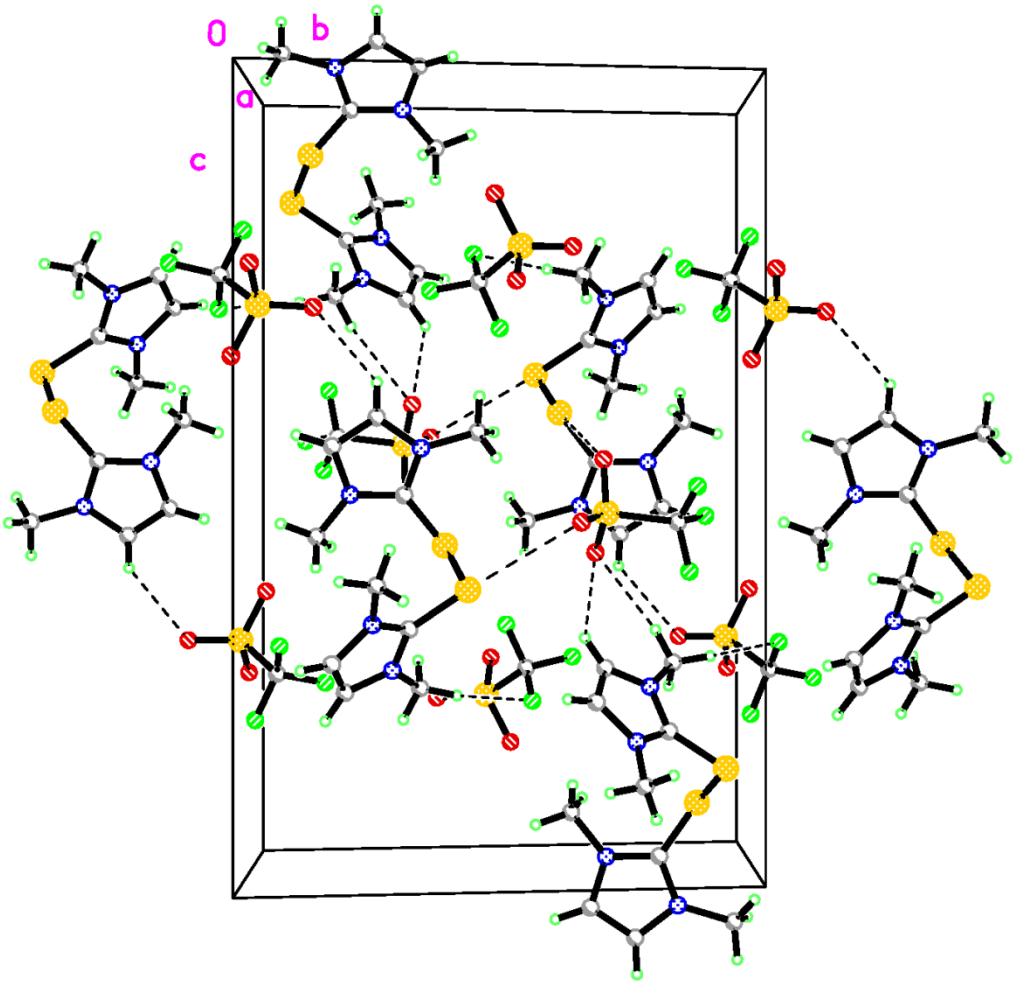

Figure 4.3. Crystal packing diagram of $[(C_5N_2H_8S)_2][(OTf)_2]$ (**2**) along the *a*-axis showing 50% probability density ellipsoids. Short contact interactions and hydrogen bonds between S-O, H-O, and F-H are shown.

The two triflate anions have short contact interactions between S(2)-O(1) (2.81 Å), S(1)-O(2) (3.24 Å), S(1)-O(4) (2.94 Å), O(3)-H(3A) (2.46 Å), O(3)-H(2B) (2.56 Å), and F(6)-H(2A) (2.53 Å) (Figure 4.3). The S-S bond distance of 2.1015(10) Å in the crystal structure of **2** is slightly longer than the previously reported disulfide dications $[(C_4H_6N_2S)_2]I_8$ (2.085(2) Å),[25] $[(C_4H_6N_2S)_2]I_3I_5$ (2.085(3) and 2.094(3) Å).[25]

X-ray structural analysis of the analogous diselenide compound **1** (Figure 4.4) shows a Se-Se bond length of 2.3598(7) Å (Table 4.2), a distance slightly shorter than the sum of their covalent radii (2.40 Å).[26] The dication is charge-balanced by two triflate anions with short contact interactions between O(1)-Se(1) (2.80 Å), O(6)-Se(2) (2.96 Å), O(1)-C(1) (2.97 Å), O(6)-H(9A) (2.35 Å), O(3)-H(7C) (2.55 Å), O(6)-H(5C) (2.52 Å), and F(5)-H(2C) (2.55 Å) (Figure 4.5). The bis(1,3-dimethylimidazolium) diselenide dication has a C(1)-Se(1)-Se(2)-C(6) torsion angle of -77.40°. The diselenide dication **1** and the unoxidized dmise have almost identical Se-C bond lengths (1.885(3) and 1.884(10) Å, respectively).[27] The Se-Se bond distance of 2.3598(7) Å in **1** is comparable to that found in $[(SeC(NH_2)_2]_2Cl_2]$ (2.381596) Å),[28] but shorter than the Se-Se bond lengths in $(C_5H_8N_2Se)_2Br_2$ (2.409(2) Å), $(C_5H_8N_2Se)_2I_2$ (2.434(2) Å), $[(C_5H_8N_2Se\text{-})_2Cl]I_3$ (2.440(2) Å).[29]

Upon treatment with anhydrous $CuCl_2$, dmise is oxidized, resulting in the formation of a red solid with the formula $[(C_5N_2H_8Se)_2][Cu_3Cl_5]$, **3** (Scheme 4.1). The X-ray structure of **3** revealed a centrosymmetric $[Cu_3Cl_5]^{2-}$ anion charge-balanced by a $[(C_5N_2H_8Se)_2]^{2+}$ dication (Figure 4.6). The diselenide dication of **3** has a slightly longer

Se-Se bond distance of 2.3946(13) Å (Table 4.3) and a positive C(1)-Se(1)-Se(1A)-C(1A) torsion angle of 70.91° compared to diselenide dication **1** (Se-Se distance of 2.3598(7) Å and a C(1)-Se(1)-Se(2)-C(6) torsion angle of -77.40°).

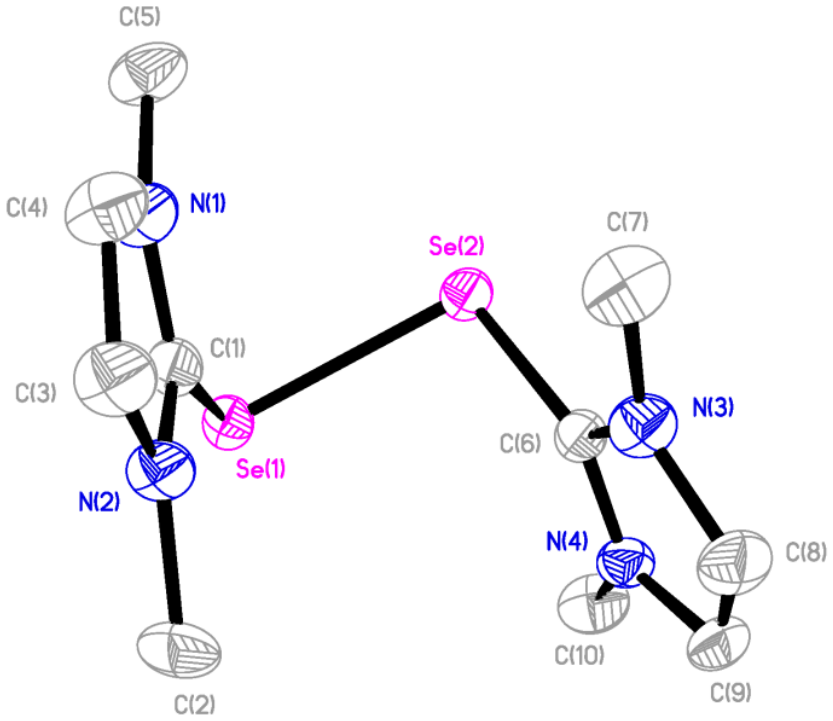

Figure 4.4. Crystal drawing of $[(C_5N_2H_8Se\text{-})_2]^{2+}$ (**1**) showing 50% probability density ellipsoids. Hydrogen atoms and counterions are omitted for clarity.

Table 4.2. Selected bond distances (Å) and angles (°) for **1**.

Se(1)-Se(2)	2.3598(7)	Se(2)-Se(1)-C(1)	95.89(9)
Se(1)-C(1)	1.885(3)	Se(1)-Se(2)-C(6)	95.75(9)
Se(2)-C(6)	1.893(3)		

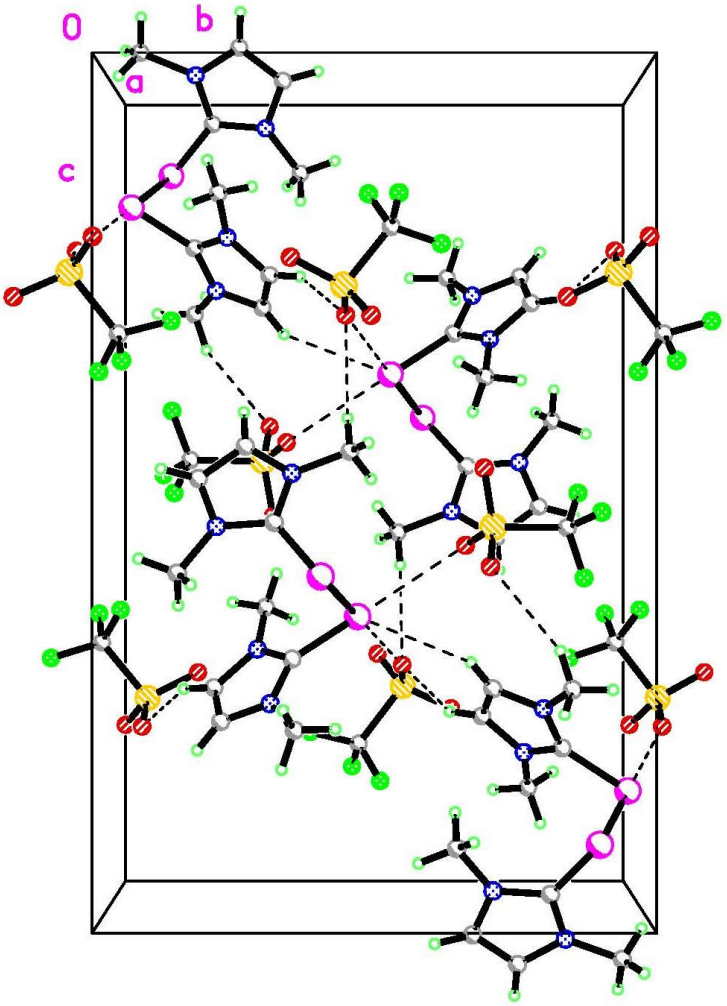

Figure 4.5. Crystal packing diagram of $[(C_5N_2H_8Se)_2][(OTf)_2]$ (**1**) along the *a*-axis showing 50% probability density ellipsoids. Short contact interactions and hydrogen bonds between Se-O, H-O, and F-H are shown.

The crystallographically centrosymmetric $[Cu_3Cl_5]^{2-}$ anion contains two geometrically different Cu^+ centers bridged by chloride atoms. Cu(1) adopts distorted trigonal geometry with an average Cu-Cl bond distance of 2.32 Å (Table 4.3), and Cl-Cu-Cl angles of 107 to 146.1°. The second Cu^+ center, Cu(2), adopts a distorted tetrahedral geometry with an average Cu-Cl bond distances of 2.38 Å and Cl-Cu-Cl

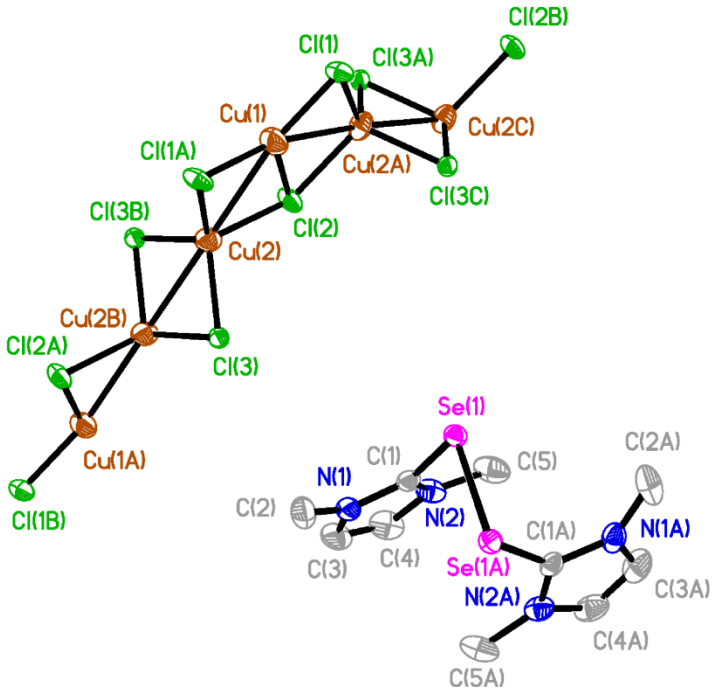

Figure 4.6. Crystal structure diagram of $[C_{10}H_{16}N_4Se_2][Cu_3Cl_5]$ (**3**) showing 50% density probability ellipsoids.

Table 4.3. Selected bond distances (Å) and angles (°) for **3**.

Se(1)-Se(1A)	2.3946(13)	Se(1A)-Se(1)-C(1)	94.01(15)
Se(1)-C(1)	1.884(5)	Se(1)-Se(1A)-C(1A)	94.01(15)
Cu(1)-Cu(2)	2.9201(12)	Cl(1)-Cu(1)-Cu(2)	161.11(7)
Cu(1)-Cl(1)	2.2346(15)	Cl(1)-Cu(1)-Cl(1A)	146.13(10)
Cu(1)-Cl(2)	2.481(3)	Cl(1)-Cu(1)-Cl(2)	106.94(5)
Cu(2)-Cl(2)	2.4910(12)	Cl(3)-Cu(2)-Cl(1A)	117.47(6)
Cu(2)-Cl(3)	2.3648(17)	Cl(1)-Cu(2)-Cl(2)	102.47(6)
		Cl(3)-Cu(2)-Cl(3B)	101.00(5)

angles ranging from 101.0° to 117.5°. The distance between the two geometrically distinct copper centers is 2.92 Å, longer than two times the sum of van der Waals radius for Cu^+ (2.80 Å),[30] suggesting minimal Cu-Cu interaction. The diselenide dications in the

crystal of **3** are arranged parallel to each other along the *b*-axis with the $[Cu_3Cl_5]^{2-}$ dianions positioned between the dications (Figure 4.7). This arrangement leads to short contact interactions between the Cl atoms of the anion and selenium and hydrogen atoms of the cation, thereby forming a two dimensional network (Figure 4.7). The Se-Cl short contact distance (3.38 Å) is significantly shorter than the sum of their van der Waals radii (3.80 Å),[30] indicating fairly strong interactions.

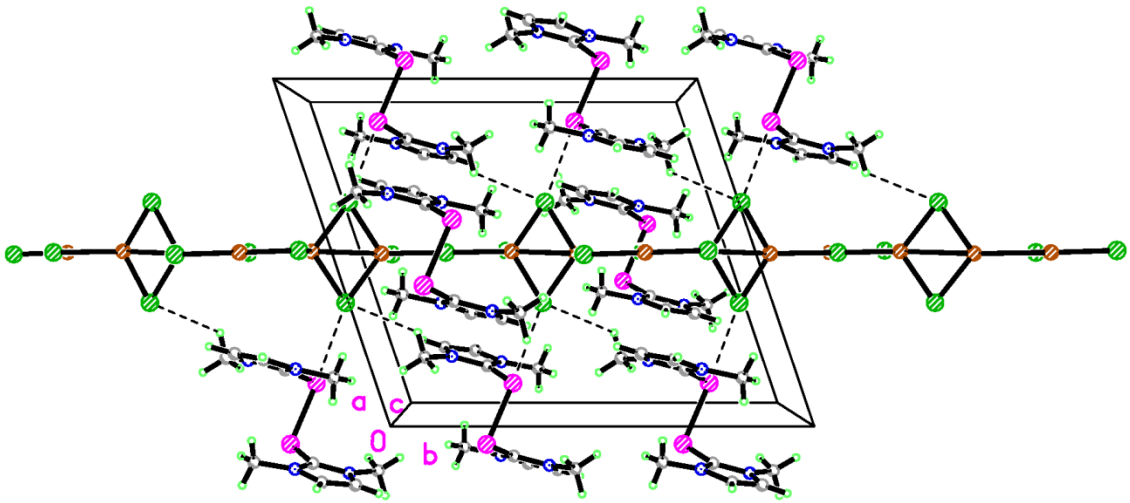

Figure 4.7. Crystal packing diagram of $[C_{10}H_{16}N_4Se_2][Cu_3Cl_5]$ (**3**) along the *b*-axis displaying 50% density probability ellipsoids. Short contact interactions between Se-Cl and H-Cl atoms are shown.

Synthesis and characterization of [Tpm^{iPr}Cu(MISeox)][(OTf)$_2$]. The Cu^{2+} $[Tpm^{iPr}Cu(MISeox)][OTf]_2$ complex (**5**) was synthesized in a two-step, two-pot procedure (Scheme 4.2). Treating $Cu(OTf)_2$ with an equimolar amount of tri(3,5-diisopropylpyrazolyl)methane (Tpm^{iPr}) in acetonitrile forms $Tpm^{iPr}Cu(OTf)_2$ (**4**)

(MALDI-MS Figure 4.12). The second step is treatment of $Tpm^{iPr}Cu(OTf)_2$ (**4**) with 1 equiv of bis(1-methylimidazolyl) diselenide (MISeox) in a mixed solvent system of dichloromethane and acetonitrile to afford **5** in relatively high yields.

Scheme 4.2

$$Cu(OTf)_2 + Tpm^{iPr} \xrightarrow[4h]{CNCH_3} Tpm^{iPr}Cu(OTf)_2$$

4; Yield 89%

$$Tpm^{iPr}Cu(OTf)_2 + MISeox \xrightarrow[4h]{CNCH_3/CH_2Cl_2} [Tpm^{iPr}Cu(MISeox)][(OTf)_2]$$

5; Yield 81%

Single crystal X-ray diffraction data were collected for $[Tpm^{iPr}Cu(MISeox)][(OTf)_2]$ (**5**), which crystallized as blue prisms. Structural parameters and selected bond lengths and angles for **5** are summarized in Tables 4.4 and 4.6, and its structure is shown in Figure 4.8. The Cu^{2+} center of **5** adopts distorted square pyramidal coordination geometry, with the Cu^{2+} bound to three nitrogen atoms from the tridentate ligand in a κ^3 fashion and to the two nitrogen atoms of bis(1-methylimidazolyl) diselenide in a κ^2 fashion. The N-Cu-N angles and Cu-N bond distances in **5** from the tris(1,3-diisopropylpyrazolyl)methane ligand range from 80.4 to 91.2º and 2.03 to 2.19 Å, respectively. Coordination of MISeox to Cu^{2+} results in N(7)-Cu-N(9) angle of 98.1° and average Cu-N bond lengths of 2.00 Å. The C-N bond distances in the bound diselenide ligand are slightly different with a Cu-N(9) distance of 1.972(6) Å and a Cu-N(7) distance of 2.027(6) Å. The geometry of the diselenide ligand changes noticeably upon

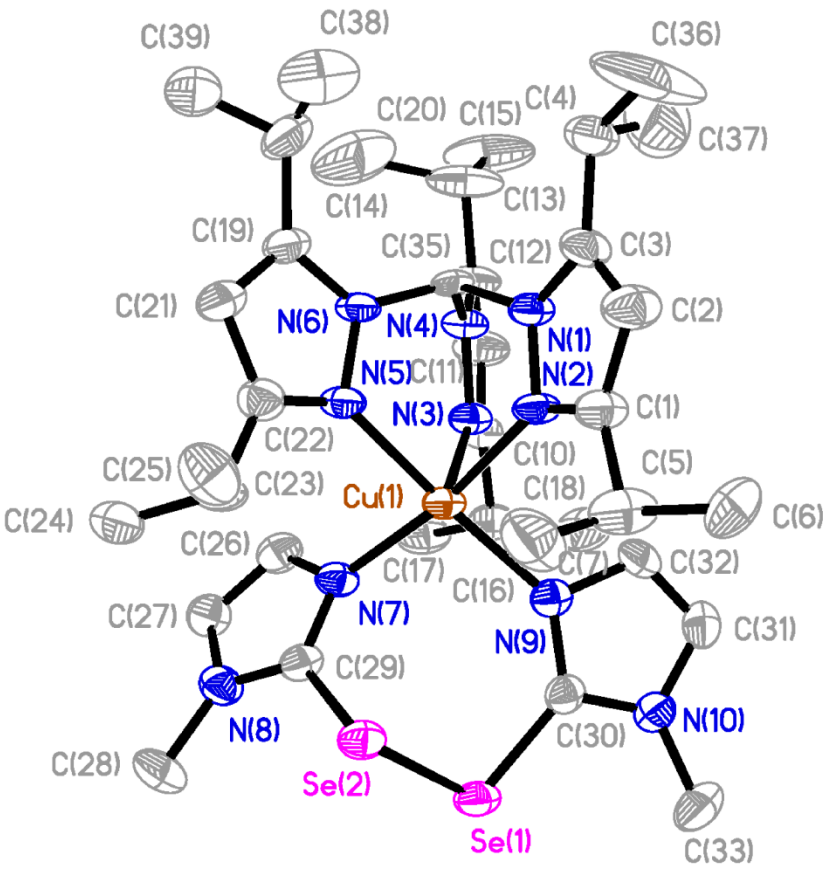

Figure4.8. Crystal structure diagram of [Tpm^{iPr}Cu(MISeox)][$(OTf)_2$] (**5**) showing 50% probability density ellipsoids. Hydrogen atoms and counterions are omitted for clarity.

Table 4.4. Selected bond distances (Å) and angles (°) for **5**.

Se(1)-Se(2)	2.3128(12)	N(9)-Cu-N(7)	98.1(2)
Cu-N(7)	2.027(6)	N(9)-Cu-N(5)	167.6(3)
Cu-N(9)	1.972(6)	N(7)-Cu-N(5)	92.6(2)
Cu-N(2)	2.055(6)	N(9)-Cu-N(2)	88.2(3)
Cu-N(5)	2.034(6)	N(7)-Cu-N(2)	170.5(2)
Cu-N(3)	2.190(6)	N(5)-Cu-N(2)	80.4(3)
		N(9)-Cu-N(3)	98.6(2)
		N(7)-Cu-N(3)	94.8(2)
		N(5)-Cu-N(3)	86.7(2)
		N(2)-Cu-N(3)	91.2(2)

binding to copper. The Se-Se distance is reduced to 2.3128(12) Å upon complexation to Cu^{2+} relative to the unbound ligand (2.3568(15) Å),[31] whereas the C-N distances in close proximity to the Cu-N bond are slightly increased. The N(9)-C(30)-Se(1) angle of 122.9(5)° does not change upon binding to Cu^{2+}, but the N(7)-C(29)-Se(2) angle of 130.5(6)° increases compared to the unbound diselenide ligand (122.8(3)°).[31]

The electrochemical behavior of bis(1-methylimidazolyl) diselenide and the Cu^{2+} complex **4** were examined by cyclic voltammetry to determine the change in the $Cu^{2+/+}$ redox potential upon copper coordination. Bis(1-methylimidazolyl) diselenide has a reduction potential of -1.067 mV versus normal hydrogen electrode (NHE), and exhibits quasi-reversible electrochemical behavior (Figure 4.9 and Table 4.5).

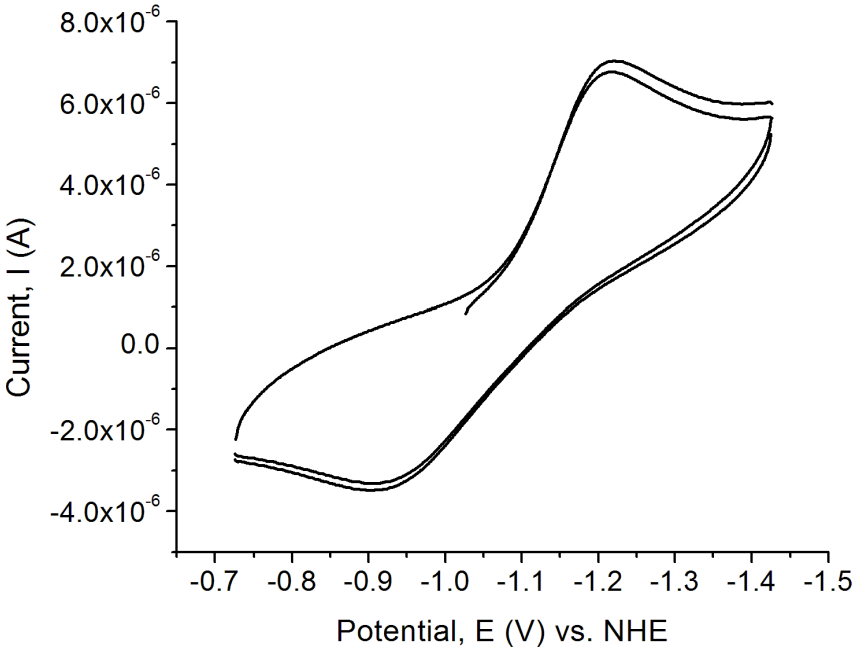

Figure 4.9. Cyclic voltammetry (CV) scan for MISeox in acetonitrile.

The cyclic voltammogram of the Tpm^{iPr}Cu(OTf)$_2$ (**4**) complex exhibits two one-electron, chemically reversible potential waves belonging to the $Cu^{2+/+}$ and $Cu^{+/0}$ reduction and oxidation processes (Figure 4.10, Table 4.5). At negative potentials, a peak corresponding to $Cu^{+/0}$ is observed at -911 mV. After switching the scan direction, the Cu^0 is then stripped off the electrode at -647 mV. The $Cu^{2+/+}$ reduction potential for Tpm^{iPr}Cu(OTf)$_2$ (**4**) is -339 mV and the complex exhibits small separation between the cathodic and anodic waves (ΔE 204 mV) relative to previously synthesized tris(pyrazolyl)Cu(I)-acetonitrile complexes (ΔE 844 to 1778 mV),[32] suggesting fast electron transfer kinetics during the voltammetry scan,[33] or small reorganization energies between a five-coordinate Cu^{2+} complex and a distorted tetrahedral Cu^{+} complex.[34]

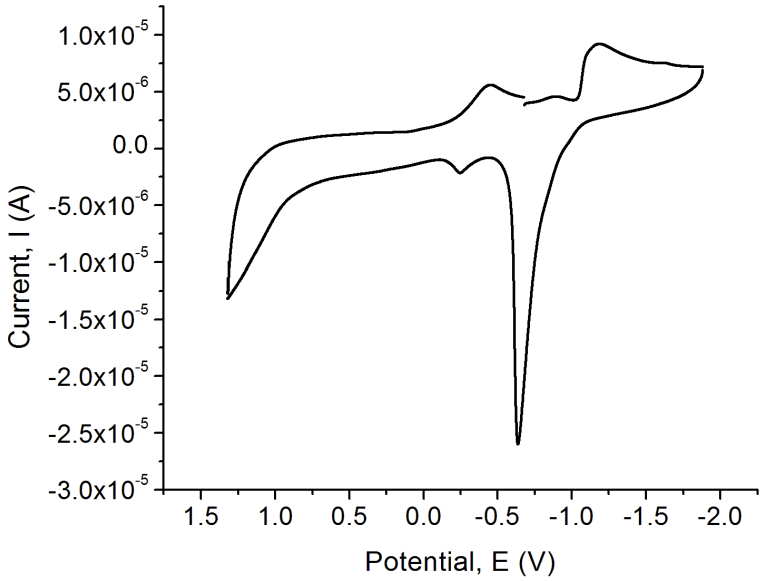

Figure 4.10. Cyclic voltammetry (CV) scan for the Tpm^{iPr}Cu(OTf)$_2$ (**4**) complex in acetonitrile vs. NHE.

The cyclic voltammogram of [Tpm^{iPr}Cu(MISeox)][(OTf)$_2$] (**5**) is very different from the analogous acetonitrile complex, Tpm^{iPr}Cu(OTf)$_2$ (**4**) due to the fact that it does not exhibit a typical $Cu^{+/0}$ reduction and oxidation wave, but instead shows two different reduction and oxidation waves (Figure 4.11). These two redox waves correspond to $Cu^{2+/+}$ reduction couples for [Tpm^{iPr}Cu(MISeox)][(OTf)$_2$] (**5**) at -508 mV and most likely a ligand (MISeox) based reduction potential at -1334 mV (Table 4.5). Complexation of MISeox to Tpm^{iPr}Cu(OTf)$_2$ (**4**) lowers the $Cu^{2+/+}$ redox potential by 170 mV. The $Cu^{2+/+}$ reduction potential of -508 in **5** is comparable to the macrocyclic copper(II) complex [Cu(dtne)]$(ClO_4)_2 \cdot CH_3CH_2OH$ (-544 mV),[35] but more negative compared to other reported Cu^{2+} complexes with nitrogen containing ligands such as [Cu(tnpa)(OH)]ClO_4 (-28 mV).[36]

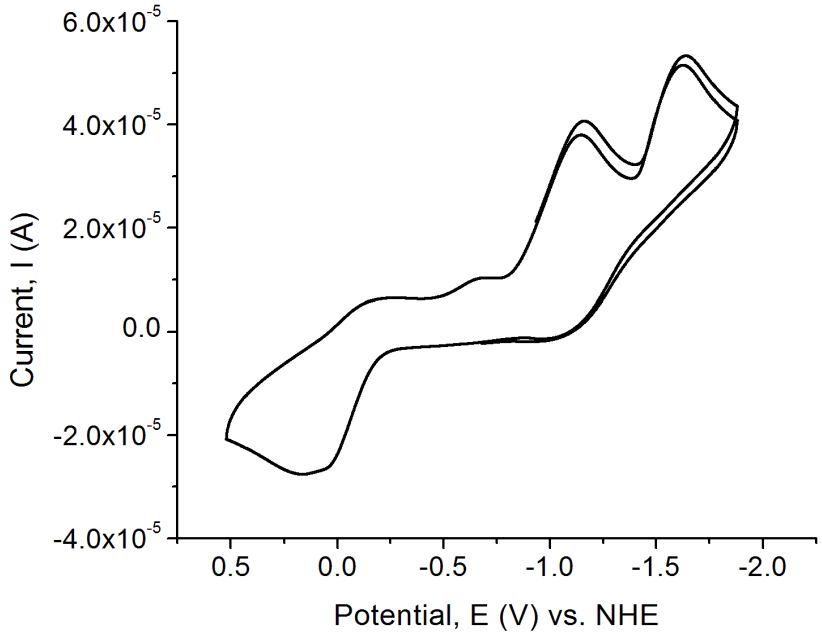

Figure 4.11. Cyclic voltammetry (CV) scan for [Tpm^{iPr}Cu(MISeox)][(OTf)$_2$] (**4**) in acetonitrile vs. NHE.

Table 5. Reduction potentials of MISeox, Tpm^{iPr}Cu(OTf)$_2$ (**4**), and [Tpm^{iPr}Cu(MISeox)][(OTf)$_2$] (**5**) vs. NHE.

	$Cu^{2+/+}$			
Compound	E_{pa} (mV)	E_{pc} (mV)	ΔE (mV)	$E_{1/2}$ (mV)
MISeox	-916	-1218	302	-1067
Tpm^{iPr}Cu(OTf)$_2$ (**4**)	-236	-440	204	-338
[Tpm^{iPr}Cu(MISeox)][(OTf)$_2$] (**5**)	129, -1037	-1146, -1630	1275, 593	-508, -1334

Table 6. $Cu^{+/0}$ reduction potential of Tpm^{iPr}Cu(OTf)$_2$ (**4**) vs. NHE.

	$Cu^{+/0}$			
Compound	E_{pa} (mV)	E_{pc} (mV)	ΔE (mV)	$E_{1/2}$ (mV)
Tpm^{iPr}Cu(OTf)$_2$ (**4**)	-647	-1175	528	-911

The bis(1-methylimidazolyl) diselenide is used to mimic coordination of naturally occurring selenoneine diselenide to biologically relevant divalent metals such as Cu^{2+}. The coordination of MISeox to Cu^{2+} occurs at the imidazolyl nitrogen atoms and alters $Cu^{2+/+}$ reduction potentials to stabilize Cu^{2+}. The $Cu^{2+/+}$ reduction potential of -508 mV for **5** is much lower than that of cellular reductant NADH (-324 mV),[37] and if similar copper complexes are formed *in vivo* their potentials may be lower enough to prevent reduction of Cu^{2+} and biological copper redox cycling.

Conclusions

Dmise and dmit ligands reduce Cu^{2+} to Cu^{+} with concomitant formation of the oxidized diselenide and disulfide dications. The reduction of Cu(OTf)$_2$ by dmise or dmit

results in formation of diselenide or disulfide dications which are stabilized by two triflate anions (**1** and **2**, respectively), whereas reduction of $CuCl_2$ by dmise forms the diselenide dication stabilized by a centrosymmetric $[Cu_3Cl_5]^{2-}$ anion (**3**). This complex anion has two geometrically distinct Cu^+ centers bridged by chloride atoms. The diselenide compound MISeox coordinates Cu^{2+} through both the imidazolyl nitrogen atoms as a bidentate ligand. X-ray structural analysis revealed that the Cu^{2+} center in $[Tpm^{iPr}Cu(MISeox)][(OTf)_2]$ (**5**) adopts a distorted square pyramidal geometry. MISeox coordination to $Tpm^{iPr}Cu(OTf)_2$ (**4**) lowers the $Cu^{2+/+}$ reduction potential by 170 mV compared to $Tpm^{iPr}Cu(OTf)_2$, thus stabilizing Cu^{2+}.

The results presented in this chapter illustrate the ability of dmise and dmit to reduce Cu^{2+}. In addition studies with Cu^{2+}-MISeox coordination shed new light on the possible coordination chemistry of selenoneine diselenide and the analogous ergothioneine disulfide with biologically relevant metal ions such as Cu^{2+}. Diselenide coordination may result in lowered $Cu^{2+/+}$ reduction potentials, and could potentially slow the rate of copper redox cycling to inhibit copper-mediated oxidative damage.

Experimental Methods

Materials. Methanol and acetonitrile were dried using standard procedures and freshly distilled prior to use. The following compounds were synthesized according to published procedures: 3,5-diisopropyl pyrazole,[38] hydrotris(3,5-diisopropyl-1-pyrazoyl)methane (Tpm^{iPr}),[39] *N,N'*-dimethylimidazole selone (dmise),[19] *N,N'*-

dimethylimidazole thione (dmit),[19] and bis(1-methylimidazolyl) diselenide.[31] The following reagents were used as received: 3,5-dimethyl-1-pyrazole (Aldrich), tetra-*n*-butylammonium bromide (Aldrich), sodium carbonate (VWR), selenium powder, sulfur powder, diisobutyrylmethane (VWR), hydrazine monohydrate (VWR), 1-methylimidazole (VWR), methyliodide (VWR) , $CuCl_2$ (VWR) and $Cu(OTf)_2$ (Alfa Aesar).

Instrumentation. ^{1}H, $^{13}C\{^{1}H\}$, $^{19}F\{^{1}H\}$, and $^{77}Se\{^{1}H\}$ NMR spectra were obtained on a Bruker AVANCE 500 or 300 NMR spectrometers. ^{1}H and $^{13}C\{^{1}H\}$NMR chemical shifts are reported in δ relative to trimethylsilane (TMS; δ 0). $^{77}Se\{^{1}H\}$ NMR chemical shifts are reported relative to dimethyl selenide (δ 0) and externally referenced to diphenyl diselenide (δ 461).[40] $^{19}F\{^{1}H\}$ NMR spectra were externally referenced to CCl_3F (δ 0).[41]

Infrared spectra were obtained using nujol mulls on KBr salt plates using a Magna 550 IR spectrometer. Abbreviations used in the description of vibrational data are as follows: vs, very strong; s, strong; m, medium; w, weak; b, broad. Electrospray ionization mass spectrometry (ESI-MS) was conducted using a QSTAR XL Hybrid MS/MS System from Applied Biosystems via direct injection of sample (0.05 mL/min flow rate) into a Turbo Ionspray ionization source. Samples were run under both positive and negative mode, with ionspray voltage of 5500, and TOF scan mode. MALDI-TOF-MS was conducted on a Bruker Microflex. Trans-2-[3-(4-tert-butylphenyl)-2-methyl-2-propenylidene]-malononitrile was used as a matrix for co-crystallization of the copper

complex characterized. All the peak envelopes matched their calculated isotopic distributions.

Formation of [($C_5N_2H_8Se)_2$][($OTf)_2$] (**1**) *by oxidation with Cu($OTf)_2$.* $Cu(OTf)_2$ (362 mg, 1 mmol) was dissolved in acetonitrile (15 mL) to give a light blue solution, and to this was cannula added a solution of dmise (175 mg, 1 mmol) in acetonitrile (10 mL). Upon addition, the solution color changed from light blue to orange. The reaction mixture was stirred for 6 h, and then the solvent volume was reduced to about 5 mL *in vacuo*. The desired product was precipitated by addition of ether, and the solid precipitate was filtered and dried *in vacuo*. Crystals of **1** were grown via slow vapor diffusion of ether into acetonitrile solution. Yield 37% (240 mg, 0.369 mmol). Mp. 227 °C. ^{1}H NMR (CD_3CN): 3.67 (s, 6 H, $2CH_3$), 7.63 (s, 2H, 2CH). $^{13}C\{^{1}H\}$ NMR (CD_3CN): 37.59 (CH_3), 125.94 (CH), 135.57 (C-Se). $^{19}F\{^{1}H\}$ NMR (CD_3CN): -79.24. $^{77}Se\{^{1}H\}$ NMR (CD_3CN): 329.37. UV-vis ($CNCH_3$): 206, 226 (shoulder), 275 nm. IR (cm^{-1}): 517 s, 573 s, 620 s, 637 vs, 666 s, 739 s, 749 vs, 778 s, 1029 vs, 1139 vs, 1223 vs, 1254 b, 1377 vs, 1407 w, 1463 vs, 1502 vs, 1566 s, 1598 w, 2728 w, 2853 b, 3128 w, 3154 w, 3177 w. ESI-MS: *m/z* positive ionization: 175.9 $[(C_5N_2H_8Se)_2]^{2+}$; negative ionization 148.97 $[(CF_3SO_3)_2]^{2-}$. Anal. Calc. for $C_{12}H_{16}N_4Se_2O_6S_2F_6$: C, 22.23; N, 8.64; H, 2.49. Found C, 22.05; N, 8.43; H, 2.28.

Formation of [($C_5N_2H_8S)_2$][($OTf)_2$] (**2**) *by oxidation with Cu($OTf)_2$.* $Cu(OTf)_2$ (362 mg, 1 mmol) was dissolved in acetonitrile (15 mL), and to this solution was cannula added dmit (192 mg, 1.5 mmol) in acetonitrile (10 mL). Upon addition, the color changed

from light blue to light yellow. The reaction mixture was stirred for 6 h, and then the solvent volume was reduced to about 5 mL *in vacuo*. The product was precipitated out using ether and the precipitate was filtered and dried *in vacuo*. Crystals of **2** suitable for X-ray diffraction analysis were grown through slow vapor diffusion of ether into acetonitrile. Yield 34% (189 mg, 0.339 mmol). Mp. 181°C. ^{1}H NMR (CD_3CN): 3.73 (s, 6 H, $2CH_3$), 7.64 (s, 2H, 2CH). $^{13}C\{^{1}H\}$ NMR (CD_3CN): 37.27 (CH_3), 126.94 (CH), 140.64 (C-S). $^{19}F\{^{1}H\}$ NMR (CD_3CN): -79.24. UV-vis ($CNCH_3$): 215, 265, 305 (shoulder) nm. IR (cm^{-1}): 517 s, 573 s, 637 vs, 679 s, 723 s, 741 s, 754 vs, 790 s, 1031 vs, 1139 vs, 1232 vs, 1259 b, 1377 vs, 1407 s, 1463 vs, 1506 vs, 1564 s, 1603 w, 2361 w, 2727 w, 2913 b, 3123 w, 3152 w. ESI-MS: *m/z* positive ionization: 128.2 $[(C_5N_2H_8S)_2]^{2+}$; negative ionization; 148.98 $[(CF_3SO_3)_2]^{2-}$. Anal. Calc. for $C_{12}H_{16}N_4S_4O_6F_6$: C, 25.99; N, 10.10; H, 2.91. Found C, 25.85; N, 9.95; H, 2.73.

Formation of $[(C_5N_2H_8Se)_2][Cu_3Cl_5]$ (**3**) *by oxidation with $CuCl_2$.* $CuCl_2$ (135 mg, 1 mmol) was dissolved in ethanol (15 mL), and to this solution was cannula added dmise (175 mg, 1 mmol) in dichloromethane (10 mL). Upon addition, the solution changed color from light brown to dark brown. The reaction mixture was stirred for 6 h and a red solid precipitated from the solution. The precipitate was filtered and dried *in vacuo*. Crystals of **3** were grown through slow vapor diffusion of ether into acetonitrile solution. Yield 20% (153 mg, 0.200 mmol). ^{1}H NMR (d_6-DMSO): 3.89 (s,12 H, $4CH_3$), 7.61 (s, 4H, 4CH). $^{13}C\{^{1}H\}$ NMR (d_6-DMSO): 37.03 (CH_3), 122.25 (CH), C-Se resonance not observed. IR (cm^{-1}): 467 w, 504 w, 660 vs, 739 vs, 761 s, 1079 w, 1155 s, 1223 vs, 1243 s, 1377 vs, 1463 vs, 1494 s, 1562 s, 2855 s, 2928 b. ESI-MS: *m/z* 175.9 $[(C_5N_2H_8Se)_2]^{2+}$.

Anal. Calc. for $C_{10}H_{16}N_4Se_2Cu_3Cl_5$: C, 16.73; N, 7.80; H, 2.25. Found C, 18.73; N, 7.84; H, 2.3.

Tpm^{iPr}Cu(OTf)$_2$ (**4**). $Cu(OTf)_2$ (362 mg, 1 mmol) was dissolved in acetonitrile (10 mL), and to this was added Tpm^{iPr} (428 mg, 1 mmol) in acetonitrile (10 mL). The reaction mixture was stirred for 4 h, dried *in vacuo*, and the obtained green solid product was washed with diethyl ether and dried *in vacuo* to afford Tpm^{iPr}Cu$(OTf)_2$. Yield: 89% (724 mg, 0.89 mmol). UV-vis (CH_3CN): 272 nm. Mp: 132°C. IR (cm^{-1}): 517 s, 573 s, 638 s, 673 s, 724 s, 755 s, 832 s, 904 w, 924 w, 1031 s, 1059 s, 1153 s, 1268 s, 1377 s, 1463 s, 1560 s, 2300 w, 2327 s, 2926 b, 3127 w. Mass spectrum (Maldi): *m/z* 529.33 [Tpm^{iPr}Cu]$^+$, 678.22 [Tpm^{iPr}Cu(OTf)]$^+$. Anal. Calc. for $C_{39}H_{60}CuF_6N_{10}O_7S_2Se_2$: C, 39.68; N, 11.86; H, 5.12. Found: C, 42.87; N, 11.13; H, 5.63.

[Tpm^{iPr}Cu(MISeox)][(OTf)$_2$] (**5**). [Tpm^{iPr}Cu$(OTf)_2$ (**4**) (414 mg, 0.5 mmol) was dissolved in acetonitrile (10 mL), and into this solution was cannula transferred MISeox (162 mg, 0.5 mmol) in dichloromethane (10 mL). Upon addition, the color of the reaction mixture changed from blue to brown. The reaction mixture was stirred for 4 h, the solvent volume was reduced to about 3 mL, and a light green solid was precipitated with ether. The solid was then filtered and dried *in vacuo*. Crystals of **4** suitable for X-ray analysis were grown by slow vapor diffusion of ether into acetonitrile solution. Yield: 81% (450 mg, 0.405 mmol). UV-vis (CH_3CN): 268 nm. IR (cm^{-1}): 517 s, 573 w, 638 s, 683 s, 725 s, 771 s, 831 s, 922 w, 944 w, 1014 w, 1030 s, 1057 s, 1156 s, 1189 w, 1224 w, 1261 s, 1378 s, 1463 s, 1560 s, 1638 w, 2286 w, 2855 s, 2926 b, 3116 s, 3470 b. Mass spectrum

(ESI-MS): *m/z* 425.6 $[Tpm^{iPr}Cu(MISeox)]^{2+}$, 321.9 $[MISeox]^{+}$. Anal. Calc. for $C_{39}H_{60}CuF_6N_{10}O_7S_2Se_2$: C, 39.68; N, 11.86; H, 5.12. Found: C, 40.12; N, 11.96; H, 5.24.

X-ray data collection and structural determination. Crystals were grown by vapor diffusion of diethyl ether into an acetonitrile solution for $[(C_5N_2H_8Se)_2][(OTf)_2]$ (**1**), $[(C_5N_2H_8S)_2][(OTf)_2]$ (**2**), $[(C_5N_2H_8Se)_2][Cu_2Cl_5]$ (**3**), and $[Tpm^{iPr}Cu(MISeox)][(OTf)_2]$ (**4**). Single crystals were mounted on a glass filament with silicon grease and immediately cooled to 168±2 K in a cold nitrogen gas stream. Intensity data were collected using a Rigaku Mercury CCD detector and an AFC8S diffractometer. The space groups $P2_1/c$ for **1** and **2**, $C2/c$ for **3**, and $P2_1/n$ for **4** were determined from the observed systematic absences. Data reduction including the application of Lorentz and polarization (Lp) effects and absorption corrections used the CrystalClear program.[42] The structures were solved by direct methods and subsequent Fourier difference techniques, and refined anisotropically, by full-matrix least squares, on F^2 using SHELXTL 6.10.[43] Crystallographic data for **1**, **2**, **3**, and **5** are summarized in Tables 4.7 and 4.8. In the final cycle of least squares, independent anisotropic displacement factors were refined for the non-hydrogen atoms and the methyl hydrogen atoms were fixed in idealized positions with C-H = 0.96 Å. Their isotropic displacement parameters were set equal to 1.5 times U_{eq} of the attached carbon atom. The high wR_2 value for complex **5** is due to disorder of the triflate anions and diisobutyl groups on the pyrazole ring.

Table 4.7. Summary of crystallographic data for complexes **1** and **2**.

	1	**2**
Chemical Formula	$C_{12}H_{16}F_6N_4O_6S_2Se_2$	$C_{12}H_{16}F_6N_4O_6S_4$
F.W. (g/mol)	648.33	554.53
Space group	$P2_1/c$	$P2_1/c$
Temp./K	168±2	168±2
Crystal system	Monoclinic	Monoclinic
a, Å	8.5501(17)	8.5235(17)
b, Å	20.249(4)	19.874(4)
c, Å	13.002(3)	12.926(3)
α, °	90	90
β, °	100.53(3)	98.29(3)
γ, °	90	90
V, $Å^3$	2236.3(8)	2166.8(8)
Z	4	4
D_{cal}, Mg/m^3	1.946	1.700
Indices (min)	[-9, -21, -16]	[-10, -22, -16]
(max)	[10, 25, 16]	[10, 24, 16]
Parameters	293	293
F(000)	1272	1128
μ, mm^{-1}	3.580	0.528
2θ range,	2.57- 26.25	2.41 – 26.32
Collected reflections	18636	18721
Unique reflections	4449	4393
Final R (obs. Data)[a], R_1	0.0346	0.0471
wR_2	0.0839	0.1192
Final R (all data), R_1	0.0383	0.0568
wR_2	0.0870	0.1304
Goodness of fit (S)	1.125	1.105
Extinction coefficient	0.0022(9)	
Largest diff. Peak	0.621	0.689
Largest diff. Hole	-0.712	-0.476

[a] $R_1 = [\Sigma||F_0| - |F_c||]/ \Sigma|F_0|$; $wR_2 = \{[\Sigma w[(F_0)^2 - (F_c)^2]^2\}^{1/2}$

Table 4.8. Summary of crystallographic data for the complexes **3**, and **4**.

	3	**4**
Chemical Formula	$C_{12}H_{16}N_4Se_2Cu_3Cl_5$	$C_{39}H_{60}CuF_6N_{10}O_7S_2Se_2$
F.W. (g/mol)	716.06	1180.55
Space group	C2/*c*	$P2_1/n$
Temp./K	168±2	168±2
Crystal system	Monoclinic	Monoclinic
a, Å	12.238(2)	15.196(3)
b, Å	12.217(2)	24.359(5)
c, Å	14.123(3)	15.260(3)
α, °	90	90
β, °	108.61(3)	116.96
γ, °	90	90
V, $Å^3$	2001.2(7)	5034.7(170
Z	4	4
D_{cal}, Mg/m^3	2.383	1.557
Indices (min)	[-10, -15, -17]	[-15, -28, -18]
(max)	[15, 15, 17]	[18, 28, 16]
Parameters	112	614
F(000)	1376	2412
μ, mm^{-1}	7.466	2.040
2θ range,	3.04-26.29	2.69-25.05
Collected reflections	8327	33101
Unique reflections	2022	8864
Final R (obs. Data)[a], R_1	0.0435	0.0771
wR_2	0.1043	0.1972
Final R (all data), R_1	0.0546	0.1001
wR_2	0.1137	0.2159
Goodness of fit (S)	1.111	1.087
Extinction coefficient		
Largest diff. Peak	1.216	1.673
Largest diff. Hole	-1.122	-0.731

[a] $R_1 = [\Sigma||F_0| - |F_c||]/ \Sigma|F_0|$; $wR_2 = \{[\Sigma w[(F_0)^2 - (F_c)^2]^2\}^{1/2}$

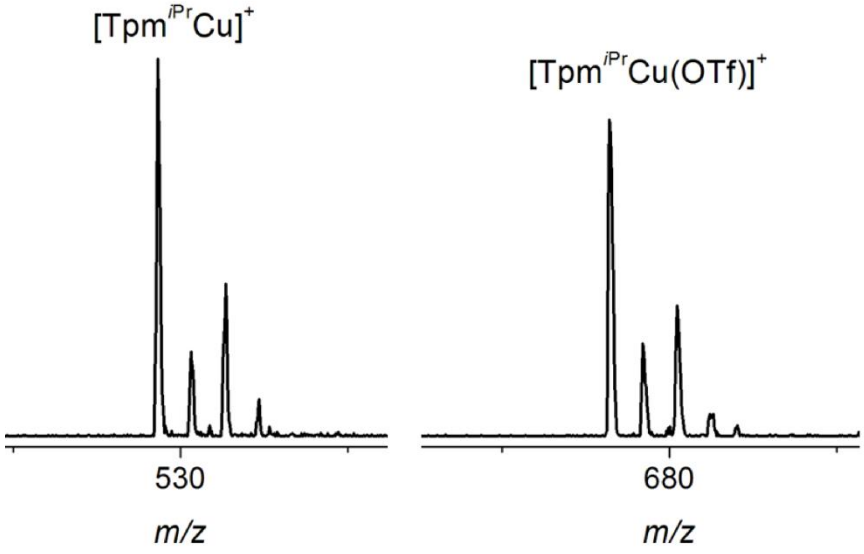

Figure 4.12. MALDI-TOF-MS for $Tpm^{iPr}Cu(OTf)_2$ (**4**)

References

(1) Raper, E. S. *Coord. Chem. Rev.* **1996**, *153*, 199-255.

(2) Raper, E. S. *Coord. Chem. Rev.* **1997**, 475-564.

(3) Akrivos, P. D. *Coord. Chem. Rev.* **2001**, *213*, 181-210.

(4) Parkin, G. *New J. Chem.* **2007**, *31*, 1996-2014.

(5) Jia, W. G.; Huang, Y. B.; Lin, Y. J.; Jin, G. X. *Dalton Trans.* **2008**, 5612-5620.

(6) Cheon, J.; Arnold, J.; Yu, K. M.; Bourret, E. D. *Chem. Mater.* **1995**, *7*, 2273-2276.

(7) Fahey, R. C. *Annu. Rev. Microbiol.* **2001**, *55*, 333-356.

(8) Seebeck, F. P. *J. Am. Chem. Soc.* **2010**, *132*, 6632-6633.

(9) Jacob, C. *Nat. Prod. Rep.* **2006**, *23*, 851-863.

(10) Yamashita, Y.; Yamashita, M. *J. Biol. Chem.* **2010**, *285*, 18134-18138.

(11) Battaglia, L. P.; Corradi, A. B.; Devillanova, F. A.; Verani, G. *Transition Met. Chem.* **1979**, *4*, 264-266.

(12) Hussein, A.; Devillanova, F. A.; Isaia, F.; Verani, G. *Transition Met. Chem.* **1985**, *10*, 368-370.

(13) Devillanova, F. A.; Diaz, A.; Isaia, F.; Battaglia, L. P.; Corradi, A. B. *J. Coord. Chem.* **1986**, *15*, 161-172.

(14) Piro, O. E.; Piatti, R. C. V.; Bolzan, A. E.; Salvarezza, R. C.; Arvia, A. J. *Acta Crystallogr. Sect. B-Struct. Sci.* **2000**, *56*, 993-997.

(15) Arner, E. S. J.; Holmgren, A. *Eur. J. Biochem.* **2000**, *267*, 6102-6109.

(16) Shchedrina, V. A.; Novoselov, S. V.; Malinouski, M. Y.; Gladyshev, V. N. *Proc. Natl. Acad. Sci. U. S. A.* **2007**, *104*, 13919-13924.

(17) Yamashita Y.; Yamashita M. *J. Biol. Chem.* **2010**, *285*, 18134-18138.

(18) Figueroa, J. S.; Yurkerwich, K.; Melnick, J.; Buccella, D.; Parkin, G. *Inorg. Chem.* **2007**, *46*, 9234-9244.

(19) Roy, G.; Das, D.; Mugesh, G. *Inorg. Chim. Acta* **2007**, *360*, 303-316.

(20) Lobana, T. S.; Castineiras, A. *Polyhedron* **2002**, *21*, 1603-1611.

(21) Beheshti, A.; Clegg, W.; Nobakht, V.; Mehr, M. P.; Russo, L. *Dalton Trans.* **2008**, 6641-6646.

(22) Popovic, Z.; Pavlovic, G.; Matkovic-Calogovic, D.; Soldin, Z.; Rajic, M.; Vikic-Topic, D.; Kovacek, D. *Inorg. Chim. Acta.* **2000**, *306*, 142-152.

(23) Bierbach, U.; Hambley, T. W.; Farrell, N. *Inorg. Chem.* **1998**, *37*, 708-716.

(24) Tomlin, D. W.; Campbell, D. P.; Fleitz, P. A.; Adams, W. W. *Acta Crystallogr. Sect. C-Cryst. Struct. Commun.* **1997**, *53*, 1153-1154.

(25) Aragoni, M. C.; Arca, M.; Demartin, F.; Devillanova, F. A.; Garau, A.; Isaia, F.; Lippolis, V.; Verani, G. *J. Am. Chem. Soc.* **2002**, *124*, 4538-4539.

(26) Cordero, B.; Gomez, V.; Platero-Prats, A. E.; Reves, M.; Echeverria, J.; Cremades, E.; Barragan, F.; Alvarez, S. *Dalton Trans.* **2008**, 2832-2838.

(27) Williams, D. J.; Fawcettbrown, M. R.; Raye, R. R.; Vanderveer, D.; Pang, Y. T.; Jones, R. L.; Bergbauer, K. L. *Heteroatom Chem.* **1993**, *4*, 409-414.

(28) Chiesi Villa, A.; Nardelli, M.; Vidoni, M. E. *Acta Cryst.* **1970**, *B26*, 1504.

(29) Bigoli, F.; Demartin, F.; Deplano, P.; Devillanova, F. A.; Isaia, F.; Lippolis, V.; Mercuri, M. L.; Pellinghelli, M. A.; Trogu, E. F. *Inorg. Chem.* **1996**, *35*, 3194-3201.

(30) Bondi, A. *J. Phys. Chem.* **1965**, *68*, 441-451.

(31) Roy, G.; Nethaji, M.; Mugesh, G. *J. Am. Chem. Soc.* **2004**, *126*, 2712-2713.

(32) Kimani, M. M.; Brumaghim, J. L.; Vanderveer, D. *Inorg. Chem.* **2010**, *49*, 9200-9211.

(33) Lee, D. H.; Hatcher, L. Y. Q.; Vance, M. A.; Sarangi, R.; Milligan, A. E.; Sarjeant, A. A. N.; Incarvito, C. D.; Rheingold, A. L.; Hodgson, K. O.; Hedman, B.; Solomon, E. I.; Karlin, K. D. *Inorg. Chem.* **2007**, *46*, 6056-6068.

(34) Balamurugan, R.; Palaniandavar, M.; Gopalan, R. S. *Inorg. Chem.* **2001**, *40*, 2246-2255.

(35) Li, Q. X.; Wang, X. F.; Cai, L.; Li, Q.; Meng, X. G.; Xuan, A. G.; Huang, S. Y.; Ai, J. *Inorg. Chem. Commun.* **2009**, *12*, 145-147.

(36) Jitsukawa, K.; Harata, M.; Arii, H.; Sakurai, H.; Masuda, H. *Inorg. Chim. Acta* **2001**, *324*, 108-116.

(37) Pierre, J. L.; Fontecave, M. *BioMetals* **1999**, *12*, 195-199.

(38) Kitajima, N.; Fujisawa, K.; Fujimoto, C.; Moro-oka, Y.; Hashimoto, S.; Kitagawa, T.; Toriumi, K.; Nakamura, A. *J. Am. Chem. Soc.* **1992**, *114*, 1277-1291.

(39) Fujisawa, K.; Ono, T.; Ishikawa, Y.; Amir, N.; Miyashita, Y.; Okamoto, K.; Lehnert, N. *Inorg. Chem.* **2006**, *45*, 1698-1713.

(40) Odom, J. D.; Dawson, W. H.; Ellis, P. D. *J. Amer. Chem. Soc.* **1979**, *101*, 5815-5823.

(41) *NMR and the Periodic Table*; Harris, R. K.; Mann, B. E., Eds.; Academic Press: London, 1978, p. 99.

(42) Crystalclear; The Woodlands: Texas, USA, 1999.

(43) Sheldrick, G. M.; Bruker Analytical X-ray Systems Inc.: Madison, WI, 2000.

CHAPTER FIVE

SYNTHESIS, CHARACTERIZATION, AND DFT STUDIES OF THIONE AND SELONE, Cu(I) COMPLEXES WITH VARIABLE COORDINATION GEOMETRIES

Introduction

There is increased interest in the chemistry of copper with soft Lewis base donors such as thiolates, thioamides, selenolates and selenoamides for use in catalysis[1] and in bioinorganic chemistry for the study of copper metallothioneins and metallochaperones.[2-5] Of particular interest is the coordination chemistry of selenium with biologically-important transition metals (Cu, Fe, Ni, Zn, Mn, Mo, etc.), since selenium has been shown to possess stronger and unique antioxidant properties relative to sulfur.[6-8] Our group has determined that copper coordination to sulfur and selenium containing ligands is a novel mechanism for selenium and sulfur antioxidant activity.[9-13] We are interested in the chemistry of *N,N'*-dimethylimidazole selone (dmise) and thione (dmit) because these and similar ligands are effective antioxidants (FFigure 5.1).[14,15] The dmise and dmit ligands are similar to methimazole, a drug currently used in the treatment of hyperthyroidism,[16] and also resemble ergothioneine[17,18] and selenoneine,[15] sulfur- and selenium-containing antioxidants naturally found in plants and animals.

The coordination of heterocyclic thioamides and selenoamides to copper results in diverse architectures ranging from mononuclear complexes to polynuclear networks with a variety of binding modes. The coordination modes of the heterocyclic

chalcogenones range from monodentate to bridging via coordination of sulfur or selenium atoms.[19-21] Mono-alkylated heterocyclic thiones and selones can also bind metals via the non-alkylated nitrogen atom.[22-24] The applications and coordination chemistry of thiones and selones with transition metals has been extensively reviewed by Raper,[25,26] Akrivos,[27] Spicer, *et al.*,[28] Pettinari,[29] and Parkin.[30] Although the coordination chemistry of *N*-alkylimidazole thiones and *N*,*N*'-dialkylimidazole thiones with transition metals is well developed,[1,20,21,25,26,31-34] few reported complexes bearing the analogous selenium ligands have been reported: $Zn(dmise)_2Cl_2$,[32,35] $Co(dmise)_2Cl_2$,[36,37] $[Cd(dmise)_4][PF_6]$,[38] $RuCl_2(PPh_3)(mt^{se})_2$, (mt^{se} = selenometh-imazolyl),[39] $HgCl_2$(N-*i*-PrImSe)$_2$, (*N*-*i*-PrImSe = *N*-isopropyl-imidazolidine-2-selone),[40] $HgCl_2(MeImSe)_3$, (MeImSe = *N*-methyl-imidazolidine-2-selone),[41] $[Tpm^RCu(dmise)]^+$, Tp*Cu(dmise),[19] $[Cu(1,10\text{-phen})_2(C_5H_{10}N_2Se)][2ClO_4]$, (phen = phenanthroline),[42] Cu_2LY_3 (Y = Cl, Br; L = *N,N'*-dimethylimidazolidine selone),[43] and $Cu_2(btseme)_3X_2$ (X = Cl, Br, NO_3, ½SO_4; btseme = *N*-methylbenzothiazole-2-selone).[44]

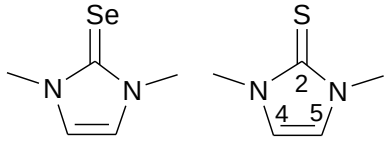

dmise dmit

Figure 5.1. Chalcogenone ligands used in this study.

This work reports the synthesis of copper halide complexes with dmise and dmit ligands, with the aim of studying their different coordination modes and electrochemistry. Complexes of the formulas $Cu_4(\mu\text{-}L_4)(\mu\text{-}X_2)X_2$, CuL_2X, CuL'_2X,

CuL_2Y and CuL'_2Y (L = dmise, L´ = dmit; X = I^-, Br^-; Y = Cl^-) have been synthesized and characterized using ^1H, $^{13}C\{^1H\}$ and $^{77}Se\{^1H\}$ NMR spectroscopy, cyclic voltammetry, X-ray structural analysis, X-ray powder diffraction (XRD), and electrospray ionization mass spectrometry (ESI-MS). Observed differences in the coordination geometries and packing orientations of these complexes are also examined using density functional theory (DFT) calculations. This chapter has been submitted to Dalton Transactions for publication (Kimani, M. M.; Brumaghim, J. L.; Bayse, C. A. *Dalton Trans*. submitted).[45]

Results and Discussion

Synthesis of Cu(I)-chalcogenone halide complexes. The target metal complexes were synthesized by treating copper halides with either one or two molar equivalents of selone or thione. The reaction of CuI and CuBr with one molar equivalent of dmise resulted in formation of tetranuclear copper complexes with bridging selone ligands (**1** and **6**; Figure 5.2A). The tetranuclear copper-iodide-selone complex (**1**) can also be synthesized via a two-step, one-pot reaction with molar equivalents of $[Cu(NCCH_3)_4][BF_4]$ and dmise in acetonitrile followed by cannula addition of KI in methanol. The reaction of CuI with dmise results in an insoluble precipitate that is redissolved by addition of KI in methanol, similar to a method previously described by Niu, *et al*.[46] Both synthetic methods result in similar yields of **1**.

Treating CuI with two molar equivalents of dmise or dmit in acetonitrile and

dichloromethane results in the formation of monomeric three-coordinate copper-iodo complexes (**2** and **3a**) characterized by intramolecular π-π interactions between the two heterocyclic five-membered rings (Figure 5.2B). In contrast, treating two molar equivalents of dmit with CuI in a mixed solvent system of ethanol and dichloromethane results in the formation of a trigonal copper complex (**3b**) with no intramolecular π-π interactions (Figure 5.2C).

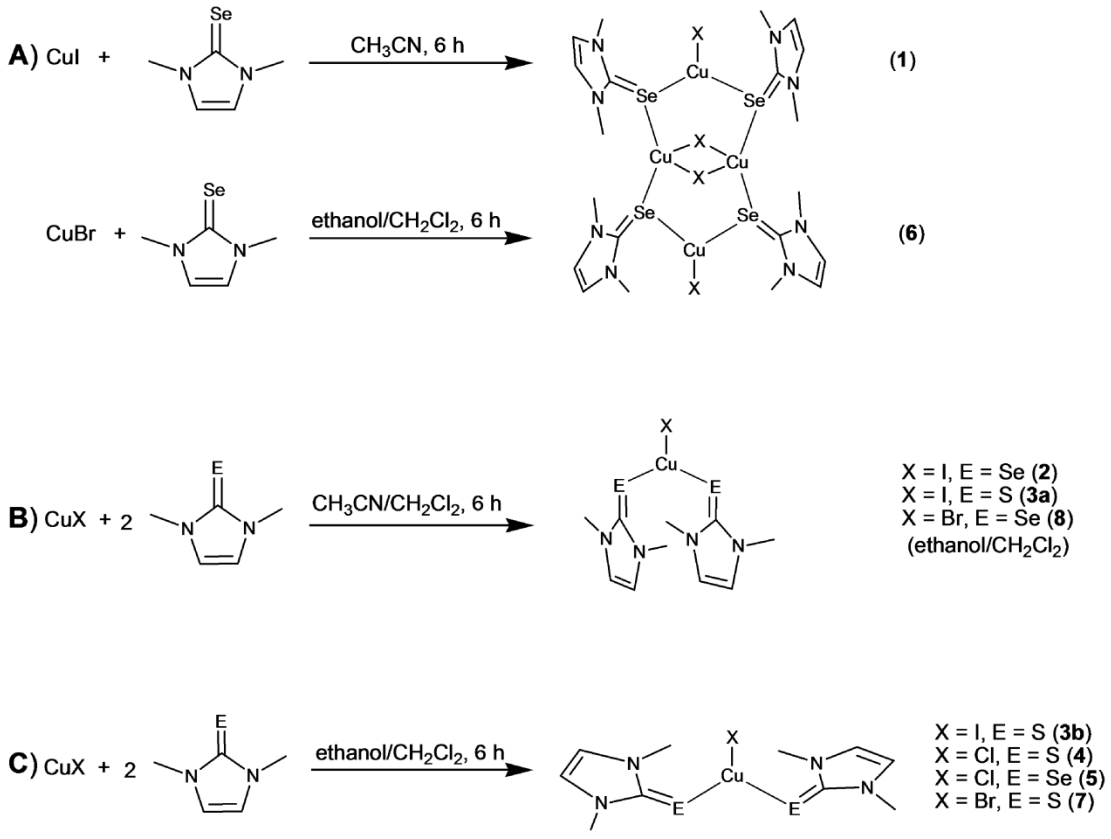

Figure 5.2. Synthetic procedures for the preparation of tetrameric and trigonal planar copper complexes.

The three-coordinate copper chloride or bromide complexes (**4**, **5**, **7**, and **8**) are

synthesized by treating two molar equivalents of dmit or dmise with CuCl or CuBr in a mixed solvent system (Figure 5.2C). The X-ray crystal structure of $Cu(dmit)_2Cl$ has been reported by Kim, *et al*. but its synthesis and characterization was not reported.[1] The trigonal copper complexes (**2**, **3a**, **3b**, **4**, **5**, **7** and **8**) can be synthesized with good yields (85-92%), whereas the tetrameric complexes **1** and **6** have an average yield of 23%. Crystals of the target metal complexes are stable in air but the Cu^+ ions are easily oxidized to Cu^{2+} in solution.

Crystallographic studies of tetrameric Cu(I) halides complexes with heterocyclic selone ligands. The X-ray crystal structures of $Cu_4(\mu\text{-dmise})_4(\mu\text{-I})_2I_2\cdot 1.5CNCH_3$ (**1**) and $Cu_4(\mu\text{-dmise})_4(\mu\text{-Br})_2Br_2\cdot 0.5CNCH_3$ (**6**) show two different coordination geometries around the copper ions (Figure 5.3). Two selenium atoms and one iodide or bromide ion coordinate to a single Cu(I) ion, forming a three-coordinate complex with the selone ligands adopting a *cis* conformation relative to I(2)/Br(2) and I(2A)/Br(2A) along the copper chalcogenone bond. The Cu(2) and Cu(2A) ions have distorted trigonal planar geometry. Trigonal copper bond angles range from 116.11(3)° to 121.81(6)° in **1** and from 119.56(3)° to 119.71(5)° for the less distorted trigonal copper centers in **6**. Cu-I and Cu-Br bond distances are 2.58 Å and 2.43 Å, respectively, for **1** and **6**, and the Cu-Se bond distances are 2.42 Å and 2.41Å, respectively.

The two additional copper centers (Cu(1) and Cu(1A)) in **1** and **6** adopt distorted tetrahedral geometries with a $Cu_2(\mu\text{-I})_2$ or $Cu_2(\mu\text{-Br})_2$ core (average Cu-Cu

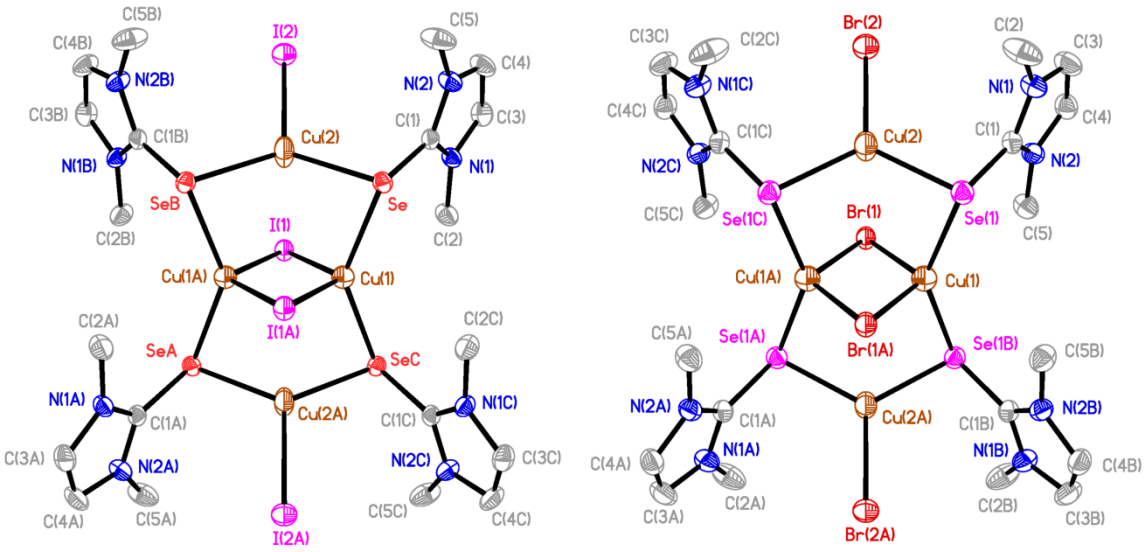

Figure 5.3. X-ray crystal structure diagrams of $Cu_4(\mu_4\text{-dmise})(\mu\text{-}I_2)I_2$ (**1**; left) and $Cu_4(\mu_4\text{-dmise})(\mu\text{-}Br_2)Br_2$ (**6**; right) showing 50% probability density ellipsoids. Hydrogen atoms are omitted for clarity.

Table 5.1. Experimental crystal data (EXP) vs. theoretical DFT calculations for selected bond lengths (Å) and angles (deg) of $Cu_4(\mu\text{-dmise})_4(\mu\text{-}I)_2I_2$ **(1)** and $Cu_4(\mu\text{-dmise})_4(\mu\text{-}Br)_2Br_2$ (**6**).

1:1 complex	X=I; Y=Se (EXP) (**1**)	X=I; Y=Se (DFT)	X=Br; Y=Se (EXP) (**6**)	X=Br; Y=Se (DFT)
Cu(1)-Y	2.4148(8)	2.470	2.4087(7)	2.446
Cu(1)-X(1)	2.7613(9)	2.731	2.6470(10)	2.582
Cu(1)-Cu(1A)	2.607(2)	2.591	2.631(2)	2.630
Cu(2)-Y(2)	2.4203(9)	2.459	2.4130(8)	2.434
Cu(2)-X(2)	2.5820(13)	2.566	2.4298(13)	2.382
Cu(2)-X(1)	3.251	3.492	3.428	3.763
Y-Cu(2)-Y	121.81(6)	119.9	119.71(5)	118.3
Y-Cu(2)-X(2)	116.11(3)	118.7	119.56(3)	120.7
Y-C(1)	1.882(5)	1.904	1.890(5)	1.900

distance 2.62 Å) and two bridging selenium atoms from the dmise ligand. Each Cu^+ ion in the core has distorted tetrahedral geometry with angles about each copper

varying from 89.6 to 140.7° in **1** and 90.3° to 142.7° in **6**. The central $Cu_2(\mu\text{-}I)_2$ core in **1** is rhomboidal with bridging Cu-I bond distances of 2.76 Å, longer than the terminal Cu-I bond distances of 2.58 Å. The angles in the $Cu_2(\mu\text{-}I)_2$ core are 56.3° for I(1)-Cu(I)-(1A) and 123.7° for Cu(1)-I(1)-Cu(1A), whereas the $Cu_2(\mu\text{-}Br)_2$ core in **6** has Br(1)-Cu(1)-Br(1A) and Cu(1)-Br(1)-Cu(1A) angles of 50.6° and 120.4°, respectively (Table 5.1). The tetrameric complex **6** has bridging Cu-Br bond distances of 2.65 Å, longer than the terminal Cu-Br bond distances of 2.43 Å.

In the X-ray structures of **1** and **6**, the average Cu-Se bond lengths of 2.41 Å are shorter or comparable to most reported bridging copper-selenium complexes in the literature[47-49] but longer than previously synthesized mononuclear copper-selone complexes such as $[Tpm^*Cu(dmise)]^+$ (2.30 Å) and Tp*Cu(dmise) (2.33 Å).[19] The bond distances for Cu(1)-I(1) (2.76 Å), Cu(2)-I(2) (2.58 Å), Cu(1)-Br(1) (2.65 Å) and Cu(2)-Br(2) (2.43 Å) are shorter than the sum of the ionic radii of Cu^+ and I^- (2.97 Å) and Cu^+ and Br^- (2.73 Å), respectively.[50] Short-contact interactions between iodine and hydrogen atoms are observed in the packing diagram of complex **1** (Figure 5.8), whereas the packing diagram of complex **6** shows no short-contact interactions. The short contact interactions of 3.16 Å between I(2)-H2B in **1** are within the sum of their van der Waals radii (3.18 Å) and possibly promote stability of this complex. The long Cu(1)-Cu(1A) distances in 1 and 6 indicate little interaction between these ions.

Density functional theory studies for tetrameric copper(I) halide complexes. Theoretical DFT calculations were conducted on the tetrameric complexes **1** and **6** to determine the effects of the halide and chalcogenone ligands on the observed crystal

structures. The DFT(B3PW91)-optimized structures of **1** and **6** were optimized in C_{2h} symmetry and are in good agreement with X-ray crystallographic data (Table 5.1) with bond distances and angles generally within 0.04 Å and 2° of experimental values. The Cu(2)-X(1) short contact is underestimated (DFT(B3PW91) = 0.25-0.35 Å; DFT(BP86) = 0.4-0.55 Å), especially for the BP86 xc functional which is known to perform poorly for non-bonding interactions. Slight overestimation of the calculated X-H2B short contacts may be attributed to the absence of intermolecular X-H interactions in the gas phase. The DFT(B3PW91)-optimized geometries of the hypothetical thione analogs (**1**(**S**) and **6**(**S**)) were similar to **1** and **6** with shorter Cu-Y bond distances. The energies of formation (ΔE+ZPE) of these species relative to the CuX(dmit/dmise) monomers were ~10 kcal/mol less favorable than for **1** and **6**.

Crystallographic studies of trigonal Cu(I) halides complexes with heterocyclic selone and thione ligands Treating copper halides with two equivalents of dmise or dmit results in the formation of monomeric three-coordinate complexes with differing geometries. The molecular structures and atom numbering schemes for $Cu(dmise)_2I$ (**2**), $Cu(dmit)_2I$ (**3a**), and $Cu(dmise)_2Br$ (**8**) are given in Figure 5.4, and Table 5.2 lists their selected bond distances and angles. X-ray structural studies established that these complexes are monomeric with two non-bridging selone and thione ligands coordinated to copper. The heterocyclic rings in complexes **2**, **3a**, and **8** adopt a *trans* conformation relative to the halogen atom along the copper-chalcogenone bond. The Cu^+ ion has distorted trigonal geometry with angles ranging from 111.56° to 136.87° for $Cu(dmise)_2I$ (**2**); 111.82° to 136.87° for $Cu(dmit)_2I$ (**3a**); and 108.0° to 144.0° for

Cu(dmise)$_2$Br (**8**). The Cu-Se and Cu-S bond distances are 2.34 Å for **2** and **8** and 2.23 Å for **3a**, whereas the avg. Cu-I bond distance of in **2** and **3a** is 2.56 Å. Short contact interactions between iodine and hydrogen atoms are found within the unit cell of Cu(dmit)$_2$I (**3a**; Figure 5.9) but are absent in the unit cell of the selenium analog Cu(dmise)$_2$I (**2**). The short contact interaction of 3.18 Å between I and H5C is equal to the sum of their van der Waals radii (3.18 Å).

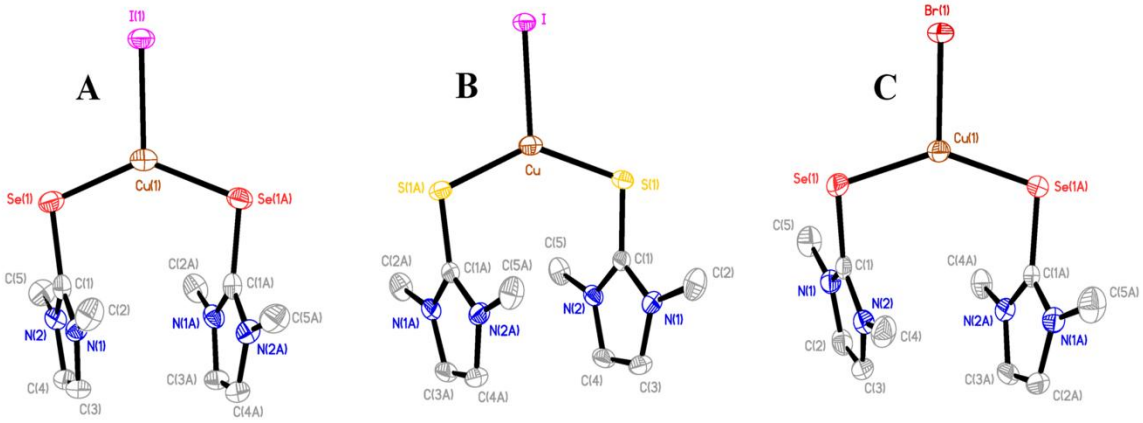

Figure 5.4. X-ray crystal structure diagrams of the *trans* structures: A) Cu(dmise)$_2$I (**2**), B) Cu(dmit)$_2$I (**3a**), and C) Cu(dmise)$_2$Br (**8**) showing 50% probability ellipsoids. Hydrogen atoms are omitted for clarity.

Table 5.2. Experimental X-ray data (EXP) vs. theoretical DFT calculations for selected bond lengths (Å) and angles (deg) for Cu(dmit)$_2$I (**3a**), Cu(dmise)$_2$I (**2**), and Cu(dmise)$_2$Br (**8**).

1:2 complex	X=I; Y=S (EXP) (**3a**)	X=I; Y=S (DFT)	X=I; Y=Se (EXP) (**2**)	X=I; Y=Se (DFT)	X=Br; Y=Se (EXP) (**8**)	X=Br; Y=Se (DFT)
Cu-X	2.5742(6)	2.497	2.5585(10)	2.507	2.4117(10)	2.334
Cu-Y	2.2345(10)	2.301	2.3351(8)	2.394	2.3430(7)	2.408
X-Cu-Y	111.823(19)	114.3	111.56(2)	111.4	107.983(17)	113.7
Y-Cu-Y	136.35(4)	131.4	136.87(4)	137.1	144.03(4)	132.6
C-Y-Cu	107.59(7)	113.2	105.55(13)	110.0	103.74(12)	110.6
Y-C(1)	1.715(2)	1.710	1.864(4)	1.871	1.867(4)	1.867

Relatively short distances between the selone heterocyclic ligands ranging from 3.63 Å (A) to 3.95 Å (B) are observed for **2** (Figure 5.5), whereas distances of 3.67 Å (A) to 3.90 Å (B) are observed between the two heterocyclic thione ligands in complex **3a**, indicating intramolecular π-π interactions are present in both. In contrast, complex **8** exhibits no intramolecular π-π interactions between the two heterocyclic rings (minimum distance 4.13 Å) due to a shift in the C(1)-Se(1)-Cu(1)-Se(1A) torsion angle (-11.08°) that results in a staggered orientation of the two five-membered rings. The copper complexes **2**, **3**, and **8** have no intermolecular π-π interactions as determined from inspection of their packing diagrams.

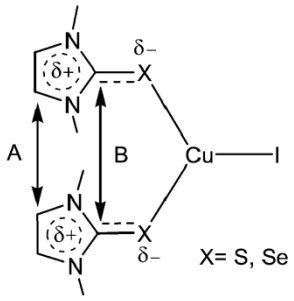

Figure 5.5. Diagram showing π-π distances between heterocyclic ligands.

Treating copper halides with two equivalents of dmit or CuCl with two equivalents of dmise also results in the formation of monomeric copper thione/selone complexes. X-ray structural analysis shows that $Cu(dmit)_2I$ (**3b**), $Cu(dmit)_2Cl$ (**4**), $Cu(dmise)_2Cl$ (**5**), and $Cu(dmit)_2Br$ (**7**) have planar, three-coordinate geometry around the Cu^+ ion with one halide anion and two terminal thione or selone ligands. In each case, the heterocyclic rings of the thione or selone ligands adopt a *cis* conformation relative to the halide atoms (Figure 5.6).

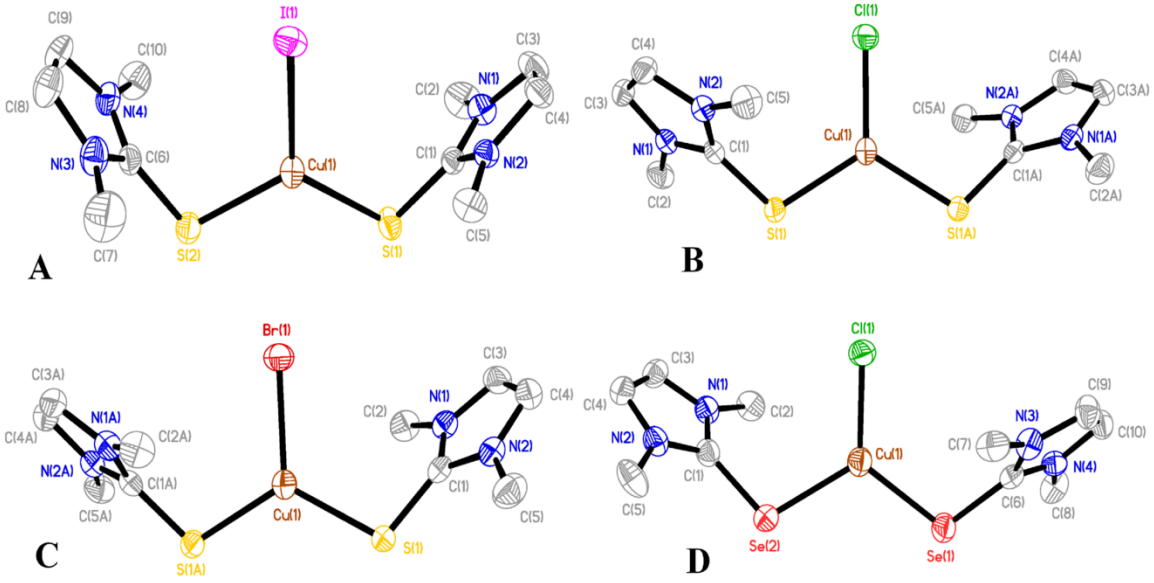

Figure 5.6. Crystal structure diagrams of A) Cu(dmit)$_2$I (**3b**), B) Cu(dmit)$_2$Cl (**4**), C) Cu(dmit)$_2$Br (**7**), and D) Cu(dmise)$_2$Cl (**5**) displaying 50% probability density ellipsoids. Hydrogen atoms are omitted for clarity.

Table 5.3. Experimental crystal data vs. theoretical DFT calculations for selected bond lengths (Å) and angles (deg) of Cu(dmit)$_2$Cl (**4**), Cu(dmit)$_2$Br (**7**).

	X=Cl; Y=S (EXP) (**4**)	X=Cl; Y=S (DFT)	X=Br; Y=S (EXP) (**7**)	X=Br; Y=S (DFT)
Cu-X	2.2497(9)	2.252	2.3857(8)	2.387
Cu-Y	2.2376(6)	2.282	2.2298(9)	2.285
X-Cu-Y	120.692(17)	121.69	118.84(2)	121.67
Y-Cu-Y	118.62(3)	116.62	122.32(5)	116.66
C-Y-Cu	106.07(7)	98.26	104.00(10)	98.84
Y-C(1)	1.714(2)	1.72	1.717(3)	1.72

Table 5.4. Experimental crystal data vs. theoretical DFT calculations for selected bond lengths (Å) and angles (deg) of $Cu(dmit)_2I$ (**3b**), $Cu(dmise)_2Cl$ (**5**).

	X=I; Y=S (EXP) (**3b**)	X=I;Y=S (DFT)	X=Cl; Y=Se (EXP) (**5**)	X=Cl; Y=Se (DFT)
Cu-X	2.5373(9)	2.550	2.238(2)	2.253
Cu-Y	2.2401(11) (avg)	2.291	2.3459(14) (avg.)	2.392
X-Cu-Y	120.085(3) (avg)	122.8	123.00(7) (avg.)	122.0
Y-Cu-Y	119.84(5)	114.5	113.89(5)	116.0
C-Y-Cu	99.425(12) (avg)	99.3	104.5(2)	94.9
Y-C(1)	1.712(3) (avg.)	1.720	1.862(8)	1.878

The Cu^+ ion has distorted trigonal geometry with angles ranging from 116.8° to 123.4° for $Cu(dmit)_2I$ (**3b**); 118.6° to 120.7° for $Cu(dmit)_2Cl$ (**4**); and 118.8° to 122.3° for $Cu(dmit)_2Br$ (**7**). The Cu-S bond distances in complexes **3a** (*trans*-$Cu(dmit)_2I$), **3b** (*cis*-$Cu(dmit)_2I$), **4**, and **7** range 2.23 to 2.41 Å (Table 5.3 and 5.4). The Cu^+ ion in complex **5** has a distorted trigonal geometry with angles ranging from 113.9° to 125.8°, and its Cu-Se bond distance of 2.34 Å is identical to that of $Cu(dmise)_2I$ (**2**) and $Cu(dmise)_2Br$ (**8**) (2.34 Å) but shorter than those found in the tetrameric copper complexes **1** (2.42 Å) and **6** (2.41 Å).

Changes in the halide ligand have no significant effects on Cu-S bond distances, since the Cu-S bond lengths of 2.2345(10) Å for *trans*-$Cu(dmit)_2I$ (**3a**), avg. 2.2401(11) Å for *cis*-$Cu(dmit)_2I$ (**3b**), 2.2376(6) Å for $Cu(dmit)_2Cl$ (**4**) and 2.2298(9) Å for $Cu(dmit)_2Br$ (**7**) are very similar. The Cu-S bond distances in **3a**, **3b**, **4**, and **7** are comparable to previously reported trigonal planar or tetrahedral coordinated copper complexes,[19,51-55] but shorter than other reported copper thione complexes such as $Cu_2X_2(mimzSH)_4$ (X = Cl, Br, I, and mimzSH = 1-methyl-1,3-

imidazoline-2-thione, 2.31-2.52 Å),[56] $Cu_2I_2(Ph_3PS)_2(NCCH_3)_2$ (2.34 Å),[57] and $[CuBr(\eta^2\text{-S-}\mu\text{-}C_5H_5NS)(p\text{-}Tol_3P)]_2$ (2.39 and 2.42 Å).[31] Coordination of the thione ligand to copper in complexes **3a**, **3b**, **4**, and **7** results in almost identical S-C(1) bond distances, 1.71-1.72 Å, which are longer than the S-C(1) bond distance in the free thione ligand (1.68 Å).[58] Increasing van der Waals radii of the halogens coordinated to copper (1.7-1.9 Å for Cl < 1.8-2.0 Å for Br < 1.95-2.12 Å for I),[50] results in decreased C(1)-S(1)-Cu(1) bond angles; $Cu(dmit)_2Cl$ (**4**; 106.1°), $Cu(dmit)_2Br$ (**7**; 104°), and *cis*-$Cu(dmit)_2I$ (**3b**; average 99.5°).

The three-coordinate copper-selone complexes $Cu(dmise)_2I$ (**2**), $Cu(dmise)_2Cl$ (**5**), and $Cu(dmise)_2Br$ (**8**) have identical Cu-Se bond distances of 2.34 Å, distances shorter than previously-reported copper selenium complexes such as $[Cu(o\text{-}C_6H_4(SeMe)_2)_2][PF_6]$ (2.42 Å),[59] and $[Cu(C_{11}H_{14}Se_2)_2][BF_4]$ (average 2.41 Å).[60] The Cu-Se bond length of 2.34 Å in complexes **2**, **5**, and **8** is longer than that in the tetrahedrally coordinated tris(pyrazolyl)copper-selone complexes $[Tpm^RCu(dmise)]^+$ (2.29-2.31 Å), and Tp*Cu(dmise) (2.33 Å).[19] Coordination of the selone ligand to copper results in relatively unchanged Se-C(1) bond lengths of 1.88 Å for **1** and 1.89 Å for **6**, but slightly shorter Se-C(1) bond lengths of 1.86 Å for **2** and **5** and 1.87 Å for **8**, relative to that of the uncoordinated dmise ligand (1.89 Å).[61] The polarizability and size differences between chloride, bromide and iodide have the most pronounced effect on the X-ray structures of complexes **1**, **2**, **3a**, **3b**, **4**, **5**, **6**, **7**, and **8**, but have no observable effects on Cu-Se or Cu-S bond lengths.

Density functional theory studies for trigonal copper halide complexes. DFT(B3PW91) geometry optimizations predict the *cis* isomer to be the lowest energy conformation for each of the 1:2 Cu:thione/selone complexes. The geometries of **3b**, **4**, **5**, and **7** agree with the X-ray structures of (Table 5.3 and 5.4) and accurately reproduce the X-H5C short contacts (3.160, 2.711, 2.742, 2.888 Å, respectively). Full optimization of complexes **2**, **3a**, and **8** in C_2 symmetry using the BP86 xc functional led to a C_{2v} configuration in which there is no π-π interaction and the imidazole rings of the thione/selone ligands form an electrostatic interaction with the halide (anion-π interaction). Surprisingly, the C_{2v} conformation is roughly degenerate ($\Delta E+ZPE < 1.0$ kcal/mol) with the experimentally observed structures indicating that the anion-π and X-H5C interactions between the halide and the dimethylimidazole fragment are similar in magnitude.

To obtain conformations with π-π interactions, the 1:2 complexes were optimized with the N2(2)-C(2)-Se-Cu dihedral angles constrained to the experimental value followed by a full optimization with a small step size in the search algorithm. The local minima with π-π interactions were found only for **2**, **3a**, and **8** and their structures generally agree with the experimental X-ray crystal data (Table 5.2). However, these structures were ~10 kcal/mol less stable than structures without intramolecular π-π interactions. In addition, the experimental structures show an apparent attractive interaction between the π-clouds of the dimethylimidazole rings (d(C1-C1A) < d(C3/4-C3/4(A)), not found in the DFT calculations. This attraction may be due to X-H3/4 interactions between molecules in the crystal, which would

explain why the 'attractive' interaction is more pronounced when X is the smaller bromide (**8**). This suggests that for the structures of **2**, **3a**, and **8**, π-π interactions may actually be preferred conformations due to the weak hydrogen-bonding interactions between units of the crystal. Such a conformation would be disfavored for X = Cl due to repulsive forces at the shorter C3/4-C3/4(A) distances required for Cl-H3/4 interactions to the smaller halogen. The lack of π-π interactions in **8** may be explained similarly if Br-H3/4 interactions are comparable to Se-H5 interactions such that complex **8** maintains the face-to-face orientation of the heterocyclic rings, but with a twist to increase the Se-H5 interaction.

For comparison to **1** and **6**, the energies of formation of the *cis* 1:2 complexes from CuX(dmit/dmise) and an additional dmit/dmise ligand were calculated. The energy per chalcogenone is lower for the selones than the thiones (ΔE+ZPE = -6.0–-6.3 versus -5.2–-5.7 kcal mol^{-1} $chalcogenone^{-1}$). These values are comparable to the formation energy per chalcogenone for the hypothetical 1:1 sulfur analogues **1**(**S**) **6**(**S**) (-5.8 and -5.5 kcal mol^{-1} $chalcogenone^{-1}$, respectively). Therefore, the 1:1 clusters are energetically preferred for selones, but, the similar energies per thione suggest that experimental conditions favor the 1:2 complexes.

Powder X-ray diffraction studies of copper(I) halide complexes. Powder X-ray diffraction (XRD) studies of both the tertrameric and monomeric copper complexes were carried out to determine whether more than one conformer was present in the reaction products. Experimental powder XRD patterns of the copper chloride complexes **4** and **5** fully matched their simulated patterns, suggesting that only the *cis*

conformer is formed and corroborating DFT calculation results (Figures 5.18-5.19). In contrast, powder XRD patterns reveal the presence of both *cis* and *trans* conformers of CuI(dmit)$_2$ (**3a** and **3b**; Figure 5.7) in powder samples. Diffraction patterns for Cu complexes **1**, **2**, **6**, **7**, and **8** also do not fully match the simulated patterns determined from their respective single crystallographic data (Figures 5.10-5.17), indicating that more than one conformer may be present. Attempts to grow crystals of additional conformers using different solvent systems, seeding the crystallization solution with an analogous crystal of the desired conformer, or crystallizing at low temperatures were not successful.

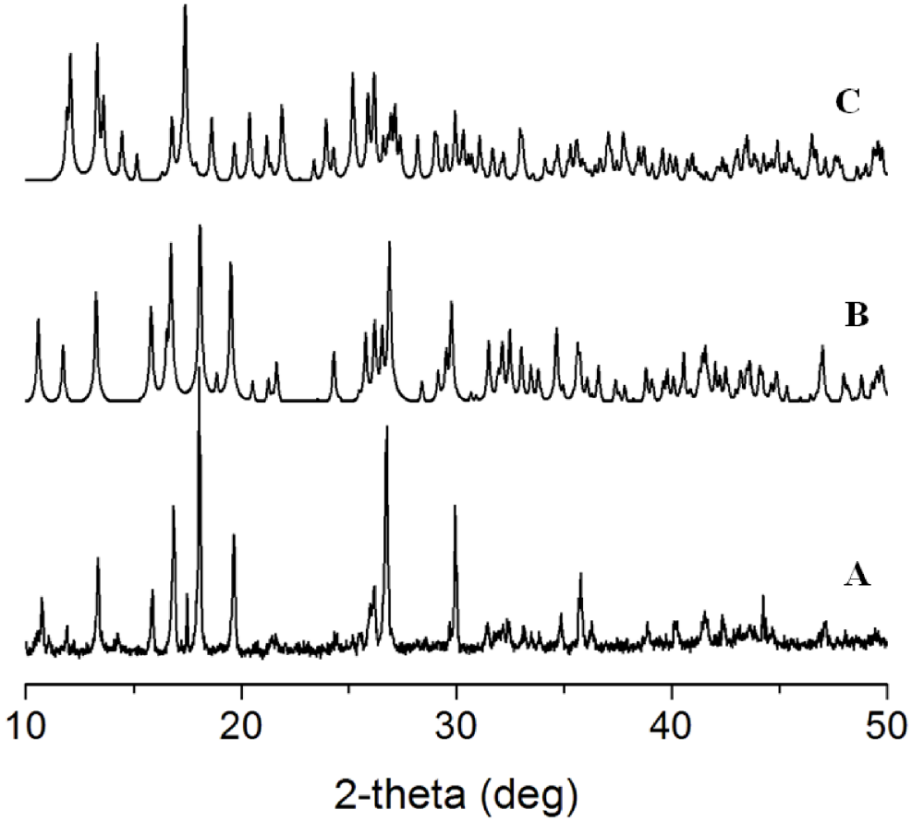

Figure 5.7. Experimental powder X-ray diffraction pattern of A) CuI(dmit)$_2$ and simulated powder patterns for B) *trans*-CuI(dmit)$_2$ (**3a**) and C) *cis*-CuI(dmit)$_2$ (**3b**).

Generally, structural and stoichiometric predictions of metal complexes depend on the geometrical flexibility of the metal ion coupled with the steric and electronic requirements of ligands. We found that changing the halide ligand had the most profound effect on the coordination number and geometry of the resulting copper-chalcogenone complexes. Similarly to previous reports,[62-64] formation of halide bridges are generally favored for the soft iodide but not for the harder chloride ligands, whereas both bridging and terminal bonding modes were observed for the bromide ligands, since bromide lies on the borderline between soft and hard Lewis bases. Formation of the tetrameric bridging selone complexes **1** and **6** are likely favored by the presence of two highly polarizable atoms, selenium and iodine or bromine, with high propensities to bridge metal centers.

The conformations obtained for the three coordinate copper complexes **2**, **3a**, **3b**, **4**, **5**, **7**, and **8**, depend on several factors, including packing forces, halide ligand, and the number and strength of stabilizing short-contact interactions between X-H or Y-H (X = I, Br, or Cl; Y = Se or S). For the trigonal complexes **2** and **3a** that have intramolecular π-π interactions between the heterocyclic rings, only very weak short contact intermolecular interactions between I-H atoms of 3.18 Å exist in **3a**, whereas **2** has no short-contact intermolecular interactions. In contrast, complexes without intramolecular π-π interactions (**3b**, **4**, **5**, **7**, and **8**) have more significant short-contact intermolecular interactions between the halides or chalcogenones and neighboring hydrogen atoms. These short- contact interactions likely stabilize the *cis* conformations (or the twisted trans conformation of **8**) of these complexes relative to

the *trans* conformations of **2** and **3a**, corroborating DFT results indicating that complexes with intramolecular π-π interactions were generally less stable than structures without intramolecular π-π interactions. The lack of short contact interactions in **2** and **3a** suggest that these complexes may be stabilized by the intramolecular π-π interactions between the heterocyclic rings, whereas complexes **3b**, **4**, **5**, **7**, and **8** are primarily stabilized by crystal packing forces resulting from short-contact intermolecular interactions between X-H (X = Cl, Br, I, Se, and S).

IR spectroscopy. In the IR spectra of the copper thione complexes, the diagnostic ν(C=S) peak appears at lower wavenumbers (1171-1173 cm^{-1}) for the trigonal complexes **3**, **3b**, **4**, and **7** compared to 1181cm^{-1} for uncoordinated dmit.[65] In contrast, the ν(C=Se) peaks are shifted to slightly higher energies (1149-1163 cm^{-1}) for complexes **1**, **2**, **5**, **6**, and **8** than uncoordinated dmise (1148 cm^{-1}).[66,67] Although it is not clear why this difference between S and Se coordination occurs between these complexes, the shift to lower energy for ν(C=S) upon coordination of dmit to copper may indicate weakening of C=S bond due to copper back-bonding, whereas the shift to higher energy for ν(C=Se) upon dmise coordination to copper indicates a slight strengthening of the C=Se bond due to Cu-Se donor bond formation. The same trend was observed for tetrahedral coordinated tris(pyrazolyl)methane/borate-copper-thione (ν(C=S) 1172-1178 cm^{-1}) and –selone (ν(C=Se) 1150-1151 cm^{-1}) complexes[19] as well as Zn^{2+} and Cd^{2+} complexes of these ligands.[32,38,68] DFT calculations assign the C=Se/S stretching band as symmetric and asymmetric modes. For **3b**, **4**, **5**, and **7**, the lower-frequency asymmetric mode is more intense, whereas the symmetric stretch is

more intense for the face-to-face complexes **2**, **3a**, and **8**.

NMR spectroscopy of copper(I) halide thione and selone complexes. For all the copper complexes **1**-**8**, the ^{1}H NMR resonances for the methyl and olefinic protons of the copper-bound dmise or dmit ligands are shifted downfield relative to unbound ligand, consistent with reports by Lobana, *et al*.,[20,21,56] Rabinovich, *et al*.,[69] and Kimani, *et al*.[19] In the ^{13}C{^{1}H} NMR spectra, upfield shift of the C-2 resonance of the dmise and dmit (both δ ~6) is also observed upon copper complexation. Similar upfield shifts for the C=Se or C=S carbon atoms were observed for Cu^{+} complexes $[Tpm^{R}Cu(L)]^{+}$ and Tp*Cu(L) (L = dmit or dmise).[19] The downfield shift of the olefinic protons resonances in the ^{1}H NMR spectra, as well as similar downfield shifts of the C-4 and C-5 resonances in the ^{13}C{^{1}H} NMR spectra, may result from minor increases in deshielding effects on C-4 and C-5 carbons due to increased electron density on the C-N bond of the heterocyclic five-membered ring upon metal complexation and concomitant weakening of the C=S/Se bond.[70,71] This explanation is consistent with the observed shift of the ν(C=S) band to lower energies upon dmit coordination, but not consistent with the observed shift of the ν(C=Se) band to higher energies, indicating differences between S and Se coordination in these complexes.

The *trans* conformer (**3a**) has thione ^{1}H resonances at δ 3.63 and 7.32 and ^{13}C{^{1}H} resonances at δ 36.0, 120.4, and 155.1, whereas the *cis* conformer (**3b**) has thione ^{1}H resonances at δ 3.59 and 7.27 and ^{13}C{^{1}H} resonances at δ 35.9, 120.2, and 155.9. When the *cis* and *trans* conformers were combined in a single NMR sample, a single set of resonances were observed in both the ^{1}H and ^{13}C{^{1}H} NMR, indicating

that the two conformers interconvert in solution, a result that is consistent with electrochemical results.

$^{77}Se\{^{1}H\}$ NMR resonances for the copper-selone complexes **1**, **2**, **5**, **6**, and **8** are shifted upfield (δ -13.4 to -75.0) upon copper coordination relative to the free dmise ligand (δ 21.8). This upfield shift is a result of the selenium atom binding to the electron-rich copper ion, but no correlation exists between Cu-Se bond lengths and $^{77}Se\{^{1}H\}$ NMR shifts.

Electrochemical studies of the copper halide complexes. Electrochemical properties of the copper(I)-halide complexes **1, 2**, **3a**, **3b**, **4**, **5**, **6**, **7**, and **8** were examined by cyclic voltammetry (CV) to determine the difference in $Cu^{2+/+}$ redox potential upon Cu-selone or Cu-thione coordination. Cyclic votammograms of these copper complexes exhibit two, one-electron, chemically-reversible potential waves for the $Cu^{2+/+}$ and $Cu^{+/0}$ redox potentials. A wave corresponding to the $Cu^{+/0}$ redox couple is observed at potentials more negative than -1000 mV vs. NHE. The Cu^{0} is then stripped off the electrode after switching the scan direction at a potential around -800 mV (Table 5.6).

Electrochemical studies of the three-coordinate copper complexes **2**, **3a**, **3b**, **4**, **5**, **7**, and **8** were carried out in acetonitrile solution with tetra-*n*-butylammonium phosphate electrolyte and a carbon working electrode. All the complexes exhibit chemically reversible $Cu^{2+/+}$ reduction waves. Complexes **2**, **4**, **5**, **7** and **8** exhibit quasi-reversible oxidation and reduction waves, whereas complexes **1**, **3a**, **3b**, and **6** exhibit irreversible electrochemical behavior for the $Cu^{2+/+}$ couple (Table 5.5). The

selone complexes **2**, **5**, and **8** have lower $Cu^{2+/+}$ reduction potentials ranging from -340 to -362 mV compared to $Cu^{2+/+}$ reduction potentials of the analogous thione complexes **3a**, **3b**, **4**, and **7**, which range from -177 to -284 mV (CV voltammograms are provided in Figures 5.20). Additionally, the thione- copper complexes show larger peak separations between the cathodic and anodic waves compared to the copper selone complexes. The large peak separations of the copper thione complexes may indicatre instability of the oxidized products during the voltammetry sweep due to slow electron transfer kinetics.[72]

The copper selone complexes $CuX(dmise)_2$ (X = I, Br and Cl) have reduction potentials more negative by an average of 108 mV relative to the copper thione complexes $CuX(dmit)_2$ (X = I, Br and Cl), consistent with previous reports.[19] The $CuI(dmit)_2$ complex **3b** (*cis*-conformation, -177 mV), has a more positive $Cu^{2+/+}$ reduction potential than complex **3a** (*trans*-conformation, -239 mV). A mixed sample of the two conformers revealed a single $Cu^{2+/+}$ at -256 mV (Figure 20G); these results coupled with ^{1}H and $^{13}C\{^{1}H\}$ NMR data, indicate that these conformers interconvert in solution.

Cyclic voltammogram for $CuCl(dmit)_2$ (**4**), $CuCl(dmise)_2$ (**5**), $CuBr(dmit)_2$ (**7**), $CuBr(dmise)_2$ (**8**), exhibit two, one-electron, waves belonging to $Cu^{2+/+}$ and $Cu^{+/0}$ redox potentials. In contrast, cyclic voltammograms of $Cu_4(\mu_4\text{-dmise})(\mu\text{-}I)_2I_2$ (**1**), $CuI(dmise)_2$ (**2**), $CuI(dmit)_2$ (**3a**), $CuI(dmit)_2$ (**3b**), and $Cu_4(\mu_4\text{-dmise})(\mu\text{-}Br)_2Br_2$ (**6**) show three distinct reduction potentials waves (Figure 5.20). Two of the waves correspond to $Cu^{2+/+}$ and $Cu^{+/0}$ redox potentials. The third reduction wave likely

corresponds to I^-/I_2 or Br^-/Br_2 reduction couples. As previously observed for copper halide complexes,[73,74] the weakly coordinated iodide ligand in complexes **1**, **2**, **3a**, and **3b** or bromide ligand in complex **6** may undergo ligand subtitution with solvent acetonitrile resulting in the observed halogen reduction peaks.

Differential pulse voltammetry (DPV) studies of complexes **1** and **6** exhibit two distinct reduction and oxidation peaks in their voltammograms, corresponding to $Cu^{2+/+}$ and their respective halogen redox potentials (Figure 5.21). Thus, the tetrameric copper complexes **1** and **6** exhibit a single $Cu^{2+/+}$ reduction potential at -452 and -365 mV, respectively, despite having two different copper centers with different geometries.

Table 5.5. Reduction potentials of $Cu^{2+/+}$ for the copper selone and thione complexes vs. NHE.

	$Cu^{2+/+}$			
Complex	**Ep_a**	**Ep_c**	**ΔE (mV)**	**$E_{1/2}$ (mV)**
$Cu_4(\mu_4\text{-dmise})(\mu\text{-}I_2)I_2$ (**1**)	83, -235	0, -986	1069	-452
$Cu_4(\mu_4\text{-dmise})(\mu\text{-}I_2)I_2$ (**1**)[a]	34, -285	126, -	92, 379	80, -475
$Cu_4(\mu_4\text{-dmise})(\mu\text{-}Br_2)Br_2$ (**6**)	-39,-178	-644	605	-342
$Cu_4(\mu_4\text{-dmise})(\mu\text{-}Br_2)Br_2$ (**6**)[a]	-106, -	-42, -	64, 381	-74, -436
$CuCl(dmise)_2$ (**5**)	-139	-570	431	-355
$CuCl(dmit)_2$ (**4**)	52	-620	672	-284
$CuBr(dmise)_2$ (**8**)	-151	-584	432	-362
$CuBr(dmit)_2$ (**7**)	41	-524	565	-241
trans-$CuI(dmit)_2$ (**3a**)	176	-653	829	-239
cis-$CuI(dmit)_2$ (**3b**)	298	-651	949	-177
Mixed (cis + trans)-$CuI(dmit)_2$	192	-705	897	-256
$CuI(dmise)_2$ (**2**)	-117	-562	445	-340

Table 5.6. Reduction potentials of $Cu^{+/0}$ for the copper selone and thione complexes vs. NHE.

	$Cu^{+/0}$			
Complex	**E_{pa}**	**E_{pc} (mV)**	**ΔE (mV)**	**$E_{1/2}$**
$Cu_4(\mu_4\text{-dmise})(\mu\text{-}I_2)I_2$ (**1**)	-866	-1355	489	-1111
$Cu_4(\mu_4\text{-dmise})(\mu\text{-}Br_2)Br_2$ (**6**)	-881	-1274	393	-1078
$CuCl(dmise)_2$ (**5**)	-821	-1211	390	-1016
$CuCl(dmit)_2$ (**4**)	-861	-1232	371	-1046
$CuBr(dmise)_2$ (**8**)	-812	-1203	391	-1008
$CuBr(dmit)_2$ (**7**)	-850	-1219	369	-1034
trans-$CuI(dmit)_2$ (**3a**)	-828	-1335	507	-1082
cis-$CuI(dmit)_2$ (**3b**)	-868	-1335	467	-1101
Mixed (cis + trans)-$CuI(dmit)_2$	-656	-1.321	665	-989
$CuI(dmise)_2$ (**2**)	-878	-1223	345	-1051

The changes in $Cu^{2+/+}$ reduction potentials of the three-coordinate complexes **2**, **3a**, **3b**, **4**, **5**, **7**, and **8** are correlated to the halide and chalcogenone ligands. For the copper thione complexes, reduction potentials are shifted to lower voltages in the following order: $CuI(dmit)_2$ (**3b**; -177 mV), $CuBr(dmit)_2$ (**7**; -241 mV), and $CuCl(dmit)_2$ (**4**; -284 mV), a trend previously observed for copper halide complexes.[74] Less polarizable halide ligands stabilize Cu^{2+} relative to Cu^{+}, resulting in a more negative $Cu^{2+/+}$ reduction potential for the copper thione complexes. The analogous copper selone complexes have more negative potentials relative to the thione complexes, but the trend observed for the thione complexes is not fully followed: $CuI(dmise)_2$ (**2**; -340 mV), $CuCl(dmise)_2$ (**5**; -355 mV), and $CuBr(dmise)_2$ (**8**; -362 mV).

Conclusions

Copper halides (CuI, CuBr, and CuCl) with selone and thione ligands have been synthesized and characterized, and their electrochemistry has been investigated and compared. The X-ray crystal structures for tetranuclear complexes **1** and **6**, and trigonal complexes **2**, **3**, **3b**, **4**, **5**, **7**, and **8** have been determined. The tetrameric omplexes **1** and **6** have two different copper coordination environments and a $Cu_2(\mu\text{-}I)_2$ or $Cu_2(\mu\text{-}Br)_2$ core coordinated to two bridging selenium atoms. In contrast, the three-coordinate thione and selone complexes **2**, **3a**, **3b**, **4**, **5**, **7** and **8** adopt distorted trigonal planar geometry, where Cu^+ is bound to a halide (Cl, Br, or I) and two thione or selone ligands. The geometry and stochiometry of the copper complexes obtained depends on several factors, including halide and chalcogenone ligand, intramolecular π-π interactions, and intermolecular short contact interactions in the crystal. DFT calculations show good correlation to the observed X-ray structures for compounds **1**-**8**. Cyclic voltammetry studies for the three-coordinate complexes show lower reduction potentials for copper selone complexes relative to the copper thione complexes regardless of the coordinated halide ligand. These results highlight the rich coordination chemistry and variable binding modes of heterocyclic selone and thione ligands.

Experimental Section

Materials. The synthesis and manipulation of all copper complexes was performed under an inert atmosphere of argon or nitrogen using standard Schlenk

techniques. Acetonitrile, methanol, dichloromethane, and ether were purified using standard procedures and freshly distilled under argon atmosphere prior to use. *N,N'*-dimethylimidazole selone (dmise), *N,N'*-dimethylimidazole thione (dmit)[75] and $[Cu(NCCH_3)_4][BF_4]$[76] were synthesized according to published procedures. Selenium powder, sulfur powder, cuprous chloride (Aldrich), cuprous iodide (Aldrich), cuprous bromide (Alfa Aesar), cuprous oxide (stabilized, Aldrich), potassium iodide (Aldrich), 1-methylimidazole (VWR), and methyliodide (VWR) were used as received.

Instrumentation. ^{1}H, $^{13}C\{^{1}H\}$, and $^{77}Se\{^{1}H\}$ spectra were obtained on a Bruker-AVANCE 500 MHz NMR spectrometer. ^{1}H and $^{13}C\{^{1}H\}$ NMR chemical shifts are reported in δ relative to tetramethylsilane (TMS) and referenced to solvent. $^{77}Se\{^{1}H\}$ NMR chemical shifts were externally referenced to diphenyl diselenide (δ 461),[77] and reported relative to dimethyl selenide (δ 0). Electrochemical experiments were performed with a BAS 100B potentiostat. A three compartment cell was used with a Ag/AgCl reference electrode, a Pt counter electrode, and a carbon working electrode. Freshly distilled acetonitrile was used as the solvent with tetra-*n*-butylammonium phosphate as the supporting electrolyte (0.1 M). Solutions containing 1 mM analyte were deaerated for 2 min by vigorous nitrogen purge. All $E^{1/2}$ values were calculated from $(Ep_a + Ep_c)/2$ at a scan rate of 100 mV/s. Differential pulse voltammetry (DPV) experiments were conducted using a pulse amplitude of 0.080 V and a pulse width of 0.050 s, in conjunction with a sample width of 0.045 s and a pulse period of 0.200 s. The powder X-ray diffraction (XRD) patterns were measured using an angle

dispersive diffractometer (Rigaku Ultima IV) with monochromated Cu-Kα (λ = 1.540) radiation at 40 kV. Infrared spectra were obtained using nujol mulls on KBr salt plates with a Magna 550 IR spectrometer. Abbreviations used in the description of vibrational data are as follows: vs, very strong; s, strong; m, medium; w, weak; b, broad. Electrospray ionization mass spectrometry (ESI-MS) was performed using a QSTAR XL Hybrid MS/MS System from Applied Biosystems via direct injection of sample (0.05 mL/min flow rate) into a Turbo Ion spray ionization source. Samples were run under positive mode, with ion-spray voltage of 5500 V, and TOF scan mode. Melting points were determined using a Barnstead Electrothermal 9100 apparatus in silicon-grease-sealed glass capillary tubes. UV-vis spectra were collected using a Shimadzu UV-3101 PC spectrophotometer in quartz cuvettes with a path length of 1 cm. Elemental analysis was performed by Atlantic Microlabs, Inc.

Theoretical methods. Geometry optimizations were performed with the B3PW91 and BP86 exchange-correlation (xc) functionals using PQS version 3.3.[78] Copper and selenium were represented by the Ermler-Christiansen relativistic effective core potential.[79] The copper basis set was modified to include the Couty-Hall 4p contraction.[80] The Wadt-Hay RECP basis set for sulfur and the halogens were augmented with a set of diffuse s- and p-functions.[81] Nitrogen, oxygen and hydrogen centers attached to non-carbon heavy atoms were represented by the Dunning split-valence triple-ζ plus polarization function basis set (TZVP).[82] Hydrocarbon fragments were double-ζ quality with polarization functions added to carbon.[83] Frequency

calculations were used to confirm that the reported structures are minima on the respective potential energy surfaces.

$Cu_4(\mu_4$-dmise)(μ-$I_2)I_2$ ***(1)****. Method 1.* The dmise ligand (176 mg, 1 mmol) was dissolved in acetonitrile (20 mL) and this solution was cannula transferred into a solution of $[Cu(CNCH_3)_4][BF_4]$ (312 mg, 1 mmol) in acetonitrile (20 mL). The reaction mixture was stirred at room temperature for 1 h until the reaction mixture was clear and colorless. Into this reaction mixture was cannula transferred KI (332 mg, 2 mmol) in methanol (15 mL) and the reaction was stirred for 5 h. The solvent was removed *in vacuo*, and the product was extracted using acetonitrile. Acetonitrile was removed *in vacuo*, yielding a white solid. Yield: 234 mg, 16%. Single crystals for X-ray analysis were grown from slow vapor diffusion of ether into an acetonitrile/DMF solution of the complex.

Method 2. The dmise ligand (176 mg, 1 mmol) was dissolved in acetonitrile (20 mL) and this solution was cannula transferred into a solution of CuI (190 mg, 1 mmol) in acetonitrile (20 mL). The reaction mixture was stirred at room temperature for 1 h, resulting in the formation of a white precipitate. Into this reaction mixture was cannula transferred KI (332 mg, 2 mmol) in methanol (15 mL), resulting in a clear solution followed by gradual formation of a white precipitate. The mixture was stirred for 6 h, dried *in vacuo*, and the desired product was extracted using acetonitrile (10 mL). The filtrate was dried *in vacuo* to yield a white powder. Single crystals for X-ray analysis were grown from slow vapor diffusion of ether into

anacetonitrile/DMF solution of the complex. Yield: 312 mg, 21%. Mp. 193 °C. Found: C, 16.83; N, 7.15; H, 2.22; requires $C_{20}H_{32}Cu_4N_8Se_4I_4$ C, 16.43; N, 7.66; H, 2.21%. UV-vis [λ_{max}, nm (ε_M, M^{-1} cm^{-1})] in CH_3CN: 245 (206,028), 276 sh (53,555). IR (cm^{-1}): 623 s, 658 s, 751 s, 773 s, 831 s, 1027 s, 1082 s, 1144 s, 1163 s, 1229 s, 1378 s, 1465 b, 1561 s, 1600 s, 1660 b, 2923 b. δ_H (500 MHz; CD_2Cl_2; Me_4Si): 3.88 (6H, s, $2CH_3$), 6.97 (2H, s, 2CH). δ_C (500 MHz; CD_2Cl_2; Me_4Si): 37.58 (CH_3), 121.60 (CH), 150.51 (C=Se). δ_{Se} (500 MHz; $(CD_3)_2SO$; PhSeSePh): -42.8; *m/z* (ESI-MS): 796.5 $[Cu_3(dmise)_3I_2]^+$,790.5 $[Cu_2(dmise)_3I]^+$, 604.7 $[Cu_2(dmise)_2I]^+$, 414.9 $[Cu(dmise)_2]^+$.

Cu(dmise)$_2$I ***(2)***. A dichloromethane solution (20 mL) of dmise (350 mg, 2 mmol) was cannula transferred into a solution of CuI (190 mg, 1 mmol) in acetonitrile (20 mL). The reaction mixture was stirred at room temperature for 6 h, resulting in the formation of a white precipitate. The white precipitate was filtered and dried *in vacuo* to yield a white powder. Single crystals for X-ray analysis were grown by slow vapor diffusion of ether into an acetonitrile/DMF solution in the complex. Yield: 459 mg, 85%. Mp. 156 °C. Found: C, 22.31; N, 10.19; H, 2.85; requires $C_{10}H_{16}CuN_4Se_2I$ C, 22.22; N, 10.36; H, 2.98%. UV-vis [λ_{max}, nm (ε_M, M^{-1} cm^{-1})] in CH_3CN: 228 (65,990). IR (cm^{-1}): 474 w, 623 s, 662 s, 724 w, 750 s, 772 s, 831 s, 1092 s, 1117 s, 1148 s, 1163 s, 1232 vs, 1378 vs, 1466 vs, 1566 vs, 1600 w, 2855 vs, 2924 b, 3110 s, 3143 s. δ_H (500 MHz; $(CD_3)_2SO$; Me_4Si): 3.70 (6H, s, $2CH_3$), 7.46 (2H, s, 2CH). δ_C (500 MHz; $(CD_3)_2SO$; Me_4Si): 37.66 (CH_3), 122.20 (CH), 147.81 (C=Se). δ_{Se} (500

MHz; $(CD_3)_2SO$; PhSeSePh): -48.9; *m/z* (ESI-MS): 414.85 $[Cu(dmise)_2]^+$, 255.04 $[Cu(dmise) + OH]^+$, 238.89 $[Cu(dmise)]^+$, 158.98 $[Cu(C_5N_2H_8)]^+$.

trans-Cu(dmit)$_2$I (***3a***). *Method 1.* A dichloromethane solution (20 mL) of dmit (260 mg, 2 mmol) was cannula transferred into a solution of CuI (190 mg, 1 mmol) in acetonitrile (10 mL). The reaction mixture was stirred at room temperature for 6 h, resulting in the formation of a white precipitate. The white precipitate was filtered and dried *in vacuo* to yield a white powder. Single crystals for X-ray analysis were grown by slow vapor diffusion of ether into an acetonitrile/DMF solution in the complex. Yield: 410 mg, 92%.

Method 2. An acetonitrile solution (20 mL) of dmit (260 mg, 2 mmol) was cannula transferred into a solution of CuI (190 mg, 1 mmol) in acetonitrile (20 mL). The reaction mixture was stirred at room temperature for 1 h, resulting in the formation of a white precipitate. To this reaction mixture was added KI (332 mg, 2 mmol) in methanol (15 mL), resulting in a clear solution that was stirred for 6 h, and then dried *in vacuo*. The desired product was extracted using acetonitrile (10 mL), and the filtrate was dried *in vacuo* to yield a white powder. Single crystals for X-ray analysis were grown from slow vapor diffusion of ether into acetonitrile solution. Yield: 401 mg, 89%. Mp. 152 °C. Found: C, 26.51; N, 12.39; H, 3.55. requires $C_{10}H_{16}CuN_4S_2I$ C, 26.88; N, 12.54; H, 3.61%. UV-vis [λ_{max}, nm (ε_M, M^{-1} cm^{-1})] in CH_3CN: 246 (38,384). IR (cm^{-1}): 629 s, 673 s, 721 s, 744 s, 826 s, 1030 s, 1082 s, 1171 s, 1227 s, 1379 s, 1466 s, 1564 s, 2926 b. δ_H (500 MHz; $(CD_3)_2SO$; Me_4Si): 3.63

(6H, s, $2CH_3$), 7.32 (2H, s, 2CH). δ_C (500 MHz; $(CD_3)_2SO$; Me_4Si): 36.02 (CH_3), 120.46 (CH), 155.12 (C=S); *m/z* (ESI-MS): 318.98 $[Cu(dmit)_2]^+$, 231.98 [Cu(dmit) + MeOH]$^+$, 190.96 [Cu(dmit)]$^+$.

*cis-Cu(dmit)$_2$I (**3b**).* A dichloromethane solution (20 mL) of dmit (260 mg, 2 mmol) was cannula transferred into a solution of CuI (190 mg, 1 mmol) in acetonitrile (20 mL). The reaction mixture was stirred at room temperature for 6 h. The reaction mixture was reduced to about 5 mL *in vacuo* and the desired product precipitated by addition of ether. The precipitate was filtered, dried *in vacuo* to yield a white powder. Single crystals for X-ray analysis were grown from slow vapor diffusion of ether into an acetonitrile/dichloromethane solution of the complex. Yield 404 mg, 90%. Mp. 152 °C. Found: C, 26.51; N, 12.39; H, 3.55; requires $C_{10}H_{16}CuN_4S_2I$ C, 26.88; N, 12.54; H, 3.61%. UV-vis [λ_{max}, nm (ε_M, M^{-1} cm^{-1})] in CH_3CN: 247 (29,773). IR (cm^{-1}): 629 s, 673 s, 721 s, 744 s, 826 s, 1030 s, 1082 s, 1171 s, 1227 s, 1379 s, 1466 s, 1564 s, 2926 b. δ_H (500 MHz; $(CD_3)_2SO$; Me_4Si): 3.59 (6H, s, $2CH_3$), 7.27 (2H, s, 2CH). δ_C (500 MHz; $(CD_3)_2SO$; Me_4Si): 35.88 (CH_3), 120.22 (CH), 155.87 (C=S); *m/z* (ESI-MS): 318.98 $[Cu(dmit)_2]^+$, 222.98 [Cu(dmit) + MeOH]$^+$, 190.96 [Cu(dmit)]$^+$.

*Cu(dmit)$_2$Cl (**4**).* A dichloromethane (20 mL) solution of dmit (260 mg, 2 mmol) was cannula transferred into a solution of CuCl (99 mg, 1 mmol) in ethanol (20 mL). The reaction mixture was stirred at room temperature for 1 h, resulting in the formation of a white precipitate. The filtrate was removed via cannula filtration and the precipitate was dried *in vacuo* yielding a white powder. Single crystals for X-

ray analysis were grown from slow vapor diffusion of ether into an acetonitrile/methanol solution of the complex. Yield: 313 mg, 87%. Mp. 158 °C. Found: C, 33.76; N, 15,67; H, 4.48; requires $C_{10}H_{16}CuN_4S_2Cl$ C, 33.80; N, 15.76; H, 4.54%. UV-vis [λ_{max}, nm (ε_M, M^{-1} cm^{-1})] in CH_3CN: 261 (22,595). IR (cm^{-1}): 663 s, 670 s, 730 s, 748 s, 763 vs, 803 w, 867 w, 1087 s, 1173 vs, 1242 vs, 1378 vs, 1464 vs, 1571 s, 1621 s, 1728 w, 2924 b, 3147 w. δ_H (500 MHz; $(CD_3)_2SO$; Me_4Si): 3.56 (6H, s, 2 CH_3), 7.28 (2H, s, 2 CH_2). δ_C (500 MHz; $(CD_3)_2SO$; Me_4Si): 35.75 (CH_3), 120.45 (CH), 154.63 (C=S); *m/z* (ESI-MS): 318.98 $[Cu(dmit)_2]^+$, 222.98 [Cu(dmit) + MeOH]$^+$, 190.96 [Cu(dmit)]$^+$, 128.03 [dmit]$^+$.

*Cu(dmise)$_2$Cl (**5**).* Complex **5** was prepared using the same procedure for **4** except that dmise (350 mg, 2 mmol) was used instead of dmit. Single crystals for X-ray analysis were grown from slow vapor diffusion of ether into an acetonitrile/DMF solution of the complex. Yield: 414 mg, 92%. Mp. 170 °C. Found: C, 26.98; N, 12.52; H, 3.51; requires $C_{10}H_{16}CuN_4Se_2Cl$ C, 26.71; N, 12.47; H, 3.59%. UV-vis [λ_{max}, nm (ε_M, M^{-1} cm^{-1})] in CH_3CN: 273 (9,844). IR (cm^{-1}): 653 s, 658 s, 719 vs, 743 vs, 764 vs, 868 w, 1027 vs, 1069 b, 1149 vs, 1243 vs, 1378 vs, 1465 vs, 1570 s, 1625 w, 2916 b. δ_H (500 MHz; $(CD_3)_2SO$; Me_4Si): 3.66 (6H, s, 2 CH_3), 7.44 (2H, s, 2 CH_2). δ_C (500 MHz; $(CD_3)_2SO$; Me_4Si): 37.55 (CH_3), 122.36 (CH), 146.23 (C=Se). δ_{Se} (500 MHz; $(CD_3)_2SO$; PhSeSePh): -39.3; *m/z* (ESI-MS): 414.85 $[Cu(dmise)_2]^+$, 270.91 [Cu(dmise) + MeOH]$^+$, 255.04 [Cu(dmise) + OH]$^+$, 238.89 [Cu(dmise)]$^+$, 158.98 $[Cu(C_5N_2H_8)]^+$.

*$Cu_4(\mu_4$-dmise)(μ-$Br_2)Br_2$ (**6**).* CuBr (144 mg, 1 mmol) was dissolved in ethanol (15 mL) and to this was cannula added a solution of dmise (175 mg, 1 mmol) in dichloromethane (15 mL). The reaction was stirred for 6 h, and the solvent reduced *in vacuo* to about 5 mL. The desired product was precipitated using ether (10 mL). This white precipitate was filtered and dried *in vacuo*. Single crystals suitable for X-ray analysis were grown by slow diffusion of ether into an acetonitrile solution of the complex. Yield: 306 mg, 24%. Mp. 212°C. Found: C, 18.89; N, 8.81; H, 2.60; requires $C_{20}H_{32}Cu_4N_8Se_4Br_4$ C, 18.83; N, 8.79; H, 2.53%. UV-vis [λ_{max}, nm (ε_M, M^{-1} cm^{-1})] in CH_3CN: 261 (26545). IR (cm^{-1}): 659 s, 744 s, 770 w, 1103 w, 1150 s, 1227 s, 1261 s, 1378 vs, 1464 vs, 1563 s, 2925 b. δ_H (500 MHz; $(CD_3)_2SO$; Me_4Si): 3.65 (6 H, s, 2 CH_3), 7.41 (2 H, s, 2 CH_2). δ_C (500 MHz; $(CD_3)_2SO$; Me_4Si): 37.43 (CH_3), 122.67 (CH), 144.69 (C=Se). δ_{Se} (500 MHz; $(CD_3)_2SO$; Me_4Si): -75.0; *m/z* (ESI-MS): 414.85 $[Cu(dmise)_2]^+$, 270.91 [Cu(dmise) + MeOH]$^+$, 255.04 [Cu(dmise) + OH]$^+$, 238.89 [Cu(dmise)]$^+$.

*Cu(dmit)$_2$Br (**7**).* CuBr (144 mg, 1 mmol) was dissolved in ethanol (15 mL), and to this was cannula added a solution of dmit (260 mg, 2 mmol) in dichloromethane (15 mL). The reaction was stirred for 6 h, the solvent was reduced *in vacuo* to about 5 ml, and the desired product was precipitated with ether (10 mL). The white precipitate was filtered and dried *in vacuo*. Single crystals suitable for X-ray analysis were grown by slow diffusion of ether into an acetonitrilesolution of the complex. Yield 347 mg, 86%. Mp. 152 °C. Found C, 29.83; N, 13.84; H, 3.90; requires $C_{10}H_{16}CuN_4Se_2Br$ C, 30.04; N, 14.01; H, 4.03%. UV-vis [λ_{max}, nm (ε_M, M^{-1}

cm^{-1})] in CH_3CN: 261 (32,442). IR (cm^{-1}): 671 s, 722 w, 757 vs, 1073 b, 1173 s, 1244 s, 1377 vs, 1464 vs, 1570 s, 1611 w, 2854 s, 2929 b, 3080 w, 3102 w, 3146 w. δ_H (500 MHz; $(CD_3)_2SO$; Me_4Si): 3.58 (6H, s, 2 CH_3), 7.25 (2H, s, 2 CH_2). δ_C (500 MHz; $(CD_3)_2SO$; Me_4Si): 35.65 (CH_3), 119.99 (CH), 156.30 (C=S); *m/z* (ESI-MS): 318.98 $[Cu(dmit)_2]^+$, 222.97 [Cu(dmit) + MeOH]$^+$, 190.95 [Cu(dmit)]$^+$, 128.03 [dmit]$^+$.

*Cu(dmise)$_2$Br (**8**).* CuBr (144 mg, 1 mmol) was dissolved in ethanol (15 mL), and to this was cannula added a solution of dmise (350 mg, 2 mmol) in dichloromethane (15 mL). The reaction was stirred for 48 h and resulted in the formation of a white precipitate, which was filtered and dried *in vacuo*. Single crystals suitable for X-ray analysis were grown by slow diffusion of ether into an acetonitrile/DMF solution of the complex. Yield 450 mg, 91%. Mp. 160 °C. Found C, 24.43; N, 11.43; H, 3.17; requires $C_{10}H_{16}CuN_4Se_2Br$ C, 24.33; N, 11.35; H, 3.27%. UV-vis [λ_{max}, nm (ε_M, M^{-1} cm^{-1})] in CH_3CN: 258 (15,611). IR (cm^{-1}): 617 w, 662 s, 740 vs, 749 vs, 804 w, 854 w, 1025 w, 1087 vs, 1150 vs, 1233 vs, 1379 vs, 1394 s, 1464 vs, 1565 vs, 1599 w. 2920 b, 3094 w, 3145 w. δ_H (500 MHz; $(CD_3)_2SO$; Me_4Si): 3.67 (s, 6 H, 2 CH_3), 7.42 (s, 2 H, 2 CH_2). δ_C (500 MHz; $(CD_3)_2SO$; Me_4Si): 37.48 (CH_3), 122.01 (CH), 147,74 (C=Se). δ_{Se} (500 MHz; $(CD_3)_2SO$; Me_4Si): -13.4; *m/z* (ESI-MS): 414.85 $[Cu(dmise)_2]^+$, 270.91 [Cu(dmise) + MeOH]$^+$, 255.04 [Cu(dmise) + OH]$^+$, 238.89 [Cu(dmise)]$^+$, 158.98 $[Cu(C_5N_2H_8)]^+$.

X-ray structural data collection and processing. Single crystals of $Cu_4(\mu_4$-

dmise)(μ-I)$_2$I$_2$ (**1**), Cu(dmise)$_2$I (**2**), Cu(dmit)$_2$I (**3a**, **3b**), Cu(dmit)$_2$Cl (**4**), Cu(dmise)$_2$Cl (**5**), Cu$_4$(μ$_4$-dmise)(μ-Br)$_2$Br$_2$ (**6**), Cu(dmit)$_2$Br (**7**), and Cu(dmise)$_2$Br (**8**) were mounted on a glass filament with silicon grease and immediately cooled to 168 ± 2 K in a cold nitrogen gas stream. Intensity data were collected using a Rigaku Mercury CCD detector and an AFC8S diffractometer. The space groups C2/*m* for **1** and **6**, C2/*c* for **2**, **3a**, **4**, **7**, and **8,** and P2$_1$/*c* for **3b** and **5** were determined from the observed systematic absences. Data reduction, including the application of Lorentz and polarization effects (Lp) and absorption corrections were performed using the CrystalClear program.[84] The structures were solved by direct methods and subsequent Fourier difference techniques, and refined anisotropically on F^2 using full-matrix least squares, with SHELXTL 6.10.[85] The presence of several residue electron density peaks in **1** and **6**, indicating disordered solvent peaks, could not be fully described and were accounted for with the Squeeze routine in PLATON.[86] Squeeze calculated a solvent-accessible void volume of 166.00 Å^3, corresponding to 29 electrons per unit cell for **1**, and a solvent-accessible void volume of 159.00 Å^3, corresponding to 26 electrons per unit cell, for **6**. The contribution of these diffusely-scattering species was removed from subsequent structure factor calculations. The reported F(000), D_{calc}, and formula weight (FW) for **1** and **6** reflect known unit cell contents only. In the final cycle of least squares, independent anisotropic displacement factors were refined for the non-hydrogen atoms and the methyl hydrogen atoms were fixed in "idealized" positions with C-H = 0.96 Å. Their isotropic displacement parameters were set equal to 1.5 times U_{eq} of the attached carbon atom.

For complex **1,** the largest peak in the final Fourier difference map (1.03 e·Å^{-3}) was located 1.62 Å from H(5A), and the lowest peak (-0.94 e·Å^{-3}) was located at a distance of 0.89 Å from I(1). The largest peak for complex **2** in the final Fourier difference map (1.20 e·Å^{-3}) was located 1.64 Å from C(3), and the lowest peak (-0.79 e·Å^{-3}) was located at a distance of 0.81 Å from I(1). The largest peak for complex 3a in the final Fourier difference map (0.53 Å) was located (1.70 Å) from H(4A), and the lowest peak (-0.80 e·Å^{-3}) was located at a distance of 0.71 Å from I. The largest peak for **3b** in the final Fourier difference map (1.12 e·Å^{-3}) was located 0.03Å from I(1), and the lowest peak (-0.99 e·Å^{-3}) was located at a distance of 0.98 Å from I(1). The largest peak for **4** in the final Fourier difference map (0.70 e·Å^{-3}) was located 1.73 Å from C(1), and the lowest peak (-0.40 e·Å^{-3}) was located at a distance of 0.80 Å from Cu1. The largest peak for **5** in the final Fourier difference map (2.05 e·Å^{-3}) was located 0.04 Å from Se(2), and the lowest peak (-0.95 e·Å^{-3}) was located at a distance of 0.93 Å from Se(2). The largest peak for **6** in the final Fourier difference map (1.69 e·Å^{-3}) was located 0.07Å from Br(1), and the lowest peak (-0.1.15 e·Å^{-3}) was located at a distance of 0.72 Å from Cu(2). The largest peak for **7** in the final Fourier difference map (1.15 e·Å^{-3}) was located 1.73 Å from H(2A), and the lowest peak (-0.49 e·Å^{-3}) was located at a distance of 0.78 Å from Cu(1). The largest peak for **8** in the final Fourier difference map (0.93 e·Å^{-3}) was located 1.72 Å from N(2), and the lowest peak (-0.93 e·Å^{-3}) was located at a distance of 0.87 Å from Se(1). Final refinement parameters for the structures of **1**, **2**, **3a**, **3b**, **4**, **5**, **6**, **7**, and **8** are given in Tables 5.7, 5.8, and 5.9; selected bond distances and angles are provided in Tables

5.7, 5.8, 5.9, and 5.10.

Table 5.7. Summary of crystallographic data for complexes **1**, **2**, and **3a**.

	1	**2**	**3a**
Chemical Formula	$C_{20}H_{32}Cu_4I_4N_8Se_4$	$C_{10}H_{16}CuIN_4Se$	$C_{10}H_{16}CuIN_4S$
F.W. (g/mol)	1462.1	540.63	446.83
Space group	C2/*m*	C2/*c*	C2/*c*
Crystal system	Monoclinic	Monoclinic	Monoclinic
a, Å	18.802(4)	15.278(3)	15.062(6)
b, Å	12.833(3)	10.874(2)	10.726(2)
c, Å	8.4800(3)	11.190(2)	11.085(2)
α, °	90	90	90
β, °	95.07(3)	118.56(3)	117.73(2)
γ, °	90	90	90
V, $Å^3$	2046.0(7)	1632.8(6)	1585.2(8)
Z	2	4	4
D_{cal}, Mg/m^3	2.374	2.199	1.864
Indices (min)	[-14, -16, -10]	[-16, -13, -13]	[-18, -13, -14]
(max)	[23, 16, 10]	[19, 13, 12]	[19, 13, 10]
Parameters	98	86	85
F(000)	1344	1016	864
μ, mm^{-1}	8.650	7.676	3.577
2θ range,	3.01 - 26.71	2.66-26.40	4.16- 26.76
Collected reflections	15543	6421	6879
Unique reflections	2263	1674	1522
Final R (obs. Data)[a],	0.0341	0.0323	0.0237
wR_2	0.0778	0.0721	0.0576
Final R (all data), R_1	0.0425	0.0395	0.0244
wR_2	0.0818	0.0775	0.0583
Goodness of fit (S)	1.107	1.132	1.203
Largest diff. Peak	1.031	1.197	0.531
Largest diff. Hole	-0.937	-0.793	-0.802

[a] $R_1 = [\Sigma||F_0| - |F_c||]/ \Sigma|F_0|$; $wR_2 = \{[\Sigma w[(F_0)^2 - (F_c)^2]^2\}^{1/2}$

Table 5.8. Summary of crystallographic data for complexes **3b**, **4**, and **5**.

	3b	**4**	**5**
Chemical Formula	$C_{10}H_{16}CuIN_4S_2$	$C_{10}H_{16}ClCuN_4S_2$	$C_{10}H_{16}ClCuN_4S$
F.W. (g/mol)	446.83	355.38	449.18
Space group	P21/c	C2/*c*	P21/*c*
Crystal system	monoclinic	Monoclinic	Monoclinic
a, Å	9.925(2)	10.348(2)	15.794(3)
b, Å	10.861(2)	9.328(19)	7.0226(14)
c, Å	14.868(3)	16.123(3)	14.263(3)
α, °	90	90	90
β, °	92.02(3)	105.64(3)	104.64(3)
γ, °	90	90	90
V, $Å^3$	1601.8(6)	1498.6(5)	1533.7(5)
Z	4	4	4
D_{cal}, Mg/m^3	1.853	1.575	1.949
Indices (min)	[-12,-11,-18]	[-12, -11, -20]	[-18,-8,-16]
(max)	[12,13,18]	[12, 10, 20]	[18,7,16]
Parameters	167	85	167
F(000)	872	728	872
μ, mm^{-1}	3.540	1.902	6.345
2θ range,	2.05-26.34	2.62 – 26.34	2.67 – 25.05
Collected reflections	13385	6856	10854
Unique reflections	3225	1522	2713
Final R (obs. Data)[a],	0.0386	0.0303	0.0684
wR_2	0.0916	0.0753	0.1680
Final R (all data), R_1	0.0422	0.0318	0.0797
wR_2	0.0943	0.0764	0.1868
Goodness of fit (S)	1.039	1.123	1.138
Largest diff. Peak	1.119	0.700	2.050
Largest diff. Hole	-0.988	-0.397	-0.949

[a] $R_1 = [\Sigma||F_0| - |F_c||]/ \Sigma|F_0|$; $wR_2 = \{[\Sigma w[(F_0)^2 - (F_c)^2]^2\}^{1/2}$

Table 5.9. Summary of crystallographic data for complexes **6**, **7**, and **8**.

	6	**7**	**8**
Chemical Formula	$C_{20}H_{32}Br_4Cu_4N$	$C_{10}H_{16}BrCuN_4S_2$	$C_{10}H_{16}BrCuN_4Se_2$
F.W. (g/mol)	1274.18	399.84	493.64
Space group	C2/*m*	C2/*c*	C2/*c*
Crystal system	Monoclinic	Monoclinic	Monoclinic
a, Å	18.374(4)	10.385(2)	10.297(2)
b, Å	12.867(3)	9.583(2)	10.390(2)
c, Å	8.4581(17)	16.002(3)	14.824(3)
α, °	90	90	90
β, °	96.71(3)	104.15 (3)	101.47(3)
γ, °	90	90	90
V, $Å^3$	1985.9(7)	1544.2(5)	1554.2(5)
Z	2	4	4
D_{cal}, Mg/m^3	2.131	1.72	2.110
Indices (min)	[-22, 0, 0]	[-12, -11, -18]	[-12,-12,-18]
(max)	[22, 15, 10]	[12, 11, 19]	[9,12,18]
Parameters	98	86	85
F(000)	1200	800	944
μ, mm^{-1}	9.826	4.261	8.648
2θ range,	2.42 - 26.26	2.93-26.27	2.80-26.28
Collected reflections	8469	6419	6449
Unique reflections	2049	1552	1560
Final R (obs. Data)[a],	0.0379	0.0346	0.0389
wR_2	0.1042	0.0842	0.0906
Final R (all data), R_1	0.0423	0.0404	0.0437
wR_2	0.1079	0.0884	0.0955
Goodness of fit (S)	1.110	1.150	1.114
Largest diff. Peak	1.693	1.15	0.933
Largest diff. Hole	-1.152	-0.489	-0.927

[a] $R_1 = [\Sigma||F_0| - |F_c||]/ \Sigma|F_0|$; $wR_2 = \{[\Sigma w[(F_0)^2 - (F_c)^2]^2\}^{1/2}$

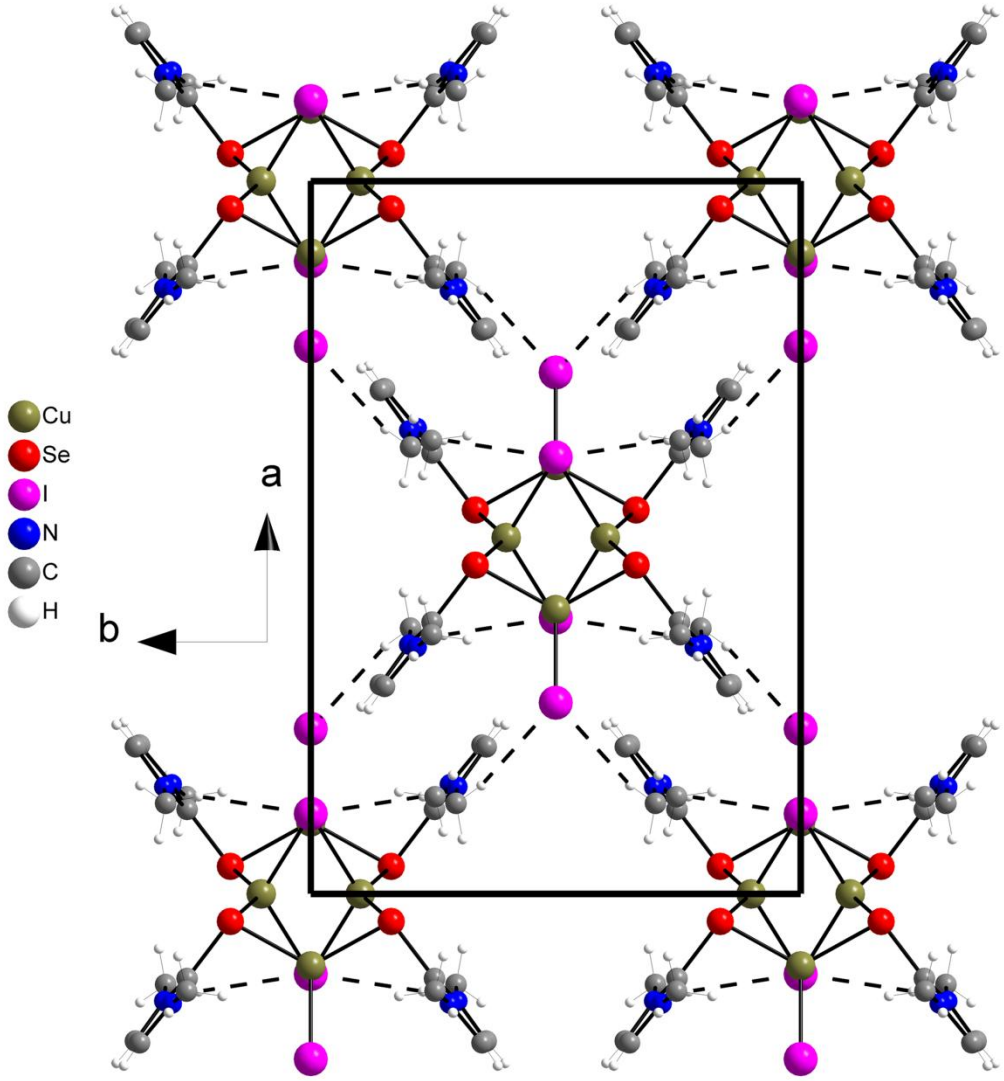

Figure 5.8. Crystal packing diagram of $Cu_4(\mu\text{-dmise})_4(\mu\text{-I})_2I_2\cdot 1.5CNCH_3$ (**1**) along the *c*-axis depicting short contact interactions between Se and H atoms.

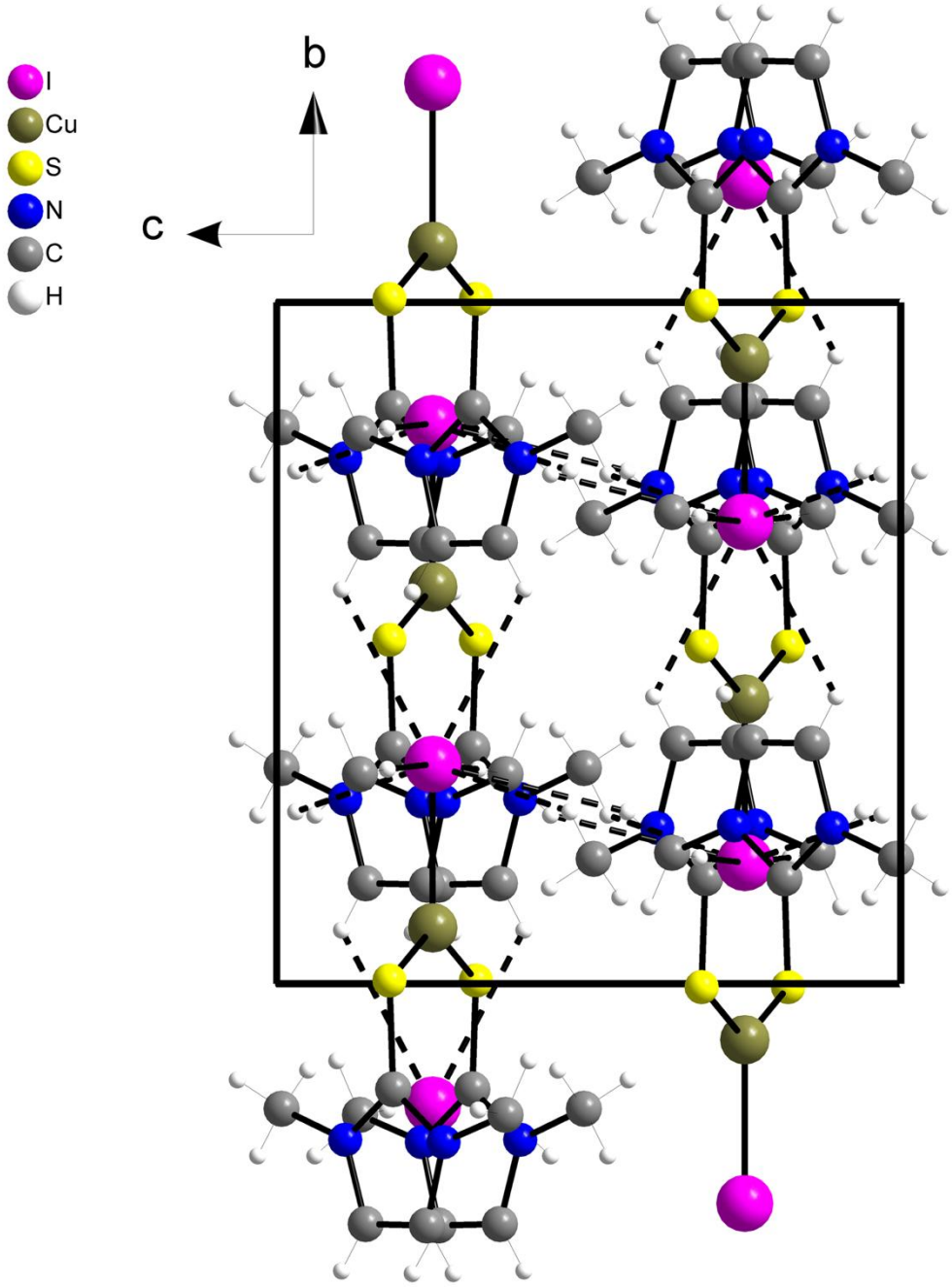

Figure 5.9. Crystal packing diagram of $CuI(dmit)_2$ (**3a**) along the *a*-axis depicting short contact interactions between Se and H atoms.

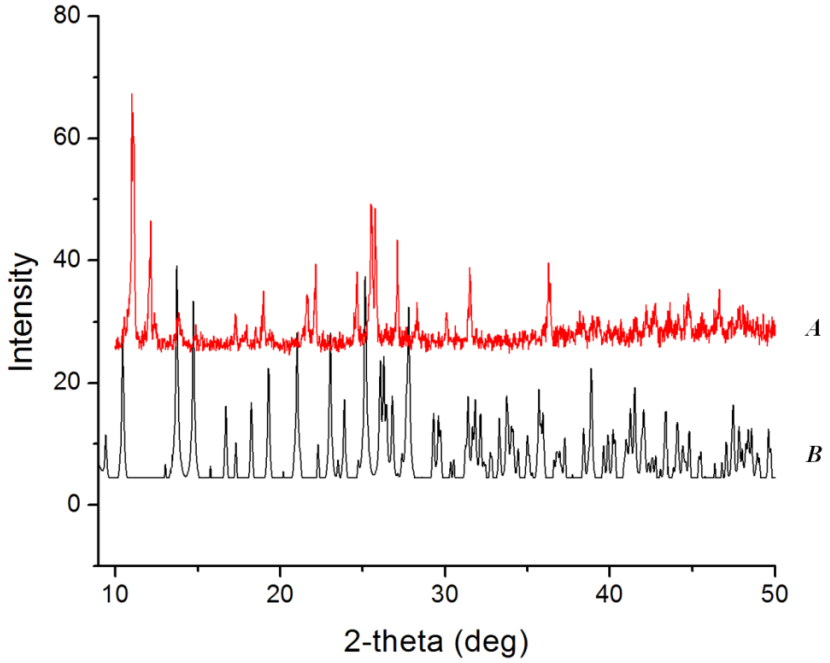

Figure 5.10. Powder X-ray diffraction pattern of A) $Cu_4(\mu\text{-dmise})_4(\mu\text{-I})_2I_2$ (**1**), vs. simulated powder pattern B) for $Cu_4(\mu\text{-dmise})_4(\mu\text{-I})_2I_2$ (**1**).

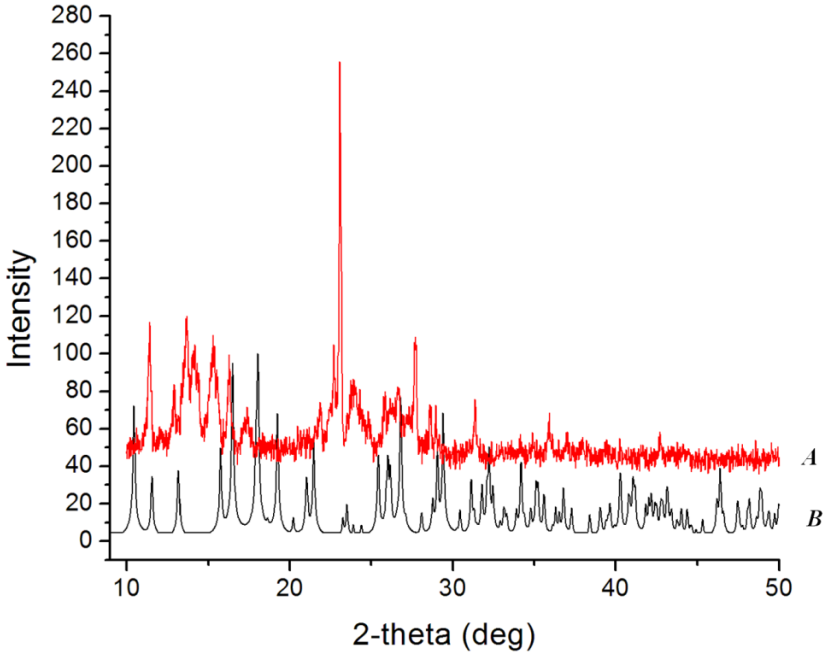

Figure 5.11. Powder X-ray diffraction pattern for **A**) $CuI(dmise)_2$ (**2**), vs. simulated powder pattern for B) $CuI(dmise)_2$ (**2**).

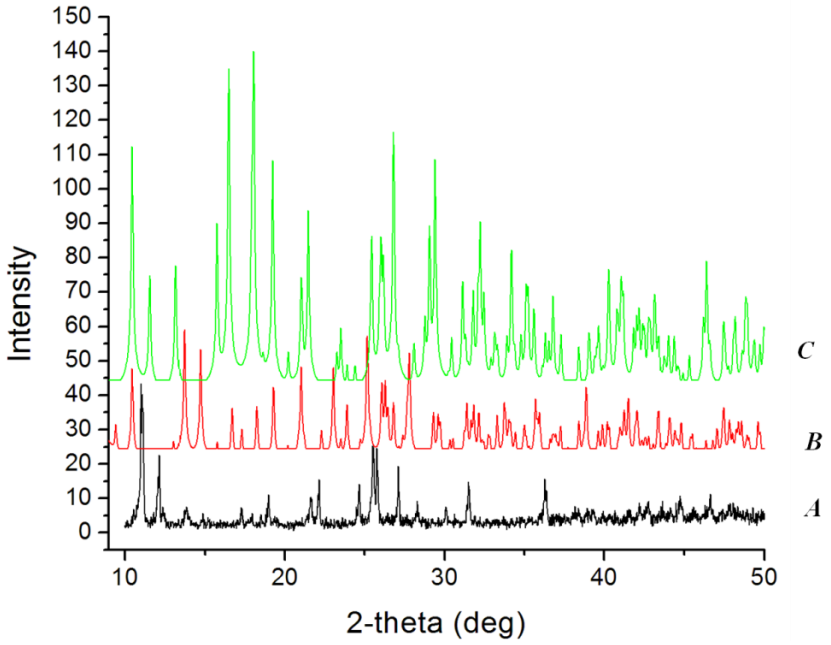

Figure 5.12. Experimental powder X-ray diffraction pattern of A) $Cu_4(\mu\text{-dmise})_4(\mu\text{-I})_2I_2$ (**1**), vs. simulated powder pattern for B) $Cu_4(\mu\text{-dmise})_4(\mu\text{-I})_2I_2$ (**1**), and C) $CuI(dmise)_2$ (**2**).

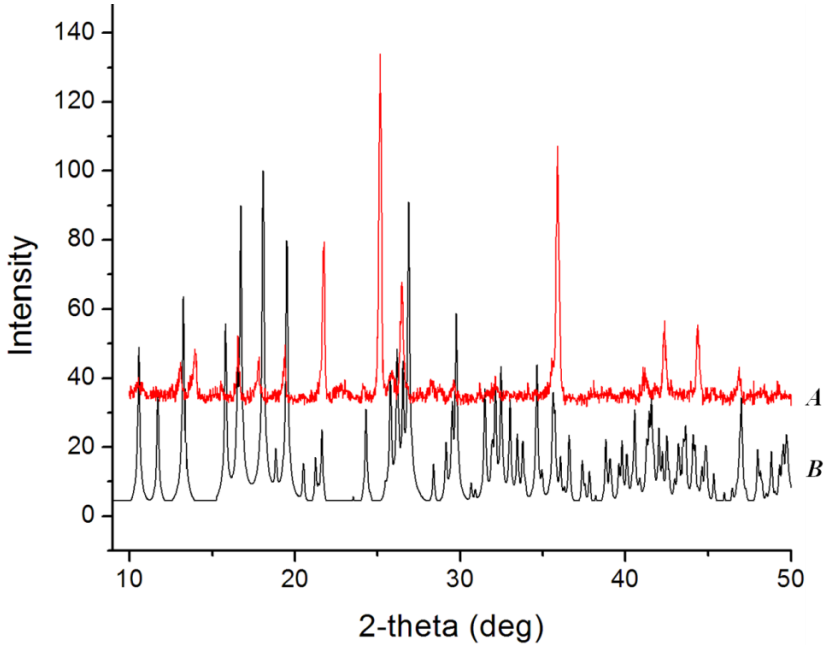

Figure 5.13. Powder X-ray diffraction pattern for A) $CuI(dmit)_2$ (**3b**) vs. simulated powder pattern for B) $CuI(dmit)_2$ (**3b**).

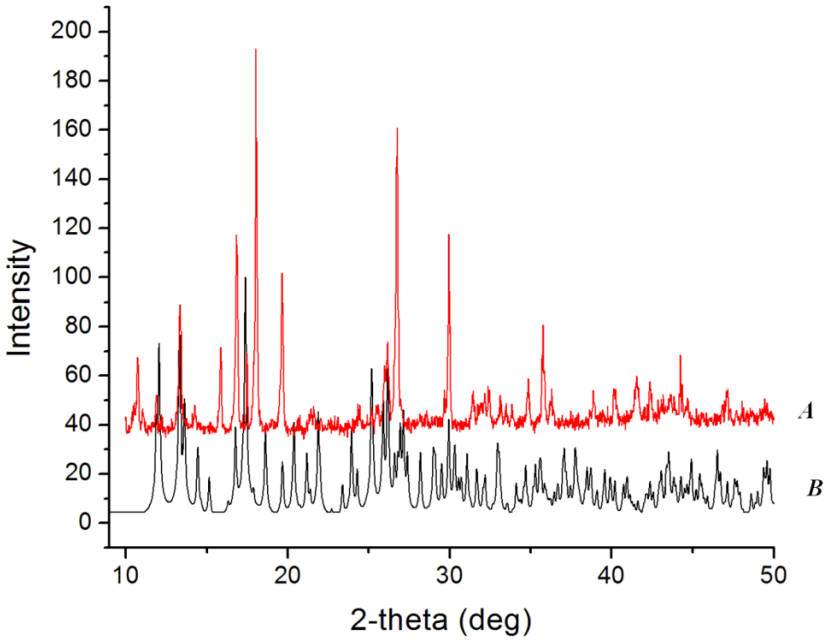

Figure 5.14. Powder X-ray diffraction pattern for **A**) $CuI(dmit)_2$ (**3a**) vs. simulated powder pattern for **B**) $CuI(dmit)_2$ (**3a**).

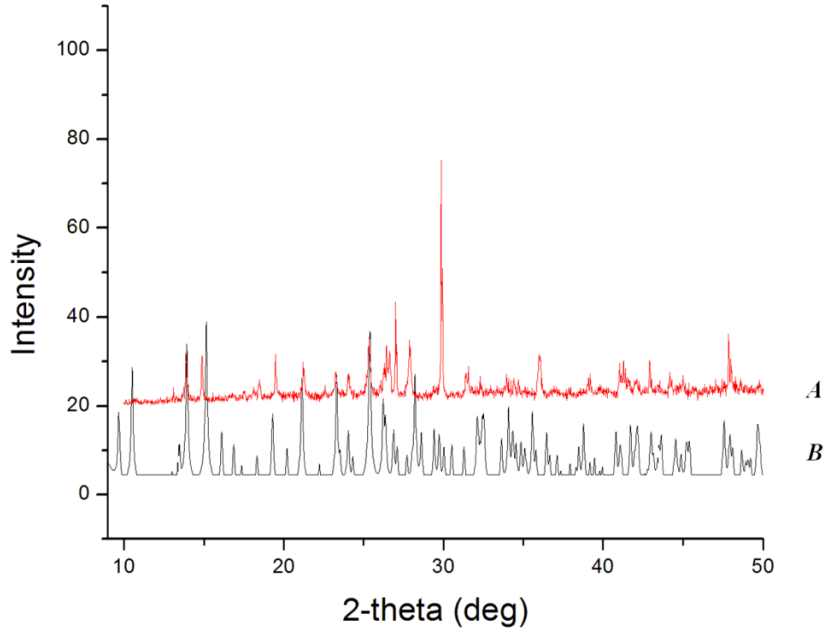

Figure 5.15. Experimental powder x-ray diffraction pattern of A) $Cu_4(\mu\text{-dmise})_4(\mu\text{-Br})_2Br_2$ (**6**) vs. simulated powder pattern B) for $Cu_4(\mu\text{-dmise})_4(\mu\text{-Br})_2Br_2$ (**6**).

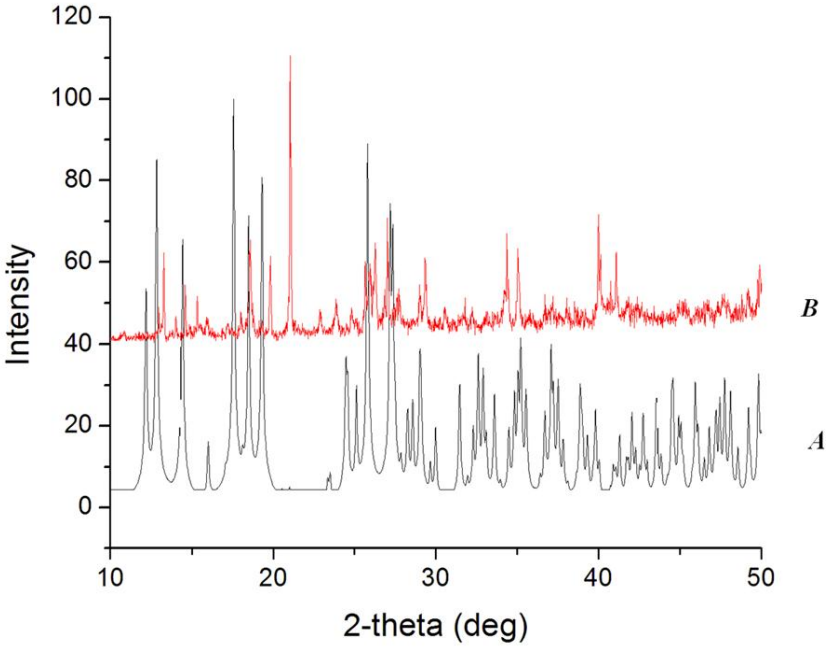

Figure 5.16. Experimental powder x-ray diffraction pattern of B) $CuBr(dmise)_2$ (**8**), vs. simulated powder pattern A) for $CuBr(dmise)_2$ (**8**).

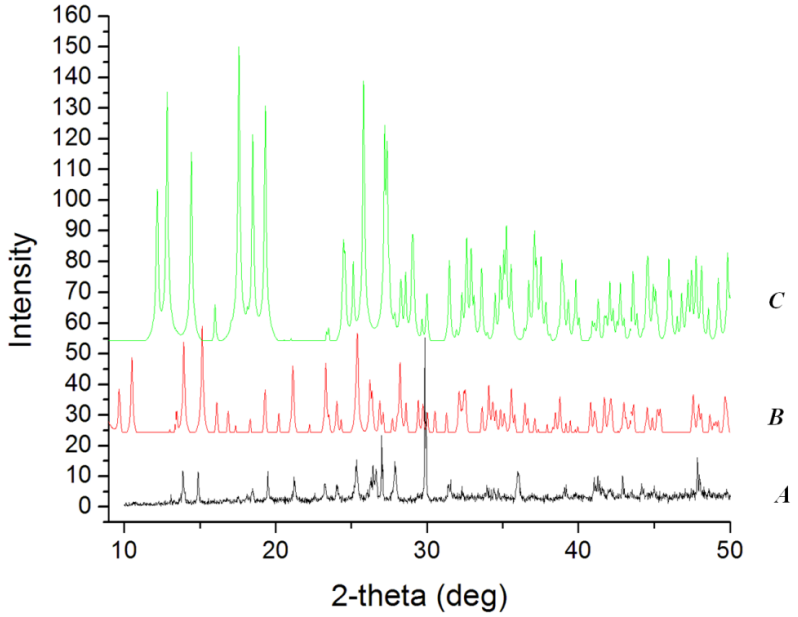

Figure 5.17. Experimental powder x-ray diffraction pattern of A) $Cu_4(\mu\text{-dmise})_4(\mu\text{-Br})_2Br_2$ (**6**), vs. simulated powder pattern B) for $Cu_4(\mu\text{-dmise})_4(\mu\text{-Br})_2Br_2$ (**6**), and C) $CuBr(dmise)_2$ (**8**).

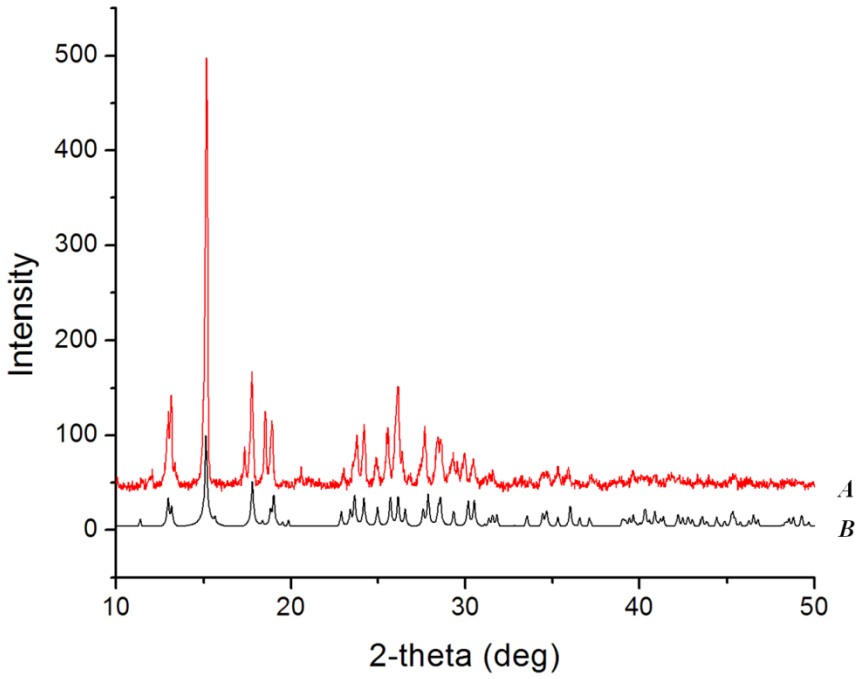

Figure 5.18. Experimental powder X-ray diffraction pattern of A) $CuCl(dmit)_2$ (**4**), vs. simulated powder pattern for B) $CuCl(dmit)_2$ (**4**).

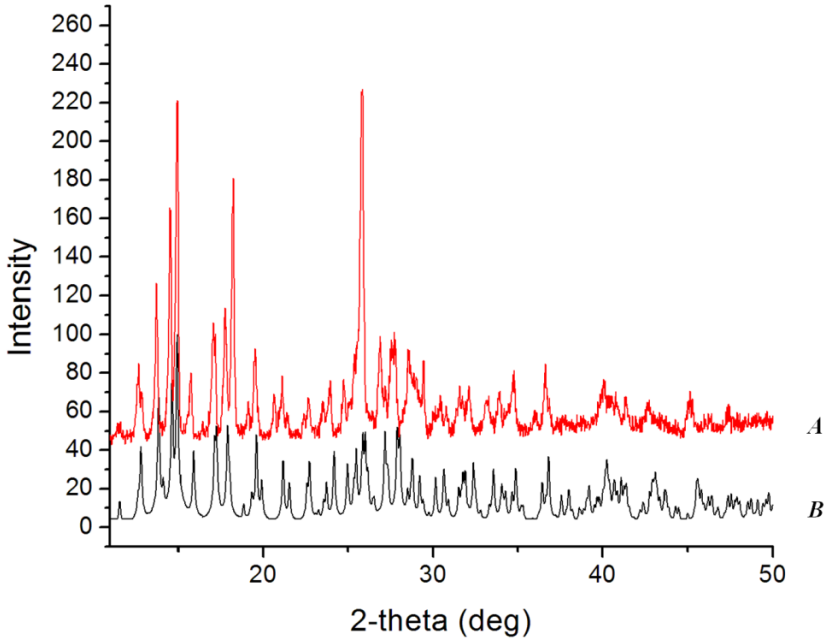

Figure 5.19. Experimental powder X-ray diffraction pattern of A) $CuCl(dmise)_2$ (**5**), vs. simulated powder pattern for B) $CuCl(dmise)_2$ (**5**).

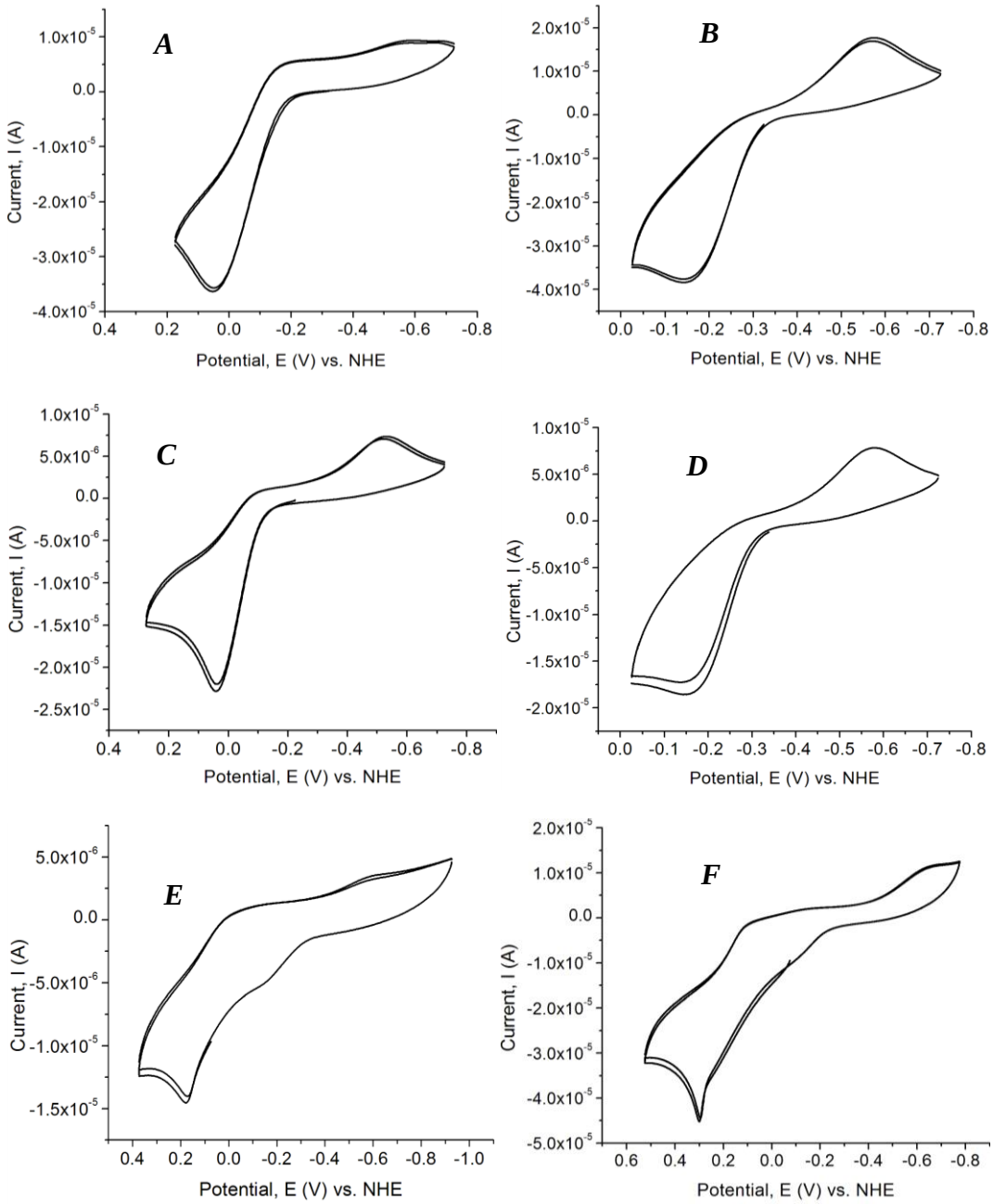

Figure 5.20. Cyclic voltammetry scans for A) $CuCl(dmit)_2$, B) $CuCl(dmise)_2$, C) $CuBr(dmit)_2$, D) $CuBr(dmise)_2$, E) $CuI(dmit)_2$ **3a**, F) $CuI(dmit)_2$ **3b**. All data collected with 1 mM complex in acetonitrile.

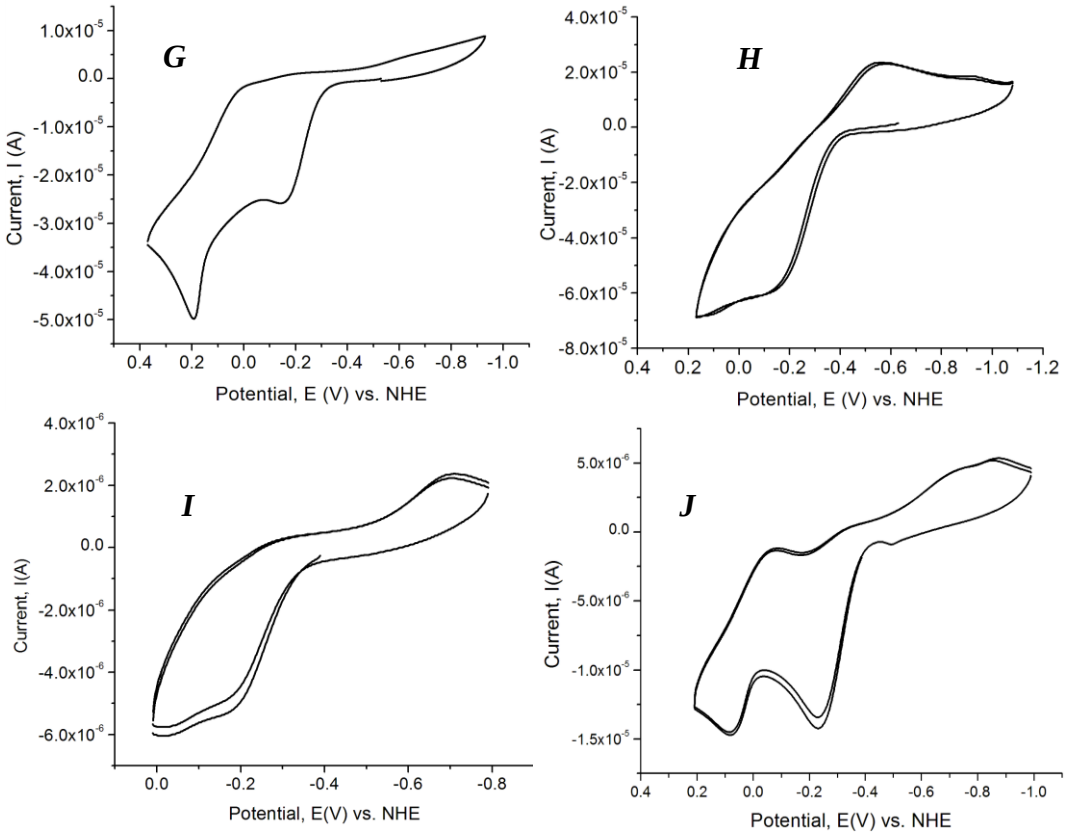

Figure 5.20 (**cont.**). Cyclic voltammetry scans for G) mixed *trans*- and *cis*-CuI(dmit)$_2$ (**3a** and **3b**), H) CuI(dmise)$_2$, I) Cu$_4$(μ-dmise)$_4$(μ-Br)$_2$Br$_2$, J) Cu$_4$(μ-dmise)$_4$(μ-I)$_2$I$_2$. All data collected with 1 mM complex in acetonitrile.

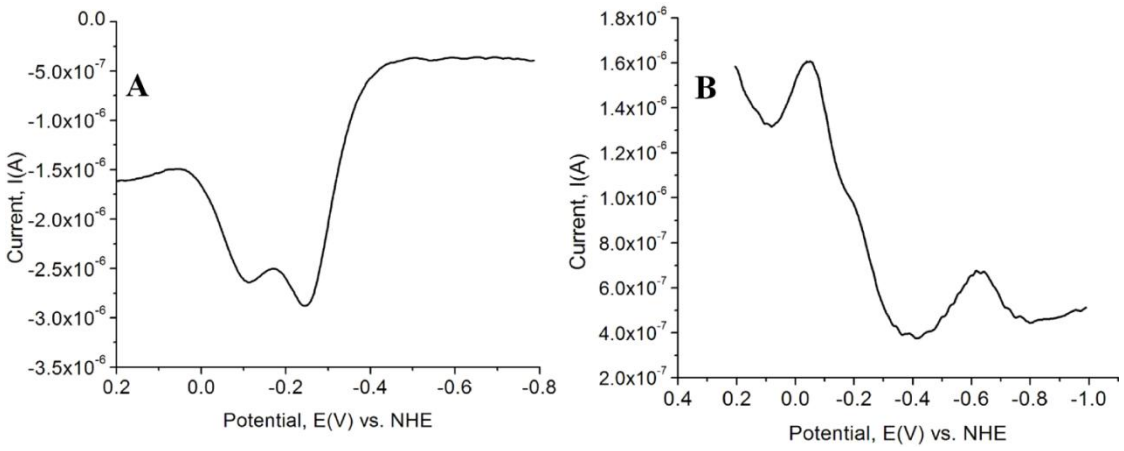

Figure 5.21. Differential pulse voltammograms: A) positive scan of $Cu_4(\mu_4\text{-dmise})(\mu\text{-}Br)_2Br_2$ (**6**); B) negative scan of $Cu_4(\mu_4\text{-dmise})(\mu\text{-}Br)_2Br_2$ (**6**). DPV data were collected at a concentration of 1 mM in acetonitrile.

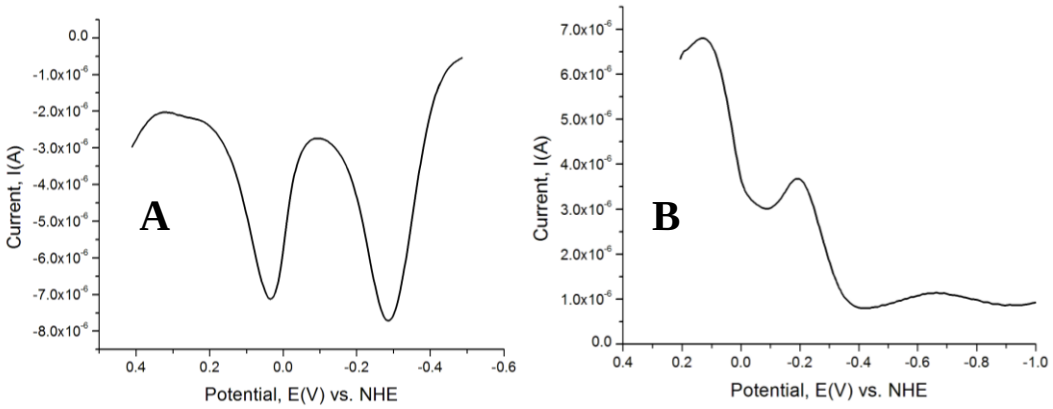

Figure 5.22. Differential pulse voltammograms: A) positive scan of $Cu_4(\mu_4\text{-dmise})(\mu\text{-}I)_2I_2$ (**1**); B) negative scan of $Cu_4(\mu_4\text{-dmise})(\mu\text{-}I)_2I_2$ (**1**). DPV data were collected at a concentration of 1 mM in acetonitrile.

References

(1) Kim, H. R.; Jung, I. G.; Yoo, K.; Jang, K.; Lee, E. S.; Yun, J.; Son, S. U. *Chem. Commun.* **2010**, *46*, 758-760.

(2) *Copper coordination chemistry: Biological and Inorganic Perspectives*; Karlin, K. D.; Zubieta, J., Eds.; Adenine Press: New York, 1985.

(3) Zeevi, S.; Tshuva, E. Y. *Eur. J. Inorg. Chem.* **2007**, 5369-5376.

(4) Davis, A. V.; O'Halloran, T. V. *Nat. Chem. Biol.* **2008**, *4*, 148-151.

(5) Holm, R. H.; Kennepohl, P.; Solomon, E. I. *Chem. Rev.* **1996**, *96*, 2239-2314.

(6) Collins, C. A.; Fry, F. H.; Holme, A. L.; Yiakouvaki, A.; Al-Qenaei, A.; Pourzand, C.; Jacob, C. *Org. Biomol. Chem.* **2005**, *3*, 1541-1546.

(7) Battin, E. E.; Brumaghim, J. L. *J. Inorg. Biochem.* **2008**, *108*, 2036-2042.

(8) Battin, E. E.; Zimmerman, M. T.; Ramoutar, R. R.; Quarles, C. E.; Brumaghim, J. L., *Metallomics*, **DOI: 10.1039/COMT0063A**.

(9) Battin, E. E.; Brumaghim, J. L. *Cell Biochem. Biophys.* **2009**, *55*, 1-23.

(10) Battin, E. E.; Brumaghim, J. L. *J. Inorg. Biochem.* **2008**, *102*, 2036-2042.

(11) Battin, E. E.; Perron, N. R.; Brumaghim, J. L. *Inorg. Chem.* **2006**, *45*, 499-501.

(12) Ramoutar, R. R.; Brumaghim, J. L. *J. Inorg. Biochem.* **2007**, *101*, 1028-1035.

(13) Ramoutar, R. R.; Brumaghim, J. L. *Main Group Chem.* **2007**, *101*, 1028-1035.

(14) Bhabak, K. P.; Mugesh, G. *Chem. Eur. J. 16*, 1175-1185.

(15) Yamashita, Y.; Yamashita, M. *J. Biol. Chem.* **2010**, *285*, 18134-18138.

(16) Roy, G.; Mugesh, G. *Chem. Biodivers.* **2008**, *5*, 414-439.

(17) Fahey, R. C. *Annu. Rev. Microbiol.* **2001**, *55*, 333-356.

(18) Seebeck, F. P. *J. Am. Chem. Soc.* **2010**, *132*, 6632-6633.

(19) Kimani, M. M.; Brumaghim, J. L.; Van Derveer, D. *Inorg. Chem.* **2010**, *49*, 9200-9211.

(20) Lobana, T. S.; Sultana, R.; Castineiras, A.; Butcher, R. J. *Inorg. Chim. Acta.* **2009**, *362*, 5265-5270.

(21) Lobana, T. S.; Sultana, R.; Hundal, G.; Castineiras, A. *Polyhedron.* **2009**, *28*, 1573-1577.

(22) Lang, E. S.; Stieler, R.; de Oliveira, G. M. *Polyhedron* **2009**, *28*, 3844-3848.

(23) Cayton, R. H.; Chisholm, M. H.; Putilina, E. F.; Folting, K. *Polyhedron* **1993**, *12*, 2627-2633.

(24) Jones, P. G.; Friedrichs, S. *Chem. Commun.* **1999**, 1365-1366.

(25) Raper, E. S. *Coord. Chem. Rev.* **1997**, 475-564.

(26) Raper, E. S. *Coord. Chem. Rev.* **1996**, *153*, 199-255.

(27) Akrivos, P. D. *Coord. Chem. Rev.* **2001**, *213*, 181-210.

(28) Spicer, M. D.; Reglinski, J. *Eur. J. Inorg. Chem.* **2009**, 1553-1574.

(29) Pattinari, C. *Scorpionates II: Chelating Borate Ligands Dedicated to Swiatoslaw Trofimenko*; Imperial College Press: London, 2008, pp. 381-415.

(30) Parkin, G. *New J. Chem.* **2007**, *31*, 1996-2014.

(31) Lobana, T. S.; Castineiras, A. *Polyhedron* **2002**, *21*, 1603-1611.

(32) Williams, D. J.; White, K. M.; VanDerveer, D.; Wilkinson, A. P. *Inorg. Chem. Commun.* **2002**, *5*, 124-126.

(33) Williams, J. D.; Concepcion, J. J.; Koether, M. C.; Arrowood, A. K.; Carmack, A. L.; Hamilton, T. G.; Luck, S. M.; Ndomo, M.; Teel, R. C.; VanDerveer, D. *J. Chem. Crystallogr.* **2006**, *36*, 453-457.

(34) Pang, K. L.; Figueroa, J. S.; Tonks, I. A.; Sattler, W.; Parkin, G. *Inorg. Chim. Acta* **2009**, *362*, 4609-4615.

(35) Williams, D. J.; Concepcion, J. J.; Koether, M. C.; Arrowood, K. A.; Carmack, A. L.; Hamilton, T. G.; Luck, S. M.; Ndomo, M.; Teel, C. R.; VanDerveer, D. *J. Chem. Crystallogr.* **2006**, *36*, 453-457.

(36) Williams, D. J.; Jones, T. A.; Rice, E. D.; Davis, K. J.; Ritchie, J. A.; Pennington, W. T.; Schimek, G. L. *Acta Crystallogr. Sect. C-Cryst. Struct. Commun.* **1997**, *53*, 837-838.

(37) Kheddar, N.; Protas, J.; Le Bacon, M.; Guglielmetti, R.; Guerchais, J. E. *Bull. Chim. Soc. Fr.* **1976**, 803-811.

(38) Williams, D. J.; McKinney, B. J.; Baker, B.; Gwaltney, K. P.; VanDerveer, D. *J. Chem. Crystallogr.* **2007**, *37*, 691-694.

(39) Dewhurst, R. D.; Hansen, A. R.; Hill, A. F.; Smith, M. K. *Organometallics* **2006**, *25*, 5843-5846.

(40) Isab, A. A.; Wazeer, M. I. M.; Fettouhi, M.; Ahmad, S.; Ashraf, W. *Polyhedron* **2006**, *25*, 2629-2636.

(41) Al-Amri, A. H. D.; Fettouhi, M.; Wazeer, M. I. M.; Isab, A. A. *Inorg. Chem. Commun.* **2005**, *8*, 1109-1112.

(42) Blake, A. J.; Lippolis, V.; Pivetta, T.; Verani, G. *Acta. Crystallogr. C* **2007**, *63*, m364-367.

(43) Devillanova, F. A.; Diaz, D.; Isaia, F.; Verani, G. *Transition Met. Chem.* **1989**, *14*, 153-154.

(44) Hussein, A.; Devillanova, F. A.; Isaia, F.; Verani, G. *Transition Met. Chem.* **1985**, *10*, 368-370.

(45) Kimani, M. M.; Bayse, C. A.; Brumaghim, J. L. *Dalton Trans.*, submitted.

(46) Niu, Y. Y.; Zhang, N.; Hou, H. W.; Zhu, Y.; Tang, M. S.; Ng, S. *J. Mol. Struct.* **2007**, *827*, 195-200.

(47) Lobana, T. S.; Mahajan, P.; Pannu, A. S.; Hundal, G.; Butcher, R. J. *J. Coord. Chem.* **2007**, *60*, 733-739.

(48) Nguyen, C. Q.; Adeogun, A.; Afzaal, M.; Malik, M. A.; O'Brien, P. *Chem. Comm.* **2006**, 2182-2184.

(49) Lobana, T. S.; Rimple; Castineiras, A.; Turner, P. *Inorg. Chem.* **2003**, *42*, 4731-4737.

(50) Bondi, A. *J. Phys. Chem.* **1965**, *68*, 441-451.

(51) Ainscough, E. W.; Brodie, A. M.; Brown, K. L. *J. Chem. Soc., Dalton Trans.* **1980**, 1042.

(52) Shen, X.; Wen, T. B.; Liu, Q. T.; Huang, X. Y.; Kang, B. S.; Wu, X. L.; Huang, Z. S.; Gu, L. Q. *Polyhedron* **1997**, *16*, 2605-2611.

(53) Li, G.; Che, D. J.; Li, Z. F.; Zhu, Y.; Zou, D. P. *New J. Chem.* **2002**, *26*, 1629-1633.

(54) Bret, J. M.; Castan, P.; Jugie, G.; Dubourg, A.; Roques, R. *J. Chem. Soc., Dalton Trans.* **1983**, 301-304.

(55) Bowmaker, G. A.; Chaichit, N.; Hanna, J. V.; Pakawatchai, C.; Skelton, B. W.; White, A. H. *Dalton Trans.* **2009**, 8308-8316.

(56) Lobana, T. S.; Sharma, R.; Butcher, R. J. *Z. Anorg. Allg. Chem.* **2008**, *634*, 1785-1790.

(57) Lobana, T. S.; Mahajan, R.; Castineiras, A. *Transition Met. Chem.* **2001**, *26*, 440-444.

(58) Tomlin, D. W.; Campbell, D. P.; Fleitz, P. A.; Adams, W. W. *Acta Cryst.* **1997**, *C53*, 1153-1154.

(59) Black, J. R.; Champness, N. R.; Levason, W.; Reid, G. *Inorg. Chem.* **1996**, *35*, 1820-1824.

(60) Booth, D. G.; Levason, W.; Quirk, J. J.; Reid, G.; Smith, S. M. *J. Chem. Soc., Dalton Trans.* **1997**, 3493-3500.

(61) Williams, D. J.; Fawcettbrown, M. R.; Raye, R. R.; Vanderveer, D.; Pang, Y. T.; Jones, R. L.; Bergbauer, K. L. *Heteroatom Chem.* **1993**, *4*, 409-414.

(62) Hadjikakou, S. K.; Aslanidis, P.; Karagiannidis, P.; Hountas, A.; Terzis, A. *Inorg. Chim. Acta* **1991**, *184*, 161-166.

(63) Hadjikakou, S. K.; Aslanidis, P.; Karagiannidis, P. *Polyhedron* **1991**, *10*, 935-940.

(64) Lecomte, C.; Skoulika, S.; Aslanidis, P.; Karagiannidis, P.; Papastefanou, S. *Polyhedron* **1989**, *8*, 1103-1109.

(65) Williams, D. J.; Ly, T. A.; Mudge, J. W.; Vanderveer, D.; Jones, R. L. *Inorg. Chim. Acta* **1994**, *218*, 133-138.

(66) Landry, V. K.; Minoura, M.; Pang, K. L.; Buccella, D.; Kelly, B. V.; Parkin, G. *J. Am. Chem. Soc.* **2006**, *128*, 12490-12497.

(67) Jia, W. G.; Huang, Y. B.; Lin, Y. J.; Wang, G. L.; Jin, G. X. *Eur. J. Inorg. Chem.* **2008**, 4063-4073.

(68) Williams, D. J.; Arrowood, K. A.; Bloodworth, L. M.; Carmack, A. L.; Gulla, D.; Gray, M. W.; Maasen, I.; Rizvi, F.; Rosenbaum, S. L.; Gwaltney, K. P.; VanDerveer, D. *J. Chem. Crystallogr.*, *40*, 1074-1077.

(69) Pinder, T. A.; VanDerveer, D.; Rabinovich, D. *Inorg. Chem. Commun.* **2007**, *10*, 1381-1384.

(70) Beheshti, A.; Clegg, W.; Nobakht, V.; Mehr, M. P.; Russo, L. *Dalton Trans.* **2008**, 6641-6646.

(71) Popovic, Z.; Pavlovic, G.; Matkovic-Calogovic, D.; Soldin, Z.; Rajic, M.; Vikic-Topic, D.; Kovacek, D. *Inorg. Chim. Acta.* **2000**, *306*, 142-152.

(72) Lee, D. H.; Hatcher, L. Y. Q.; Vance, M. A.; Sarangi, R.; Milligan, A. E.; Sarjeant, A. A. N.; Incarvito, C. D.; Rheingold, A. L.; Hodgson, K. O.; Hedman, B.; Solomon, E. I.; Karlin, K. D. *Inorg. Chem.* **2007**, *46*, 6056-6068.

(73) Chuaysong, R.; Chooto, P.; Pakawatchai, C. *Scienceasia* **2008**, *34*, 440-442.

(74) Miyamoto, R.; Santo, R.; Matsushita, T.; Nishioka, T.; Ichimura, A.; Teki, Y.; Kinoshita, I. *Dalton Trans.* **2005**, 3179-3186.

(75) Roy, G.; Das, D.; Mugesh, G. *Inorg. Chim. Acta.* **2007**, *360*, 303-316.

(76) Kubas, G. J. *Inorg. Synth.* **1990**, *28*, 68-70.

(77) Odom, J. D.; Dawson, W. H.; Ellis, P. D. *J. Amer. Chem. Soc.* **1979**, *101*, 5815-5823.

(78) Solutions, P. Q.; Parallel Quantum Solutions: Fayetteville AR 72703.

(79) Hurley, M. M.; Pacios, L. F.; Christiansen, P. A.; Ross, R. B.; Ermler, W. C. *J. Chem. Phys.* **1986**, *84*, 6840-6853.

(80) Couty, M.; Hall, M. B. *J. Comput. Chem.* **1996**, *17*, 1359-1370.

(81) Wadt, W. R.; Hay, P. J. *J. Chem. Phys.* **1985**, *82*, 284-298.

(82) Dunning, T. H. *J. Chem. Phys.* **1971**, *55*, 716-723.

(83) Dunning, T. H. *J. Chem. Phys.* **1970**, *53*, 2823-2833.

(84) Crystalclear; The Woodlands: Texas, USA, 1999.

(85) Sheldrick, G. M. *Acta Crystallogr. Sect. A* **2008**, *64*, 112-122.

(86) Spek, A. L. *J. Appl. Crystallogr.* **2003**, *36*, 7-13.

CHAPTER SIX

SYNTHESIS , CHARACTERIZATION AND ELECTROCHEMICAL STUDIES OF DINUCLEAR Cu(I)-COMPLEXES WITH BIS(SELENO/THIOIMIDAZOLYL)METHANE OR ETHANE AND *N*,*N*'-DIMETHYLIMIDAZOLE SELONE AND THIONE LIGANDS

Introduction

The chemistry of monodentate and bidentate "soft" sulfur and selenium Lewis donor ligands with soft and borderline metals has recently received much attention due to their potential applications in catalysis,[1,2] radiopharmaceuticals,[3] supramolecular, bioinorganic, organometallic and coordination chemistry.[4] Great strides have been made in understanding the coordination chemistry of bis(thioimidazolyl)borate and methane ligands first pioneered by Parkin[5] and Reglinski,[6] but the neutral selenium analog, bis(selenoimidazolyl)methane, has received relatively little attention. We are interested in the coordination chemistry of *N*,*N*'-dimethylimidazole selone, *N*,*N*'-dimethylimidazole thione, bis(thioimidazolyl)methane and bis(selenoimidazolyl)methane, bis(thioimidazolyl)ethane and bis(selenoimidazolyl)ethane ligands with copper in the hope of understanding the fundamentals of copper-selenium/sulfur coordination and it's effects on $Cu^{2+/+}$ reduction potentials. The high propensity for selenium and sulfur to bridge also results in diverse coordination architectural frameworks[7] and these ligands are

also potential synthons for the formation of heterocyclic carbenes via potassium metal reduction.[8] There is also increased interest in copper chalcogenolates and mixed chalcogenolates as single source precursors in the synthesis of semiconductor materials via metal organic chemical vapor deposition.[9]

Different coordination models of mbit with metal ions such as Pb^{2+},[10,11] Sn^{2+},[12] Sb^{3+},[13] Bi^{3+},[13] Ag^{+},[14] Rh^{3+},[1,15] Re^{+},[3] Ni^{2+},[16] Co^{2+},[16] and Ir^{3+},[1] have been reported, but it's rather surprising that their Cu^{+} complexes have not been synthesized to date. While the coordination chemistry of mbit with transition metals is well established, that of the analogous selenium ligand (mbis) is very uncommon. Only a handful of transition metal complexes with mbis or ebis ligands have been reported: [Cp*Ir(ebis)Cl][Cl], [Cp*Rh(mbis)Cl][Cp*$RhCl_3$],[1] $NiBr_2$(mbis), $NiBr_2$(ebis), $[CoCl_2(mbis)]_n$ and $[CoCl_2(ebis)]_n$.[16] It is expected that coordination of mbis and ebis to copper should have stronger coordination bonds relative to mbit and ebit due to increased nucleophilicity and polarizability of selenium compared to that of sulfur.[17]

In this chapter, we report the synthesis and crystal structures of dinuclear, three- and four-coordinate Cu^{+} complexes with the aim of understanding their modes of coordination and the effect of the alkane linker and chalcogenone binding on $Cu^{2+/+}$ reduction potentials. The $Cu^{2+/+}$ reduction potentials can also be tuned by synthesizing homoleptic copper complexes using a variety of different selone and thione ligands or heteroleptic copper complexes using mixed chalcogenone ligands. Such redox tuning has practical applications ranging from understanding biological processes such as electron

transfer in blue copper proteins and respiration,[18] to industrial and synthetic applications in catalysis.[2,19] Copper(I) complexes bearing homogeneous and heterogeneous monodentate (dmise or dmit) and bidentate (mbis, mbit, ebis and ebit) chalcogenone ligands have been synthesized and characterized using ^{1}H, $^{13}C\{^{1}H\}$, $^{19}F\{^{1}H\}$ and $^{77}Se\{^{1}H\}$ NMR spectroscopy, X-ray structural analysis, electrospray ionization mass spectrometry and cyclic voltammetry.

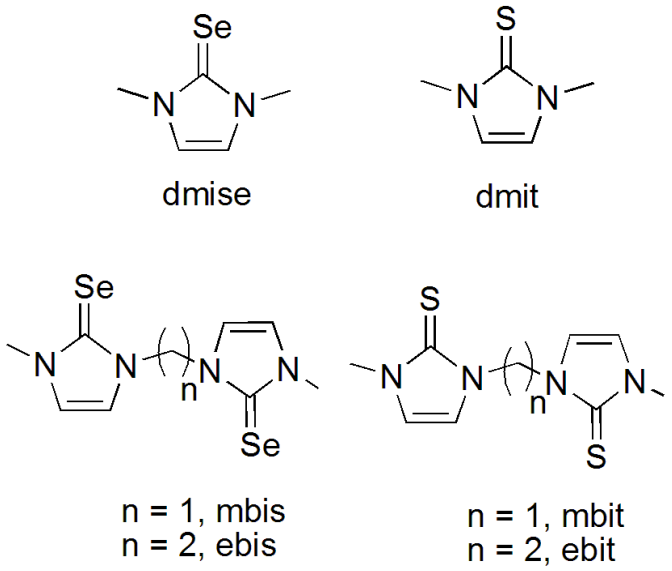

Figure 6.1. Chalcogenone ligands used in this study.

Results and Discussion

Synthesis of dinuclear Cu(I) selone and thione complexes. Homoleptic dinuclear copper complexes were synthesized via the reaction of appropriate amounts of $[Cu(NCCH_3)_4][BF_4]$ with *N,N'*-dimethylimidazole selone (dmise) and

N,N'-dimethylimidazole thione (dmit) in acetonitrile (Scheme 6.1, reaction 1) or bis(selenoimidazolyl)methane (mbis), bis(selenoimidazolyl)ethane (ebis), bis(thioimidazolyl)methane (mbit), and bis(thioimidazolyl) ethane (ebit) in a mixed solvent system of acetonitrile and dichloromethane (Scheme 6.1, reactions 2 and 3).

Scheme 6.1

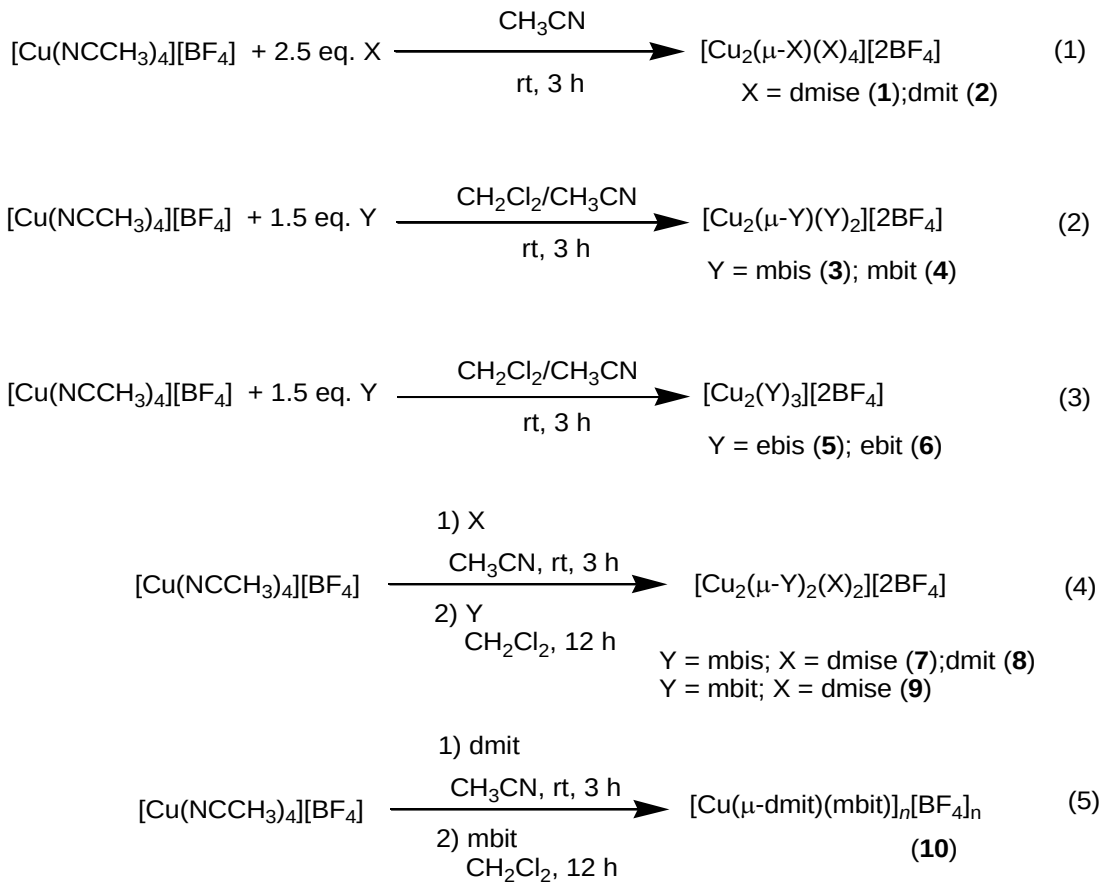

Heteroleptic dinuclear complexes of Cu^{+} were synthesized via a convenient two-step, one-pot synthesis by treating equimolar amounts of $[Cu(NCCH_3)_4][BF_4]$ and dmise or dmit in acetonitrile, followed by cannula addition of mbis or mbit in dichloromethane (Scheme 6.1, reaction 4). Treating equimolar amounts of $[Cu(NCCH_3)]_4[BF_4]$ with dmit

in acetonitrile followed by addition of equimolar amount of mbit in dichloromethane afforded a copper complex with infinite chains of mbit and dmit (Scheme 6.1, reaction 5).

Structural analysis of dinuclear copper complexes. Single crystal diffraction data were collected for $[Cu_2(\mu\text{-dmise})(dmise)_4][2BF_4]\cdot CH_3CN$ (**1**), $[Cu_2(\mu\text{-mbis})(mbis)_2]$-$[2BF_4]\cdot CH_3CN$ (**3**), $[Cu_2(ebit)_3][2BF_4]$ (**6**), $[Cu_2(\mu\text{-mbis})_2(dmise)_2][2BF_4]$ (**7**), $[Cu_2(\mu\text{-mbis})_2(dmit)_2][2BF_4]$ (**8**), and $[Cu(mbit)(\mu\text{-dmit})]_n[BF_4]_n$ (**10**), which crystallized as colorless plates. The structural parameters for **1**, **3**, **6**, **7**, **8**, and **10** are summarized in Tables 6.1 to 6.4, and their structures are shown in Figures 6.2 to 6.5.

The X-ray crystal structure of $[Cu_2(\mu\text{-dmise})(dmise)_4][2BF_4]\cdot CH_3CN$ (**1**) is shown in Figure 6.2, and selected bond lengths and angles are given in Table 6.1. The structural unit of $[(Cu(dmise)_2)(\mu\text{-dmise})][2BF_4]$ is made up of a dimer with two Cu^+ centers, with one of the Se atoms of the dimethylimidazole selone (dmise) bridging two Cu atoms, forming a trigonal Cu_2Se core. Each copper atom is further bonded to two selenium atoms from dmise and thus each copper adopts a distorted trigonal geometry. The Cu-Cu bond distance, 2.63 Å is longer than sum of ionic radii of Cu^+ (1.48 Å). The average Cu-Se bond distance is 2.37 Å which is slightly longer than monomeric copper selone complexes reported by Kimani, *et al*.[20] The average bond length of bridging Cu-Se bond (2.42 Å) is longer than the average non bridging Cu-Se bond length (2.35 Å). The dinuclear copper selone complex **1** adopts a distorted trigonal planar geometry with average Cu-Se bond lengths of 2.37 Å, longer than the previously synthesized three-

coordinate copper-selone complexes $Cu(dmise)_2X$, (X = I, Br, or Cl) with Cu-Se bond distances of 2.34 Å,[21] $[Cu_3I_3\{Ph_2P(Se)\text{-}(CH_2)_3\text{-}P(Se)Ph_2\}_2]_n$ (2.35 Å).[22]

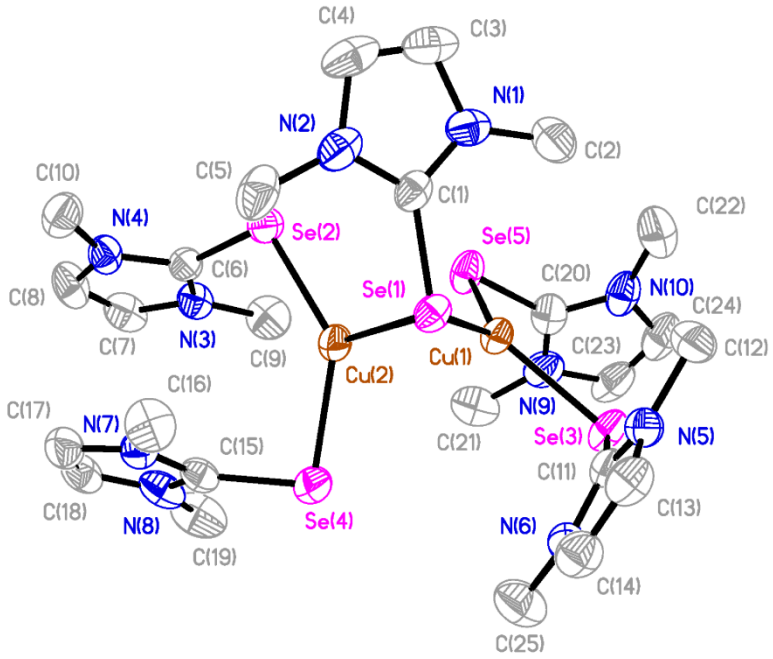

Figure 6.2. The crystal structure diagram of $[Cu_2(\mu\text{-dmise})(dmise)_4][2BF_4]\cdot CH_3CN$ (**1**) showing 50% probability ellipsoids. Hydrogen atoms, counterions, and the solvent molecule are omitted for clarity.

Table 6.1. Selected bond lengths (Å) and angles (°) for **1**.

Cu(1)-Se(1)	2.3986(9)	Se(5)-Cu(1)-Se(3)	118.37(4)
Cu(2)-Se(1)	2.4382(10)	Se(5)-Cu(1)-Se(1)	128.11(4)
Cu(1)-Se(3)	2.3460(10)	Se(3)-Cu(1)-Se(1)	113.34(3)
Cu(1)-Se(5)	2.3377(9)	Se(2)-Cu(1)-Se(4)	133.26(4)
Cu(2)-Se(2)	2.3458(11)	Se(2)-Cu(1)-Se(1)	111.91(4)
Cu(2)-Se(4)	2.3592(12)	Se(4)-Cu(1)-Se(1)	112.68(4)
Cu(1)-Cu(2)	2.6326(11)		

The molecular structure of $[Cu_2(\mu\text{-mbis})(mbis)_2][2BF_4]\cdot CH_3CN$ (**3**) is shown in Figure 6.3 and the selected bond lengths and angles are given in Table 6.2. The structural

unit of $[Cu_2(\mu\text{-mbis})(mbis)_2][2BF_4]$ (**3**) is made up of a Cu^+ dimer, and two of the Se atoms from bis(seleno-methylimidazole) methane (mbis) bridge two copper atoms forming a Cu_2Se_2 core. The Cu^+ ions are bound to two additional selenium atoms from the bidentate mbis ligand, hence each Cu^+ ion adopts a distorted tetrahedral geometry with angles ranging from 100.50 to 123.36°. The Cu-Cu distance, 2.96 Å is longer than the sum of their ionic radii, suggesting the absence of Cu-Cu interactions. The average bond length of the bridging Cu-Se bonds (2.54 Å) is longer than the average non-bridging Cu-Se bond length (2.45 Å).

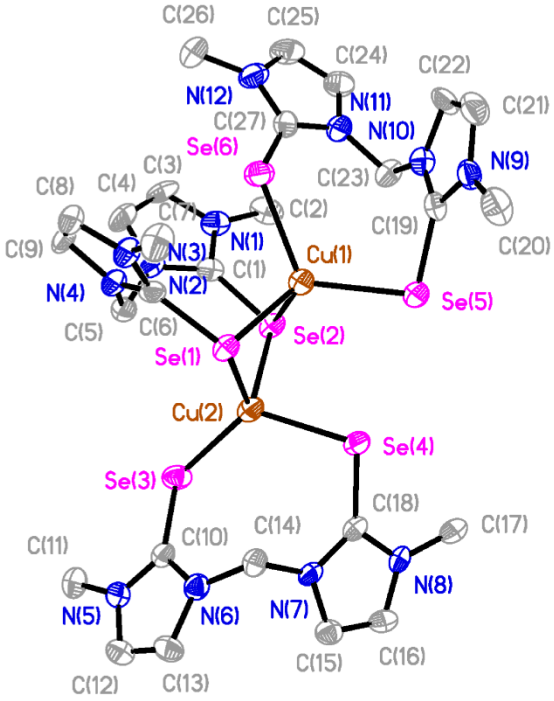

Figure 6.3. The crystal structure diagram of $[Cu_2(\mu\text{-mbis})(mbis)_2][2BF_4]$ showing 50% probability ellipsoids. Hydrogen atoms, counterions and the solvent molecules are omitted for clarity.

Table 6.2. Selected bond distances (Å) and angles (°) for **3**.

Cu(1)-Se(1)	2.5128(12)	Se(1)-Cu(1)-Se(2)	100.50(4)
Cu(1)-Se(2)	2.5617(13)	Se(1)-Cu(1)-Se(5)	115.76(4)
Cu(1)-Se(5)	2.4221(11)	Se(1)-Cu(1)-Se(6)	100.21(4)
Cu(1)-Se(6)	2.4315(12)	Se(5)-Cu(1)-Se(2)	110.93(4)
Cu(2)-Se(1)	2.5073(12)	Se(5)-Cu(1)-Se(6)	115.10(5)
Cu(2)-Se(2)	2.4981(12)	Se(1)-Cu(2)-Se(2)	102.43(4)
Cu(2)-Se(3)	2.4091(15)	Se(1)-Cu(2)-Se(3)	122.52(4)
Cu(2)-Se(4)	2.4267(11)	Se(1)-Cu(2)-Se(4)	95.13(4)
Cu(1)-Cu(2)	2.9616(18)	Se(2)-Cu(2)-Se(3)	107.50(4)
		Se(2)-Cu(2)-Se(4)	102.71(4)
		Se(3)-Cu(2)-Se(4)	123.36(4)

The copper complex $[Cu_2(ebit)_3][2BF_4]$ (**6**) (Figure 6.4) has two Cu^+ centers, each arranged in a distorted trigonal planar geometry. The distorted trigonal geometry results from coordination of sulfur atoms from the ebit ligand and a third sulfur atom from an additional ebit ligand that bridges the two separate copper centers. The angles around the copper centers are 117.72(5)° for S(3)-Cu(1)-S(2), 114.70(6)° for S(4)-Cu(1)-S(3) and 122.49(5)° for S(4)-Cu(1)-S(2), with an average Cu-S bond distance of 2.29 Å (Table 6.3).

The molecular structure of $[Cu_2(\mu\text{-mbis})_2(dmise)_2][2BF_4]$ (**7**) is shown in Figure 6.5, and the selected bond length and angles are given in Table 6.4. The structural unit of $[Cu_2(\mu\text{-mbis})_2(dmise)_2][2BF_4]$ is dimeric, with two of the Se atoms from bis(seleno-methylimidazole) methane (mbis) bridging two Cu^+ ions to form a Cu_2Se_2 core that resembles a parallelogram. The copper ions are bound to two additional selenium atoms,

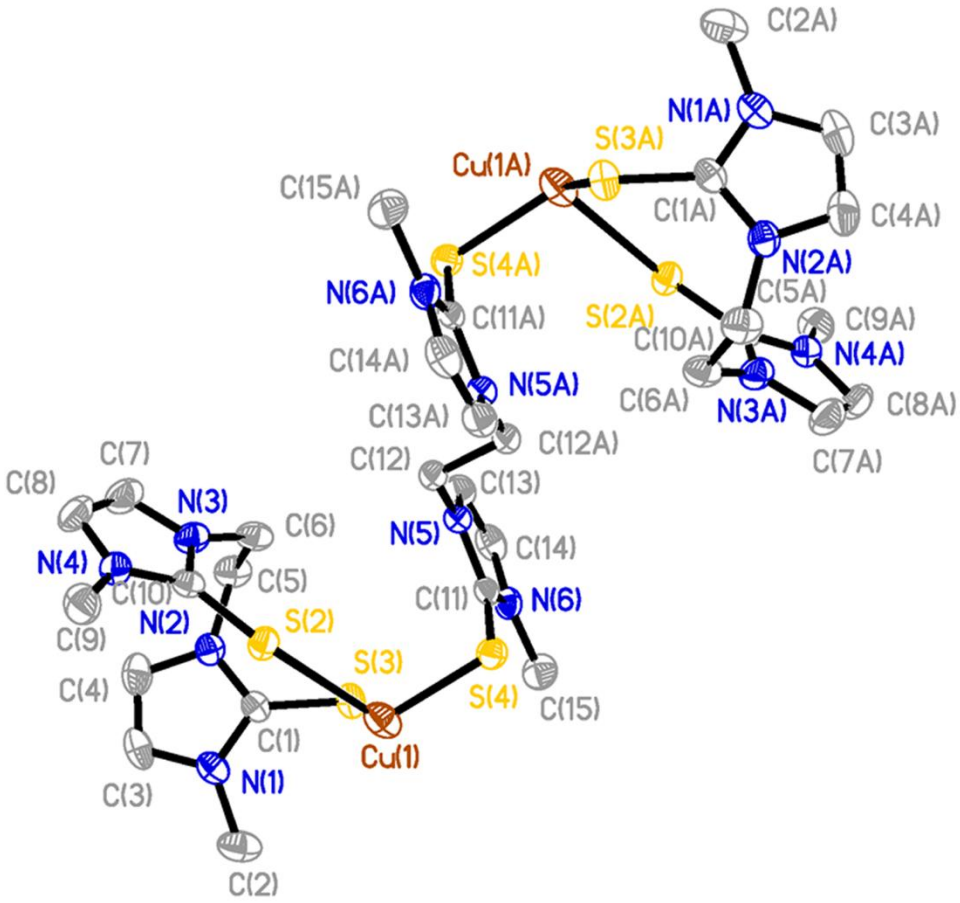

Figure 6.4. Crystal structure diagram of $[Cu_2(ebit)_3][2BF_4]$ (**6**) displaying 50% probability density ellipsoids. Hydrogen atoms are omitted for clarity.

Table 6.3. Selected bond lengths (Å) and angles (°) for $[Cu_2(ebit)_3][2BF_4]$ (**6**).

Cu(1) - S(4)	2.2871(16)
Cu(1) - S(3)	2.3030(16)
Cu(1) - S(2)	2.2900(14)
S(4) - Cu(1) - S(2)	122.49(5)
S(4) - Cu(1) - S(3)	114.70(6)
S(3) - Cu(1) - S(2)	117.72(5)

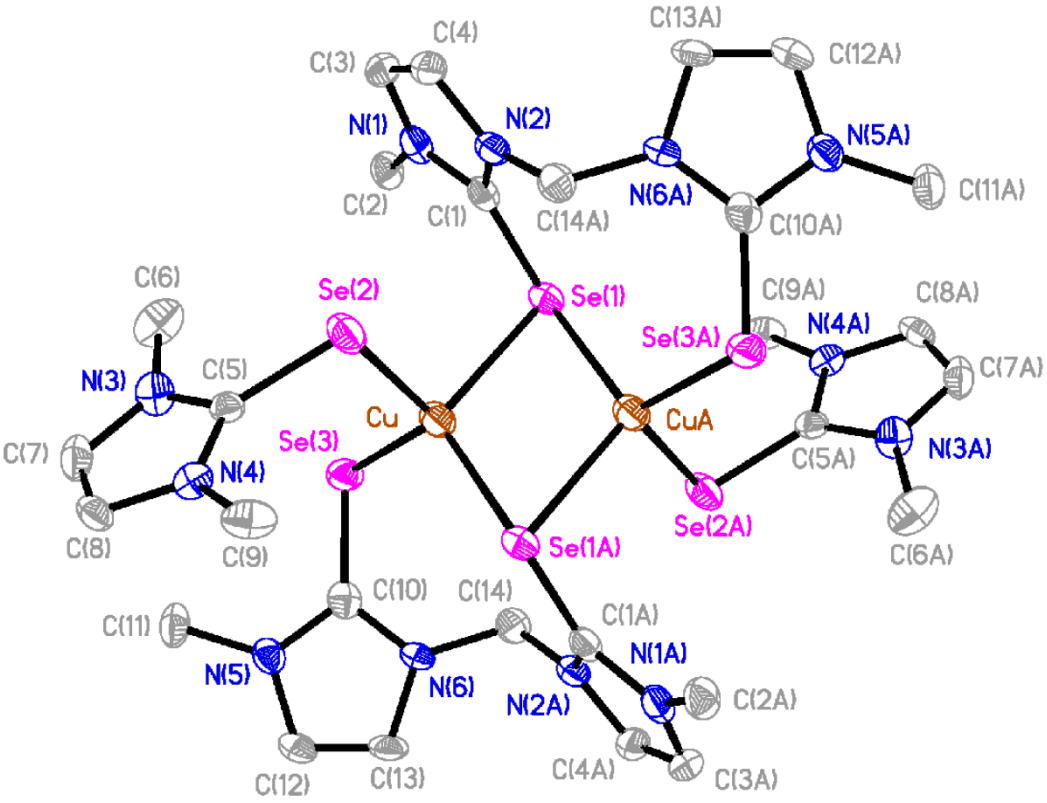

Figure 6.5. Crystal structure diagram of $[Cu_2(\mu\text{-mbis})_2(dmise)_2][2BF_4]$ (**7**) showing 50% probability ellipsoids. Hydrogen atoms and counterions are omitted for clarity.

Table 6.4. Selected bond distances (Å) and angles (°) for**7**.

Cu-Se(1)	2.5349(12)	Se(1)-Cu-Se(2)	105.02(5)
Cu-Se(A1)	2.4950(13)	Se(1)-Cu-Se(3)	107.35(5)
Cu-Se(2)	2.4583(13)	Se(1)-Cu-Se(A1)	114.02(5)
Cu-Se(3)	2.4238(14)	Se(2)-Cu-Se(3)	115.95(5)
Cu(A)-Se(1)	2.4950(13)	Se(2)-Cu-Se(A1)	94.97(5)
Cu-Cu(A)	2.739(2)	Se(3)-Cu-Se(A1)	118.58(4)

one from an mbis ligand, and the other from a dmise ligand, hence each Cu^+ center adopts a distorted tetrahedral geometry with angles ranging from 105.02 to 115.95°.The

Cu-Cu distance, 2.74 Å, is slightly shorter than the sum of their van der Waals radii, suggesting weak Cu-Cu interactions. The average length of the bridging Cu-Se bonds (2.52 Å) is longer than the average non-bridging Cu-Se bond length (2.44 Å).

The X-ray crystal structure diagram of $[Cu_2(\mu\text{-mbis})_2(dmit)_2][2BF_4]$ (**8**) is shown in Figure 6.6, and the selected bond length and angles are given in Table 6.5. The dimer in the structural unit of **8** with a Cu_2Se_2 core is similar to that found in **7**. The copper ions in complex **8** are bound to two bridging and two terminal Se atoms from bis(seleno-methylimidazole) methane (mbis) and two additional sulfur atoms from dmit ligand. Each Cu^+ ion adopts a distorted tetrahedral geometry with angles ranging from 95.38 to

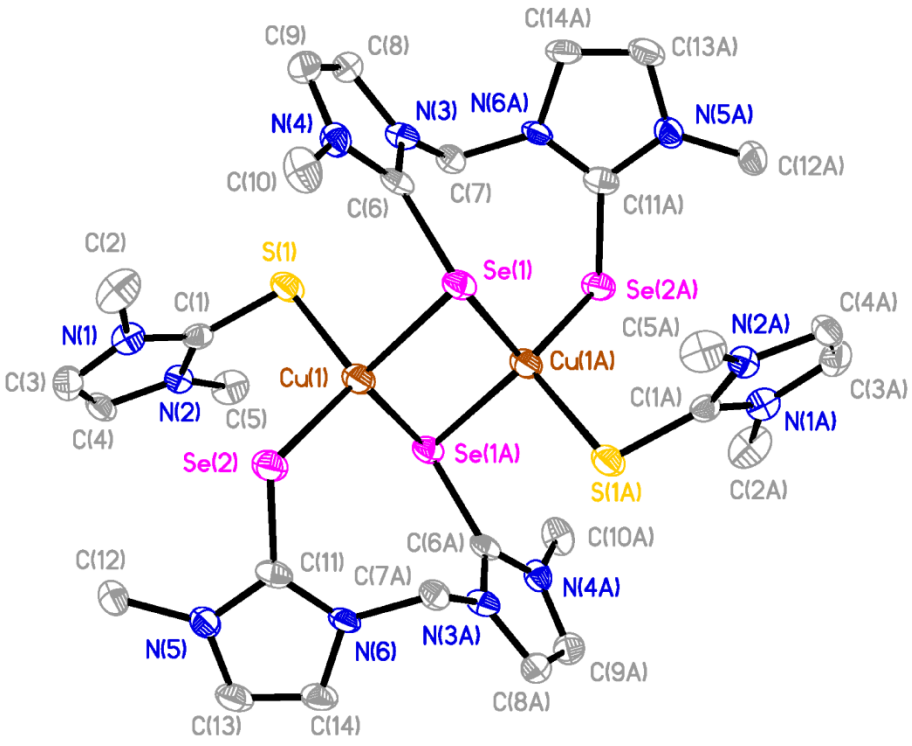

Figure 6.6. Crystal structure diagram of $[Cu_2(\mu\text{-mbis})_2(dmit)_2][2BF_4]$ (**8**) showing 50% probability ellipsoids. Hydrogen atoms and counterions are omitted for clarity.

Table 6.5. Selected bond distances (Å) and angles (°) for **8**.

Cu(1)-S(1)	2.3455(16)	S(1)-Cu(1)-Se(2)	116.36(6)
Cu(1)-Se(2)	2.4222(12)	S(1)-Cu(1)-Se(1A)	95.38(5)
Cu(1)-Se(1A)	2.5013(11)	Se(2)-Cu(1)-Se(1A)	118.61(4)
Cu(1)-Se(1)	2.5328(11)	S(1)-Cu(1)-Se(1)	105.58(5)
Se(1)-Cu(1A)	2.5013(11)	Se(2)-Cu(1)-Se(1)	105.96(4)
Cu(1)-Cu(1A)	2.7297(19)	Se(1A)-Cu(1)-Se(1)	114.33(4)

118.61°. The Cu-Cu distance, 2.73 Å is slightly shorter than the sum of their van der Waals radii, suggesting weak Cu-Cu interaction. The average Cu-Se bond distance is 2.45 Å, whereas the Cu-S bond length is 2.35 Å. The average bond length of bridging Cu-Se bond (2.52 Å) is longer than the average non bridging Cu-Se bond length (2.42 Å).

The X-ray crystal structure of $[Cu(mbit)(\mu\text{-}dmit)]_n[BF_4]_n$ reveals an infinite chain of tetrahedrally coordinated Cu^+ centers bound to two sulfur atoms from a bidentate mbit ligand and to bridging sulfur atom from dmit ligand (Figure 6.7). The geometry around Cu(1) is best described as distorted tetrahedral geometry with S-Cu-S angles ranging from 95.06° to 123.18°, and avg. Cu-S bond lengths of 2.36 Å (Figure 6.8, Table 6.6).

The tetrahedrally coordinated dinuclear copper selone complexes **3**, **7**, and **8** have average Cu-Se bond lengths of 2.48 Å, longer than the average Cu-Se bond distance of 2.30 Å for $[Tpm^RCu(dmise)][BF_4]$ (R = H, Me, and *i*Pr), 2.33 Å Tp*Cu(dmise),[20] $Cu(C_{11}H_{14}Se_2)_2][BF_4]$ (avg. 2.41 Å),[23] but slightly shorter than the Cu-Se bond distance of 2.49 Å found in $[Cu(1,10\text{-}phen)_2(C_5H_{10}N_2Se)][2ClO_4]$.[24] The Se-C bonds in **1**, in the

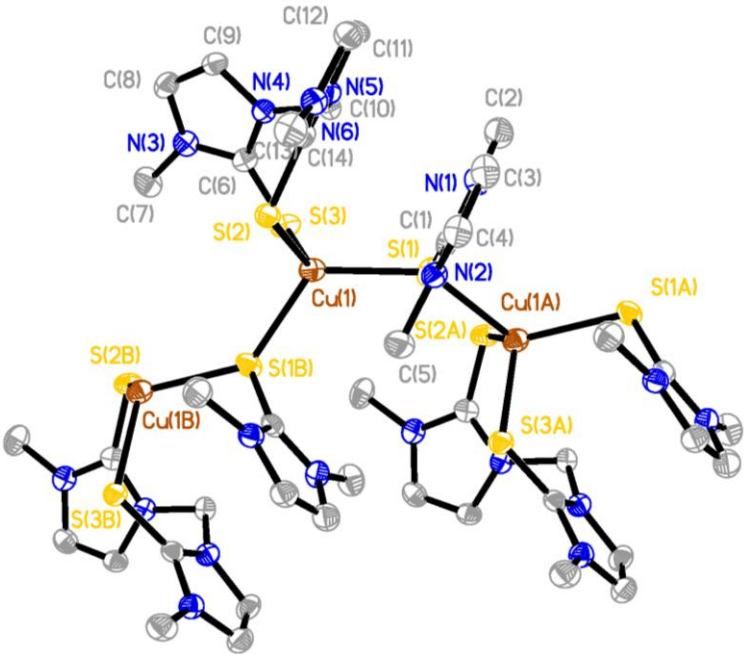

Figure 6.7. Crystal structure diagram of $[Cu(mbit)(\mu\text{-dmit})]_n[BF_4]_n$ (**10**) showing the extended chain network. Hydrogen atoms and counterions are omitted for clarity.

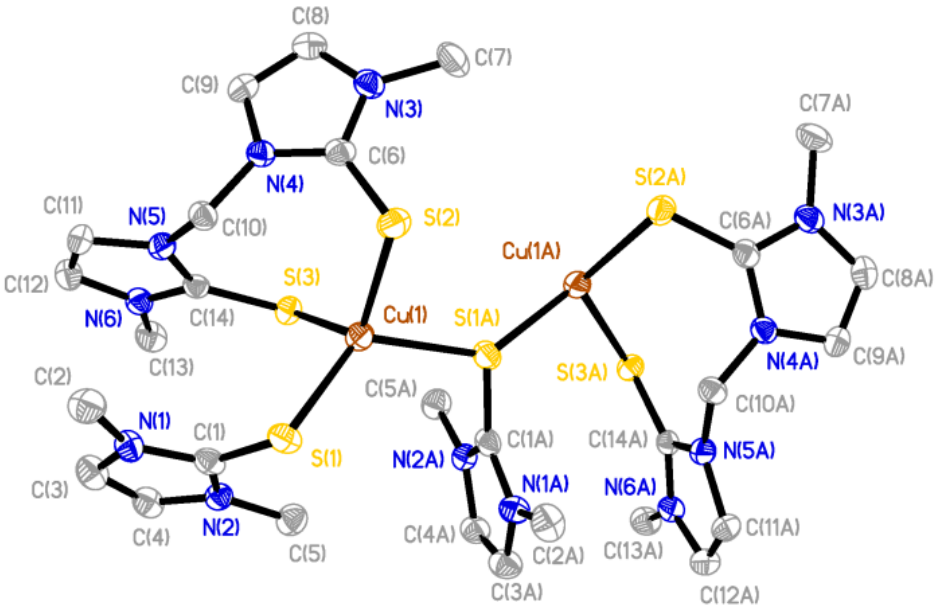

Figure 6.8. Crystal structure diagram of $[Cu(mbit)(\mu\text{-dmit})]_n[BF_4]_n$ (**10**). Hydrogen atoms and counterions omitted for clarity.

Table 6.6. Selected bond distances (Å) and angles (°) for **10**.

Cu(1)-S(1)	2.3689(10)	S(1)-Cu(1)-S(2)	110.51(5)
Cu(1)-S(2)	2.3748(10)	S(1A)-Cu(1)-S(2)	95.06(4)
Cu(1)-S(3)	2.3347(10)	S(1A)-Cu(1)-S(1)	123.18(2)
Cu(1)-S(1A)	2.3520(10)	S(3)-Cu(1)-S(1)	105.05(4)
Cu(1A)-S(1)	2.3520(10)	S(3)-Cu(1)-S(1A)	105.05(4)
S(1)-C(1)	1.718(3)	S(3)-Cu(1)-S(2)	117.58(3)
S(2)-C(6)	1.698(3)	C(1)-S(1)-Cu(1)	104.53(11)
S(3)-C(14)	1.694(3)	C(6)-S(2)-Cu(1)	99.25(11)

range of 1.85-1.88 Å, are slightly lengthened relative to those in uncoordinated dmise (1.89 Å).[25]

The copper thione complexes **6**, **8**, and **10** have average Cu-S bond distances of 2.33 Å, longer than most previously reported copper thione and thiolate complexes such as $[Tpm^{R}Cu(dmit)][BF_4]$ (2.20 Å, R = H, Me), Tp*Cu(dmit),[20] $[Cu(diditme)_2Cl]$ (2.23 Å),[26] $Cu_3(Bm^{Me})_3$ (avg. 2.28 Å), $Cu(Bm^{Me})(PPh_3)$ (2.28 Å),[27] but shorter than $[Cu(PPh_3)_2(bzimH_2)Cl]$ (2.38 Å),[28] $[CuCl(1\kappa S\text{-}imzSH)(PPh_3)_2]$ (2.36 Å),[29]and $[Cu(HB(3,5\text{-}iPrPz)_3(SMeIm)]$ (2.45 Å).[30] The S-C bond lengths in complexes **6**, **8**, and **10** (1.694-1.704 Å), are slightly lengthened relative to those in uncoordinated dmit (1.68 Å),[31]and 1-methyl-4-imidazoline-2-thione (1.68 Å).[32]

NMR spectroscopy of dinuclear copper thione and selone complexes. The dinuclear copper complexes were characterized by ^{1}H, $^{13}C\{^{1}H\}$, $^{77}Se\{^{1}H\}$, and $^{19}F\{^{1}H\}$ NMR spectroscopy. In the ^{1}H NMR spectra of dmise, dmit, mbis, mbit, ebis, and ebit the olefinic CH protons on the heterocyclic ring are shifted downfield by δ 0.2 to 0.5 from its position in the free ligand upon coordination to copper. This same downfield shift was

observed by Rabinovich, *et al.*,[11] for $[Pb_2(Bmm^{Me})_5](ClO_4)_4$, Gardinier, *et al.*, for $[Ag(mbit)_2]^+$,[14] and Kimani *et al.*, for $[Tpm^RCu(X)]^+$ (R = H; Tpm, R = Me; Tpm*, R = *i*Pr; Tpm^{iPr}; X = dmise, or dmit) complexes.[20] $^{13}C\{^1H\}$ NMR resonances for the complexed and uncomplexed selone and thione ligands are given in Table 6.7. Substantial shifting of the C=Se/S resonances of the dmise, dmit, mbis, and mbit carbon atoms are observed upon complexation to copper. Coordination of the selones and thiones via the selenium and sulfur atoms results in upfield shifts of δ 5 to 8 for both the C=Se and C=S carbons. The upfield shift in C=Se/S resonance results in decreased double bond character of the seleno- and thio-carbonyl bond while enhancing that of the adjacent C-N single bond.[27,33]

Table 6.7. $^{13}C\{^1H\}$ and $^{77}Se\{^1H\}$ NMR chemical shifts of the selone and thione ligands before and after complexation with copper.

	C=Se	C=S (dmit)	^{77}Se
Dmise	155.57^t		-6
Dmit		162.42^t	
Mbis	157.03^b		16.02
Mbit		163.71^b	
Ebis	155.63^b		22.65
Ebit		162.29^b	
$[Cu_2(\mu\text{-dmise})(dmise)_4][2BF_4]$ (**1**)	147.19^t		
$[Cu(dmit)][BF_4]$ (**2**)		157.34^t	
$[Cu_2(mbis)_3][BF_4]_2$ (**3**)	149.67^b		-28.01
$[Cu_2(mbit)_3][BF_4]_2$ (**4**)		158.04^b	
$[Cu_2(ebis)_3][BF_4]_2$ (**5**)	147.98^b		-42.91
$[Cu_2(ebit)_3][BF_4]_2$ (**6**)		155.22^b	
$[Cu_2(\mu\text{-mbis})_2(dmise)_2][2BF_4]$ (**7**)	148.99^t, 151.27^b		-26.01
$[Cu_2(\mu\text{-mbis})_2(dmit)_2][2BF_4]$ (**8**)	151.63^b	157.65^t	-24.20
$[Cu_2(mbit)_2(dmise)_2][2BF_4]$ (**9**)	149.25^t	158.75^b	
$[Cu(\mu\text{-dmit})(mbit)]_n[BF_4]_n$ (**10**)		156.61^t, 158.40^b	

^{t} = terminal, ^{b} = bridging

$^{77}Se\{^{1}H\}$ NMR spectroscopy studies revealed upfield shifts of selenium resonance in the copper complexes relative to those of the free mbis and ebis ligands. The $^{77}Se\{^{1}H\}$ NMR signal for complex **1** could not be obtained, whereas all the complexes with mbis and ebis ligands exhibited upfield selenium resonance shifts ~δ 40 upon coordination to copper. This upfield shift of $^{77}Se\{^{1}H\}$ NMR resonance upon copper binding is direct evidence that mbis and ebis ligands bind to copper in a bidentate fashion via the selenium atoms.

Electrochemical studies of the dinuclear copper complexes. Cyclic voltammetry studies of the chalcogenones and their dinuclear copper complexes were conducted to determine the influence of the alkyl linker on the redox potential of the chalcogenone ligands and the change in $Cu^{2+/+}$ reduction potential upon coordination of the chalcogenone ligands to copper. All the uncoordinated chalcogenone ligands exhibit chemically reversible and quasi-reversible electrochemical behavior, with the selone ligands having more negative reduction potentials relative to the analogous thione ligands. The unbound bidentate ethylene-bridged ligands (ebis and ebit) have larger peak separation between the oxidized and reduced products relative to the methylene- bridged ligands (mbis and mbit), suggesting faster electron transfer in the latter.[34] The reduction potentials of the unbound selone ligands are: dmise -367 mV < ebis (-342 mV) < mbis (-333 mV). The analogous thione ligands follow the same trend: dmit (-169 mV) < ebit (-148 mV) < mbit (-118 mV), versus normal hydrogen electrode (NHE; Table 6.10). The reduction potentials of the uncoordinated bidentate chalcogenones indicate that

increasing the length of the alkyl linker from methylene to ethylene results in more negative reduction potentials.

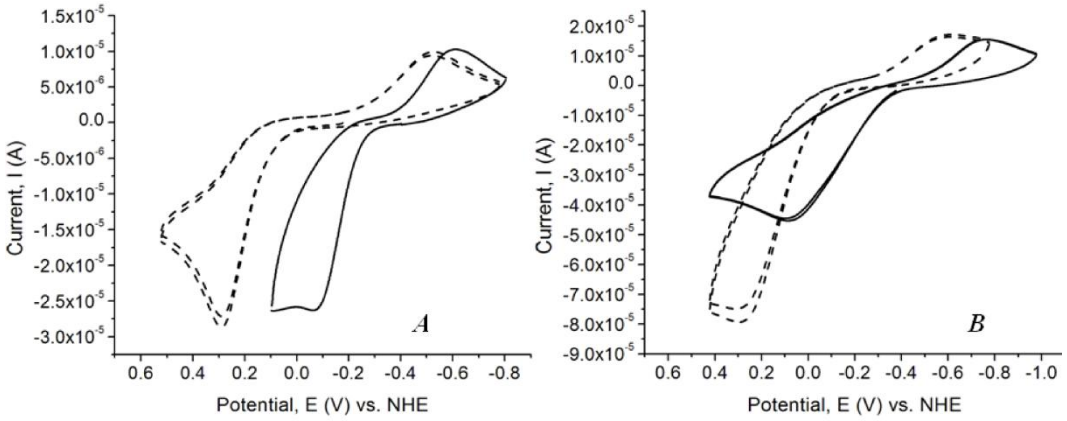

Figure 6.9. Cyclic voltammetry (CV) scan for A) mbit (dashed lines) and mbis (solid lines), B) ebit (dashed lines) and ebis (solid lines). All data were collected with 1mM complex in acetonitrile.

The $Cu^{+/2+}$ redox potentials of the complexes versus NHE are given in Table 6.10. The cyclic voltagrams (CV) of the copper complexes **1**, **2**, **3**, **4**, **5**, **6**, **7**, and **10** exhibit two, one-electron redox potential waves belonging to the $Cu^{+/2+}$ and $Cu^{+/0}$ couples, with exception of complexes **8** and **9** which exhibit three, one-electron redox potential waves. The $Cu^{+/0}$ redox couple commences at potentials more than -1000 mV vs. NHE and after switching the scan direction at potentials close to 750 mV, Cu^0 is stripped off the electrode (Figure 6.10). All the dinuclear copper selone and thione complexes exhibit chemically reversible, $Cu^{+/2+}$ one-electron oxidation and reduction, but the peak separation between the anodic and cathodic waves is much higher relative to the

ferrocene/ferrocenium couple at the same conditions, suggesting an electrochemically quasi-reversible process (Figures 6.10-6.12).

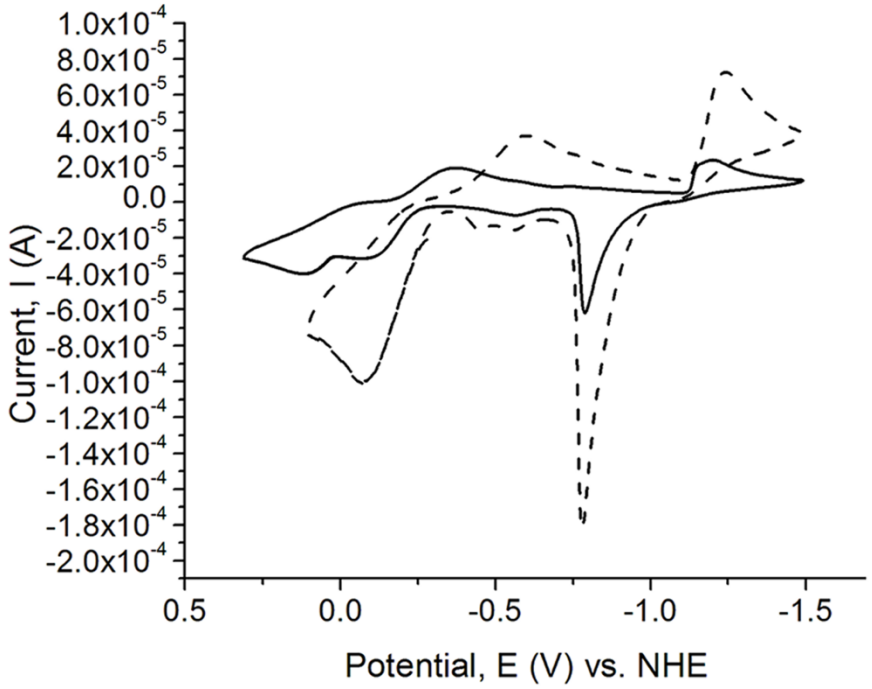

Figure 6.10. Cyclic voltammetry (CV) scans for $[Cu_2(\mu\text{-mbis})_2(dmise)_2][2BF_4]$ (**7**), (dashed lines) and $[Cu_2(\mu\text{-mbis})_2(dmit)_2][2BF_4]$ (**8**) (solid line) in acetonitrile.

Upon examination of the reduction potentials for the copper complexes **1**, **2**, **3**, **4**, **5**, and **6**, it is clear that the selone containing complexes exhibit more negative reduction potentials relative to the analogous thione complexes, a similar trend observed by Kimani, *et al.*, for the electrochemistry of $[Tpm^RCu(X)]^+$ complexes (X = dmise or dmit).[20] Interestingly, increasing the length of the alkyl bridge in the bidentate ligands from methylene to ethylene results in lower reduction potentials for $[Cu_2(ebis)_3][2BF_4]$ (**5**) (-369 mV) compared to $[Cu_2(\mu\text{-mbis})(mbis)_2][2BF_4]$ (**3**) (-306 mV), and the same trend is observed for the thione complex $[Cu_2(ebit)_3][2BF_4]$ (**6**) (-203 mV) relative to

Table 6.8. Redox potentials and $Cu^{+/2+}$ potentials of dinuclear copper complexes vs. NHE.

	E_{pa}	E_{pc}	ΔE	$E_{1/2}$
Dmise	39	-773	812	-367
Dmit	424	-761	1158	-167
Mbis	-53	-613	560	-333
Mbit	289	-525	814	-118
Ebis	83	-768	851	-342
Ebit	292	-587	879	-148
$[Cu_2(\mu\text{-dmise})(dmise)_4][2BF_4]$ (**1**)	-101	-603	502	-352
$[Cu_2(dmit)_5][2BF_4]$ (**2**)	147	-565	712	-210
$[Cu_2(\mu\text{-mbis})(mbis)_2][2BF_4]$ (**3**)	-37	-575	538	-306
$[Cu_2(mbit)_3][2BF_4]$ (**4**)	120	-500	620	-180
$[Cu_2(ebis)_3][2BF_4]$ (**5**)	-131	-606	475	-369
$[Cu_2(ebit)_3][2BF_4]$ (**6**)	228	-634	862	-203
$[Cu_2(\mu\text{-mbis})_2(dmise)_2][2BF_4]$ (**7**)	-68	-645	577	-356
$[Cu_2(\mu\text{-mbis})_2(dmit)_2][2BF_4]$ (**8**)	192, -6	-44, -478	225, 439	74, -242
$[Cu_2(mbit)_2(dmise)_2][2BF_4]$ (**9**)	174, -23	31, -608	149, 585	102, -315
$[Cu(\mu\text{-dmit})(mbit)]_n[BF_4]_n$ (**10**)	147	-535	682	-195

Table 6.9. $Cu^{+/0}$ reuction potentials of dinuclear copper complexes vs. NHE.

	E_{pa}	E_{pc}	ΔE	$E_{1/2}$
$[Cu_2(\mu\text{-dmise})(dmise)_4][2BF_4]$ (**1**)	-724	-1107	383	-920
$[Cu_2(dmit)_5][2BF_4]$ (**2**)	-747	-1129	382	-938
$[Cu_2(\mu\text{-mbis})(mbis)_2][2BF_4]$ (**3**)	-796	-1336	540	-1066
$[Cu_2(mbit)_3][2BF_4]$ (**4**)	-742	-1298	556	-1020
$[Cu_2(ebis)_3][2BF_4]$ (**5**)	-936	-1152	216	-1044
$[Cu_2(ebit)_3][2BF_4]$ (**6**)	-816	-1299	483	-1058
$[Cu_2(\mu\text{-mbis})_2(dmise)_2][2BF_4]$ (**7**)	-774	-1231	457	-1003
$[Cu_2(\mu\text{-mbis})_2(dmit)_2][2BF_4]$ (**8**)	-710	-1119	409	-915
$[Cu_2(mbit)_2(dmise)_2][2BF_4]$ (**9**)	-671	-1107	436	-889
$[Cu(\mu\text{-dmit})(mbit)]_n[BF_4]_n$ (**10**)	-791	-1222	431	-1007

$[Cu_2(mbit)_3][2BF_4]$ (**4**) (-180 mV). The dinuclear copper complex **7** with both mbis and dmise ligands has a lower reduction potential of (-356 mV) relative to complex **10** which has both mbit and dmit ligands (-195 mV) (Table 6.8).

The heterogeneous dinuclear complex $[Cu_2(\mu\text{-mbis})_2(dmit)_2][2BF_4]$ (**8**; Figure 6.12I) exhibits two different reduction and oxidation potentials for the $Cu^{2+/+}$ couple, whereas $[Cu_2(\mu\text{-mbit})_2(dmise)_2][2BF_4]$ (**9**; Figure 6.12H) exhibits three oxidation and reduction waves. One reduction and oxidation wave in the dinuclear copper complex **9** likely corresponds to the reduction potential of the bidentate mbit ligand ($E_{1/2}$ = -51 mV), whereas the remaining two waves correspond to $Cu^{2+/+}$ reduction potentials, similar to those observed for complex **8**. These two different $Cu^{2+/+}$ reduction potentials are only observed for the dinuclear copper complexes with mixed sulfur and selenium ligands (Table 6.8).

The unbound dmise and dmit have more negative reduction potentials than the bidentate chalcogenones (mbis, mbit, ebis and ebit). The reduction potentials from the bidentate chalcogenones indicate that increasing the length of the alkyl linker from methylene to ethylene results in more negative reduction potentials. All the synthesized copper-selone complexes have more negative $Cu^{2+/+}$ reduction potentials relative to the analogous copper-thione complexes. The copper-selone complexes stabilize the Cu^{2+} oxidation state more effectively than the copper-thione complexes by an average of 144 mV, consistent with previously observed results.[20,21] The $Cu^{2+/+}$ reduction potential of the dinuclear copper chalcogenone complexes **1** to **10** can be tuned from a range of 102 mV

to -369 mV by simply changing the chalcogenone and denticity of selone and thione ligands. Compared to naturally occurring cupredoxins with $Cu^{2+/+}$ reduction potential range of 90 mV to 670 mV,[35] the synthesized copper chalcogenone complexes have more negative $Cu^{2+/+}$ reduction potentials.

Conclusions

Dinuclear homoleptic and heteroleptic Cu^{+} complexes with monodentate and bidentate chalcogenone ligands have been synthesized and characterized, and the electrochemistry of the resulting Cu^{+} complexes has been investigated and compared. Treating the Cu^{+} starting material $[Cu(NCCH_3)_4][BF_4]$ with bidentate (mbit, mbis, ebit, and ebis) and monodentate chalcogenone ligands (dmise and dmit) results in the formation of dinuclear copper complexes (**1**, **2**, **3**, **4**, **5**, and **6**). The dinuclear copper complexes adopt either trigonal or tetrahedral coordinate geometries with both terminal and bridging selone or thione ligands. The heterogeneous dinuclear copper complexes $[Cu_2(\mu\text{-mbis})_2(dmise)_2][2BF_4]$ (**7**) and $[Cu_2(\mu\text{-mbis})_2(dmit)_2][2BF_4]$ (**8**) adopt distorted tetrahedral geometry where each copper is coordinated to three selenium atoms from mbis ligand and one selenium atom from dmise for **7** and one sulfur atom from dmit for **8**. Interestingly, the mixed ligand complex **10** consist of infinite chains of tetrahedrally coordinated Cu^{+} ions bound to two sulfur atoms from a mbit ligand and a bridging sulfur atom from a dmit ligand.

The copper selone complexes **1**, **3**, **5**, and **7** have more negative $Cu^{2+/+}$ reduction potentials relative to their sulfur analogs (**2**, **4**, **6**, and **10**), and increasing the length of the

alkyl linker in the bidentate chalcogenone ligands results in more negative reduction potentials for their copper complexes. This study provides detailed comparative coordination chemistry of selones and thiones with copper and its effect on the $Cu^{2+/+}$ reduction potentials. Simply changing the chalcogens and denticity of the selone and thione ligands results in $Cu^{2+/+}$ reduction potentials of the synthesized copper chalcogenone complexes that can be tuned in a range of 471mV, a difference that would have significant effects in redox-mediated reactions.

Experimental Section

Materials. The synthesis and manipulation of all copper complexes was performed under an inert atmosphere of argon or nitrogen using standard Schlenk techniques. Acetonitrile, methanol, and ether were purified using standard procedures and freshly distilled under argon atmosphere prior to use. *N,N'*-Dimethylimidazole-selone (dmise), *N,N'*-dimethylimidazole thione (dmit),[36] $[Cu(NCCH_3)_4][BF_4]$,[37] bis (selono-imidazolyl)methane (mbis), bis (thio-imidazolyl)methane (mbit), bis(selono-imidazolyl)ethane (ebis), bis(thio-imidazolyl)ethane (ebit)[1] were synthesized according to published procedures. The following reagents were used as received: selenium powder (VWR), sulfur powder (VWR), cuprous oxide (stabilized, Aldrich), 1-methylimidazole (VWR), methyliodide (VWR), and dibromomethane (Alfa Aesar).

Instrumentation. ^{1}H, $^{13}C\{^{1}H\}$,$^{77}Se\{^{1}H\}$ and $^{19}F\{^{1}H\}$ spectra were obtained on Bruker-AVANCE 300 and 500 MHz NMR spectrometers. ^{1}H and $^{13}C\{^{1}H\}$ NMR

chemical shifts are reported in δ relative to tetramethylsilane (TMS) and referenced to solvent. $^{19}F\{^{1}H\}$ NMR spectra were externally referenced to CCl_3F (δ 0).[38] The $^{77}Se\{^{1}H\}$ NMR chemical shifts were obtained in $CDCl_3$ and externally referenced to diphenyl diselenide (δ 461),[39] and reported relative to dimethyl selenide (δ 0).

Electrochemical experiments were performed with a BAS 100B potentiostat. A three compartment cell was used with an Ag/AgCl reference electrode, Pt counter electrode, and a glassy carbon working electrode. Freshly-distilled acetonitrile was used as the solvent with tetra-*n*-butylammonium phosphate as the supporting electrolyte (0.1 M). Solutions containing 1 mM analyte were deaerated for 2 min by vigorous nitrogen purge. The measured potentials were corrected for junction potentials relative to ferrocenium/ferrocene (0.586 mV vs. Ag/AgCl).[40] All $E_{1/2}$ values were calculated from $(E_{pa} + E_{pc})/2$ at a scan rate of 100 mV/s, and $\Delta E = E_{pa} - E_{pc}$.

Infrared spectra were obtained using Nujol mulls on KBr salt plates with a Magna 550 IR spectrometer. Abbreviations used in the description of vibrational data are as follows: vs, very strong; s, strong; m, medium; w, weak; b, broad. Electrospray ionization mass spectrometry (ESI-MS) was conducted using a QSTAR XL Hybrid MS/MS System from Applied Biosystems via direct injection of sample (0.05 mL/min flow rate) into a Turbo Ionspray ionization source. Samples were run under positive mode, with ionspray voltage of 5500 V, and TOF scan mode. MALDI-TOF-MS was conducted on a Bruker Microflex. Trans-2-[3-(4-tert-butylphenyl)-2-methyl-2-propenylidene]-malononitrile was used as a matrix for co-crystallization of the copper complex characterized. All the peak

envelopes matched their calculated isotopic distributions. Melting points were determined using a Barnstead Electrothermal 9100 apparatus in silicon-grease-sealed glass capillary tubes. Absorption spectra were collected using a Varian Cary-50 Bio spectrophotometer in quartz cuvettes with a path length of 1 cm.

*$[Cu_2(\mu\text{-dmise})(dmise)_4][2BF_4]$ (**1**).* Dmise (437 mg, 2.5 mmol) was dissolved in acetonitrile (30 mL) and cannula transferred to a solution of $[Cu(NCCH_3)_4][BF_4]$ (312 mg, 1 mmol) in acetonitrile (20 mL). The reaction was stirred at room temperature for 3 h, and the solvent volume was reduced *in vacuo* to about 5 mL. The product was precipitated with diethyl ether (10 mL) to afford an off-white solid that was dried *in vacuo*. Single crystals for X-ray analysis were grown from slow vapor diffusion of diethyl ether into acetonitrile solution. Yield: 85% (496 mg, 0.425 mmol). Mp. 126°C. ^{1}H NMR (CD_3CN): 3.69 (s, 6H, $2CH_3$), 7.16 (s, 2H, 2CH). $^{13}C\{^1H\}$ NMR (CD_3CN): 37.06 (CH_3), 121.58 (CH), 147.19 (C=Se). $^{19}F\{^1H\}$ NMR (CD_3CN): -151.56, -151.61. IR (cm^{-1}): 521 s, 624 w, 660 s, 744 s, 933 s, 1021 b, 1238 s, 1285 s, 1378 s, 1457 s, 1570 s, 1818 w, 2252 w, 2276 vs, 2304 vs, 2918 b, 3139 w, 3172 w, 3230 w. MALDI-TOF-MS: 415.07 $[Cu(dmise)_2]^+$. Anal. Calc. for $C_{25}H_{40}Cu_2N_{10}Se_5B_2F_8$: C, 25.53; N, 11.91; H, 3.43. Found: C, 25.42; N, 11.73; H, 3.45.

*$[Cu_2(dmit)_5][2BF_4]$ (**2**).* Complex **2** was prepared following the same procedure for **1** except that dmit (322 mg, 2.5 mmol) was used instead of dmise. Yield: 74% (350 mg, 0.371 mmol). Mp. 132°C. ^{1}H NMR (CD_3CN): 3.63 (s, 6H, $2CH_3$), 6.99 (s, 2H, 2CH). $^{13}C\{^1H\}$ NMR (CD_3CN): 35.13 (CH_3), 120.35 (CH), 157 (C=S). IR (cm^{-1}): 521 s, 672 vs,

724 vs, 746 vs, 801 s, 1047 b, 1175 vs, 1236 vs, 1284 v, 1378 s, 1464 vs, 1569 vs, 1684 w, 2276 s, 2304 s, 2723 w, 2859 b, 3118 w, 3142 w. MALDI-TOF-MS: 319.51 $[Cu(dmit)_2]^+$. Anal. Calc. for $C_{25}H_{40}Cu_2N_{10}S_5B_2F_8$: C, 31.89; N, 14.87; H, 4.28. Found: C, 31.80; N, 14.56; H, 4.23.

*$[Cu_2(mbis)_3][BF_4]_2$ (**3**).* Mbis (215 mg, 0.75mmol) was dissolved in dichloromethane (20 mL) before being cannula transferred to a solution of $[Cu(CNCH_3)_4][BF_4]$ (160 mg, 0.5 mmol) in acetonitrile (10mL). The reaction mixture was stirred at room temperature for 3 h. The solvent volume in the reaction mixture was then reduced to about 5 mL and the product was precipitated with diethyl ether. Single crystals for X-ray analysis were grown from slow vapor diffusion of ether into acetonitrile solution. Yield: 45% (262 mg, 0.225 mmol). ^{1}H NMR (DMSO): 3.54 (s, 6H, $2CH_3$), 6.82 (s, 2H, CH_2), 7.59 (d, J_{HH} 2.0, 2H, 2CH), 7.33 (d, J_{HH} 2.0, 2H, $2CH_3$). $^{13}C\{^1H\}$ NMR (DMSO): 37.46 (CH_3), 59.67 (CH_2), 121.33 (CH), 123.43 (CH), 149.67 (C=Se). $^{19}F\{^1H\}$ NMR (DMSO): -151.59, -151.63. ^{77}Se NMR (DMSO): -28.008. UV-vis (CH_3CN): 291.6 nm. Mp. 139°C; 460 s, 473 w, 521 vs, 604 w, 655 s, 697 s, 731 vs, 779 w, 790 s, 1059 b, 1207 s, 1234 s, 1249 s, 1318 s, 1378 s, 1464 vs, 1575 vs, 1676 vs, 2727 b, 3145 w. Mass spectrum (ESI-MS): *m/z* 1216.59 $[Cu_2(mbis)_3(BF_4)]^+$, 882.68 $[Cu_2(mbis)_2(BF_4)]^+$, 796.67 $[Cu_2(mbis)_2]^{2+}$, 398.83 $[Cu(mbis)]^+$. Anal. Calc. for $C_{29}H_{39}Cu_2N_{13}Se_6B_2F_8$: C, 25.91; N, 13.55; H, 2.92. Found: C, 25.98; N, 13.12; H, 3.04.

*$[Cu_2(mbit)_3][BF_4]_2$ (**4**).* Complex **4** was prepared following the same procedure for **3** except that mbit (186 mg, 0.75 mmol) was used instead of mbis. The growth of

single crystals for X-ray analysis was attempted from slow vapor diffusion of diethyl ether into acetonitrile solution. Yield: 56% (297 mg, 0.283 mmol). ^{1}H NMR (CD_3CN): 3.54 (s, 6H, $2CH_3$), 6.51 (s, 2H, CH_2), 7.08 (d, J_{HH} 2.5, 2H, 2CH), 7.29 (d, J_{HH} 2.5, 2H, $2CH_3$). $^{13}C\{^{1}H\}$ NMR (CD_3CN): 35.97 (CH_3), 57.55 (CH_2), 119.04 (CH), 121.61 (CH), 158.04 (C=S). $^{19}F\{^{1}H\}$ NMR: -151.57, -151.63, (s, $^{10}BF_4$, $^{11}BF_4$). UV-vis (CH_3CN): 274.4 nm. Mp. 128°C; IR (cm^{-1}): 521 s, 604 w, 663 s, 703 s, 734 s, 759 s, 784 s, 1046 b, 1168 s, 1215 s, 1238 s, 1286 s, 1319 s, 1378 s, 1398 s, 1467 s, 1576 s, 1700 w, 2272 w, 2304 w, 2727 w, 2855 b, 3141 w. Anal. Calc. for $C_{27}H_{36}Cu_2N_{12}S_6B_2F_8$: C, 31.74; N, 16.45; H, 3.55. Found: C, 30.07; N, 16.25; H, 3.61.

*$[Cu_2(ebis)_3][BF_4]_2$ (**5**).* Complex **5** was prepared following the procedure for **3** except that ebis (223 mg, 0.75 mmol) was used in place of mbis. Yield: 30% (174 mg, 0.153 mmol). ^{1}H NMR ($(CD_3)_2SO$): 3.58 (s, 6H, $2CH_3$), 4.73 (s, 4H, $2CH_2$), 7.33 (d, 2H, 2CH), 7.47 (d, 2H, 2CH). $^{13}C\{^{1}H\}$ NMR: 39.70 (CH_3), 47.46 (CH_2), 121.47 (CH), 122.76 (CH), 147.98 (C=Se). $^{19}F\{^{1}H\}$ NMR: -148.10, -148.16 (s, $^{10}BF_4$, $^{11}BF_4$). ^{77}Se NMR: -42.91 (s, Se). UV-vis (CH_3CN): 288.4 nm; Mp. 270°C; IR (cm^{-1}): 522 s, 666 vs, 724 vs, 738 vs, 747 vs, 800 w, 930 w, 1057 vs, 1128 vs, 1183 vs, 1223 s, 1246 vs, 1287 w, 1378 vs, 1409 vs, 1467 vs, 1569 vs, 2854 vs, 2919 b, 3114 w, 3146 w, 3173 w. Anal. Calc. for $C_{30}H_{42}Cu_2N_{12}Se_6B_2F_8$: C, 26.79; N, 12.49; H, 3.15. Found: C, 26.97; N, 12.48; H, 3.12.

*$[Cu_2(ebit)_3][BF_4]_2$ (**6**).* Complex **6** was prepared following the procedure for **3** except ebit (191 mg, 0.75 mmol) was used in place of mbis. Yield: 47% (252 mg, 0.236 mmol). ^{1}H NMR ($(CD_3)_2SO$): 3.52 (s, 6H, $2CH_3$), 4.63 (s, 4H, $2CH_2$), 7.18 (d, 2H, 2CH),

7.30 (d, 2H, 2CH). $^{13}C\{^{1}H\}$ NMR: 35.59 (CH_3), 45.67 (CH_2), 119.70 (imidazole), 120.89 (imidazole), 155.22 (C=S). $^{19}F\{^{1}H\}$ NMR: -148.31, -148.35, (s, $^{10}BF_4$, $^{11}BF_4$). UV-vis (CH_3CN): 272.5 nm; Mp. 230°C; IR (cm^{-1}): 501 w, 522 s, 622 w, 670 s, 680 s, 720 vs, 736 vs, 1059 vs, 1137 w, 1197 s, 1227 s, 1247 vs, 1287 w, 1378 vs, 1415 vs, 1466 vs, 1570 vs, 1694 w, 2927 b, 3137 w. Anal. Calc. for $C_{30}H_{42}Cu_2N_{12}S_6B_2F_8$: C, 33.87; N, 15.50; H, 3.98. Found: C, 29.88; N, 13.68; H, 3.45.

$[Cu_2(\mu\text{-mbis})_2(dmise)_2][2BF_4]$ (7). Dmise (176 mg, 1 mmol) was dissolved in acetonitrile (20 mL) and cannula transferred to a solution of $[Cu(NCCH_3)_4][BF_4]$ (312 mg, 1 mmol) in acetonitrile (10 mL). The reaction was stirred at room temperature for 3 h, resulting in the formation of a yellow solution. To this reaction mixture was cannula added mbis (336 mg, 1 mmol) in dichloromethane (10 mL) and stirred overnight. The solvent volume was reduced *in vacuo* to about 3 mL and the product was precipitated with diethyl ether to afford an off-white solid which was dried *in vacuo*. Single crystals for X-ray analysis were grown from slow vapor diffusion of diethyl ether into acetonitrile solution. Yield: 46% (558 mg, 0.456 mmol). ^{1}H NMR (CD_3CN): 3.62 (s, 6H, $2CH_3$), 3.68 (s, 6H, $2CH_3$), 6.68 (s, 2H, CH_2), 7.14 (s, 2H, 2CH), 7.24 (d, J_{HH} 2.0, 2H, 2CH), 7.40 (d, J_{HH} 2.0, 2H, 2CH). $^{13}C\{^{1}H\}$ NMR: 36.45(CH_3), 37.82 (CH_3), 60.53 (CH_2), 121.05 (CH), 122.04 (CH), 123.67 (CH), 148.99 (C=Se (dmise)), 151.27 (C=Se (mbis)). $^{19}F\{^{1}H\}$ NMR (CD_3CN): -151.56, -151.61. ^{77}Se NMR (CD_3CN): -26.01. UV-vis (CH_3CN): 277.6 nm. Mp. 193°C. IR (cm^{-1}): 521 s, 623 s, 650 s, 658 s, 724 s, 745 s, 791 s, 837 s, 1055 b, 1176 s, 1207 s, 1230 vs, 1248 s, 1287 s, 1320 s, 1378 b, 1464 vs, 1571 vs, 1673 s, 2925 b, 3132 b.; Mass spectrum (ESI-MS): *m/z* 732.76 $[Cu(mbis)_2]^+$, 572.81

[(dmise)Cu(mbis)]$^{+}$, 398.83 [Cu(mbis)]$^{+}$, 239.02 [Cu(dmise)]$^{+}$. Anal. Calc. for $C_{28}H_{40}Cu_2N_{12}Se_6B_2F_8$: C, 25.49; N, 12.74; H, 3.06. Found: C, 24.85; N, 12.48; H, 3.00.

*$[Cu_2(\mu\text{-mbis})_2(dmit)_2][2BF_4]$ (**8**).* Complex **8** was prepared following the same procedure for **7** except that dmit (129 mg, 1 mmol) was used instead of dmise. Single crystals for X-ray analysis were grown from slow vapor diffusion of diethyl ether into acetonitrile solution. Yield: 38% (427 mg, 0.378 mmol). ^{1}H NMR (CD_3CN): 3.60 (s, 6H, $2CH_3$), 3.62 (s, 6H, $2CH_3$), 6.65 (s, 2H, CH_2), 6.98 (s, 2H, 2CH), 7.23 (d, J_{HH} 2.5, 2H, 2CH), 7.38 (d, J_{HH} 2.0, 2H, 2CH). ^{13}C{^{1}H} NMR: 35.84(CH_3), 37.77 (CH_3), 60.51 (CH_2), 120.02 (CH), 121.00 (CH), 123.31 (CH), 151.63 (C=Se (mbis)), 157.65 (C=S (dmit)). ^{19}F{^{1}H} NMR (CD_3CN): -151.52, -151.57. ^{77}Se{^{1}H} NMR (CD_3CN): -24.20. UV-vis (CH_3CN): 273.7 nm. Mp. 209 °C. IR (cm^{-1}): 508 s, 521 s, 611 s, 640 s, 650 s, 657 s, 676 s, 723 vs, 746 vs, 790 vs, 839 s, 867 s, 1033 b, 1145 s, 1177 s, 1207 s, 1229 s, 1249 s, 1290 s, 1321 s, 1372 s, 1395 s, 1465 s, 1571 vs, 1602 s, 1673 s, 2920 b, 3088 s.; Mass spectrum (ESI-MS): *m/z* 732.73 [Cu(mbis)$_2$]$^{+}$, 526.85 [(dmit)Cu(mbis)]$^{+}$, 398.82 [Cu(mbis)]$^{+}$, 318.97 [Cu(dmit)$_2$]$^{+}$, 190.95 [Cu(dmit)]$^{+}$. Anal. Calc. for $C_{28}H_{40}Cu_2N_{12}Se_4S_2B_2F_8$: C, 27.44; N, 13.72; H, 3.29. Found: C, 27.28; N, 13.60; H, 3.27.

*$[Cu_2(dmise)_2(mbit)_2][2BF_4]$ (**9**).* Complex **9** was prepared following the same procedure for **7** except that mbit (242 mg, 1 mmol) was used in place of mbis. The growth of single crystals for x-ray analysis was attempted from slow vapor diffusion of diethyl ether into acetonitrile solution. Yield: 30% (347 mg, 0.302 mmol). ^{1}H NMR (CD_3CN): 3.52 (s, 6H, $2CH_3$, mbit), 3.69 (s, 6H, $2CH_3$, dmise), 6.48 (s, 2H, CH_2), 7.04

(d, J_{HH} 3.0, 2H, 2CH), 7.14 (s, 2H, 2CH, dmise), 7.26 (d, J_{HH} 3.0, 2H, 2CH). $^{13}C\{^1H\}$ NMR: 35.88 (CH_3), 37.74 (CH_3), 57.45 (CH_2), 118.91 (CH), 121.40 (CH), 122 (CH), 149.25 (C=Se (dmise)), 158.75 (C=S (mbit)). $^{19}F\{^1H\}$ NMR (CD_3CN): -151.48, -151.53. UV-vis (CH_3CN): 268.9 nm. Mp. 174°C; IR (cm^{-1}): 521 s, 672 vs, 725 vs, 741 vs, 761 vs, 796 vs, 848 s, 983 s, 1033 b, 1217 vs, 1234 vs, 1250 vs, 1287 s, 1314 s, 1376 vs, 1401 vs, 1429 s, 1464 b, 1571 vs, 1699 b, 2851 b, 3141 s, 3171 s. Anal. Calc. for $C_{28}H_{40}Cu_2N_{12}Se_2S_4B_2F_8$: C, 29.72; N, 14.85; H, 3.56. Found: C, 29.60; N, 14.61; H, 3.53.

*$[Cu(mbit)(\mu\text{-}dmit)]_n[BF_4]_n$ (**10**).* Complex **10** was prepared following the same procedure for **7** except that dmit (129 mg, 1 mmol) was used in place of dmise and mbit (242 mg, 1 mmol) was used instead of mbis. Single crystals for x-ray analysis were grown from slow vapor diffusion of diethyl ether into acetonitrile solution. Yield: 34% (354 mg, 0.335 mmol). ^1H NMR (CD_3CN): 3.52 (s, 6H, $2CH_3$, mbit), 3.62 (s, 6H, $2CH_3$, dmit), 6.49 (s, 2H, CH_2), 7.00 (s, 2H, 2CH), 7.06 (d, J_{HH} 2.5, 2H, 2CH), 7.25 (d, J_{HH} 2.5, 2H, 2CH). $^{13}C\{^1H\}$ NMR: 35.94 (CH_3), 57.52 (CH_2), 119.00 (CH), 120.30 (CH), 121.50 (CH), 156.61 (C=S (dmit)), 158.40 (C=S (mbit)). $^{19}F\{^1H\}$ NMR (CD_3CN): -151.30, -151.35. UV-vis (CH_3CN): 267.8 nm. Mp. 159°C; IR (cm^{-1}): 503 s, 521 s, 603 s, 633 s, 670 vs, 729 vs, 760 s, 782 s, 848 s, 1032 b, 1174 s, 1234 vs, 1286 s, 1395 vs, 1464 vs, 1572 vs, 1684 b, 2250 s, 2725 s, 2921 b, 3140 b. Anal. Calc. for $C_{28}H_{40}Cu_2N_{12}S_6B_2F_8$: C, 32.41; N, 16.20; H, 3.88. Found: C, 32.55; N, 16.15; H, 3.97.

X-ray data collection and structural determination. Single crystals grown from vapor diffusion were mounted on a glass filament with silicon grease and immediately

cooled to 168.15K in a cold nitrogen gas stream. The crystals were grown by vapor diffusion of diethyl ether into an acetonitrile solution for $[Cu_2(\mu\text{-dmise})(dmise)_4][2BF_4]$ (**1**), $[Cu_2(\mu\text{-mbis})(mbis)_2][2BF_4]$ (**3**), $[Cu_2(ebit)_3][BF_4]_2$ (**6**), $[Cu_2(\mu\text{-mbis})_2(dmise)_2][2BF_4]$ (**7**), $[Cu_2(\mu\text{-mbis})_2(dmit)_2][2BF_4]$ (**8**), and **[**$Cu(mbit)(\mu\text{-dmit})]_n[BF_4]_n$ (**10**). Intensity data were collected using a Rigaku Mercury CCD detector and an AFC8S diffractometer. The space groups P-1 for **1**, **3**, **6**, **8**, and **10** and $P2_1/c$ for 7 were determined from the observed systematic absences. Data reduction including the application of Lorentz and polarization (Lp) effects and absorption corrections used the CrystalClear program.[41] The structures were solved by direct methods and subsequent Fourier difference techniques, and refined anisotropically, by full-matrix least squares, on F^2 using SHELXTL 6.10.[42] In the final cycle of least squares, independent anisotropic displacement factors were refined for the non-hydrogen atoms and the methyl hydrogen atoms were fixed in "idealized" positions with C-H = 0.96 Å. Their isotropic displacement parameters were set equal to 1.5 times U_{eq} of the attached carbon atom.

For complex **1,** the largest peak in the final Fourier difference map (1.08 $e \cdot A^{-3}$) was located 0.83 Å from Se(4) and the lowest peak (-0.81 $e \cdot A^{-3}$) was located at a distance of 0.86 Å from Se(4). The largest peak for complex **3** in the final Fourier difference map (0.82 $e \cdot A^{-3}$) was located 0.08 Å from Se(4) and the lowest peak (-0.79 $e \cdot A^{-3}$) was located at a distance of 0.77 Å from Se(5). The largest peak for **7** in the final Fourier difference map (1.16 $e \cdot A^{-3}$) was located 1.19 Å from H(6C) and the lowest peak (-0.74 $e \cdot A^{-3}$) was located at a distance of 0.92 Å from Se(1). The largest peak for **8** in the final Fourier difference map (1.10 $e \cdot A^{-3}$) was located 1.23 Å from N(5) and the lowest peak (-0.78

$e \cdot A^{-3}$) was located at a distance of 0.88 Å from Se(1). The largest peak for **10** in the final Fourier difference map (0.42 $e \cdot A^{-3}$) was located 1.73 Å from S(1), and the lowest peak (-0.42 $e \cdot A^{-3}$) was located at a distance of 0.76 Å from Cu(1). Final refinement parameters for the structures of **1**, **3**, **6**, **7**, **8**, and **10** are given in Tables 6.10 and 6.11.

Table 6. 10. Summary of crystallographic data for complexes **1**, **3**, and **6**.

	1	**3**	**6**
Chemical Formula	$C_{27}H_{43}Cu_2N_{11}Se_5B_2F_8$	$C_{29}H_{39}Cu_2N_{13}Se_6B_2F_8$	$C_{33}H_{46}Cu_2N_{13}S_6B_2F_8$
F.W. (g/mol)	1217.22	1344.19	1437.29
Space group	P-1	P-1	P-1
Crystal system	Triclinic	Triclinic	Triclinic
a, Å	11.712(2)	11.972(2)	10.368(2)
b, Å	14.126(3)	14.325(3)	10.699(2)
c, Å	14.800(3)	15.568(3)	10.804(2)
α, °	87.32(3)	89.58(3)	98.29(3)
β, °	73.78(3)	77.29(3)	116.81(3)
γ, °	71.01(3)	68.69(3)	91.25(3)
V, $Å^3$	2220.5(8)	2418.7(8)	1053.4(4)
Z	2	2	2
D_{cal}, Mg/m^3	1.821	1.846	1.677
Indices (min)	[-14, -17, -18]	[-14, -17, 0]	[-12, -11, -13]
(max)	[14, 17, 18]	[14, 17, 19]	[12, 11, 13]
Parameters	508	548	274
F(000)	1184	1296	542
μ, mm^{-1}	5.124	5.462	1.384
2θ range,°	3.19 - 26.38	2.94-26.34	3.09- 26.30
Collected reflections	18943	9716	9129
Unique reflections	8943	9716	9129
Final R (obs. Data)[a], R_1	0.0461	0.0470	0.0553
wR_2	0.1125	0.1116	0.1363
Final R (all data), R_1	0.0616	0.0666	0.0553
wR_2	0.1263	0.1276	0.1581
Goodness of fit (S)	1.117	1.062	1.046
Largest diff. Peak	1.081	0.817	0.929
Largest diff. Hole	-0.813	-0.792	-0.880

[a] $R_1 = [\Sigma||F_0| - |F_c||]/ \Sigma|F_0|$; $wR_2 = \{[\Sigma w[(F_0)^2 - (F_c)^2]^2\}^{1/2}$

Table 6.11. Summary of crystallographic data for complexes **7**, **8**, and **10**.

	7	**8**	**10**
Chemical Formula	$C_{28}H_{40}Cu_2N_{12}Se_6B_2F_8$	$C_{28}H_{40}Cu_2N_{12}S_2Se_4B_2F_8$	$C_{28}H_{40}Cu_2N_{12}S_6B_2F_8$
F.W. (g/mol)	1319.18	1225.38	1037.78
Space group	P-1	P-1	$P2_1/c$
Crystal system	Triclinic	Triclinic	Monoclinic
a, Å	8.21868(16)	8.1987(16)	9.4763(19)
b, Å	11.247(2)	11.198(2)	27.970(6)
c, Å	12.904(3)	12.935(3)	7. 8016(16)
α, °	66.67(3)	65.68(3)	90
β, °	84.64(3)	84.17(3)	99. 89 (3)
γ, °	77.72(3)	77.75(3)	90
V, $Å^3$	1066.1(4)	1057.5(4)	2037.1(7)
Z	1	1	2
D_{cal}, Mg/m^3	2.055	1.924	1.692
Indices (min)	[-10, -14, 16]	[-12, -21, -24]	[-11, -34, -7]
(max)	[9, 14, 11]	[11, 21, 26]	[11, 34, 9]
Parameters	266	267	266
F(000)	636	600	1056
μ, mm^{-1}	6.194	4.622	1.429
2θ range,°	3.12-26.75	2.95- 26.35	2.18 - 26.31
Collected reflections	9066	8161	16881
Unique reflections	4435	4221	4096
Final R (obs. Data)[a], R_1	0.0503	0.0455	0.0440
wR_2	0.1120	0.1049	0.0984
Final R (all data), R_1	0.0796	0.0658	0.0591
wR_2	0.1319	0.1182	0.1074
Goodness of fit (S)	1.093	1.100	1.089
Largest diff. Peak	1.158	1.097	0.416
Largest diff. Hole	-0.736	-0.778	-0.424

[a] $R_1 = [\Sigma||F_0| - |F_c||]/ \Sigma|F_0|$; $wR_2 = \{[\Sigma w[(F_0)^2 - (F_c)^2]^2\}^{1/2}$

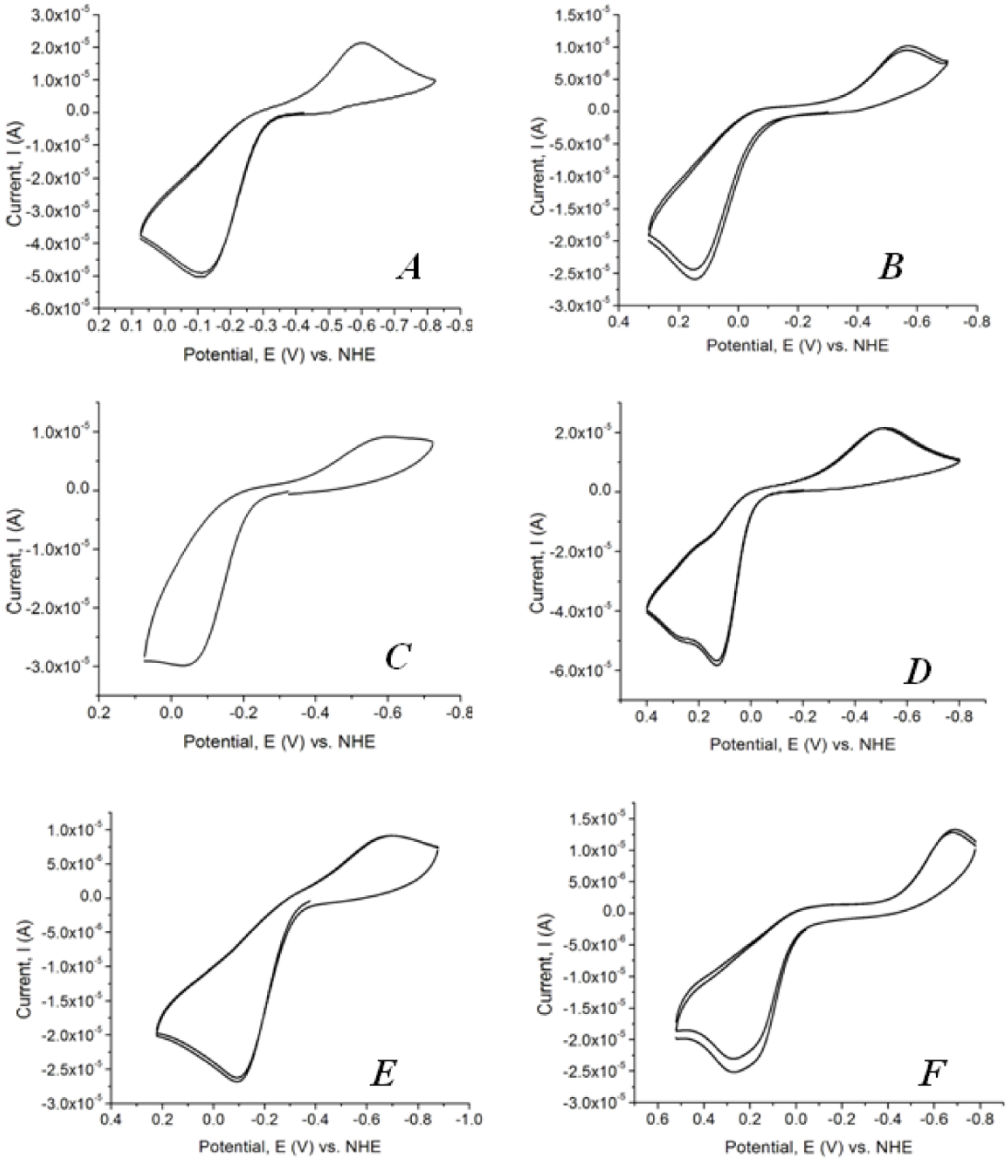

Figure 6.11. Cyclic voltammetry (CV) scans for A) $[Cu_2(\mu\text{-dmise})(dmise)_4][2BF_4]$ (**1**), B) $[Cu_2(dmit)_5][2BF_4]$ (**2**), C) $[Cu_2(\mu\text{-mbis})_3][2BF_4]$ (**3**), D) $[Cu_2(mbit)_3][2BF_4]$ (**4**), E) $[Cu_2(ebis)_3][2BF_4]$ (**5**), F) $[Cu_2(ebit)_3][2BF_4]$ (**6**). All data collected with 1 mM complex in acetonitrile.

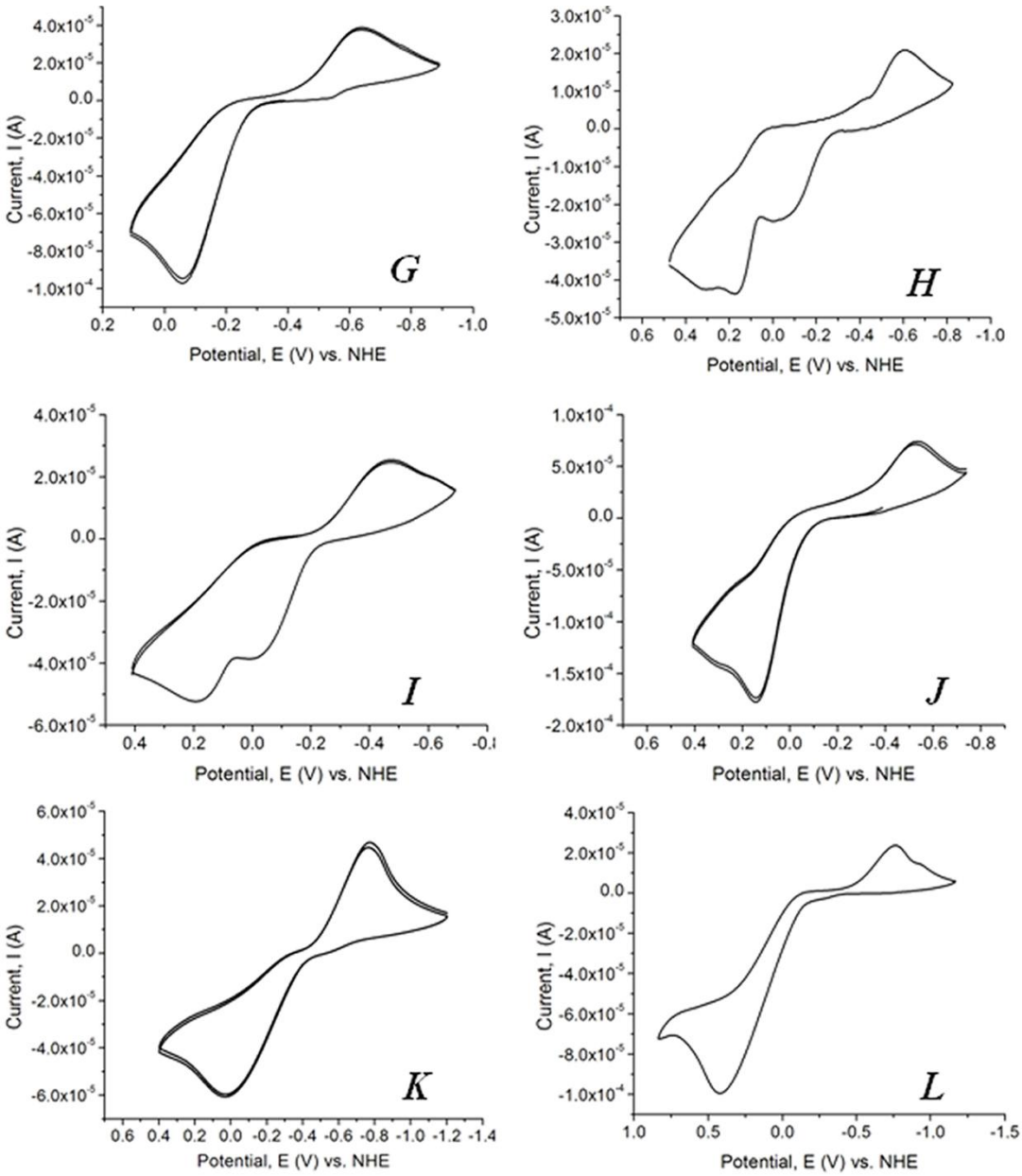

Figure 6.11(cont.). Cyclic voltammetry (CV) scans for G) $[Cu_2(\mu\text{-mbis})_2(dmise)_2][2BF_4]$ (**7**), H) $[Cu_2(mbit)_2(dmise)_2][2BF_4]$ (**8**), I) $[Cu_2(\mu\text{-mbis})_2(dmit)_2][2BF_4]$ (**9**), J) $[Cu(mbit)(\mu\text{-dmit})]_n[BF_4]_n$ (**10**), K) dmise, F) dmit. All data collected with 1 mM complex in acetonitrile.

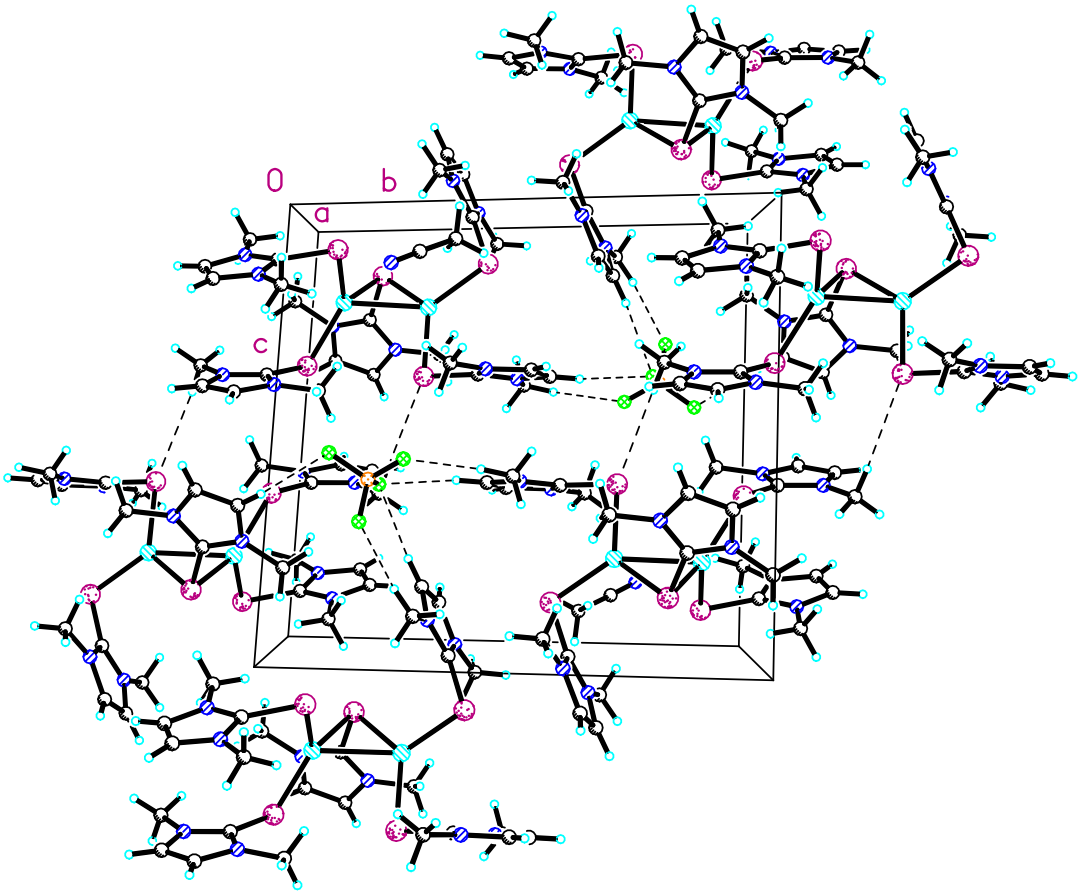

Figure 6.12. Crystal packing diagram of $[Cu_2(\mu\text{-dmise})(dmise)_4][2BF_4]$ (**1**) showing 50% probability density ellipsoids displaying H-F and H-Se short contact interactions along the *a*-axis.

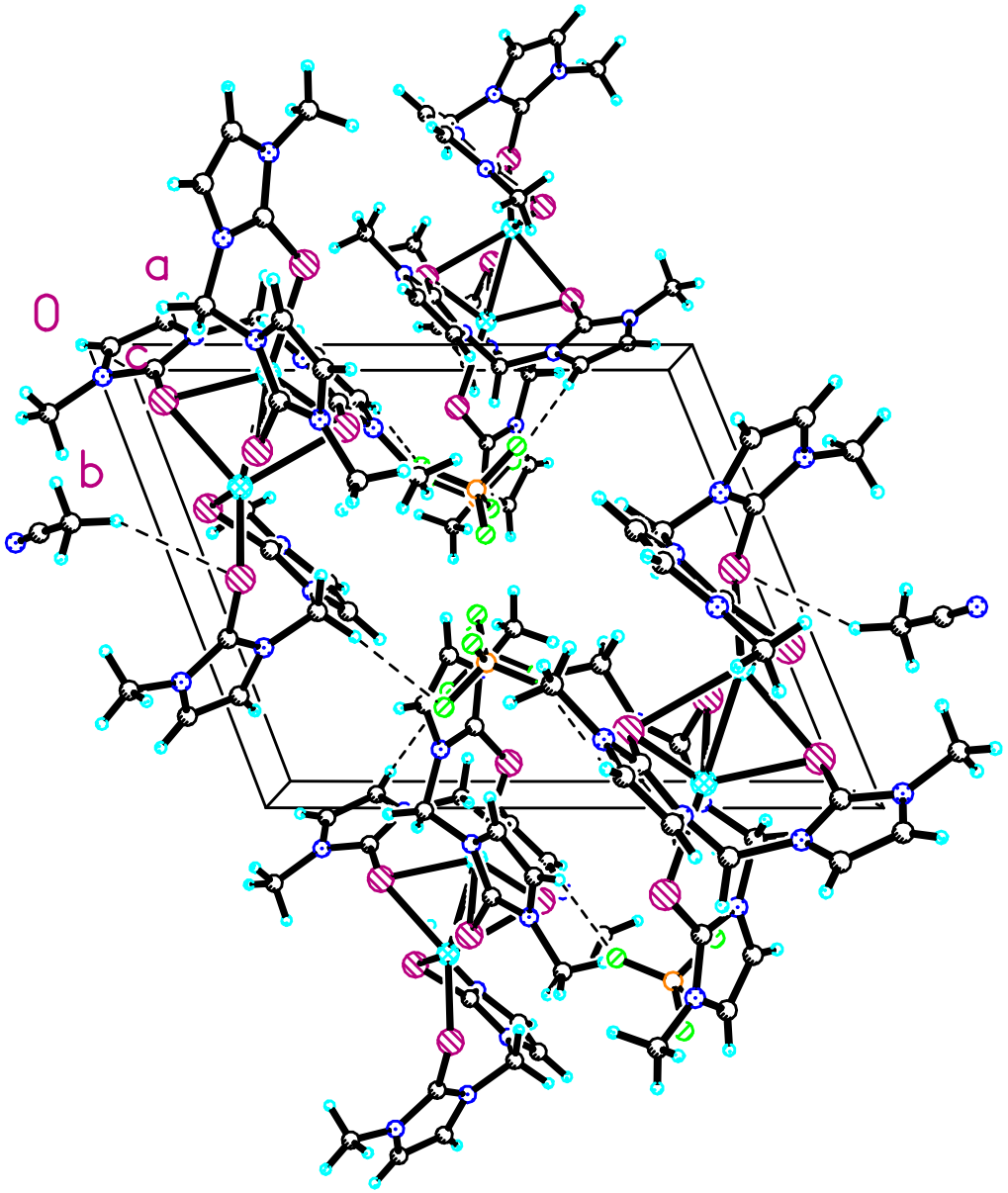

Figure 6.13. Crystal packing diagram of $[Cu_2(\mu\text{-mbis})(mbis)_2][2BF_4]$ (**3**) showing 50% probability density ellipsoids and displaying H-F short contact interactions along the *c*-axis. The short-contact interaction between the acetonitrile solvent molecule and the selenium atom is also shown.

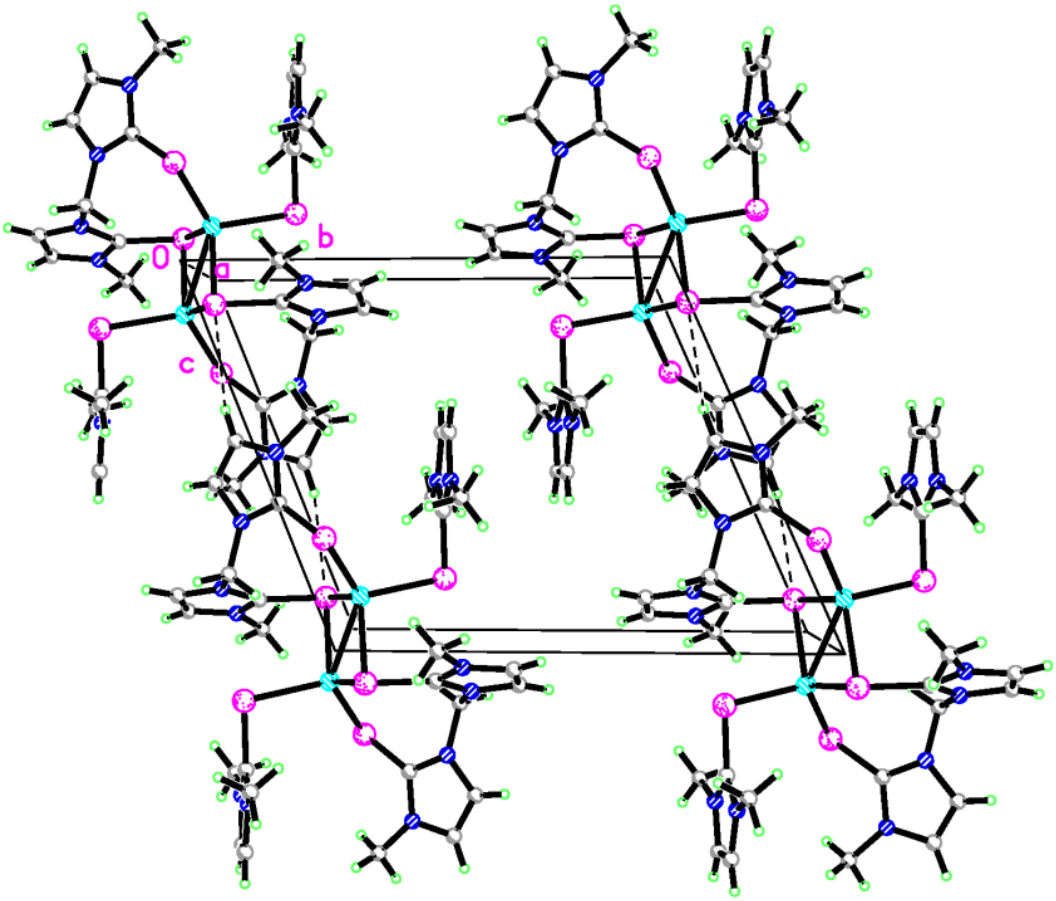

Figure 6.14. Crystal packing diagram of $[Cu_2(\mu\text{-mbis})_2(dmise)_2][2BF_4]$ (**7**) showing 50% probability density ellipsoids and H-Se short-contact interactions along the *a*-axis. The counterions are omitted for clarity.

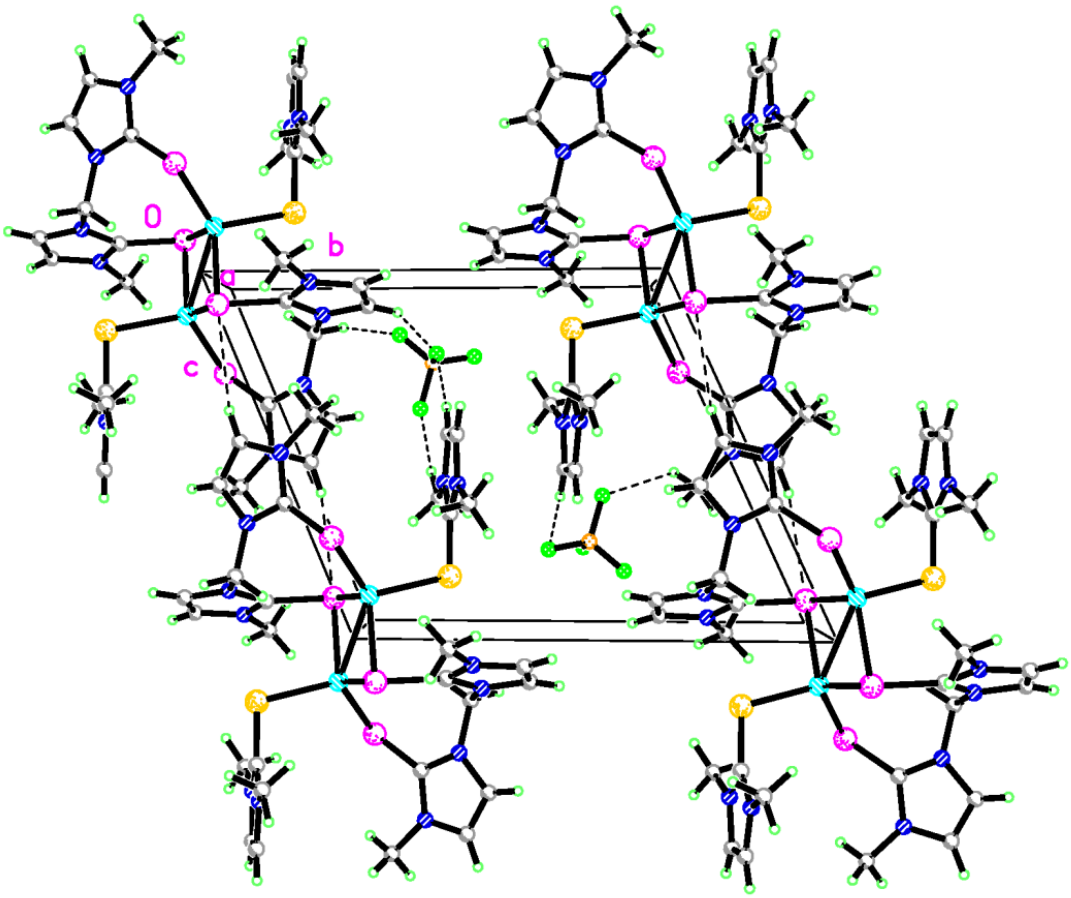

Figure 6.15. Crystal packing diagram of $[Cu_2(\mu\text{-mbis})_2(dmit)_2][2BF_4]$ (**8**) showing 50% probability density ellipsoids and the H-F and H-Se short-contact interactions along the *a*-axis.

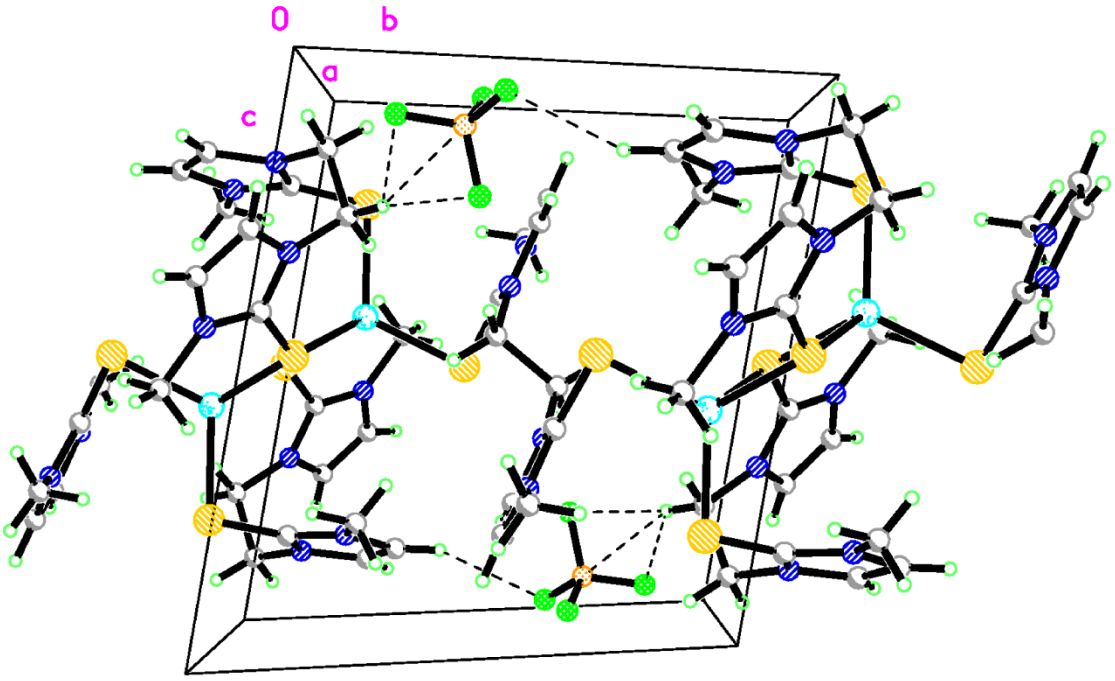

Figure 6.16. Crystal packing diagram of $[Cu_2(ebit)_3][2BF_4]$ (**6**) showing 50% probability density ellipsoids and the H-F short contact interactions along the *a*-axis.

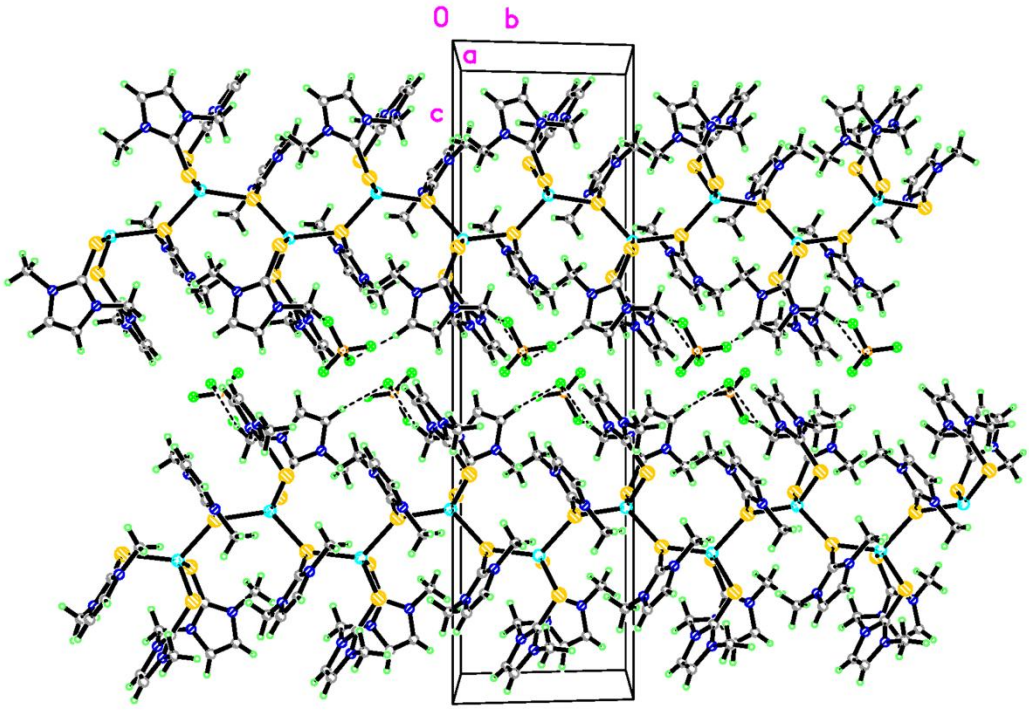

Figure 6.17. Crystal packing diagram of **[**Cu(mbit)(μ-dmit)]$_n$[BF_4]$_n$ (**10**) showing 50% probability density ellipsoids and the H-F short-contact interactions along the *a*-axis.

References

(1) Jia, W. G.; Huang, Y. B.; Lin, Y. J.; Jin, G. X. *Dalton Trans.* **2008**, 5612-5620.

(2) Kim, H. R.; Jung, I. G.; Yoo, K.; Jang, K.; Lee, E. S.; Yun, J.; Son, S. U. *Chem. Commun.* **2010**, *46*, 758-760.

(3) Maria, L.; Moura, C.; Paulo, A.; Santos, I. C.; Santos, I. *J. Organomet. Chem.* **2006**, *691*, 4773-4778.

(4) Parkin, G. *New J. Chem.* **2007**, *31*, 1996-2014.

(5) Kimblin, C.; Bridgewater, B. M.; Churchill, D. G.; Hascall, T.; Parkin, G. *Inorg. Chem.* **2000**, *39*, 4240-4243.

(6) Slavin, P. A.; Reglinski, J.; Spicer, M. D.; Kennedy, A. R. *J. Chem. Soc.-Dalton Trans.* **2000**, 239-240.

(7) Awaleh, M. O.; Badia, A.; Brisse, F. *Inorg. Chem.* **2007**, *46*, 3185-3191.

(8) Kuhn, N.; Kratz, T. *Synthesis* **1993**, 561.

(9) Cheon, J.; Arnold, J.; Yu, K. M.; Bourret, E. D. *Chem. Mater.* **1995**, *7*, 2273-2276.

(10) Williams, D. J.; Shilatifard, A.; VanDeveer, D.; Lipscomb, L. A.; Jones, R. L. *Inorg. Chim. Acta* **1992**, *202*, 53-57.

(11) Pinder, T. A.; VanDerveer, D.; Rabinovich, D. *Inorg. Chem. Commun.* **2007**, *10*, 1381-1384.

(12) Bigoli, F.; Deplano, P.; Devillanova, F. A.; Lippolis, V.; Mercuri, M. L.; Pellinghelli, M. A.; Trogu, E. F. *Inorg. Chim. Acta* **1998**, *267*, 115-121.

(13) Williams, D. J.; VanDerveer, D.; Jones, R. L.; Menaldino, D. S. *Inorg. Chim. Acta* **1989**, *165*, 173-178.

(14) Silva, R. M.; Smith, M. D.; Gardinier, J. R. *Inorg. Chem.* **2006**, *45*, 2132-2142.

(15) Crossley, I. R.; Hill, A. F.; Humphrey, E. R.; Smith, M. K. *Organometallics* **2006**, *25*, 2242-2247.

(16) Jia, W. G.; Huang, Y. B.; Lin, Y. J.; Wang, G. L.; Jin, G. X. *Eur. J. Inorg. Chem.* **2008**, 4063-4073.

(17) Landry, V. K.; Buccella, D.; Pang, K. L.; Parkin, G. *Dalton Trans.* **2007**, 866-870.

(18) Marshall, N. M.; Garner, D. K.; Wilson, T. D.; Gao, Y. G.; Robinson, H.; Nilges, M. J.; Lu, Y. *Nature* **2009**, *462*, 113-U127.

(19) Strieter, E. R.; Bhayana, B.; Buchwald, S. L. *J. Am. Chem. Soc.* **2009**, *131*, 78-88.

(20) Kimani, M. M.; Brumaghim, J. L.; VanDerveer, D. *Inorg. Chem.* **2010**, *49*, 9200-9211.

(21) Kimani, M. M.; Brumaghim, J. L.; Bayse, C. A. *Dalton Trans.*, submitted.

(22) Balamurugan, R.; Palaniandavar, M.; Gopalan, R. S. *Inorg. Chem.* **2001**, *40*, 2246-2255.

(23) Booth, D. G.; Levason, W.; Quirk, J. J.; Reid, G.; Smith, S. M. *J. Chem. Soc., Dalton Trans.* **1997**, 3493-3500.

(24) Blake, A. J.; Lippolis, V.; Pivetta, T.; Verani, G. *Acta. Crystallogr. C* **2007**, *63*, m364-367.

(25) Williams, D. J.; Fawcettbrown, M. R.; Raye, R. R.; Vanderveer, D.; Pang, Y. T.; Jones, R. L.; Bergbauer, K. L. *Heteroatom Chem.* **1993**, *4*, 409-414.

(26) Devillanova, F. A.; Verani, G.; Battaglia, L. P.; Corradi, B. A. *Transition Met. Chem.* **1980**, *5*, 362-364.

(27) Beheshti, A.; Clegg, W.; Nobakht, V.; Mehr, M. P.; Russo, L. *Dalton Trans.* **2008**, 6641-6646.

(28) Aslanidis, P.; Hadjikakou, S. K.; Karagiannidis, P.; Cox, P. J. *Inorg. Chim. Acta* **1998**, *271*, 243-247.

(29) Lobana, T. S.; Sharma, R.; Butcher, R. J. *Z. Anorg. Allg. Chem.* **2008**, *634*, 1785-1790.

(30) Basumallick, L.; George, S. D.; Randall, D. W.; Hedman, B.; Hodgson, K. O.; Fujisawa, K.; Solomon, E. I. *Inorg. Chim. Acta* **2002**, *337*, 357-365.

(31) Tomlin, D. W.; Campbell, D. P.; Fleitz, P. A.; Adams, W. W. *Acta Cryst.* **1997**, *C53*, 1153-1154.

(32) Raper, E. S.; Creighton, J. R.; Oughtred, R. E.; Nowell, I. W. *Acta Crystallogr. Sect. B-Struct. Commun.* **1983**, *39*, 355-360.

(33) Lobana, T. S.; Castineiras, A. *Polyhedron* **2002**, *21*, 1603-1611.

(34) Lee, D. H.; Hatcher, L. Y. Q.; Vance, M. A.; Sarangi, R.; Milligan, A. E.; Sarjeant, A. A. N.; Incarvito, C. D.; Rheingold, A. L.; Hodgson, K. O.; Hedman, B.; Solomon, E. I.; Karlin, K. D. *Inorg. Chem.* **2007**, *46*, 6056-6068.

(35) Dennison, C. *Coord. Chem. Rev.* **2005**, *249*, 3025-3054.

(36) Roy, G.; Das, D.; Mugesh, G. *Inorg. Chim. Acta* **2007**, *360*, 303-316.

(37) Kubas, G. J. *Inorg. Synth.* **1990**, *28*, 68-70.

(38) *NMR and the Periodic Table*; Harris, R. K.; Mann, B. E., Eds.; Academic Press: London, 1978, p. 99.

(39) Odom, J. D.; Dawson, W. H.; Ellis, P. D. *J. Amer. Chem. Soc.* **1979**, *101*, 5815-5823.

(40) Connelly, N. G.; Geiger, W. E. *Chem. Rev.* **1996**, *96*, 877-910.

(41) Crystalclear; The Woodlands: Texas, USA, 1999.

(42) Sheldrick, G. M.; Bruker Analytical X-ray Systems Inc.: Madison, WI, 2000.

APPENDIX A

COPYRIGHT PERMISSION FOR WORK PRESENTED IN CHAPTER TWO

This is a License Agreement between Martin M. Kimani ("You") and American Chemical Society ("American Chemical Society") provided by Copyright Clearance Center ("CCC"). The license consists of your order details, the terms and conditions provided by American Chemical Society, and the payment terms and conditions.

All payments must be made in full to CCC. For payment instructions, please see information listed at the bottom of this form.

License Number	2573691239471
License Date	Dec 21, 2010
Licensed content publisher	American Chemical Society
Licensed content publication	Inorganic Chemistry
Licensed content title	Probing the Antioxidant Action of Selenium and Sulfur Using Cu(I)-Chalcogenone Tris(pyrazolyl)methane and -borate Complexes
Licensed content author	Martin M. Kimani et al.
Licensed content date	Oct 1, 2010
Volume number	49
Issue number	20
Type of Use	Thesis/Dissertation
Requestor type	Not specified
Format	Electronic
Portion	50% or more of original article
Author of this ACS article	Yes
Order reference number	
Title of the thesis / dissertation	synthesis and characterization of biologically relevant Cu(I) selone and thione complexes
Expected completion date	Dec 2010
Estimated size(pages)	230
Billing Type	Invoice
Billing Address	50 keoway dr apt a4 seneca, SC 29672 United States
Customer reference info	
Total	0.00 USD
Terms and Conditions	

Thesis/Dissertation

ACS / RIGHTSLINK TERMS & CONDITIONS
THESIS/DISSERTATION

INTRODUCTION

payment is received from you (by CCC) as provided in CCC's Billing and Payment terms and conditions. If full payment is not received on a timely basis, then any license preliminarily granted shall be deemed automatically revoked and shall be void as if never granted. Further, in the event that you breach any of these terms and conditions or any of CCC's Billing and Payment terms and conditions, the license is automatically revoked and shall be void as if never granted. Use of materials as described in a revoked license, as well as any use of the materials beyond the scope of an unrevoked license, may constitute copyright infringement and publisher reserves the right to take any and all action to protect its copyright in the materials.

COPYRIGHT NOTICE: DISCLAIMER

You must include the following copyright and permission notice in connection with any reproduction of the licensed material: "Reprinted (“Adapted” or “in part”) with permission from REFERENCE CITATION. Copyright YEAR American Chemical Society."

WARRANTIES: NONE

Publisher makes no representations or warranties with respect to the licensed material.

INDEMNITY

You hereby indemnify and agree to hold harmless publisher and CCC, and their respective officers, directors, employees and agents, from and against any and all claims arising out of your use of the licensed material other than as specifically authorized pursuant to this license.

NO TRANSFER OF LICENSE

This license is personal to you or your publisher and may not be sublicensed, assigned, or transferred by you to any other person without publisher's written permission.

NO AMENDMENT EXCEPT IN WRITING

This license may not be amended except in a writing signed by both parties (or, in the case of publisher, by CCC on publisher's behalf).

OBJECTION TO CONTRARY TERMS

Publisher hereby objects to any terms contained in any purchase order, acknowledgment, check endorsement or other writing prepared by you, which terms are inconsistent with these terms and conditions or CCC's Billing and Payment terms and conditions. These terms and conditions, together with CCC's Billing and Payment terms and conditions

(which are incorporated herein), comprise the entire agreement between you and publisher (and CCC) concerning this licensing transaction. In the event of any conflict between your obligations established by these terms and conditions and those established by CCC's Billing and Payment terms and conditions, these terms and conditions shall control.

JURISDICTION

This license transaction shall be governed by and construed in accordance with the laws of the District of Columbia. You hereby agree to submit to the jurisdiction of the courts located in the District of Columbia for purposes of resolving any disputes that may arise in connection with this licensing transaction.

THESES/DISSERTATION TERMS

Regarding your request for permission to include **your** paper(s) or portions of text from **your** paper(s) in your thesis/dissertation, permission is now automatically granted; please pay special attention to the **implications** paragraph below. The Copyright Subcommittee of the Joint Board/Council Committees on Publications approved the following:

Copyright permission for published and submitted material from theses and dissertations ACS extends blanket permission to students to include in their theses and dissertations their own articles, or portions thereof, that have been published in ACS journals or submitted to ACS journals for publication, provided that the ACS copyright credit line is noted on the appropriate page(s).

Publishing **implications** of electronic publication of theses and dissertation material

Students and their mentors should be aware that posting of theses and dissertation material on the Web prior to submission of material from that thesis or dissertation to an ACS journal may affect publication in that journal. Whether Web posting is considered prior publication may be evaluated on a case-by-case basis by the journal's editor. If an ACS journal editor considers Web posting to be "prior publication", the paper will not be accepted for publication in that journal. If you intend to submit your unpublished paper to ACS for publication, check with the appropriate editor prior to posting your manuscript electronically.

Reuse/Republication of the Entire Work in Theses or Collections: Authors may reuse all or part of the Submitted, Accepted or Published Work in a thesis or dissertation that the author writes and is required to submit to satisfy the criteria of degree-granting institutions. Such reuse is permitted subject to the ACS' "Ethical Guidelines to Publication of Chemical Research" (http://pubs.acs.org/page/policy/ethics/index.html); the author should secure written confirmation (via letter or email) from the respective ACS journal editor(s) to avoid potential conflicts with journal prior publication*/embargo policies. Appropriate citation of the Published Work must be made. If the thesis or dissertation to be published is in

electronic format, a direct link to the Published Work must also be included using the ACS Articles on Request author-directed link - see

http://pubs.acs.org/page/policy/articlesonrequest/index.html

* Prior publication policies of ACS journals are posted on the ACS website at http://pubs.acs.org/page/policy/prior/index.html

If your paper has not yet been published by ACS, please print the following credit line on the first page of your article: "Reproduced (or 'Reproduced in part') with permission from [JOURNAL NAME], in press (or 'submitted for publication'). Unpublished work copyright [CURRENT YEAR] American Chemical Society." Include appropriate information.

If your paper has already been published by ACS and you want to include the text or portions of the text in your thesis/dissertation in **print or microfilm formats**, please print the ACS copyright credit line on the first page of your article: "Reproduced (or 'Reproduced in part') with permission from [FULL REFERENCE CITATION.] Copyright [YEAR] American Chemical Society." Include appropriate information.

Submission to a Dissertation Distributor: If you plan to submit your thesis to UMI or to another dissertation distributor, you should not include the unpublished ACS paper in your thesis if the thesis will be disseminated electronically, until ACS has published your paper. After publication of the paper by ACS, you may release the entire thesis (**not the individual ACS article by itself**) for electronic dissemination through the distributor; ACS's copyright credit line should be printed on the first page of the ACS paper.

v1.2

Gratis licenses (referencing $0 in the Total field) are free. Please retain this printable license for your reference. No payment is required.

If you would like to pay for this license now, please remit this license along with your payment made payable to "COPYRIGHT CLEARANCE CENTER" otherwise you will be invoiced within 48 hours of the license date. Payment should be in the form of a check or money order referencing your account number and this invoice number RLNK10903421.

Once you receive your invoice for this order, you may pay your invoice by credit card. Please follow instructions provided at that time.

Make Payment To:
Copyright Clearance Center
Dept 001
P.O. Box 843006
Boston, MA 02284-3006

If you find copyrighted material related to this license will not be used and wish to cancel, please contact us referencing this license number 2573691239471 and noting the reason for cancellation.